

UNIVERSITY OF CANBERRA  
FACULTY OF APPLIED SCIENCE

# Digital imaging & image processing techniques for the comparison of human hair features

Carolyn Jane McLaren

A thesis submitted in fulfilment of the requirements for the  
Degree of Doctor of Philosophy

June 2012



## Abstract

The role of the forensic hair examiner is to determine whether a questioned hair recovered from a crime scene could or could not be from the same source as a known sample and therefore whether it should be included or excluded as probative evidence. Arguably, traditional hair microscopy is a largely subjective process that relies heavily on the training and experience of the examiner. The aim of this project was to investigate three objective analytical methods—two based on image analysis and one based on infrared spectroscopy—to produce a hair examination protocol that balances qualitative microscopic observations with quantitative measures.

First, numerical colour measurements were investigated for allocating hair to one of six nominal categories and for distinguishing one participant's hair from another's within a subpopulation of similar coloured hair. Overall, between 69.3 and 76.2% correct classification to the categories was achieved with the RGB and CIE L\*a\*b\* colour models returning the highest prediction accuracy, and CIE XYZ colour model returning generally poor results, particularly among the darker hair categories. In an effort to refine and improve these results, analyses were repeated that incorporated only a limited set of categories and predictor variables. Correct allocation increased slightly for the dark hair categories while no improvement was observed for the light hair categories. For distinguishing between individual hairs within a subpopulation of similarly coloured hair, aside from the red hair category, the discriminating power was considered to be too low for the method to be recommended as a routine tool in forensic hair examination.

Second, a novel image analysis technique was evaluated that involved applying threshold operations to image montages, in order to compare pigmentation characteristics in three separate hair populations—Fair, Medium and Dark shaded hair. The average pixel area of each black on white object and the length of the major and minor axes, as well as calculated measurements such as density, the percentage of small, medium and large objects, and the percentage of two nominal configurations—'streaks' and 'clumps'—were evaluated as potential variables. The novel technique did not support discrimination between the selected participants. The Medium sample population resulted in the lowest number of images correctly allocated, with only 32% prediction accuracy, the Fair sample population resulted in 54% prediction accuracy and the Dark sample population showed the highest correct allocation, with 62% prediction accuracy. No obvious relationships

were observed between each of the populations in terms of the number of variables selected, the strongest predicting variable or the overall prediction accuracy.

Finally, ATR–FTIR spectroscopy was assessed for identifying trace contaminants—specifically, hair treatments—on the hair surface. Seven product types were evaluated following dense and sparse application to individual hairs. Infrared absorption peaks were apparent for six product types with only one type showing no significant absorption. Discriminant analysis comprising 254 wavenumbers between 1632 and 652 (at a spacing of  $3.857\text{ cm}^{-1}$ ) resulted in 100% accuracy for 60 reference spectra of the products evaluated, albeit only one brand per product type was included in this analysis. The strongest predictor variables were generally between 1300 and  $1000\text{ cm}^{-1}$  corresponding to the CO absorbance bands for ethers and esters, and at  $1450\text{ cm}^{-1}$  corresponding to the  $\text{CH}_3$  asymmetrical bend vibration. Variations in the spectra most likely due to molecular interactions (e.g., hydrogen bonding), were observed following dense application to the hair. Only 73% of those spectra were correctly classified by product type. Following sparse application to hair, trace contaminants were not observed on the majority of samples. On the few samples where traces were observed, spectra of the product type could not be clearly resolved.

Difficulties associated with improving the discriminating power of hair examinations were identified two decades ago, including that considerable intra-individual variation exists and that microscopic hair features are difficult to assess objectively (Robertson, 1982). Emerging technologies could assist future examinations with classifying—or potentially individualising—forensic hair evidence. However, successful quantification and discrimination of hair characteristics has not yet been achieved, despite attempts made in this research. Until there is a universally applicable technique that will mimic microscopic analysis, current evaluations made by an experienced examiner are the best option available.

# Certificate of Authorship of Thesis

Except where clearly acknowledged in footnotes, quotations and the bibliography, I certify that I am the sole author of the thesis submitted today entitled –

## **Digital imaging & image processing techniques for the comparison of human hair features**

I further certify that to the best of my knowledge the thesis contains no material previously published or written by another person except where due reference is made in the text of the thesis.

The material in the thesis has not been the basis of an award of any other degree or diploma except where due reference is made in the text of the thesis.

The thesis complies with University requirements for a thesis as set out in –

*Gold Book Part 7: Examination of Higher Degree by Research  
Theses Policy, Schedule Two (S2).*

Refer to <http://www.canberra.edu.au/research-students/goldbook>

.....

Signature of Candidate

.....

Signature of Chair of the Supervisory Panel

Date: .....



## Acknowledgements

There are many people who provided advice, encouragement and support throughout my PhD research. I am tremendously grateful to everyone who gave up their time to assist. In particular, I would like to thank my supervisors for their excellent guidance over the last three and a half years. My supervisory chair, Professor Chris Lennard, played devil's advocate at almost every cross-road I came to along the way (although, personally, I believe he enjoys this role!). In addition, Chris meticulously reviewed all of my written work, for which I am very grateful. My secondary supervisory, Dr James Robertson, generously gave me direction on many different aspects of the project and consistently drew me back to the bigger picture. Thank you both.

I offer a big thank you to Elizabeth Brooks for getting this project started in the first place. Liz supported me in many ways during the first few years of my research; I am especially appreciative to Liz and David Parry, for patiently training me on microscopic examination and the science of hair. I would like to thank David Pederson, Alice Richardson and Tamsin Kelly who each assisted on different aspects of the statistical analyses, as well as David Royds, Brian Reedy and Nopporn Song-im who got me through spectroscopy. FTIR spectroscopy is an amazing technique that I knew very little about before now. Thank you all for the tips and tricks that got me on my way. I also wish to thank Bruce Comber, David Meere and James Irwin who helped me understand the *VPascal* image analysis scripts used in this research; (an extra big thank you to Bruce for actually writing the scripts in the first place!).

I would like to acknowledge my fellow researchers and the staff at the National Centre for Forensic Studies, University of Canberra who have made my research journey all the more enjoyable—particularly, Tamsin Kelly, Sam Venables, Nopporn Song-im, Greg Adcock, Shirani Katupitiya, David Royds, Dennis McNevin and Melissa Clark. Thanks goes also to my non-Uni friends whom I haven't had a great deal of time to see over the last few years, yet still let me phone them up occasionally just to “vent”—particularly, Dave and Kate Meere, Amy McKenzie, Ash Taylor and Jenni O.

Finally, I would like to thank my family for their continuous support since my return to university, seven long years ago. You have sat through at least twelve practice presentations and plenty more tantrums. I promise that I will now move my laptop and

books from the kitchen table—for good! To my partner, Jimmy, thank you for all your support and encouragement and for pretending to be interested in statistics, at least some of the time. If we can make it through this, I trust we can make it through almost anything! To my beautiful daughter, Jordan, you were only three when I left work and enrolled in my undergraduate degree. I started this journey so I could be a better role model for you and I sincerely hope, seven years later, that is now the case. Thank you for putting up with my many absences from school presentations and weekend sports. I promise that I will now go to work only and not spend my weekends studying—“just like a normal mum”.

This research would not have occurred without a linkage grant generously awarded from the Australian Research Council (ARC) and additional funding provided by the Australian Federal Police. I hope the research presented in this thesis—along with that conducted by my ARC Linkage grant co-researcher, Janette Edson, at the University of Adelaide—provide an important and useful contribution to the science of forensic hair examination.



## Table of Contents

<i>Abstract</i> .....	<i>i</i>
<i>Certificate of Authorship of Thesis</i> .....	<i>iii</i>
<i>Acknowledgements</i> .....	<i>v</i>
<i>Table of Contents</i> .....	<i>vii</i>
<i>List of Figures</i> .....	<i>x</i>
<i>List of Tables</i> .....	<i>xi</i>
<i>Abbreviations</i> .....	<i>xii</i>
<b>Chapter 1. INTRODUCTION</b> .....	<b>1</b>
1.1. <i>Hair Growth and Physiology</i> .....	2
1.2. <i>Forensic Hair Examination</i> .....	4
1.2.1. Microscopic Examination .....	4
1.2.2. DNA Analysis .....	5
1.2.3. Hair as Evidence.....	6
1.2.4. Probative Value of Hair Evidence.....	8
1.2.5. Individualisation.....	10
1.3. <i>Digital Imaging and Image Processing</i> .....	12
1.3.1. Application and Diversity in Forensic Science .....	12
1.3.2. Application to Animal Fibres .....	13
1.3.3. Image Analysis of Hair .....	14
1.4. <i>Aim and Scope of this Project</i> .....	17
1.4.1. Chapter 2: COLOUR.....	17
1.4.2. Chapter 3: PIGMENTATION .....	17
1.4.3. Chapter 4: SPECTROSCOPY .....	18
<b>Chapter 2. COLOUR</b> .....	<b>19</b>
2.1. <i>Introduction</i> .....	20
2.1.1. Colour Classification.....	20
2.1.2. Colour Science .....	21
2.1.3. Colour Models.....	23
2.1.4. Research on Hair Colour .....	26
2.1.5. Research Focus.....	31
2.2. <i>Materials and Methods</i> .....	33
2.2.1. Sample Preparation .....	33
2.2.2. Image Acquisition .....	34
2.2.3. Image Preparation .....	36
2.2.4. Colour Measurement.....	37

2.2.5. Colour Transformation .....	37
2.2.6. Exposure Correction .....	39
2.2.7. Data Preparation .....	41
2.2.8. Discriminant Analysis .....	41
2.2.9. Analysis of Variance .....	44
2.2.10. Nominal Colour Categories .....	45
2.2.11. Probability Distribution Curve .....	46
<i>2.3. Results and Discussion</i> .....	48
2.3.1. Allocation to Categories (Preliminary).....	48
2.3.2. Allocation to Categories (Secondary).....	56
2.3.3. Main Source of Variance .....	59
2.3.4. Allocation to Participants .....	59
2.3.5. Discriminative Analysis Considerations .....	62
2.3.6. Colour Comparison between Two Samples .....	63
2.3.7. Confidence Interval Considerations .....	69
<i>2.4. Conclusion</i> .....	70
<b>Chapter 3. PIGMENTATION .....</b>	<b>71</b>
<i>3.1. Introduction</i> .....	72
3.1.1. Hair Colour .....	72
3.1.2. Melanogenesis and Pigment Patterns .....	72
3.1.3. Research on Hair Pigmentation .....	74
3.1.4. Quantification of Pigmentation .....	75
3.1.5. Research Focus .....	76
<i>3.2. Materials and Method</i> .....	78
3.2.1. Preliminary Evaluation — Sample Preparation.....	78
3.2.2. Preliminary Evaluation — Pigmentation Measurement .....	80
3.2.3. Preliminary Evaluation — Summary .....	83
3.2.4. Data Preparation .....	85
3.2.5. Analysis of Variance .....	86
3.2.6. Discriminant Analysis .....	87
<i>3.3. Results and Discussion</i> .....	89
3.3.1. Main Source of Variance .....	89
3.3.2. Allocation to Participants .....	95
<i>3.4. Conclusion</i> .....	101
<b>Chapter 4. SPECTROSCOPY .....</b>	<b>103</b>
<i>4.1. Introduction</i> .....	104
4.1.1. Principles of Molecular Spectroscopy .....	104
4.1.2. Spectroscopy Instrumentation and Sampling Techniques.....	108
4.1.3. Chemical Imaging.....	113

4.1.4. Research on Hair .....	114
4.1.5. Research Focus.....	119
<b>4.2. Materials and Methods .....</b>	<b>121</b>
4.2.1. Sample Preparation .....	121
4.2.2. Instrumentation.....	123
4.2.3. Data Preparation.....	124
4.2.4. Chemical Imaging .....	124
4.2.5. Discriminant Analysis .....	125
<b>4.3. Results and Discussion .....</b>	<b>128</b>
4.3.1. Hair Product References.....	128
4.3.2. Allocation to Product Class.....	140
4.3.3. Product Densely Applied .....	142
4.3.4. Allocation to Product Class.....	149
4.3.5. Product Sparsely Applied.....	151
4.3.6. Chemical Imaging .....	157
<b>4.4. Conclusion .....</b>	<b>161</b>
<b>Chapter 5. CONCLUSION.....</b>	<b>163</b>
5.1. Conclusion .....	164
5.1.1. Colour.....	164
5.1.2. Pigmentation.....	166
5.1.3. Spectroscopy .....	167
5.2. Conclusion – Recommendations for Future Research .....	169
<b>References.....</b>	<b>171</b>
<b>Appendices .....</b>	<b>183</b>
Appendix A.....	184
Appendix B.....	193
Appendix C.....	196
Appendix D .....	197
Appendix E.....	199
Appendix F.....	202

## List of Figures

Figure 1.1-1 – The Hair Bulb.....	2
Figure 2.1-1 – Visible Continuous Spectrum .....	21
Figure 2.1-2 – Depiction of Colour Interpolation .....	23
Figure 2.1-3 – RGB Colour Gamut.....	24
Figure 2.1-4 – CIE XYZ Colour Gamut .....	25
Figure 2.1-5 – CIE L*a*b* Colour Space .....	26
Figure 2.2-1 – Depiction of Z–range Relative to Hair Shaft .....	35
Figure 2.2-2 – Example Z–stack and Final Montage.....	36
Figure 2.3-1 – RGB Canonical Discriminant Functions.....	50
Figure 2.3-2 – CIE XYZ Canonical Discriminant Functions .....	52
Figure 2.3-3 – CIE L*a*b* Canonical Discriminant Functions .....	54
Figure 2.3-4 – Dark Category Canonical Discriminant Functions .....	57
Figure 2.3-5 – Light Category Canonical Discriminant Functions.....	58
Figure 2.3-6 –Montage Representing a Individual, Questioned Hair .....	64
Figure 2.3-7 – Probability Distribution and Colour Variation of Participant 2002044 .....	65
Figure 2.3-8 – Probability Distribution and Colour Variation of Participant 2002185 .....	66
Figure 2.3-9 – Montages Representing a Question and Known Comparison Hair .....	67
Figure 2.3-10 – Box Plots of Mean, Upper and Lower RGB Measurements .....	68
Figure 3.2-1 – Pigment Pattern Matching Value Generation for Analysis 1 .....	81
Figure 3.3-1 – Images Acquired for Fair Sample Population.....	90
Figure 3.3-2 – Images Acquired for Medium Sample Population.....	92
Figure 3.3-3 – Images Acquired for Dark Sample Population .....	93
Figure 3.3-4 – Fair Participant Canonical Discriminant Functions .....	96
Figure 3.3-5 – Dark Participant Canonical Discriminant Functions.....	98
Figure 4.1-1 – Electromagnetic Spectrum .....	105
Figure 4.1-2 – Molecular Vibrations .....	107
Figure 4.1-3 – Depiction of the FTIR Interferometer .....	109
Figure 4.1-4 – Total Internal Reflection .....	110
Figure 4.1-5 – Typical Hair Keratin Spectra .....	115
Figure 4.2-1 – Depiction of FTIR Sampling Substrate.....	122
Figure 4.3-1 – Hairspray Reference Spectra.....	129
Figure 4.3-2 – Gel Reference Spectra.....	131
Figure 4.3-3 – Mousse Reference Spectra .....	133
Figure 4.3-4 – Finishing Gloss Reference Spectra .....	135
Figure 4.3-5 – Styling Wax Reference Spectra .....	136
Figure 4.3-6 – Smoothing Balm Reference Spectra .....	138
Figure 4.3-7 – Product Reference Spectra Canonical Discriminant Functions .....	141
Figure 4.3-8 – Smoothing Balm Reference and Densely Applied Spectra.....	143
Figure 4.3-9 – Finishing Gloss Reference and Densely Applied Spectra.....	144
Figure 4.3-10 – Hairspray Reference and Densely Applied Spectra .....	145
Figure 4.3-11 – Gel Reference and Densely Applied Spectra .....	146

Figure 4.3-12 – Mousse Reference and Densely Applied Spectra .....	147
Figure 4.3-13 – Styling Wax Reference and Densely Applied Spectra .....	148
Figure 4.3-14 – Dendogram of Densely Applied Spectra .....	150
Figure 4.3-15 – Mousse Reference and Sparsely Applied Spectra .....	154
Figure 4.3-16 – Styling Wax Reference and Sparsely Applied Spectra.....	155
Figure 4.3-17 – Chemical Image of Keratin.....	158
Figure 4.3-18 – Chemical Image of Hairspray .....	159

## List of Tables

Table 1.2-1 – Classification of Morphological Hair Features .....	4
Table 2.2-1 – sRGB Values for Exposure Correction .....	40
Table 2.2-2 – Sample Numbers for Nominal Hair Colour Categories .....	46
Table 2.3-1 – RGB Predicted Colour Allocation (%) .....	49
Table 2.3-2 – CIE XYZ Predicted Colour Allocation (%) .....	51
Table 2.3-3 – CIE L*a*b* Predicted Colour Allocation (%).....	53
Table 2.3-4 – Source of Variance for Sample Population.....	59
Table 2.3-5 – Summary of Prediction Accuracy .....	60
Table 2.3-6 – RGB Values of an Individual, Questioned hair and a Comparison Hair .....	68
Table 3.2-1 – Threshold levels for Fair, Medium and Dark Shaded Hair .....	79
Table 3.2-2 – V++ Object Analysis Measured Parameters.....	82
Table 3.2-3 – Manual versus Automatic Generation of Pigmentation Measurements.....	84
Table 3.3-1 – Summary of Main Source of Variance .....	94
Table 3.3-2 – Fair Participant Predicted Allocation (%) .....	95
Table 3.3-3 – Medium Participant Predicted Allocation (%).....	97
Table 3.3-4 – Dark Participant Predicted Allocation (%) .....	97
Table 4.1-1 – Hair Keratin Components and Oxidation Products.....	116
Table 4.2-1 – <i>Thermo–Nicolet</i> FTIR Operating Parameters .....	123
Table 4.3-1 – Product Sparsely Applied Summary of Spectra Resolved.....	153

## Abbreviations

AFM	Atomic Force Microscope
ANOVA	Analysis of Variance
ATR	Attenuated Total Reflectance
B	Measure of blue (RGB colour model)
bmp	Bitmap Image File
CCD	Charged Couple Device
CIE	<i>Commission Internationale de l'Eclairage</i>
CIE a*	Measure of green to red (CIE L*a*b* colour model)
CIE b*	Measure of blue to yellow (CIE L*a*b* colour model)
CIE L*	Measure of lightness (CIE L*a*b* colour model)
CIE X	Measure of red (CIE XYZ colour model)
CIE Y	Measure of green and luminescence (CIE XYZ colour model)
CIE Z	Measure of blue (CIE XYZ colour model)
CMYK	Cyan, Magenta, Yellow, Key
CSV	Comma Separated Value
DTGS	Deuterated triglycine sulfate
e*	Electron
FPA	Focal Plane Array
FTIR	Fourier Transform Infrared
G	Measure of green (RGB colour model)
HPLC	High Performance Liquid Chromatography
HSB	Hue, Saturation, Brightness
IR	Infrared
LAS	<i>Leica</i> Application Suite
linRGB	Linear RGB colour space
LSA	Large Sampling Accessory
LCTF	Liquid crystal tuneable filter
Mc1r	Melanocortic 1 receptor
MCT	Mercury cadmium telluride
ms	Millisecond
mtDNA	Mitochondrial deoxyribose nuclease
n	Population size

NATA	National Association of Testing Authorities
nDNA	Nuclear deoxyribose nuclease
nm	Nanometre
PASW	Predictive Analytical Software
PCR	Polymerase Chain Reaction
PEG	Polyethylene glycol
R	Measure of red (RGB colour model)
RI	Refractive Index
SEM	Scanning Electron Microscope
Sig.	Level of significance (F ratio)
SPSS	Statistical Package for the Social Sciences
sRGB	Standard RGB colour space
Std Dev	Standard Deviation
Std Dev <sup>2</sup>	Total Variance
TEM	Transmission Electron Microscope
TGS	Triglycine sulfide
TIFF	Tagged Image File Format
US	United States
UV	Ultra Violet
UV–Visible	Ultra Violet–Visible
$\alpha$	Alpha, statistical level of significance
$\lambda$	Lambda, wavelength
$\pi$	Pi
$\phi$	Phi, angle of incidence
$\mu\text{m}$	Micron, micrometre



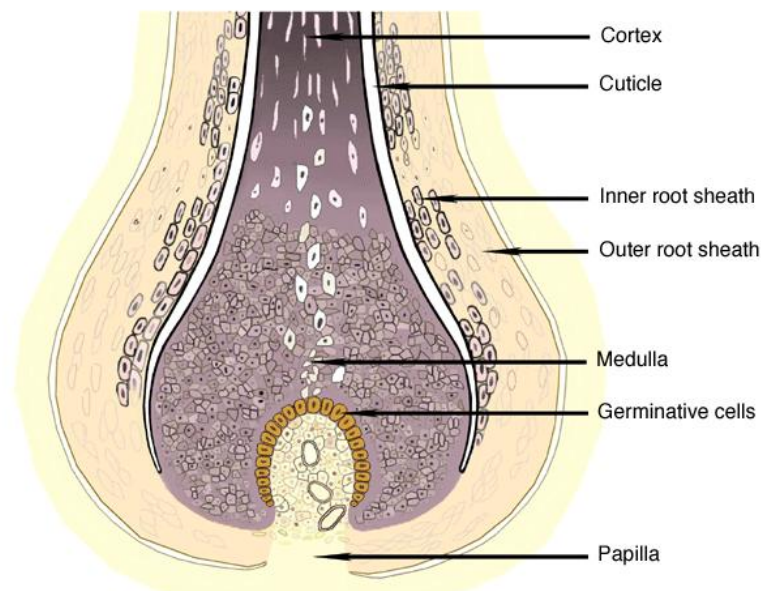


# Chapter 1. INTRODUCTION

---

## 1.1. Hair Growth and Physiology

Hair is essentially a series of dead keratinised cells. The hair shaft is generated from a matrix of living cells within the hair bulb that undergo successive mitotic division, pushing the oldest cells upward (Chase, 1954; Kaszynski, 1985). Two main types of hair are found on the human body, vellus and terminal, the former hair type being the fine hairs present over most of the body and the latter type being the thick, coarser, pigmented hair that appears on the scalp and face (Gaudette, 2000; Stenn & Paus, 2001; Wilson & Gilbert, 2006). All hair has three basic structural components—the cuticle, cortex and medulla, as depicted in Figure 1.1-1. The central medulla contains loosely connected cells and large air spaces, the medial cortex contains tight, interlocking cells with small air spaces, while the outermost cells of the cuticle fuse with the follicle to anchor the hair in position (Robins, 1991). One of the essential characteristics that differentiates human hair from animal hair is the medullar cells' clear ultra-structure as well as the small size of the medulla, whose index is typically less than 0.30 (Clement *et al.*, 1981; Clement *et al.*, 1982). Together, the cuticle, cortex and medulla create a fibre of considerable tensile strength.



**Figure 1.1-1 – The Hair Bulb**

The central medulla contains loosely connected cells and large air spaces; the medial cortex contains tight, interlocking cells with small air spaces; while the outermost cells of the cuticle fuse with the follicle to anchor the hair in position. (Source: Natural Nigerian, 2012).

Hair growth is cyclic over three stages—anagen, catagen and telogen. In humans, growth cycles are unsynchronised whereby neighbouring follicles are in different development stages at any one time (Chase, 1954; Kaszynski, 1985; Stenn & Paus, 2001). Typically, about 80% of follicles are actively growing in the anagen stage that can last from two to seven years, while 20% are non-growing hairs, resting in their respective follicles for up to several months during the telogen stage (Petraco *et al.*, 1988; Houck & Bisbing, 2005). Following release of the telogen hair, a follicle regenerates and the anagen cycle recommences. Less than 1% of human hairs are in the catagen stage, which is the transition between anagen and telogen that only lasts for several weeks (Houck & Bisbing, 2005).

Melanocytes are specialised dendrite cells responsible for the synthesis of the pigment ‘melanin’ within membrane-bound organelles called melanosomes. In human hair, the enzyme tyrosinase is responsible for the formation of melanin, which occurs as two types—eumelanin, a black-brown pigment, and phaemelanin, a yellow-red pigment (Jimbow *et al.*, 1983; Robins, 1991; Ito & Wakamatsu, 2003; Rees, 2003). Melanosomes are dispersed within the cytoplasm of keratinocytes as either solitary particles or as aggregates of more than two particles, a factor that appears to be determined by their size (Robins, 1991). Natural hair colour is therefore perceived as a consequence of the amount and type of melanin content transferred to keratinocytes as well as the number, size and density of the granules themselves. Hairs perceived as light to dark in colour are correlated with increasing pigmentation and therefore increasing light absorption, while white hair that has no melanin, reflects almost all incident light (Robins, 1991; Rees, 2003).

## 1.2. Forensic Hair Examination

### 1.2.1. Microscopic Examination

Forensic hair examinations typically begin with a complete and detailed microscopic evaluation of each hair followed by a side-by-side comparison between the unknown and exemplar hairs. This non-destructive technique has been well established in forensic laboratories for over sixty years (Houck & Bisbing, 2005) and is analogous to the techniques employed by histologists and pathologists to identify tissue samples, cell types, disorders and other abnormalities based on microscopic cell morphology (Houck *et al.*, 2004). With hair, morphological patterns or trends are often apparent throughout the length of the shaft and may be recognised in hairs from the same or different sources (Verma *et al.*, 2002). Such morphological hair features can be grossly classed as macroscopic and microscopic characteristics (Robertson & Aitken, 1986; Robertson, 1999; Verma *et al.*, 2002; Houck & Bisbing, 2005), as shown in Table 1.2-1.

**Table 1.2-1 – Classification of Morphological Hair Features**

Macroscopic	Microscopic
Colour	Pigment distribution, aggregation, density and size
Treatment	Proximal (root) and distal (tip) shape
Spatial configuration	Shaft shape and diameter
Length	Medulla appearance and index
Coarseness	Cuticle margin
	Cortical fusi presence or absence
	Cortical texture and diffusion

While the description of individual hairs encourages systematic and documented evaluations, at present, a side-by-side hair comparison is the only effective method for comparing individual features and overall patterns along the hair length (Robertson & Aitken, 1986; Robertson, 1999). Unlike a stand-alone description to determine the properties of a sample, the side-by-side microscopic hair comparison is considered a powerful technique utilised by other biological disciplines, such as anthropology and zoology, to assess hair fibres (Houck *et al.*, 2004). A significant difference between two hairs, or several fundamental dissimilarities, is a strong indication that the hairs originated from different sources. As such, positive associations between hairs rely not only on the

presence of several indistinguishable traits, but on the absence of significant dissimilarities as well (Houck & Bisbing, 2005).

With the exception of identical twins, every individual has a unique genetic make-up that has been nurtured by the environment so theoretically, hair colour and pigmentation are unique to each person (Bisbing & Wolner, 1984). In practice however, this concept is difficult to observe or measure with conventional microscopic hair examination techniques. One issue is the absence of uniform nomenclature to define various hair features. Hair colour, for example, is a qualitative trait subjectively perceived by the examiner and the process of applying descriptive phrases to characterise colour has not been standardised (Bednarek, 2003). Borders between shades are undefined in most colour classification systems, resulting in complications and inconsistencies when the same hair evidence is evaluated by more than one examiner (Bednarek, 2003). A questionnaire regarding microscopic hair features that was widely circulated to forensic hair examiners during the mid-1980s, highlighted the need for standardised terminology to clearly define microscopic features, as many respondents described the same feature in different ways (Robertson & Aitken, 1986). Most respondents to the same questionnaire rated non-numerical features as highly useful (Aitken & Robertson, 1986) while more recently Houck and Bisbing (2005) maintain that the potential rate of error in microscopic comparisons of human hair is very low, dependent on the examiner's training and experience. Although qualitative features are still considered significant and the potential rate of error is perceived as low, human hair currently cannot be associated with a single source to the exclusion of all others based on qualitative methods. (For more information on hair biology, microscopic characteristics and forensic examinations, Houck (2002) provides a comprehensive list of literary resources.)

### **1.2.2. DNA Analysis**

Telogen hairs – the most common type encountered in forensic casework – are not routinely submitted for DNA analysis due to the cessation of cellular activity in the root end and the limiting amount of cellular material present in the root sheath (Kolowski *et al.*, 2004; Wilson & Gilbert, 2006; Boonen *et al.*, 2008). Boonen and colleagues (2008) describe a screening method using DAPI, a fluorescent DNA stain, to estimate the number of cell nuclei in telogen hair roots so that only the most promising samples are submitted for nuclear DNA (nDNA) analysis. That study found that a significant increase in the

nDNA success rate occurred for hair roots containing more than 50 visible nuclei. Anagen hairs are not naturally shed and tend to be encountered only in instances where they have been forcibly removed, such as during a struggle. Unlike telogen hairs, actively growing anagen hairs contain an abundance of nucleated cells within the root and surrounding follicular material, meaning nDNA profiling from anagen hair roots can be highly successful (Houck & Bisbing, 2005). However, the recovery of nDNA from hair can be technically problematic. The hair pigment melanin is an inhibitor of the polymerase chain reaction (PCR), the predominant tool used in DNA amplification; peroxides and bleaches used in some hair treatments can reduce DNA yields and there is also a risk of sample contamination due to external sources of nDNA associated with the hair shaft (Wilson & Gilbert, 2006).

Non-destructive extraction methods such as ‘Charge Switch’ can be used to extract nDNA from anagen roots while still maintaining the hair’s overall integrity (Brooks, 2009). Conversely, extraction of mitochondrial DNA (mtDNA) is destructive and consumes a portion of the hair, although the ability to recover mtDNA from small pieces of hair is viable due to the high copy number of mitochondria organelles per cell. A transmission electron microscope (TEM) was used by Linch (2009) to investigate the presence of mitochondria and nuclei along the hair shaft. Nuclei and mitochondria were not observed in tissue sections at the level where the cuticle becomes fully keratinised in the hair root stem; melanosomes were the only recognisable cytoplasm organelle beyond this point (Linch, 2009). This supports earlier studies on medulla cells that describe a form of progressive degeneration, whereby the nucleus disappears and cell organelles such as mitochondria are destroyed (Parakkal & Matoltsy, 1964; Roth & Helwig, 1964).

### **1.2.3. Hair as Evidence**

Individuals lose approximately 75 to 100 head hairs each day as a result of normal activities (Gaudette, 2000; Wilson & Gilbert, 2006) and, unlike other biological tissues, hairs are resistant to degradation. Resting telogen hairs are loosely held in the follicle until being released through normal handling and therefore they are the most common type encountered in casework. Hair may occur at a crime scene, not only by natural shedding, but because they have been pulled out by force or following transfer from one object or person to another. Hair evidence is especially important in cases where no biological fluids are available, such as physical or sexual assaults involving no bloodshed or seminal

ejaculation (Taupin, 1996). In many cases hairs are the only evidence, or only one of a number of trace materials of possible evidentiary significance (Robertson, 1999). A number of authors (e.g. Smith & Linch, 1999; Houck *et al.*, 2004) have found that when DNA analysis is not possible the microscopic hair comparison is an effective independent analysis for most casework, provided that aspects of examiner training, caution and proficiency are addressed to reduce any potential error. Robertson and Roux (2010) assert that there is a current over-emphasis on the value of identification in forensic science, outweighing the value that can be provided by trace evidence, such as hair, in establishing 'what happened?'. Moreover, Robertson (1999) argues that critics who over-emphasise the need to assign numerical values to positive findings of identification, such as those provided by DNA population statistics, often fail to recognise the importance of exclusionary evidence. For example, a clump of hairs found clutched in a murder victim's hand and excluded as having come from neither the victim nor the suspect, would be highly significant (Gaudette, 1999).

Hair is ubiquitous in nature and can be used to associate or exclude a suspect, victim or witness with a crime scene but just as importantly, hair evidence is valuable for reconstructing events, providing investigative leads, as well as refuting or corroborating witness statements. In one case, dyed brown head hairs originating from the partner of an accused, was located on an abduction victim's clothing, indicating secondary transfer (Taupin, 1996). In a separate instance, hair found on duct tape supported the scenario that the victim's head was wrapped in tape (Tafaro, 2000). A distinctive opaque ellipsoidal band ("putrid root") appearing approximately 0.5 mm above the root bulb of post-mortem anagen hair samples has been used to determine whether a sample was transferred ante- or post-mortem (Petrao *et al.*, 1988; Linch & Prahlow, 2001). Post-mortem banding observed in recovered questioned hairs helped investigators reconstruct events in two murder investigations in New Orleans, USA (Tafaro, 2000). Finally, as part of an investigation into a series of sexual assaults committed in the UK over a two year period, microscopic examination of hair samples from 118 individuals of Afro-Caribbean descent was conducted (Lamb & Tucker, 1994). Only 11 samples (9.3%) could not be excluded from samples recovered from the crime scene, demonstrating that microscopic examination is a useful and relatively quick technique for the elimination of suspects from police inquiry (Lamb & Tucker, 1994). In many case scenarios, the number, location and condition of hairs can provide useful information for reconstructing events and, where

such hairs are not examined, it can be more difficult to determine the circumstances and facts of the particular case, for both investigator and jury members (Robertson, 1999).

#### **1.2.4. Probative Value of Hair Evidence**

In the United States (US), evidence based on microscopic hair examinations has traditionally been accepted in all levels of court, having met the scientific evidence requirements of Rule 702 of the US Federal Rules of Evidence and *Frye v United States* (1923); that is, a technique is admissible if it is generally accepted by the scientific community. Seventy years after that case, *Daubert v Merrell Dow Pharmaceuticals Inc.* (1993) found that, in addition to general acceptance, scientific evidence must also show testability, peer review and have a known error rate. Therefore, Rule 702 was subsequently altered to ensure that scientific evidence was reliable on two levels – first, the level of principle and methods, and second, the application of those principles and methods to the facts of the case (Beach, 2009). In Australia, the statutory requirement for the admissibility of expert evidence is outlined in the *Evidence Act 1995 (Commonwealth)* or each state's equivalent. Section 79 of the Act allows the admissibility of expert testimony, while Sections 135–137 determine the admissibility of evidence. Broadly, evidence presented by the expert must be derived from a body of knowledge or experience that is sufficiently recognised and accepted as reliable (McClellan J, 2009). To ensure the trustworthiness and reliability of a particular science or technique, an approach has been taken by a number of Australian states to impose a “threshold requirement” on the reliability of evidence—this often refers to approaches taken in the United States (McClellan J, 2009). Furthermore, an Australian Standard that aims to provide guidelines for the interpretation of observations and analytical results to obtain information and knowledge, is currently under development (Forensic Standards Working Group, 2012). This standard will emphasise the value of the examiner's professional judgement and the components which contribute to such judgement, including qualification, training, competence, contemporary knowledge and continuous professional development (Forensic Standards Working Group, 2012).

It has been argued that hair associations based on the comparison of macro– and microscopic features cannot uniquely identify an individual, nor currently can they be used to make claims regarding probabilities or frequencies with which particular characteristics are distributed in the population (Robertson, 1982; Smith & Linch, 1999; Kolowski *et al.*, 2004; Houck & Bisbing, 2005). The rate of error for hair examination depends on the



quality and maintenance of microscopes, as well as the experience of the examiner. Following the evaluation of a number of hair studies, Gaudette (1999) concluded that, while type II errors (false positives) due to coincidental matches do occur in forensic hair comparisons, such errors are relatively rare when the examination has been conducted by qualified, well-trained examiners. Furthermore, macroscopic and microscopic hair comparisons generally produce good corroborative evidence but that this evidence depends on all stages of the physical evidence process, including recovery, analysis, interpretation and presentation of results (Gaudette, 1999).

According to Houck and colleagues (2004), the rates of error for hair examination are statistically determined by a particular set of circumstances and data, and therefore cannot be used to predict the probabilities in a different set of circumstances, as the actual error rates depend on the sample data. Errors will exist in qualitative microscopic examinations but they are often not susceptible to the quantitative analyses that yield a value of uncertainty, therefore the use of appropriate non-parametric statistics could be considered to support any opinion evidence derived (Forensic Standards Working Group, 2012). Isolated cases in the US, such as *State v McGrew* (1997) and *Williamson v Reynolds* (1995), have ruled microscopic hair examination inadmissible under the requirements of *Daubert* because the known error rate requirement was not met or was too high. Moreover, a report on forensic science in the US (National Research Council of the National Academies, 2009) found that there were no uniform standards on the number of features a hair must possess before an examiner may declare an association. The same report emphasised that disciplines relying on subjective assessments to match characteristics require a body of research to identify sources of variability and potential bias, and to establish quantifiable measures of uncertainty and limitations. It has been stated that no forensic method has consistently demonstrated a connection between the evidence and an individual or specific source with the same high degree of certainty that nDNA evidence has shown (National Research Council of the National Academies, 2009). Others propose that it is unfounded to compare qualitative comparisons that deal with phenotypic variation with DNA analysis that deals with quantified genetic information and that over-reliance on rigid, statistical probabilities can diminish otherwise well-founded scientific methods (Houck *et al.*, 2004). Nonetheless, attempts have been made to use human hair as an individual identification tool.

### 1.2.5. Individualisation

The number of hair follicles, their growth rate, distribution, pigmentation and structural characteristics are all determined by proteins under genetic control (Kaszynski, 1985). In the 1970s, Lee and colleagues analysed electrophoretic patterns of keratin matrix components from hair strands of over 300 participants in an attempt to observe individual genetic differences (Lee *et al.*, 1978). Fourier Transform Infrared (FTIR) spectroscopy has also been used to investigate keratin residues to determine whether genetic variations between the quantity and type of amino acids present in human hair were distinctive enough to individualise hair samples (Hopkins *et al.*, 1991). Also using FTIR, Panayiotou and Kokot (1999) reportedly discriminated between two similarly aged female Caucasians with the same hair colour, length and treatment as well as between hair collected from the left and right side of the participants' heads.

To evaluate the practical effectiveness of morphological comparative hair analysis, the individualisation of 100 hairs randomly selected from 12 individuals was undertaken by Bednarek (2003). Ninety-one hair samples were correctly allocated based on intensity coordinated determined by the RGB colour model system compared with 74 hair samples correctly allocated based on a method involving colour standards (Bednarek, 2003). Barrett and colleagues (2011) also attempted to individualise hair samples based on natural hair colour measurements derived from microspectrophotometry. Following several discriminant analyses, those researchers concluded that the technique was not able to successfully discriminate between 25 natural hair samples, with only 22% of participants correctly classed.

Bisbing and Wolner (1984) investigated the forensic hair examiner's ability to distinguish between duplicate head hair samples from 17 pairs of twins and one set of identical triplets. In the first phase of their study, the examiners were able to correctly distinguish the hairs with the correct duplicate sample in every case, and never incorrectly with a twin's sample. In the second phase of the study simulating typical casework, seven unknown hairs were compared with several potential sources, and on more than one occasion the questioned hairs were incorrectly identified and sourced to another participant's head hair. In a separate study, 27 volunteers each collected 50 pubic hairs to compare the identification success rates of nDNA genotyping with microscopic examination (Kolowski *et al.*, 2004). A full nDNA profile of unknown hairs were allocated

to the correct source in 3 out of 5 instances, while microscopic examination resulted in correct sourcing of hairs in 4 out of 5 instances, thereby indicating that microscopic hair examination had a higher success rate than nDNA analysis in this study. However, it is worth emphasising that hair samples not correctly sourced following nDNA analysis were the result of no profiles or partial profiles, whereas hair not correctly assigned following microscopic examination were wrongly allocated to another source.

While the microscopic hair examination is a quick and inexpensive technique, at present it cannot provide the level of individualisation that nDNA genotyping can, nor can it provide mathematical statements regarding the strength of association; comparatively, DNA analysis is a time consuming and expensive process. As proposed by a number of authors (Linch *et al.*, 1998; Kolowski *et al.*, 2004; Boonen *et al.*, 2008) a coordinated approach may yield the most useful information, by first applying microscopic examination to screen the hair samples and narrow down the scope of the investigation, followed by DNA genotyping to individualise those indistinguishable hairs with abundant nuclei present.

Notwithstanding, a quantitative method for analysing hair evidence is warranted to substantiate claims based on qualitative, microscopic observations. Traditional microscopic approaches rely on the human element to make observations and interpretations, and this depends heavily on proper instrument use, the brain's ability to correlate hundreds of data points and a high level of consistency when repeating these tasks (Tontarski & Thompson, 1998). It has previously been considered difficult to improve the discriminating power of hair examinations due to the considerable variation in features within a sample of hairs from the same individual and because microscopic features of hair are difficult to assess in an objective manner, among other reasons (Robertson, 1982). Emerging technologies in image processing, pattern recognition and computer science could assist future evidence examinations with classifying, or potentially individualising, forensic evidence. There is a need to investigate universally applicable techniques that will mimic microscopic analysis and provide a complimentary evaluation to subjective assessments made by an experienced examiner. However, as noted by Verma and colleagues (2002), the judgement of any automated system is limited by the information of its database, just as the judgement of a human examiner is limited by their own experience.

### **1.3. Digital Imaging and Image Processing**

#### **1.3.1. Application and Diversity in Forensic Science**

Over the last few decades increased application of image processing technology has surfaced as a powerful tool in the forensic sciences. As early as 1975, digital methods originally developed to provide clear transmission of images from space exploration were applied to an obscured palm print photographed in blood on a textured bed sheet, enhancing the print and enabling identification (Blackwell & Crisci, 1975). The palm print ridge detail was enhanced by filtering the bed sheet weave pattern noise in the frequency domain, then reverse transforming the image to produce the conventional image in the spatial domain. Facey and colleagues (1992) describe a method that permits extraction of wear information from high-end images of shoe marks, wear pattern contours and isobars of the pressure distribution under foot. Images in this study were also enhanced by forward transforming the original arrays into the Fourier domain and filtering them to remove high frequency patterns relating to tread pattern and noise (Facey *et al.*, 1992). The US Bureau of Alcohol, Tobacco and Firearms have applied a technique based on image analysis to evaluate fired bullet *striae*, cartridge case breech faces and firing pin impressions (Tontarski & Thompson, 1998). Furthermore, a quantitative, non-destructive method for discriminating between different types of paper using image analysis, Fourier transformation and cross-correlation matching has also been proposed (Miyata *et al.*, 2002). The described procedure was able to discriminate 10 out of 12 commercial photocopier paper specimens, with only two samples producing similar periodicity (Miyata *et al.*, 2002). Another method has been developed for discriminating blue ballpoint pen inks and for comparing those inks on paper, based on innovative image analysis software that evaluates scanned, thin layer chromatograms (Djozan *et al.*, 2008). The retention factor values, colour range and intensity of separated ink components of 41 blue ballpoint pens were analysed and distinguished with high reliability and 92.8% discriminating power (Djozan *et al.*, 2008). Finally, computerised image analysis was found to be useful for determining morphometric changes in epidermal cells for discrimination between electrocution, flame burn and abrasion type lesions (Akyildiz *et al.*, 2009). The described method provided objectivity to morphological examination using light microscope, by measuring length, perimeter, diameter and darkness of epidermal cell nuclei (Akyildiz *et al.*, 2009).

### 1.3.2. Application to Animal Fibres

In light of the increasing demand for quantitative examinations, a number of other science disciplines have also investigating automated, digital techniques to evaluate fibres. In the past, microscopy was consistently the most widely accepted technique for the identification of animal hairs and other fibres in the textile industry, providing much information on the nature of the fabric, including internal structure and colour information (Robson, 1993). Image analysis in that arena is now proving to be a useful tool for identifying materials consistently and overcoming inaccuracies associated with measurements that depend on an evaluator's ability to subjectively rate a fabric article (Wagner, 1998). Image analysis has greatly advanced the evaluator's ability to characterise a diverse range of both natural and synthetic fibres. This versatility is highlighted by Wagner (1998) who describes a range of image analysis applications, including yarn assessments to determine fabric denier, squareness and pilling; evaluations of pore openings of filters used in aerospace; and, tennis ball size and seam uniformity measurements. Properties that effect the mechanical, functional and aesthetic properties of thread have also been quantitatively investigated, such as the fibre distribution and blend irregularities of wool/acrylic yarns (Shaikhzadeh Najar *et al.*, 2003 ).

An ideal method for assessing both animal and hair fibres might involve a database of measured parameter information, suitable for statistical analysis. Huang and Xu (2002) describe a system that acquires sequential images of cotton fibre segments then outputs both fineness and maturity predictions, based on statistical data derived from a larger cotton fibre sample population. Those authors introduce a series of algorithms that deal with sharpening fibre edges, edge tracing, transverse scanning, scan validation and merging separate fibre segments. Following execution of those algorithms, the number of scans, length of scanned segments, fibre width maximum, minimum, mean and standard deviation, as well as the number of twists, can be calculated for each cotton fibre (Huang & Xu, 2002). Robson (1993) reviewed techniques that have enabled the surface architecture of an animal fibre section to be characterised by Fourier transformation to the frequency domain to create a 2-D Power Spectrum image. That author also underlined the potential for using fibre surface frequency data to quantify cuticle scale pattern variations along the human hair and to provide the basis for applying pattern recognition techniques.

### 1.3.3. Image Analysis of Hair

Microscopic image processing techniques have been investigated for application to hair examination. The Atomic Force Microscope (AFM) produces ultra-high resolution images using a mechanical probe to feel across the surface of the sample to be analysed. It is a non-invasive technique that requires little to no sample preparation, though measurements are limited to the topographic morphology of the sample plane as subsurface information cannot be detected (Gurden *et al.*, 2004). Images produced by AFM have been used to measure cuticle step height, as described by Smith (1998) who recommended this technique for other measureable hair characteristics, including cuticle length and surface roughness. Swift and Smith (2000) applied AFM to investigate the surface architecture of the entire lengths of human hair. An algorithm for the automatic analysis of AFM images of human hair was also presented by Gurden and colleagues (2004). Multivariate analysis of such measurements as step height, tilt angle and cuticle density were processed, thereby allowing quantitative analysis and comparison of the hair samples. Swift and Smith (2000) found the hair surface of freshly emergent hair was quite different from most of its length after about 20mm, while Gurden and colleagues (2004) found there were fewer cuticle layers toward the distal hair end due to physio-chemical stresses and cosmetic treatments that gradually chip away the cuticle edge. In a forensic context, such inter-individual changes could provide information on the lifestyle of the hair's owner. However, the AFM technique is restricted to imaging within the width and top surface of a clean, individual hair fibre; each image is typically captured in 10 minutes, so does not enable rapid scrutiny along the hair, unlike the real-time observational capabilities of other instruments (Swift & Smith, 2000) or the human examiner.

A classification for mammalian hair identification was proposed following studies involving the Scanning Electron Microscope (SEM) to observe the morphology of the medulla on longitudinal hair sections, in coordination with a transmission electron microscope (TEM) to observe structural characteristics of medullar cells on hair cross-sections (Clement *et al.*, 1981). Physical variations of cuticle scale patterns in mammalian hair have also been evaluated from SEM images, including area, perimeter, density, width-to-height ratio and index (Meyer *et al.*, 1997; Meyer *et al.*, 2000). The SEM can provide rapid, valuable detail about the hair surface. Though, one study found that height (z) information is not easily obtainable as SEM datasets contain image intensity of x, y coordinates only and that some surface information can be 'overwhelmed' by subsurface

signals thereby conveying a smoother impression of the cuticle scales (Swift & Smith, 2000). In the reflection mode, Confocal Microscopy can also be used to quantify cuticle morphology and exogenous deposits at the hair surface, as well as perform high-resolution 3-D reconstructions of thick biological specimens (Hadjur *et al.*, 2002).

To overcome depth-of-field problems often associated with 3-D samples, Brooks (2007) imaged the full depth of the hair shaft and applied an optical sectioning technique to create a single montage image. Microscopic optical sectioning involves acquiring a series of images—optical slices—throughout the full depth of the hair shaft (z-plane) then using a unique range of algorithms to produce a single, composite montage from the optical slices. Previously, Hadjur and colleagues (2002) used the optical sectioning property of the confocal microscope to obtain a z-series of 80 optical slices that were then used to create a single, in-focus projection image of the hair surface and a 3-D reconstruction of the sample. However, the microscope's fluorescence mode was required to investigate the internal hair structure by this method, relying on fluorescent probes such as Rhodamine to stain the sample, therefore rendering this method ineffective for characterising natural hair colour.

Verma and colleagues (2002) describe an automated Hair-MAP system that assesses whether two hairs are associated, following a digitised evaluation of microscopic images. The system consists of distinct modules that automatically extract separate hair features such as medulla type, cuticle texture and shaft diameter that then undergo multivariate analysis to indicate whether two hairs were from the same source (Verma *et al.*, 2002). In the reported study, Hair-MAP imaged, segmented and extracted the feature values of five morphological characteristics from each of 25 hairs from nine participants and returned accurate hair associations 83% of the time (Verma *et al.*, 2002). Sato (2003) investigated morphological comparisons between Japanese head hairs using data also obtained by image analysis. Following statistical evaluations, six values were derived that showed larger inter-individual variations than intra-individual variations (Sato, 2003). Based on this preliminary study, the author proposed that numerical data obtained from image analysis was important for constructing an objective screening procedure for evidential hairs, especially for Japanese hairs that are thought to show limited variation in morphological features (Sato, 2003). Finally, Ball and colleagues (2002) used image analysis to determine whether morphological differences could be demonstrated between

the head hair from Egyptian mummies and living Caucasoid and Oriental individuals. An image analyser was used to scan images projected from a Leitz Wezlar Prado projector (with micro attachment) that were then analysed using multivariate and discriminate analysis. The authors concluded that there were significant morphometric differences between head hair from different races and from different genders within the same race.



## **1.4. Aim and Scope of this Project**

This project aims to investigate three objective analytical methods for the examination of human hair to provide an objective, quantitative approach to balance the qualitative observations made by a forensic examiner. To achieve this aim, the following research was undertaken.

### **1.4.1. Chapter 2: COLOUR**

Colour is one of the main hair characteristics subjectively assessed as part of the forensic hair examination process and the absence of uniformity to define this feature has not been resolved. The research focus of Chapter 2 involved assigning numerical colour measurements to such assessments. The initial analyses were designed to address forensic casework in the broader context, whereby an inexperienced hair examiner or scene of crime officer may be required to process multiple hairs or bulk samples during evidence triage. This chapter aimed to determine which of three selected colour models (RGB, CIE XYZ and CIE L\*a\*b\*) could provide the best statistical model for allocating to one of six nominal colour categories, namely Red, Blonde, Light Brown, Medium Brown, Dark Brown and Black, and for distinguishing a participant's hair from another's, within a subpopulation of similar coloured hair.

Subsequent analyses were designed to investigate whether numerical colour measurements could provide an additional tool for the experienced forensic examiner when performing comparisons. Confidence intervals derived from probability distribution curves were used to demonstrate that numerical colour measurements could aid the examiner with comparisons between a single, questioned hair and hair from a known source.

### **1.4.2. Chapter 3: PIGMENTATION**

Pigmentation patterns or trends that are often apparent throughout the length of the hair shaft may be recognised in hairs from the same source, given the relationship between genotype and hair melanin. While pigmentation may be visually observed, such differences often resist quantification. Previously reported studies involving the numerical classification of hair characteristics have focused on hair morphology in terms of the form or structure of the shaft, or on comparisons between pixel intensity values, rather than the

pigmentation itself. The research focus of Chapter 3 involved assigning numerical values to hair pigmentation. This preliminary study introduced a novel technique designed to measure the density, size and shape of the pigment aggregations, as represented by pixel variations within montage images. Specifically, discriminant analyses were used to address the question of whether the selected measurements could discriminate between participants within three populations of similar shaded hair.

### **1.4.3. Chapter 4: SPECTROSCOPY**

Identifying trace contaminants on the hair surface resulting from the popular use of cosmetic products such as hairsprays, gels and mousse, is not currently part of the hair examination process. Research on hair involving Attenuated Total Reflectance (ATR) FTIR spectroscopy, to date, has focused on hair keratin, the effects of chemical-based hair treatments and/or sunlight exposure; very few studies have been reported on hair surface contamination. Chapter 4 focused on evaluating ATR-FTIR spectroscopy for detecting trace contaminants on the hair surface as a means to increase the evidential value of human hair in a forensic context.

Visual evaluations and spectral interpretation software were used to establish whether constituents of hair product could be detected. Statistical analyses were used to determine whether multiple spectra of the absorbing constituents could be broadly distinguished and classed based on product type, including following dense and sparse application to single hair samples. Chemical imaging was also investigated to determine whether the spatial data provided by this technique could be employed to assist the examiner with locating trace contaminants along the hair surface.

## Chapter 2. COLOUR

---

## 2.1. Introduction

### 2.1.1. Colour Classification

Hair colour is one of the most diverse human characteristics and, along with skin colour, provides one of the clearest variations in the population. There has long been the need for uniform nomenclature of colours and an exact definition of terms to avoid the common situation where two examiners allocate different descriptions to the same sample, or the same description to dissimilar samples. One examiner may classify hair ‘Light Brown’ whereas another may classify the same colour as ‘Medium Brown’ and this inhibits a direct comparison of results.

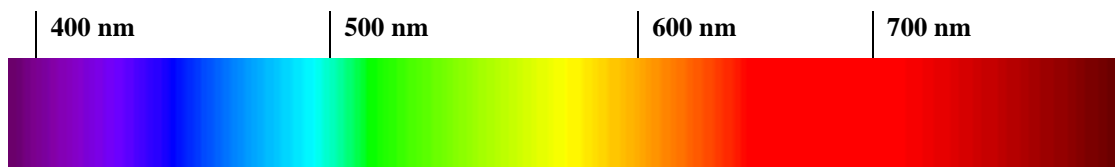
Crude hair colour classifications can also make it difficult to interpret observations resulting from different populations and by different authors. Structures to appropriately classify hair colour have been investigated in anthropology since as early as the last quarter of the nineteenth century (for a full review of early papers see Trotter, 1939). Many proposals for the classification and description of hair colour now exist, but they are mainly limited to presenting all possible colour profiles and their differentiation, rather than defining colour or borders between shades which is left to the interpretation of the examiner (Bednarek, 2003). As noted by Naysmith and colleagues (2004), misclassification of a continuous variable such as hair colour, will diminish the power of statistical testing and the strength of any relationship observed. The application of technical advances to hair examination is helping to overcome these problems. For example, measures of hair melanin offer the advantages of objectivity and the ability to handle colour quantitatively (Rees, 2003).

Casework involving cosmetically treated hair introduces a number of distinct variables such as the length of natural regrowth and signs of chemical wear. Unlike natural variance and characteristics, the unique characteristics resulting from chemical treatments often have the greatest potential for forensic casework (Verma *et al.*, 2002). For example, scanning near-field optical microscopy is employed in the cosmetics industry to investigate the penetration and diffusion pathways of chemical treatments in human hair (Kelch *et al.*, 2000; Formanek *et al.*, 2006). Treated hair colour can hence be a critical feature, whereas a naturally coloured hair provides far less information. There is clearly a

need to develop methods that can measure natural hair colour both objectively and accurately.

### 2.1.2. Colour Science

The phenomenon of ‘colour’ is essentially a response of the human visual system to the interpretation of light at different wavelengths (Grey, 2006). It is convenient to define colour by the wavelength of its light, as each part of the visible colour spectrum corresponds to light waves of different wavelengths (Hunt, 1987; Grey, 2006). As depicted in Figure 2.1-1, the main spectral colours occupy the wavelength bands from approximately 380 nm to 780 nm and include a gradual transition from one colour to another throughout the spectrum (Hunt, 1987; Grey, 2006).



**Figure 2.1-1 – Visible Continuous Spectrum**

Different parts of the visible continuous spectrum correspond to light waves of different wavelengths. The main spectral colours occupy the wavelength bands from approximately 380 to 780 nm, with a gradual transition from one colour to another.

Hue is the property of colour that distinguishes one colour from another; it is the dominant wavelength of light that is often identified with a name, such as ‘red’, ‘orange’, ‘purple’, etc. Colours seen by the human eye are not only subject to variations in hue but also lightness (relative brightness) and colourfulness (chroma and saturation). Lightness is a measure of the amount of light reflected or emitted by an object. Colourfulness, which incorporates chroma and saturation, is the property of colour that describes purity and so is responsible for any given colour’s vibrancy or dullness.

The retina of the human eye contains two main types of photoreceptors. ‘Rods’ number approximately 120 million and are very light sensitive but do not have a role in the perception of colour, while ‘cones’ number approximately 6–7 million and provide all of our colour sensitivity (Grey, 2006). When a visual signal is received, photoreceptors judge the hue and the brightness of the signal and the overall combination of these signals determines the colour perceived by the brain. The eye’s retina is also responsible for the ‘triple’ nature of colour. The basic principle of trichromatic colour is that all the colours

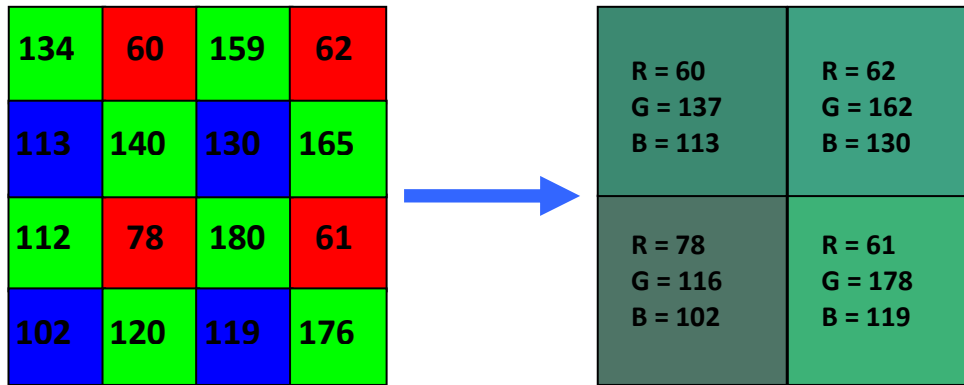
can be reproduced by blending together in different proportions the three primary colours – red (R), green (G) and blue (B). Consequently, the human eye has three types of cones, with each type being sensitive to either red green or blue radiation. Colour blindness is characterised by the absence of one type of cone.

### 2.1.2.1 Colour Interpolation

Objects absorb, transmit and reflect light of different wavelengths in a variety of combinations. To produce a colour digital image using a microscope operating in the transmission mode, the wavelengths of light transmitted by a sample must be ‘read’ by the microscope’s camera then converted to the picture elements (pixels) of the digital image.

First, light from the sample is focused on the camera’s charged–coupled device (CCD), an electronic instrument that captures images as variations in light intensity. The principal component of the CCD is the silicon wafer chip sensor that carries a rectangular array of millions of light–sensitive diodes (Brown, 2004). Photodiodes incorporate filters that separate intensity data for the red, green and blue bands of the spectrum, creating individual photosites that correspond to pixels in the final image (Brown, 2004). When a photon of light strikes the surface of the sensor, the energy imparted by the photon releases an electron that is stored in the photodiode (Rieke, 1994). Each diode produces an electrical charge proportional to the amount of light it captures from the sample.

Second, signals from the sensor pass into an analogue–to–digital converter that translates the electrical charges into numerical pixel values. The numerical value is assigned to each photodiode’s charge, according to the number of electrons it contains. Experiments have shown that output signals are linear with respect to exposure time (ms) until close to saturation (Theuwissen, 2010). As each photosite is filtered to record only one of three colours, the data from each one cannot completely determine the final colour of the pixel. As depicted in Figure 2.1-2, colour interpolation algorithms obtain the single channel data from the photosites, which have distinct red, green and blue values, and recalculate new values so that each pixel in the final digital image will contain discrete RGB data (Brown, 2004). Therefore, a digital image is essentially an array of pixels that are each an exact square representing a uniform flat value of colour (Rivard, 2006).



**Figure 2.1-2 – Depiction of Colour Interpolation**

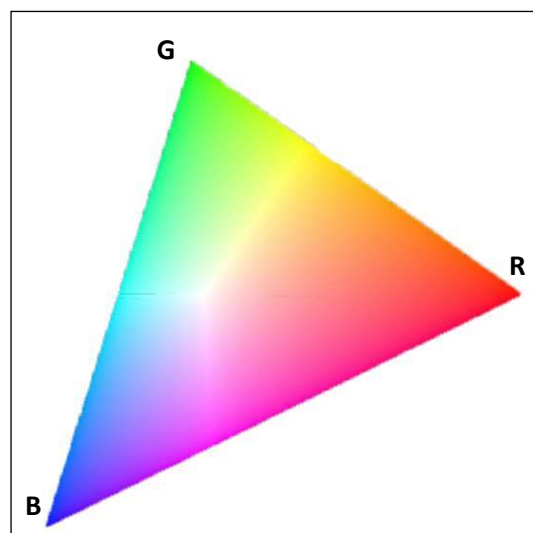
An analogue-to-digital converter assigns numerical values to each photodiode's charge, depending on the number of electrons it contains. Colour interpolation involves recalculating new pixel values for the digital image based on each photosite's single-channel data, having distinct red, green and blue values.

### 2.1.3. Colour Models

Colour models provide an organisational system for digital images by translating the wavelength and light intensities of specific attributes from an image into numerical values. Each model relies on different attributes and therefore describes the same colour in a numerically different manner. For example, one model (RGB) describes colour based on the level of red, green and blue required to reproduce a colour, while another model (HSB) describes colour based on its hue, saturation and brightness.

#### 2.1.3.1 RGB Colour Model

The RGB colour model characterises colour based on the three primary components red (R), green (G) and blue (B). Monochromatic light of these primaries include wavelengths of 650 nm for red, 530 nm for green and 460 nm for blue (Hunt, 1987). Theoretically, combining all three components at their most saturated (monochromatic) levels produces pure white while alternatively omitting all three components produces pure black. The two-dimensional (2D) RGB colour gamut presented in Figure 2.1-3 depicts every colour that can be produced within the RGB colour space at its highest level of luminosity. In reality, the gamut is three dimensional (3D) with primary colours forming the triangle vertices and the intermediate colours forming a weighted average of those three primaries in different proportions (Kay, 2007). As the gamut is 3D, the darker pixels are 'hidden' beyond the pixels shown.



**Figure 2.1-3 – RGB Colour Gamut**

The 2D gamut depicts every colour possible within the RGB colour model at its highest luminosity. The primary colours form the triangle vertices while the intermediate colours form a weighted average of those three primaries in different proportions. The darker pixels are ‘hidden’ beyond the pixels shown. (Source: Kay, 2007).

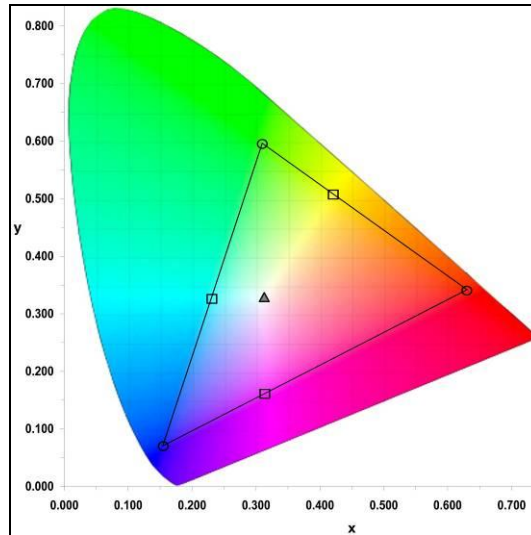
On a digital monitor, characters are represented by strings of eight binary digits (‘0’s and ‘1’s). For a greyscale image, each pixel can be one of 256 levels of grey (comprising integers between 0 and 255) that corresponds to a particular combination of binary digits ( $2^8 = 256$ ). For an RGB colour image, each pixel is represented by three colour channels that are each represented by 256 saturation levels of red, green and blue, together creating over 16 million colours ( $2^{(3*8)} = 16,777,216$ ). Theoretically, the full range of colour in the visible spectrum can be represented in digital media by combining red, green and blue pixels at different intensities (Brinkman, 2008). However, there is some colour visible to the human eye that is located outside the RGB colour space.

### **2.1.3.2 CIE XYZ Colour Model**

The CIE XYZ tri-stimulus model was developed in 1931 by the International Commission on Illumination (in French, the *Commission Internationale de l’Éclairage* or CIE). The colour models CIE XYZ and CIE L\*a\*b\* (described next) were designed on precise measurements of how humans perceive colour, incorporating properties of hue and saturation, rather than being designed on how colour is produced as was the case with the RGB colour model design (Grey, 2006; Rofin, 2006). The CIE X, Y and Z components do not represent real colour values, rather, they represent artificial primary colours (x, y and z) derived from a mathematical model (Rivard, 2006).



The CIE XYZ colour gamut is shown in Figure 2.1-4. The x and y axes specify the colour, while luminescence lies orthogonally in and out of the plane of the gamut, with the bottom black and top white (Hancock, 2010). Plotting red, green and blue on the CIE XYZ colour gamut establishes the boundaries of the RGB colour gamut and those particular colours that fall within and outside the RGB model.



**Figure 2.1-4 – CIE XYZ Colour Gamut**

Colour is specified by the x and y axes, while luminescence lies orthogonally in and out of the plane of the gamut, with black at the bottom and white at the top. The boundaries of the RGB colour gamut are also displayed as a triangle formed by the three primary colours. (Source: Hancock, 2010).

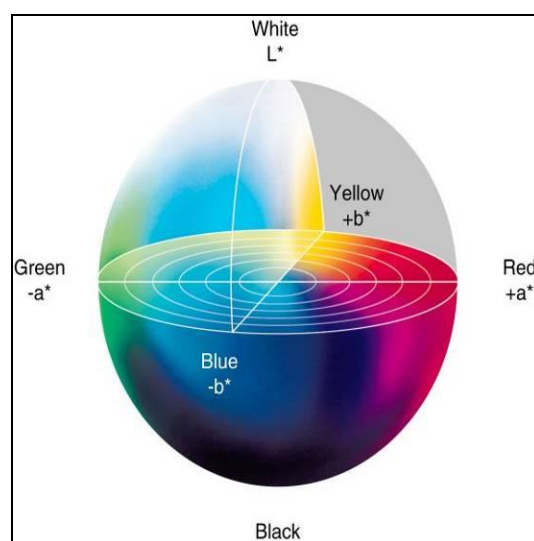
For any colour characterised by the CIE XYZ model, the CIE Y component (measured from 0 to 100) represents both the amount of artificial green primary and how sensitive the human eye is to light. Therefore, CIE Y is also a measure of the total luminescence in an image (Overheim & Wagner, 1982; Hunt, 1987). The CIE X component represents the amount of artificial red primary in an image and CIE Z represents the amount of artificial blue primary in an image. Variations in the amounts of CIE X and Z only affect the colour, leaving luminescence unchanged (Hunt, 1987). Moreover, to produce some colours, negative red, green or blue values are required so the artificial primary colours of the CIE XYZ colour model are derived in such a way that they are always positive (Overheim & Wagner, 1982; Christie *et al.*, 2000).

### 2.1.3.3 CIE L\*a\*b\* Colour Model

Some dimensions of colour perception, such as hue, colourfulness (chroma and saturation) and lightness, are not easily interpreted from the CIE XYZ model, which lead

to the design of the CIE  $L^*a^*b^*$  tri-stimulus model. The CIE  $L^*a^*b^*$  measurements correspond to trichromatic human perception and encompass every possible visible colour within which all RGB and CMYK (the subtractive colour model, Cyan Magenta Yellow and Key (black)) colour spaces are plotted (Rivard, 2006).

Akin to RGB and CIE XYZ, the CIE  $L^*a^*b^*$  colour model also consists of three components to describe colour, but it is best represented in a 3D space as depicted in Figure 2.1-5. The component  $L^*$  is purely a measure of lightness (measured from 0 to 100) and corresponds as much as possible to the human perception of lightness. Hence, CIE  $L^*$  is entirely devoid of hue and saturation, while CIE  $a^*$  and  $b^*$  account for all the saturation and hue, measured along two axes between -100 and +100 (Rivard, 2006). The component CIE  $a^*$  is represented by one axis between red (where  $a^* > 0$ ) and green (where  $a^* < 0$ ) while the component CIE  $b^*$  is represented by the second axis between yellow (where  $b^* > 0$ ) and blue (where  $b^* < 0$ ).



**Figure 2.1-5 – CIE  $L^*a^*b^*$  Colour Space**

The CIE  $L^*a^*b^*$  model comprises three components to describe colour. CIE  $L^*$  is purely a measure of lightness and corresponds to the human perception of lightness. The other two components account for both saturation and hue. CIE  $a^*$  is measured on an axis between red and green, while CIE  $b^*$  is measured on an axis between yellow and blue. (Source: Thyon Design, 2010)

## **2.1.4. Research on Hair Colour**

### **2.1.4.1 Spectrophotometry**

Shriver and Parra (2000) used reflective spectrophotometry to compare two methods for the determination of skin and hair pigmentation: a narrow-band spectrometer

(*DermaSpectrometer*) that measures the melanin index, and a tristimulus colorimeter (*Photovolt Colour Walk*) that measures luminescence within the CIE L\*a\*b\* colour space. The researchers obtained triplicate measures of the parietal region of the heads of 55 European, 9 African, 7 South Asian and 9 East Asian participants, all with naturally coloured hair. A clear correlation between the level of luminescence (CIE L\* variable) and the melanin index was observed, and the researchers concluded that both instruments provide accurate estimates of pigmentation in skin and hair (Shriver & Parra, 2000).

Naysmith and colleagues (2004) investigated the relationship between human pigmentation and the Mc1r genotype by comparing the DNA sequence diversity, hair colour and melanin measures of 59 participants. To measure hair colour, the researchers obtained triplicate measures represented in the CIE L\*a\*b\* colour space, of the parietal region of the participants' heads using a tristimulus colorimeter (*Minolta Chromameter CR300*) and quantified the amount of eumelanin and phaemelanin using high performance liquid chromatography (HPLC). It was observed that the predictive power of the genotype for hair colour (Mc1r) was greatest for the CIE b\* score that measures on a scale from blue to yellow, followed by CIE a\* that measures on a scale from green to red (Naysmith *et al.*, 2004).

In a series of papers on hair colour, Vaughn and colleagues evaluated reflective spectrophotometry as a method to objectively describe hair colour (2008), to compare macroscopic and microscopic hair colour measurements as well as hair thickness (2009a), and compare hair colour measurement by digital image analysis with reflective spectrophotometry (2009b). For their research, CIE L\*a\*b\* colour measurements were derived from both digital image and reflective spectrophotometry scans of the back and sides of participants' heads.

In order to categorise hair colour, several two-step cluster analyses (Euclidean distance and log-likelihood method) were performed based on the CIE L\*a\*b\* colour measurements obtained from reflective spectrophotometry (Vaughn *et al.*, 2008). The same CIE L\*a\*b\* colour measurements and the respective category allocations were then used to perform several discriminant analyses, a method that predicts group measurements based on similarities within categories. Nearly all the two-step cluster models reportedly classed more than 95% of the samples into the correct categories (Vaughn *et al.*, 2008). The high degree of prediction accuracy reported was not surprising considering that both

the ‘predicted’ and ‘original’ category allocations were based on exactly the same measurements. When the authors categorised the colour measurements according to observer–reported colours, only 73.1% of cases were correctly classified (Vaughn *et al.*, 2008). The lower result was most likely because cluster analyses evaluate the raw variable scores and groups them accordingly, irrespective of the overall colour perceived by the human eye.

A further study compared CIE L\*a\*b\* measurements using reflective spectrophotometry, with measurements obtained using the *V++ precision digital imaging system* from digital images of hair from the same individuals (Vaughn *et al.*, 2009b). Based on the category allocations determined by reflective spectrophotometry in an earlier study (Vaughn *et al.*, 2008), the authors performed a discriminant analysis using the digital imaging measurements as the predictor variables (Vaughn *et al.*, 2009b). Several analyses resulted in low to moderate prediction accuracies, ranging from 51.5 to 85.8%. Had the digital imaging measurements been used to establish the original category allocations, it can reasonably be assumed that the digital image measurements would result in higher prediction accuracy than the reflective spectrophotometry measurements as again both the predicted and original category allocations would be based on the same variables. However, this was not investigated by Vaughn and colleagues (2009b), who concluded that the digital imaging method was inaccurate and inconsistent, and thus of limited value for forensic use.

While reflective spectrophotometry may be a reliable method for accurately measuring macroscopic hair colour, it would be useful if cluster categories actually corresponded to the hair colours most people already use, such as ‘Blonde’ and ‘Dark Brown’, as noted by Vaughn and colleagues (2008). When the authors divided the hairs into six categories based solely on the spectrophotometric measurements, the observer–reported Red (n = 4) and White (n = 2) colours were reportedly very clearly discriminated, while the other colours were “somewhat less distinct ... [and were] roughly divided” into the categories Fair, Light, Medium and Dark (combined n = 134) (Vaughn *et al.*, 2008, pp93). When statistical criteria is the sole basis for categorising colour data, the predictive model created will be devoid of meaning with respect to the human perception of colour.

Other researchers studied the ability of ultra violet–visible (UV–visible) microspectrophotometry to successfully discriminate the colour of dyed hair (Barrett *et al.*,

2010; 2011). Although they focused on discriminating between chemically treated hair some natural hair colour assessments were incorporated in the research. Twenty five participants, reportedly representing a variety of natural shades from Light Blonde to Dark Brown, were classed into four categories following hierarchical cluster analysis (Euclidean distance and Ward's aggregation criterion) (Barrett *et al.*, 2011). The authors also used discriminant analysis to evaluate the ability of microspectrophotometry to differentiate natural hair colour between the four classes. Based on the mean of 25 spectra per participant (five scans from five hairs), 84% were correctly classed while, based on the mean of five spectra per hair (five hairs per participant), only 71% were correctly classed, as more opportunity for cross variations between hairs of the same shade was introduced (Barrett *et al.*, 2011).

Furthermore, Barrett and colleagues (2011) attempted to individualise the natural hair colours. Based on several discriminant analyses, the researchers concluded that the microspectrophotometry technique was not able to successfully discriminate between the 25 natural hair samples, with only 22% of participants correctly classed.

#### 2.1.4.2 Alternative Research Methods

While reflective spectrophotometry can be used to accurately measure hair colour at the macroscopic level, it can be cumbersome to use on a large number of individuals and such instruments are generally not portable (Vaughn *et al.*, 2009b). As noted by Robertson (1982), methods based on the colour analysis of pigmentation (such as UV-visible microspectrophotometry), which have been successfully applied for many forensic applications, have limited value in classifying natural hair colour since the pigment in all hair is composed of only two components—eumelanin and phaemelanin.

Research by Bednarek (2003) aimed to determine whether hair colours described as Blonde and Brown corresponded to narrow, non-overlapping ranges of the three components of the RGB colour model and also to define the practical effectiveness of morphological comparative hair analysis. Hair samples were classified as being either Blonde (n = 50) or Brown (n = 50) in accordance with the Ogle and Fox criteria that compares the colour of hair observed microscopically, with standards published in their Hair Atlas (see Ogle & Fox, 1999). Bednarek (2003) selected Blonde hair samples that compared to the D01–D03 Ogle and Fox classification and Brown hair samples that compared to the D21–D25 Ogle and Fox classification. The researcher used *Lucia 4.51*

*Image Analysis Software* to obtain digital images of the hair samples at 10, 40 and 60x magnification and to calculate the mean RGB value for the pixels making up each image. The author found that the *Lucia* imaging method could precisely detect and characterise strand colour in a digital manner without error from overlap between colour ranges. The Blonde RGB coordinates were 243, 224, 206 (lightest blonde) to 207, 182, 57 (darkest blonde) and the Brown RGB coordinates were 179, 154, 131 (lightest brown) to 117, 98, 76 (darkest brown), all calculated from the mean  $\pm$  one standard deviation (Bednarek, 2003).

Furthermore, to evaluate the practical effectiveness of morphological comparative hair analysis, the individualisation of 100 hairs randomly selected from 12 individuals was undertaken by both the method proposed by Ogle and Fox and the comparative analysis of RGB intensity values (Bednarek, 2003). Correct personal identification was obtained for 74 hairs using the Ogle and Fox comparison to standards method, compared to 91 hairs correctly identified using intensity values determined by the RGB colour model system (Bednarek, 2003). The author concluded that the RGB digital image method provides a reliable basis for forensic hair comparisons.

Birngruber and colleagues (2009) investigated the effectiveness of obtaining hair colour profiles using *SpectraCube*<sup>®</sup>, a spectral imaging device that combines a CCD-based camera to acquire high resolution digital images, spectroscopy to acquire the spectra of each pixel, and light microscopy to observe morphological features. The authors' evaluated spectral data from each of three hairs from 25 participants with both chemically treated and naturally coloured hair, to determine whether the *SpectraCube*<sup>®</sup> could be used to attribute human head hair to an individual on the basis of its colour profile. While the sensitivity range of the human eye is limited to wavelengths between 380 and 780 nm, the *SpectraCube*<sup>®</sup> was used to image hair samples between 450 and 1020 nm (Birngruber *et al.*, 2009).

Extreme intra-individual variability in the colour of individual hairs was observed and the researchers considered that this would diminish the significance of the results (Birngruber *et al.*, 2009). The authors found that, while spectroscopic data was able to confirm microscopic findings, it could not provide additional levels of discrimination for indistinguishable hairs. The research indicated that it was not possible to definitively provide identification with a compound light microscope and a *SpectraCube*<sup>®</sup> based solely

on the colour of an individual hair and that the method is not suitable for forensic hair evidence (Birngruber *et al.*, 2009).

Finally, Brooks and colleagues (2011) combined traditional microscopic techniques with digital imaging to evaluate the use of numerical image values for measuring colour. The authors obtained five high resolution digital images from each of ten hairs from ten nominally brown hair participants. Numerical colour values were determined for each image using three colour models, namely, RGB, CIE XYZ and CIE L\*a\*b\* using a *V++ precision digital imaging system*. The authors used discriminant analyses to evaluate and compare the ability of the three colour models to allocate hair samples to the rightful participant. They reported that the RGB colour model correctly classed 64% of the hair samples, CIE XYZ correctly classed 68% samples and CIE L\*a\*b\* correctly classed 58% of the samples (Brooks *et al.*, 2011).

Canonical discriminant plots were also produced by those researchers to facilitate the statistical validity of the analyses, representing two functions for each model and describing almost all of the variation in the data (Brooks *et al.*, 2011). For each colour model, two shades of brown were distinguished and, within the shades, it was reportedly possible to identify trends where all hairs were associated with the correct participant within the population sampled (Brooks *et al.*, 2011). Of all the research methods on hair colour presented here, Brooks and colleagues (2011) showed the highest prediction accuracy for individualising hair samples based on colour alone. However, as only a small population ( $n = 10$ ) was examined by the researchers, a greater number of participants would need to be included in the sample population to assess the full utility of the proposed approach. This, then, became the focus of the research presented in this chapter.

### **2.1.5. Research Focus**

Hairs are a ubiquitous material in our environment and one of the most common forms of evidence found at crime scenes. The role of the forensic hair examiner is to determine whether a questioned hair recovered from a crime scene is or is not consistent with a known sample, through the employment of microscopic examination and comparison (Brooks, 2007). As colour is one of the main hair characteristics assessed and scored as part of this process, the research focus of this chapter involved assigning numerical values to such assessments.

The initial analyses were designed to address forensic casework in the broader context, whereby an inexperienced hair examiner or scene of crime officer may be required to process multiple questioned hairs or bulk samples during evidence triage. Discriminant analysis was used to distinguish between multiple hair samples. First, attempts were made to develop a statistical model that could assign a nominal hair colour to any given questioned hair, based on numerical colour values. Predictive models were established using the numerical values of approximately 1050 hair samples measured in this research. Second, to assess the evidential power of numerical colour values, attempts were made to allocate multiple hairs of visually similar colour to the correct participants.

The follow-up analyses were designed to investigate whether numerical colour measurements could provide an additional tool for the experienced forensic examiner when performing colour comparisons. As opposed to colour components that were considered collectively as multivariate entities, for the follow-up analyses they were tested as individual variables regardless of the overall colour perceived by the human observer. That is, they were considered on a purely numerical basis for comparative purposes. Confidence intervals were applied to distinguish between an individual, questioned hair and multiple hairs from a known source. Issues pertaining to hair-to-hair comparisons were also provided. However, as a number of statistical requirements were not met due to the sampling method employed in this research, the follow-up analyses were included as a demonstration for potential future work only.



## 2.2. Materials and Methods

### 2.2.1. Sample Preparation

In accordance with the University of Canberra Committee for Ethics in Human Research (approval number 08–65), hair samples were received from 154 participants, comprising males and females aged between 18 and 65 years. Six nominal hair colour categories were targeted, namely Red, Blonde, Light Brown, Medium Brown, Dark Brown and Black, with 20 participants from each nominal category actively sought. Participants were asked to complete a short questionnaire regarding their age, gender, ancestry, hair colour, chemical treatment and product usage. All documents given to the participants including the questionnaire are provided in Appendix A<sup>1</sup>. Each participant and their associated samples were identified by a unique number between 200000 and 200250, anonymously allocated when the sample collection kits were distributed, that were retained throughout the entirety of the project.

Combed head hair was requested to increase the number of telogen hairs in each sample set, as this hair type is the most common encountered during forensic casework and not generally suitable for nDNA analysis. Hair from each participant was collected in A3 size white office paper that was folded and placed in a plastic snap–seal bag for return and subsequent storage. Returned hair samples were screened under light microscope. Only samples comprising at least ten hairs with distal (root) end attached and natural, untreated colouring (or where chemically treated, approximately 3 cm or more of naturally coloured regrowth) were retained for use in this study. Following screening, ten hairs from each participant were longitudinally mounted in pairs on Livingstone Premium Microscopes Glass Slides (76.2 x 25.4 mm, thickness 1.0–1.2 mm) using HistoMount™ mounting medium (*National Diagnostics*, supplied by *Geneworks*, South Australia) and size 1 Deckglaser microscope cover glass (1 oz, 22 x 55 mm). The samples were then numbered 01 to 10. Hair extending beyond the length of the microscope slide were correspondingly numbered, removed by cutting and stored in the original A3 folded paper. Glass slides were placed in a controlled oven (Contherm digital series, Cat. 2100, *Contherm Scientific*

---

<sup>1</sup> In addition to hair samples, participants were also asked to provide a DNA sample using two sterile cheek swabs. The DNA was collected on behalf of a second hair research project involving the recovery and characterisation of nDNA from Telogen hairs, being conducted at the University of Adelaide.

Co., New Zealand) at  $37^{\circ}\text{C} \pm 2^{\circ}\text{C}$  overnight to dry the mounting medium and prevent sample movement during image acquisition. Finally, the underside of each slide was marked at three equidistant points along the pigmented hair length, indicating where each image would subsequently be acquired.

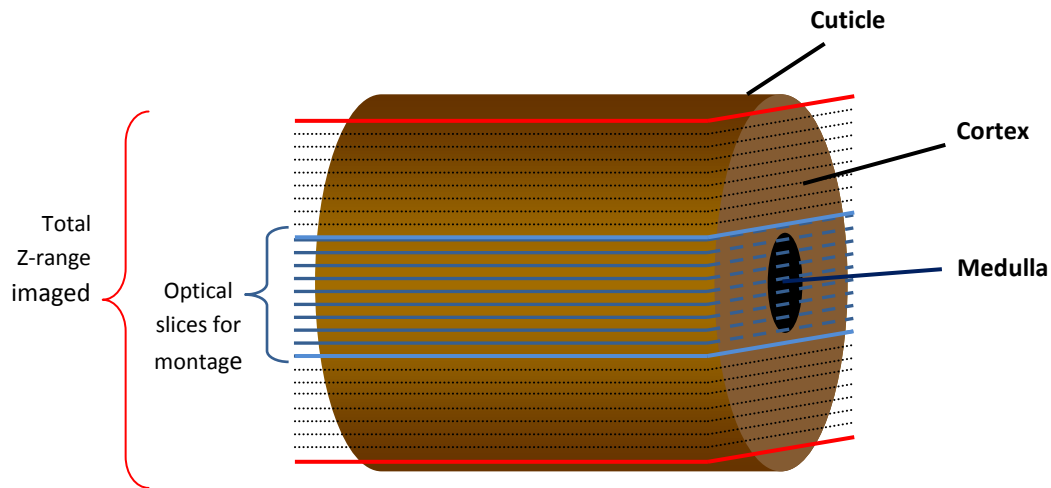
## **2.2.2. Image Acquisition**

### **2.2.2.1 Microscope Specifications**

All image acquisition was conducted with the *Leica DM6000* (Light Microscope series, *Leica Microsystems CMS GmbH*, Wetzlar, Germany), a fully automated upright microscope system as well as its associated image management software, the *Leica Application Suite (LAS)*. The high resolution images were captured in colour format, 1392 x 1040 mm, full frame HQ (real size = 203.59 x 152.1  $\mu\text{m}$ ) and saved as Tagged Image File Format (TIFF) files. Bright field transmitted light contrast method was selected with all images captured through a 63x glycerine objective (Immersion Oil G,  $n_e^{21}$ : 1,451, *Leica Microsystems*). The following conditions were established at the beginning of the research, following observation of a random selection of hair samples: 1.50 saturation, 1.13 gamma, 1.0x gain and 7.19 ms exposure. Toward the end of the image acquisition phase, these parameters were found to be unsuitable for a few hair samples comprising nominally dark black hair so the exposure time was reset to 17.3 ms to capture these few samples (discussed in detail at 2.2.6 Exposure Correction).

### **2.2.2.2 Z-Stack Acquisition**

Montage images were acquired at three equidistant points along the proximal end of the hair shaft for all ten hairs belonging to each participant. At each point, the microscope was manually focused on the optical plane lying immediately below the cuticle area at the topmost part of the hair. This z-plane location was then ‘locked’ into the *LAS* software memory. The microscope camera was manually focused on the optical plane lying immediately above the cuticle area at the lowermost part of the hair and also ‘locked’ into software memory. Depending on the depth of the hair, the z-range distance was typically 28–35  $\mu\text{m}$  deep. Once each z-range was selected, the camera automatically re-focused at 30 equidistant optical planes within the range, approximately 1  $\mu\text{m}$  apart. An image or “optical slice” was automatically acquired at each of these focal planes. From those 30 optical slices, the researcher manually selected ten from the core region, as shown in Figure 2.2-1, to create a single, multi-focus montage image.



**Figure 2.2-1 – Depiction of Z–range Relative to Hair Shaft**

The microscope camera was manually focused on the focal plane immediately below the cuticle area, at the topmost part of the hair (red line) and then on the focal plane immediately above the cuticle area at the lowermost part of the hair (red line). Depending on the depth of the hair, the z–range distance was typically 28–35  $\mu\text{m}$  deep. The camera automatically re–focused at 30 equidistant optical planes within the range, approximately 1  $\mu\text{m}$  apart, and acquired an optical slice at each plane. From those 30 optical slices, 10 slices predominately from the central region (blue) were used to create the final montage.

### 2.2.2.3 Multi–focus Montage Generation

Digital information from the individual optical slices that can be retained in the final montage image depends on user preferences. For this project, fixed method was selected with a patch size of 10 and a preference for accuracy over speed. Given hair’s cylindrical form, when observed through a microscope the width of the hair shaft (y plane) decreases at the focal planes furthest from the central region; the hair shaft is widest at the central region. Optical slices, acquired from focal planes where the hair appears narrowest, were found to create an overlapping effect that obscured pigmentation on other slices included in the same montage. Therefore, only the ten optical slices from the widest, central region were selected as the z–stack to create montages in this project. Also, it was judged that little pigment detail would be lost using this method, as the majority of pigmentation is nonetheless observed in the central region during microscopic forensic hair examinations (Brooks, 2009). An example of a z–stack and final montage created by this method is provided in Figure 2.2-2.

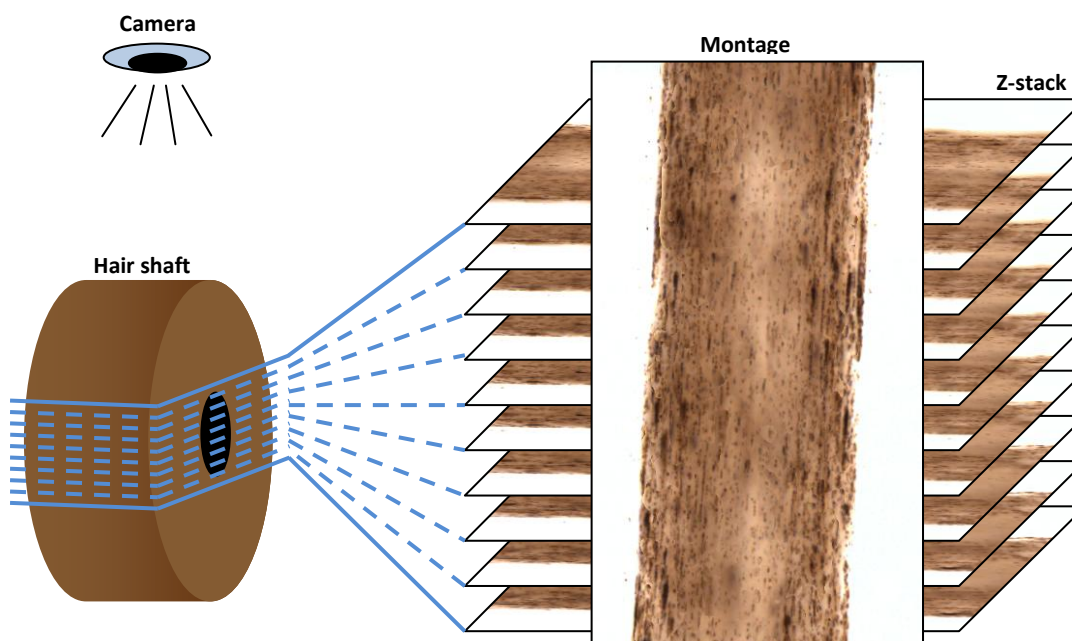


Figure 2.2-2 – Example Z-stack and Final Montage

Montage images were created from the ten optical slices acquired from the widest, central region of the hair shaft. This avoided obscured pigment detail in the final montage that can sometimes occur when optical slices of the narrower part of the hair (those regions at the nominal top and bottom of the cylindrical shaft) are included in the Z-stack. The majority of pigmentation detail is also thought to be observed in this central region regardless.

### 2.2.3. Image Preparation

Numerical colour values from the montage images (TIFF files) were measured using Digital Optics *V++ precision digital imaging system* software, version 5.0 (*Digital Optics Limited*, Auckland, New Zealand). Each image was normalised prior to the colour values being measured. This involved first using the *V++ Geometry* function to align each image so that the hair appeared horizontal across the monitor. As the angle of rotation differed for each montage and the image boundary was not enlarged during the process, the final normalised images differed markedly in size. Second, 4-point mapping, also part of the *V++ Geometry* function, was used to map a quadrant boundary rectangle of only the hair image, thereby cropping out any of the microscope slide observed in the image background. A bilinear interpolation filter was used to smooth the results during this process. Bilinear interpolation is a technique used to calculate the appropriate intensity of a new pixel when it is moved from another position. The transformation matrix is based on the intensity of the four nearest neighbouring pixels in the new pixel position (Rofin, 2006).

### 2.2.4. Colour Measurement

The *V++* Statistics function was used to measure and record the mean pixel value contained within each digital image. The Statistics dialogue updates colour measurements continuously, depending on the image selected at a given time. The three colour models compared in this project, namely RGB, CIE XYZ and CIE L\*a\*b\*, are each expressed by three components so a measure of the mean pixel value was recorded for each component. For example, for the RGB model, the mean level of red (R) in the normalised image was recorded, as well as the average level of green (G) and blue (B). In total, nine mean values were recorded for each normalised image.

### 2.2.5. Colour Transformation

Multiple colour models can be supported by *V++*, including RGB, CMY, HSV, YIQ and CIE XYZ. Normally, a standard 3 x 3 colour transformation matrix is performed to convert between RGB and CIE XYZ coordinates. However, like most modern cameras, by default the *DM6000* camera produces pixel values in the standard RGB (sRGB) colour model and was therefore non-linear with respect to CIE XYZ. Conversion between sRGB and the *V++* inbuilt CIE XYZ coordinates could not be performed correctly, without first converting sRGB to linear RGB (linRGB).

Furthermore, the CIE L\*a\*b\* colour model was not one of the multiple colour models automatically included with *V++*, though it can be mathematically derived from the CIE XYZ coordinates. The programming language of *V++*, *VPascal*, was used to automate most of the colour transformation and measurement tasks in this research. The original *VPascal* script for transformation between the colour models was provided by Comber (2006a) with some alterations. The final *VPascal* script used to transform between colour model coordinates, is provided in Appendix B.

#### 2.2.5.1 Standard RGB to linear RGB

To transform sRGB coordinates to linRGB coordinates, the following calculation was applied to each respective component:

- $linR = (sR / 255)$   
     and if  $(linR > 0.04045)$   
     then  $((linR + 0.055) / 1.055)^{2.4}$  or else  $(linR / 12.92)$

- $\text{linG} = (sG / 255)$   
and if  $(\text{linG} > 0.04045)$   
then  $((\text{linG} + 0.055) / 1.055)^{2.4}$  or else  $(\text{linG} / 12.92)$
- $\text{linB} = (sB / 255)$   
and if  $(\text{linB} > 0.04045)$   
then  $((\text{linB} + 0.055) / 1.055)^{2.4}$  or else  $(\text{linB} / 12.92)$

### 2.2.5.2 Linear RGB to CIE XYZ

To transform linRGB coordinates to CIE XYZ coordinates, the following calculation was applied to each respective component. (NB– the returned CIE XYZ values were percentages of the full scale (0–255).)

- $\text{CIE X} = (\text{linR} * 0.412453) + (\text{linG} * 0.357580) + (\text{linB} * 0.180423)$
- $\text{CIE Y} = (\text{linR} * 0.212671) + (\text{linG} * 0.715160) + (\text{linB} * 0.072169)$
- $\text{CIE Z} = (\text{linR} * 0.019334) + (\text{linG} * 0.119193) + (\text{linB} * 0.950227)$

### 2.2.5.3 CIE XYZ to CIE L\*a\*b\*

To transform CIE XYZ coordinates to CIE L\*a\*b\* coordinates, the temporary variables XX, YY and ZZ were first calculated. The following calculations were applied to each respective component.

- $\text{XX}_{(\text{temp. variable})} = \text{CIE X} / (0.412453 + 0.357580 + 0.180423)$   
and if  $(\text{XX}^* > 0.008856)$   
then  $(\text{XX}^*)^{1/3}$  or else  $(\text{XX}^* 7.787) + 0.1379310345$
- $\text{YY}_{(\text{temp. variable})} = \text{CIE Y} / (0.212671 + 0.715160 + 0.072169)$   
and if  $(\text{YY}^* > 0.008856)$   
then  $(\text{YY}^*)^{1/3}$  or else  $(\text{YY}^* 7.787) + 0.1379310345$
- $\text{ZZ}_{(\text{temp. variable})} = \text{CIE Z} / (0.019334 + 0.119193 + 0.950227)$   
and if  $(\text{ZZ}^* > 0.008856)$   
then  $(\text{ZZ}^*)^{1/3}$  or else  $(\text{ZZ}^* 7.787) + 0.1379310345$

CIE L\*a\*b\* coordinates were calculated from the temporary variables XX, YY and ZZ. The CIE L\* value was scaled from 0 to 100, whereas the CIE a\* and b\* values were scaled from -100 to +100.

- $\text{CIE L}^*_{(\text{true scale})} = (\text{YY}^* 116) - 16$
- $\text{CIE a}^*_{(\text{true scale})} = 500 * (\text{XX} - \text{YY})$

- $CIE\ b^*_{(true\ scale)} = 200 * (YY - ZZ)$

As the values of CIE  $a^*$  and  $b^*$  were scaled from -100 to +100, and some imaging and statistical software packages do not cope with negative numbers, the CIE  $L^*a^*b^*$  coordinates were rescaled from 0 to 255.

- $CIE\ L^*_{(positive\ scale)} = 255 * (CIE\ L^*_{(true\ scale)} / 100)$
- $CIE\ a^*_{(positive\ scale)} = 255 * ((CIE\ a^*_{(true\ scale)} + 100) / 200)$
- $CIE\ b^*_{(positive\ scale)} = 255 * ((CIE\ b^*_{(true\ scale)} + 100) / 200)$

Quality control of the colour measurements and transformations in this research was conducted at various times throughout the data collection process, including after the exposure correction calculations (discussed next). A selection of ten sRGB measurements were entered into an online colour conversion program (Logicol Color Technology, 2008) and the CIE XYZ and  $L^*a^*b^*$  returned measurements were compared with the V++ returned measurements. In addition, the same ten sRGB coordinates were transformed to the other two colour models by manually writing *Excel for Windows* syntax and these results also compared with the V++ returned measurements. Minor differences were observed between the online colour conversion and the other methods but this was expected, as numbers used in calculations will be rounded-off at different levels by different programmers.

### 2.2.6. Exposure Correction

A number of parameters must remain consistent during the image acquisition phase, in order for the comparison of numerical colour measurements to be valid. Bednarek (2003) established that these parameters include image magnification, light intensity, hair-mounting medium, and the parameters of the optical device receiving the image.

In this research, all images were captured through a 63x glycerine objective with 7.19 ms exposure, 1.13 gamma, 1.50 saturation and 1.0x gain. However, during the research, these parameters were found to be unsuitable for some samples, particularly nominally dark brown and black hairs. The parameters lead to images that were considered too dark to (a) manually focus beyond the cuticle to set the z-range correctly, and (b) accurately observe the pigment detail in the final montage required for the pigment pattern recognition algorithms applied in Chapter 3: PIGMENTATION.

As established in section 2.1.2.1, Colour Interpolation, the number of electrons contained at a photosite affects its electrical charge, which then determines the numerical pixel value assigned in the final digital image. Experiments by Theuwissen (2010) showed that output signals are linear with respect to exposure time (ms) until close to saturation. Therefore, to capture the darker hair samples, the exposure time was increased from 7.19 to 17.3 ms, determined experimentally.

To correct for the increased exposure time, a sample of 19 hairs ranging in perceived colour from medium/dark brown to dark black were selected and imaged using both the original exposure (7.19 ms) and the longer exposure (17.3 ms), and separate regression plots for sR, G and B were constructed using *Excel* (see Appendix D). All other microscope, camera and lighting configurations, as well as image acquisition and colour measurement procedures, were identical to those applied to the main research samples. A strong relationship was found to exist between the two exposure times for each component ( $R^2 > 95\%$ ). Table 2.2-1 indicates the minimum and maximum values, the regression equation and the r-squared values, for sR, G and B.

**Table 2.2-1 – sRGB Values for Exposure Correction**

Colour Component	Min Value	Max Value	Regression Equation*	R-squared
sR	9.86	253.16	$y = 0.4342x - 3.4379$	0.9760
sG	6.45	229.57	$y = 0.3499x + 1.425$	0.9824
sB	5.28	174.23	$y = 0.3265x + 1.8766$	0.9696

\*Where 'y' is for 7.19 ms exposure values and 'x' is for 17.3 ms exposure values

Regression equations are only valid for measurements occurring within the original sample range. The following syntax was employed to define the minimum and maximum values and an example calculation based on values for sR (RGB) colour is also presented (where “.” denotes values outside the minimum and maximum range).

- *IF (logical test [1], value if [1] true, IF (logical test [2], value if [2] true), value if [1] [2] false)*
- $R_{(7.19\text{ ms})} = IF (R_{(17.3\text{ ms})} > 253.16, ".", IF (R_{(17.3\text{ ms})} > 9.86, (0.4342 * R_{(17.3\text{ ms})}) - 3.4379, ".")$



Following sRGB exposure correction for the dark hair samples, the CIE XYZ and CIE L\*a\*b\* coordinates were derived from the sRGB coordinates using the same mathematical equations employed in the *VPascal* script (see Appendix B) and as described in detail above (2.2.5 Colour Transformation).

### 2.2.7. Data Preparation

Numerical colour measurements were pasted directly from the V++ clipboard to an *Excel* spreadsheet for initial observations and for cross-correlation. Raw data from *Excel* was then exported directly to *PASW (Predictive Analytical Software) Statistics for Windows*, version 17.0.2 (SPSS Statistics IBM Corporation, 2008) for analysis. The *PASW* program was chosen for its full range of predictive analytical features that can handle both simple and complex inputs. In addition, *PASW* features are accessible via simple pull-down menus or command syntax programming, giving the benefit of ease of use and reproducibility.

The complete *Excel* data sheet contained over 3000 cases and included individual colour measurements for three images per hair for every participant. The *PASW* Aggregation function can combine multiple data points into single cases based on, for example, summary functions for numerical variables, including mean, median, standard deviation and sum, and then creates a new file containing only this data (SPSS Statistics IBM Corporation, 2008). For the present data, the Aggregate function was used to combine single colour measurements for each hair calculated from the mean of the three images originally measured, to avoid software memory issues that were encountered during preliminary tests.

### 2.2.8. Discriminant Analysis

Discriminant analysis focuses on the prediction of group membership. It is used to determine whether two or more known groups can be distinguished, based on a linear combination of multiple independent (predictor) variables (Norusis, 2008). The independent variables are combined into discriminant functions in such a way that the group centroids, being the means of the discriminant functions, will be similar for cases in the same group but different for cases in different groups (Norusis, 2008; Kinnear & Gray, 2010). This analysis treats cases as both mutually exclusive and collectively exhaustive

(Norusis, 2008); that is, each case belongs to only one group and all cases are members of at least one group.

Discriminant analysis [probability of F criteria (entry 0.05, removal 0.10) and Wilks' lambda stepwise method] was used in this research, first to allocate individual hairs to one of six nominal hair colour categories and second to allocate multiple hairs to the correct participant within one of six subpopulations of similar hair colour. The nominal categories and the participants in the respective analyses were the grouping variables, while the colour components – R, G, B, CIE X, Y, Z, CIE L\*, a\* and b\* – were the regressors from which group membership was predicted.

The discriminant function coefficients categorised cases by assigning them to one group when the colour coordinates fell within a certain criterion or to another group when the coordinates fell within another criterion. The more widely separated the discriminant function distributions, the more successful the prediction of group membership from those functions (Kinnear & Gray, 2010). The percentage of cases allocated to the correct group was primarily used to evaluate the success of three colour models for this type of analysis.

#### **2.2.8.1 Hierarchical Cluster Analysis**

Hierarchical cluster analysis is used when the group membership for a set of cases is not known. While, for each hair, information about the participant they belonged to was available, information about the colour category each hair belonged to was not available. Hierarchical cluster analysis (Squared Euclidean distance and Ward's Method) was used to facilitate the allocation of hairs to one of six nominal colour categories, namely Blonde, Red, Light Brown, Medium Brown, Dark Brown and Black.

#### **2.2.8.2 Canonical Discriminant Analysis**

Canonical discriminant analysis measures the degree of association between discriminant scores and the predicted groups (Norusis, 2008) and was used here to evaluate the success of the colour models for discriminating firstly between categories and secondly between participants. Function 1 always explains the greatest variance in the data and Function 2, being uncorrelated to the first, explains the second greatest variance in the data, etc (Norusis, 2008). Individual function coefficients represent the discriminating power of each of the variables independently.

Canonical analyses are often performed on data where each group has an equal probability of occurring in a population, or where information on the probability of occurrence is not available and is therefore ignored (Norusis, 2008). In this research, at least 20 participants from each of the six colour categories were actively sought; however, despite significant efforts, an overwhelming number of Medium Brown category samples and relatively few Red and Black category samples were returned. Therefore, prior probabilities were considered unequal for the canonical discriminant analyses performed. When sample proportions are unequal, the rate of correct classification is known to increase (Norusis, 2008).

The canonical correlation produced by *PASW* is the overall variance that each function explains. A high correlation (up to 100%) indicates that most of the observed variability in the discriminant scores for a particular function is explained by differences between the groups. The canonical discriminant function plot represents discriminant scores of predictor variables that showed the greatest discriminating power (Norusis, 1985; Brooks, 2007). Misclassification can occur due to lack of separation between the group centroids in the canonical space.

### **2.2.8.3 Assumptions**

As discriminant scores are based on the calculated mean of the group centroid, they are sensitive to outliers. Also, the covariance matrix of the predictor variables should be the same for all populations and violations of this assumption can affect both hypothesis testing and classification (Norusis, 2008). ‘Box Ms’ produced by *PASW* can be used to test whether the population covariance matrices are equal. The Box test, however, is notoriously sensitive, with even relatively minor departures from homogeneity resulting in small observed significance levels, especially for large size sample populations (Leech *et al.*, 2008; Norusis, 2008; SPSS Statistics IBM Corporation, 2008; Kinnear & Gray, 2010). Therefore, in many situations, small observed significance levels can be ignored with impunity (Norusis, 2008; Kinnear & Gray, 2010), i.e., the statistical significance may not equally represent the practical significance.

The discriminant analyses were designed to emulate forensic casework, whereby an inexperienced hair examiner or scene of crime officer may be required to process multiple questioned hairs during evidence triage. Two specific questions were addressed. Namely,

which of the three selected colour models, RGB, CIE XYZ and CIE L\*a\*b\*, provided the best statistical model for:

- Allocating individual hairs to one of six nominal hair colour categories; and
- Allocating individual hairs to the correct participant, within a subpopulation of similarly coloured hair.

### 2.2.9. Analysis of Variance

Analysis of variance (ANOVA) is used to compare two or more population or sample means, by focusing on the variance within the data being compared. Variance is the extent to which the measures of a single variable are distributed in a particular population, as opposed to covariance which is the extent to which two or more variables, vary together (i.e., how much they co-vary).

Mixed-model ANOVA (linear) was used to confirm whether the main source of variance in the sample population was ‘between participants’. Attempting to distinguish one participant’s hair colour from another’s based on numerical colour measurements would be superfluous if ‘within participant’ variance was found to be greater. The colour components – R, G, B, CIE L\*, a\* and b\* – were the dependent variables while ‘within hair’, ‘within participant’ and ‘between participants’ were the factors under investigation. [The colour components CIE X, Y and Z were not investigated here based on initial results and because the assumption of normality was not met (see Appendix E).] As measurements from the three images per hair (‘within hair’) was one of the factors under investigation, the complete data file containing over 3000 cases had to be analysed. To avoid software memory issues, the complete data file was randomly halved with each half analysed separately and the mean of both results provided.

#### 2.2.9.1 Assumptions

The ANOVA statistic is only reliable when applied to normally distributed data. Normality was determined by observing histograms, QQ- and stem-and-leaf plots produced by *PASW*. Homogeneity of variance is also required however this assumption is actually tested as part of the analysis.

### 2.2.10. Nominal Colour Categories

As previously described, colour is trichromatic and also incorporates hue, lightness and colourfulness (chroma and saturation). The colour models evaluated in this research numerically describe three specific attributes that combine to produce an overall colour that is, essentially, a visual experience dependant on the human observer for description, such as ‘Blonde’ or ‘Dark Brown’ in relation to hair colour. As one of the purposes of this research was to overcome the subjectiveness associated with hair colour perceptions, an appropriate method for allocating hair to nominal categories had to be derived that was as objective as possible. Multiple allocation methods were employed.

Firstly, hierarchical cluster analyses were used to facilitate the allocation of hair samples to six nominal categories. They were performed separately for each of the three colour models, using the mean hair values calculated from three images. For each colour model, the researcher assigned nominal colour to each of the six clusters (cluster 01 = Blonde, cluster 02 = Red, etc.). A large number of hairs were allocated to the same colour category by all three models, though some inconsistencies between the allocations were observed. Cluster analyses separate data based on the raw variable scores and groups them accordingly, irrespective of meaning or interpretation of the variables. Even minor deviations in the statistical criteria could have had a profound effect on the importance of any given colour component, thus altering the significance of the model produced.

While subjective in nature, participant–reported information on hair colour, along with observations of the original images by the researcher, were also used to facilitate the colour category allocation processes to ensure, in part, that the human perception of colour would be incorporated in the final statistical model. In their research on hair colour measurement and variation, Vaughn and colleagues (2008) found that self–reported hair colours were statistically similar to observer–reported hair colours. Those authors found that 85.7% of individuals had the same hair colour reported by themselves and an independent observer and, where there were discrepancies, the observer was more likely to report darker shades. As a wide variety of colour was sought in this project, participants were likewise asked to nominate the colour (Red, Blonde, Brown or Black) and shade (Light, Medium or Dark) of their own natural hair. (A short questionnaire pertaining to the participant’s ancestry, gender, age, hair colour, chemical treatment and product usage, was

included as part of the sample collection process and is provided in Appendix A.) Table 2.2-2 indicates the final number of hair samples allocated to each category.

**Table 2.2-2 – Sample Numbers for Nominal Hair Colour Categories**

<b>Blonde</b>	<b>Red</b>	<b>Light Brown</b>	<b>Medium Brown</b>	<b>Dark Brown</b>	<b>Black</b>	<b>Total</b>
n = 106	n = 71	n = 162	n = 361	n = 256	n = 53	1009*

\*A total of 1050 hairs would be expected given ten hairs from 105 participants. However, some colour measurements could not be obtained for various reasons causing a decrease in the total number expected. For example, some dark hairs fell outside the regression range (max/min) during the exposure conversion calculations.

### 2.2.11. Probability Distribution Curve

The probability distribution curve (or Gaussian distribution) serves as a model for the variation of a given measurement in a given population. A probability distribution curve can be derived from a mean value that describes where the population distribution of  $x$  is centred, as well as the standard deviation that describes variability within the population distribution (Devore & Peck, 2005). Natural hair colour varies to some degree with, for example, position on the head, and because numerical colour measurements have some level of uncertainty also. When a forensic examiner compares two hair samples, the result will always be based on the degree of difference between the samples, even when they are from the same source. A probability distribution curve representing variation in one person's hair colour can be used to test how probable it is that a difference in colour would be obtained if a questioned hair had the same origin.

The area under the probability distribution curve equals 1.0 in total. The approximate probability of observing a value at any given point lies along the curve and above that point on the  $x$  axis (Devore & Peck, 2005). However, determining the probability of occurrence of an exact occurrence ( $x$ ) within a continuous random variable is impractical as an infinitely small probability would result. It is more convenient to calculate the cumulative probability between two intervals ( $x_1 - x_2$ ). The *Excel* normal distribution syntax: NORM DIST( $x$ , mean, standard deviation, true) was used in this research to calculate the cumulative probability between -1.96 and +1.96 standard deviations of the mean, being the 95% confidence interval.

When the population standard deviation is unknown, the sample standard deviation can be used but only when the sample size is greater than 30 (Devore & Peck, 2005). For every participant ten hairs were collected, with triplicate measures per hair ( $n = 30$ ). However, as it was the ‘within participant’ hair colour variance being examined here and not the ‘within hair’ colour variance, ideally, a hair sample size of 30 would provide a more accurate representation of the distribution. Therefore, the results presented can provide an example for potential future work only.

The analyses were designed to investigate whether numerical measurements could assist the experienced forensic hair examiner with colour comparisons. Specifically, confidence intervals were used here to address the question:

- Can numerical colour measurements aid the examiner with colour comparisons between the individual, questioned hair and a sample from a known source

## 2.3. Results and Discussion

Hair samples from 154 participants were received for this research, from which only 105 were found suitable for analysis in regard to sample size, natural colouring (or extensive regrowth), lack of damage, and intact hair roots. Approximately 3150 montage images were acquired from those suitable hair samples, being three images from ten hairs for every participant. Using *V++*, numerical colour coordinates from the mean pixel colour within each image were measured in respect of the three chosen colour models, namely RGB, CIE XYZ and CIE L\*a\*b\*. Discriminant analyses were performed on the numerical colour measurements in *PASW* to assess which colour model could provide the best statistical model for assigning each hair to one of six nominal categories and for distinguishing a participant's hair from another's, within a subpopulation of similar hair colour. Probability distribution curves were then performed in *Excel* to assess whether numerical colour measures could be used to aid the experienced examiner with colour comparisons between question and known sources. The latter analyses were provided as an example for potential future work.

### 2.3.1. Allocation to Categories (Preliminary)

#### 2.3.1.1 RGB Category Allocation

The discriminant analysis involving R, G and B as the predictor variables resulted in the highest number of hairs correctly classed, with 76.2% prediction accuracy. Table 2.3-1 illustrates the predicted categories (%) based on the RGB measurements. Rows indicate the original colour category; columns indicate the category predicted by the RGB colour model measurements.



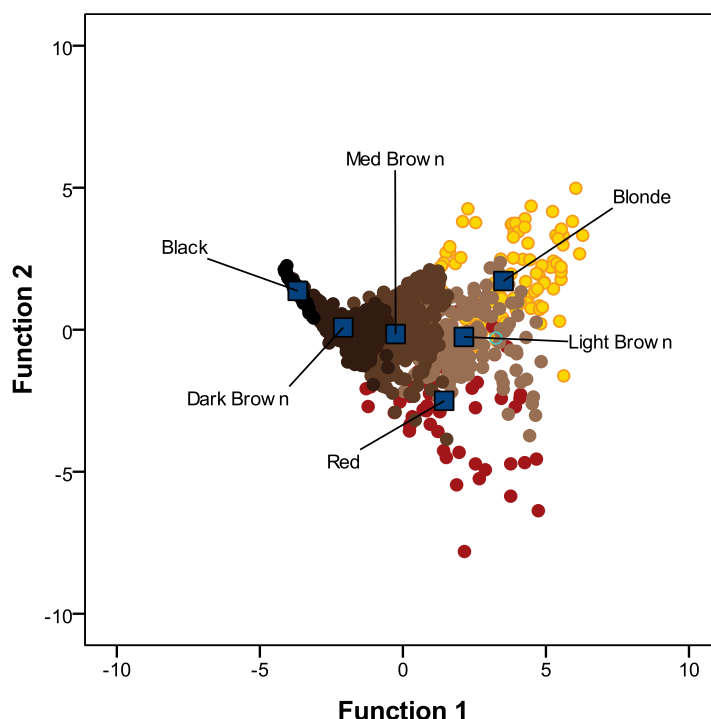
Table 2.3-1 – RGB Predicted Colour Allocation (%)

		PREDICTED						
		Blonde	Red	Light B	Med B	Dark B	Black	Total %
ORIGINAL	Blonde	69.8		22.6	7.5			100
	Red		59.2	15.5	23.9	1.4		100
	Light B	11.7	4.9	59.9	23.5			100
	Med B		1.7	1.7	87.8	8.9		100
	Dark B				18.8	77.3	3.9	100
	Black					22.6	77.4	100

When there is an unequal prior probability of belonging to a category, the rate of correct classification always increases as the larger groups can overwhelm the information in the discriminant scores (Norusis, 2008). However, it was found that, while 87.8% of the medium brown hairs have been correctly classed, this was not at the expense of the other categories, showing correct classification in between 59.2 and 77.4% of cases.

Figure 2.3-1 represents discriminant scores for the RGB colour model. Each hair is represented by the original allocated colour, but located in canonical space with respect to the two highest discriminant functions. It was observed that group centroids (mean discriminant functions) for Black, Dark Brown, Medium Brown and Light Brown, were best separated by Function 1 along the horizontal axis. For this function, the R variable that measured the intensity of red in an image was the strongest predictor variable, showing a high individual coefficient (0.961). In comparison, the other two predictors contributed very little to Function 1 (G, -0.215 and B, 0.285). The canonical correlation indicates that Function 1 explained 89.5% of the data variance.

Alternatively, group centroids for Red, Blonde and, again, Light Brown were best separated by Function 2 along the vertical axis. For this function, the B variable that measured the intensity of blue in an image was the strongest predictor variable, showing a high individual coefficient (2.141). The R variable was the second highest predictor (-1.346), while the G variable that measured the intensity of green in an image was again the smallest contributor (-0.571).



**Figure 2.3-1 – RGB Canonical Discriminant Functions**

The *PASW* canonical plot illustrates the two highest discriminant functions for the RGB colour model. Group centroids for Black, Dark Brown, Medium Brown and Light Brown were best separated along the horizontal axis, being Function 1, whereas Red, Blonde and again, Light Brown, were best separated along the vertical axis, being Function 2.

Bednarek (2003) found that the *Lucia 4.51 Image Analysis Software* that was used to calculate mean RGB pixel values, could precisely detect and characterise strand colour without error from overlap between Blonde and Brown colour ranges. Based on the same method of calculation (category mean  $\pm$  one standard deviation), the Blonde and Brown RGB coordinates in this research did not correspond well to those coordinates reported by Bednarek (2003). Bednarek reported the Blonde RGB coordinates as being 243,224,206 (lightest) to 207,182,57 (darkest) while this research found 206,171,148 (lightest) to 141,112,91 (darkest). Bednarek reported the Brown RGB coordinates as being 179,154,131 (lightest) to 117,98,76 (darkest), while this research found 173,132,101 (lightest) to 121,89,63 (darkest). The Light Brown category from this research was used in the above comparison, as it corresponded better than either the Medium or Dark Brown categories.

The difference between RGB coordinates reported by Bednarek (2003) and those reported in this research were most likely due to differences between the optical device

conditions for acquiring the two separate sets of digital images. Generally, the coordinates reported here were darker with the exception of B for the Blonde upper limit (lightest) and R for the Brown upper limit (lightest).

### 2.3.1.2 CIE XYZ Category Allocation

The discriminant analysis involving CIE X, Y and Z as the predictor variables resulted in the lowest number of hairs correctly classed, with only 69.3% prediction accuracy. Table 2.3-2 illustrates the predicted categories (%) based on the CIE XYZ measurements.

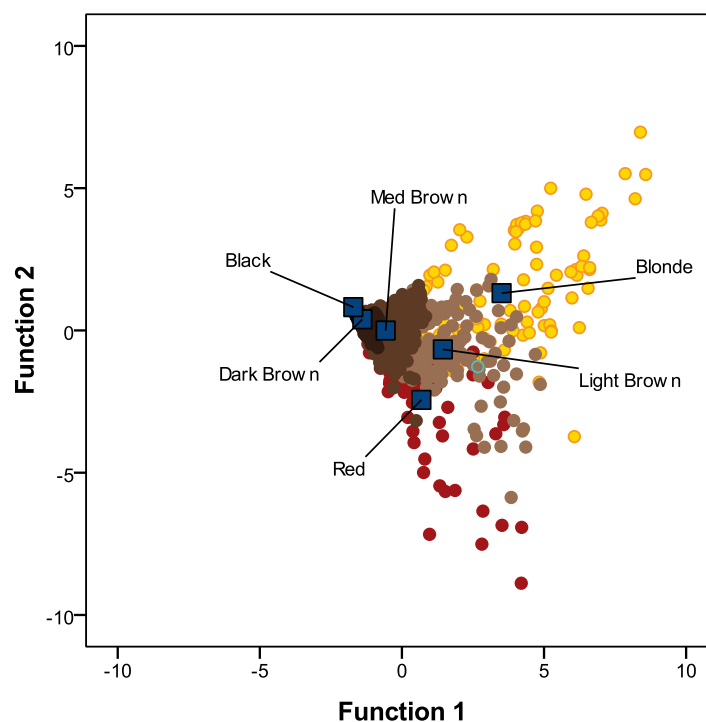
Table 2.3-2 – CIE XYZ Predicted Colour Allocation (%)

		PREDICTED						
		Blonde	Red	Light B	Med B	Dark B	Black	Total %
ORIGINAL	Blonde	58.5		25.5	16.0			100
	Red		46.5	15.5	38.0			100
	Light B	6.8	6.8	54.3	32.1			100
	Med B		0.6	0.3	96.7	2.5		100
	Dark B				34.8	65.2		100
	Black					100		100

While 96.7% of the medium brown hairs were correctly classed, a high number of hairs were also incorrectly classed as Medium Brown and all of the black hairs were incorrectly classed as Dark Brown. These results suggest that the large Medium Brown category may have overwhelmed the information in the discriminant scores due to unequal prior probability.

In addition, unlike the RGB and CIE L\*a\*b\* colour models, normality assessments for the X, Y and Z variables indicated negatively skewed distributions (see Appendix E). The majority of hairs recorded low scores when measured within the CIE XYZ colour space, while much fewer high scoring hairs were recorded. This skewness likely affected close distribution of the discriminant functions, thus decreasing prediction of group membership from those functions, particularly for the lower valued Medium Brown, Dark Brown and Black categories. Figure 2.3-2 represents discriminant scores for the CIE XYZ colour model.

For CIE XYZ, the canonical discriminant function plot was ambiguous, with little separation between group centroids, particularly for Medium Brown, Dark Brown and Black. Even for Function 1, the highest discriminant function explaining the greatest amount of variance (canonical correlation 84.2%), all the individual coefficients were low. However, similar to the RGB results (Figure 2.3-1) the variable that measured the level of red in an image (CIE X) was the strongest predictor variable, with an individual coefficient of 1.432 for Function 1. The other two variables, namely CIE Y that measured the artificial level of green plus luminescence together, and CIE Z that measured the artificial level of blue, contributed even less (-0.674 and 0.258, respectively).



**Figure 2.3-2 – CIE XYZ Canonical Discriminant Functions**

Output from *PASW* illustrates the discriminant functions that showed the greatest discrimination. The low prediction accuracy of the CIE XYZ colour model has resulted in an ambiguous plot, with little separation between group centroids, particularly for Medium Brown, Dark Brown and Black.

It was also observed that group centroids for Red, Blonde and Light Brown were again best separated along the vertical axis by Function 2. However, for the CIE XYZ colour model, the level of artificial red (CIE X) showed as the strongest predictor for both Function 1 and Function 2 (individual coefficient for Function 2, -7.731).

### 2.3.1.3 CIE L\*a\*b\* Category Allocation

The discriminant analysis involving CIE L\*, a\* and b\* as the predictor variables, resulted in the second highest number of hairs correctly classed with 75.5% prediction accuracy, almost as high as the RGB results (76.2%). Table 2.3-3 illustrates the predicted categories (%) based on the CIE L\*a\*b\* measurements. This result is consistent with previous research involving CIE L\*a\*b\* by Vaughn and colleagues (2009b) who observed prediction accuracies ranging from 51.5 to 85.8% following several discriminant analyses. Those researchers nominated six colour categories (Red, White, Fair, Light, Medium and Dark) based on reflective spectrophotometry and digital image measurements as the predictor variables.

In contrast to the CIE XYZ results where no black hairs were correctly allocated, for CIE L\*a\*b\*, Black showed the highest category allocation with 92.5% correctly classed. This was even higher than Medium Brown, the largest category, where 86.7% were correctly classed. This indicates that, similar to the RGB results, high prediction accuracy of the largest group was most likely not at the expense of the smaller groups, despite unequal prior probabilities.

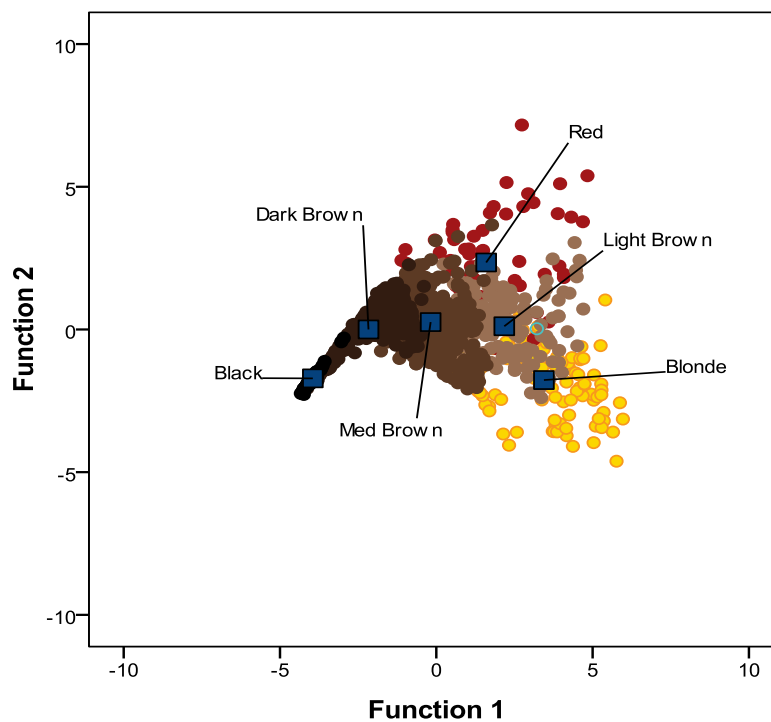
**Table 2.3-3 – CIE L\*a\*b\* Predicted Colour Allocation (%)**

		PREDICTED						
		Blonde	Red	Light B	Med B	Dark B	Black	Total %
ORIGINAL	Blonde	69.8		23.6	6.6			100
	Red		57.7	16.9	23.9	1.4		100
	Light B	13.0	3.7	59.3	24.1			100
	Med B	0.3	1.7	3.9	86.7	7.5		100
	Dark B				20.3	73.8	5.9	100
	Black					7.5	92.5	100

Figure 2.3-3 represents discriminant scores for the CIE L\*a\*b\* colour model. It was observed that group centroids for Dark Brown, Medium Brown and Light Brown were best separated by Function 1 along the horizontal axis. For this function, the CIE L\* variable, which measures the level of lightness in an image was the strongest predictor, showing the highest individual coefficient (0.977). In comparison, the two other predictor variables contributed very little to this function (-0.186 and -0.010, respectively). The

canonical correlation indicated that Function 1 explained 89.9% of the data variance. In a study on reflective spectrophotometry and the determination of skin and hair pigmentation, Shriver and Parra (2000) also observed a clear correlation between the level of luminescence measured by CIE  $L^*$  and the melanin index.

Group centroids for Red, Blonde and, again, Light Brown were best separated along the vertical axis by Function 2. The variable that measured the level of blue to yellowness in an image was the strongest predictor variable (CIE  $b^*$ ), showing a high individual coefficient (0.967). The CIE  $L^*$  variable was the second highest predictor (-0.482) for Function 2, while CIE  $a^*$ , which measures the level of green to redness, contributed very little (0.092).



**Figure 2.3-3 – CIE  $L^*a^*b^*$  Canonical Discriminant Functions**

The *PASW* canonical plot illustrates the two highest discriminant functions for the CIE  $L^*a^*b^*$  colour model. Group centroids for Dark Brown, Medium Brown and Light Brown were best separated along the horizontal axis by Function 1, whereas Red, Blonde and again Light Brown were best separated along the vertical axis by Function 2.

The individual coefficients for the CIE  $L^*a^*b^*$  results for Function 2 were consistent with those of Vaughn and colleagues (2008). Following discriminant analysis on CIE  $L^*a^*b^*$  coordinates measured by reflective spectroscopy and from digital images,

those researchers found the  $b^*$  component of colour to be the strongest predictor variable and  $L^*$  the second strongest predictor variable. Interestingly, Naysmith and colleagues (2004) found that CIE  $b^*$  also had the strongest correlation with *Mc1r*, the gene that controls the production of eumelanin and pheomelanin.

#### 2.3.1.4 Summary of Allocation to Categories (Preliminary)

Application of the three colour models resulted in between 69.3 and 76.2% correct classification of individual hairs to six colour categories. These results were similar to those reported by Barrett and colleagues (2011), who correctly classed 71% of individual hairs to four colour categories based on microspectrophotometry measurements.

Of the three colour models evaluated, RGB returned the highest prediction accuracy; albeit CIE  $L^*a^*b^*$  returned an almost similar number of correctly classed samples. Conversely, the CIE XYZ results were generally poor, comprising low prediction accuracy and an ambiguous discriminant function plot, particularly among the darker categories. Lack of separation between group centroids of the darker categories most likely affected a high number of misclassifications including, most notably, classing all the black hairs to the Dark Brown category.

Moreover, it was observed that the discriminant analysis relied on similar measurements to discriminate between two types of categories – ‘Dark’ and ‘Light’. On one side, group centroids for Black, Dark Brown, Medium Brown and Light Brown were predominantly distinguished by a single function that incorporated measures of red and luminescence in an image. Alternatively, group centroids for Light Brown, Red and Blonde were predominantly distinguished by a single function that incorporated measures of blue or blue to yellowness in an image.

Vaughn and colleagues (2008) employed log-likelihood cluster analyses that classed their population into two categories (when the number of category allocations was not dictated) based on CIE  $L^*a^*b^*$  measurements. Their results showed that one category incorporated the ‘Dark’ observer-reported hair colours Black, Dark Brown, Light Brown and the four darkest Blonde participants, while the second category incorporated the ‘Fair’ observer-reported hair colours including the remaining Blonde, Red and White participants. In later research, the same authors observed that, as the number of categories increased, the percent of individuals correctly classified decreased (Vaughn *et al.*, 2009b).

Given this observation and the fact that prediction accuracy can increase when variables showing low individual coefficients are removed (Norusis, 1985), further analyses in this research were considered.

### **2.3.2. Allocation to Categories (Secondary)**

In an effort to increase the number of correctly classed hairs, analyses were repeated that incorporated only a limited set of categories and predictor variables. Accordingly, the nominally ‘Dark’ categories were separated from the nominally ‘Light’ categories and only the strongest predictor variables for those respective categories were included in each discriminant analysis.

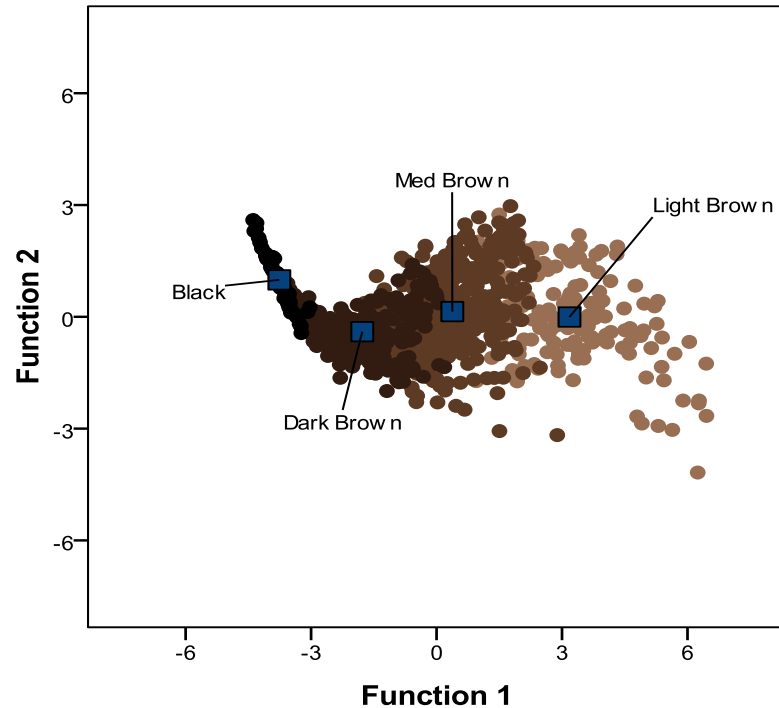
A few considerations need to be highlighted. First, preliminary results showed that the Light Brown category is discriminated from the darker brown categories along the Function 1 axes, as well as from the lighter categories along the Function 2 axes (see Figure 2.3-1 and Figure 2.3-3). Thus, while the nominally Dark and Light groups were separated, the Light Brown category was included in both analyses. Second, given the generally poor CIE XYZ results, variables from this colour model were not included further. Finally, one of the aims of this project was to evaluate which colour model provides the best statistical framework for categorising hair to one of six nominal categories; the secondary analyses do not address that aim. Rather, the secondary analysis aimed to refine and improve the preliminary results by further investigating the more significant observations.

#### **2.3.2.1 Dark Category Allocation**

One secondary analysis comprised Black, Dark Brown, Medium Brown and Light Brown hairs. Only the stronger predictor variables for these categories were included, namely, the level of red in an image measured by R (RGB) and the level of luminescence in an image measured by CIE L\*.

As a result of category and variable limitations, the prediction accuracy increased to 81.9%. The CIE L\* variable was the poorer predictor variable compared with the R (RGB) variable, showing individual coefficients of -0.033 and 1.032, respectively. Figure 2.3-4 represents discriminant scores for this analysis and shows that group centroids were well separated along the horizontal axis by Function 1.





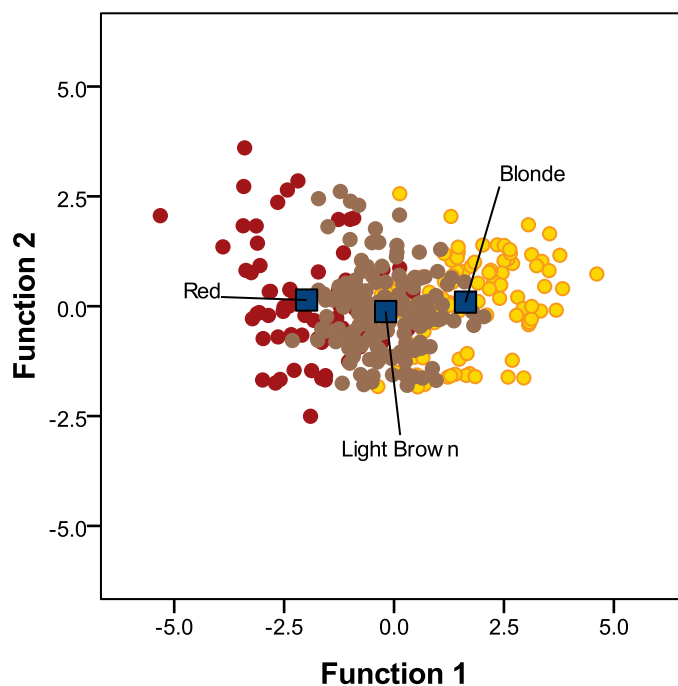
**Figure 2.3-4 – Dark Category Canonical Discriminant Functions**

Output from *PASW* illustrates the discriminant scores for the R (RGB) and L\* variables. Group centroids for Black, Dark Brown, Medium Brown and Light Brown were well separated along the horizontal axis by Function 1. However, only 81.9% of the original colour categories were correctly classified.

### 2.3.2.2 Light Category Allocation

The other secondary analysis was limited to Light Brown, Red and Blonde classed hairs. Again, only the stronger predictor variables for these categories were included, namely the level of blue in an image measured by B (RGB) and the level of blue to yellow in an image measured by CIE b\*.

Prediction accuracy for this analyses remained at only 74.4%. The level of blue in an image (B) was the slightly stronger predictor variable compared with the measurement of blue to yellow in an image (CIE b\*), both showing individual moderate coefficients of 0.786 and -0.598, respectively. As these two variables measured the same colour attribute in part, equivalent predicting strength was expected. Figure 2.3-5 represents the discriminant scores for this analysis and shows that group centroids for the lighter categories were best separated along the horizontal axis by Function 1.



**Figure 2.3-5 – Light Category Canonical Discriminant Functions**

Output from *PASW* illustrates the discriminant scores for the B (RGB) and  $b^*$  variables. Group centroids for Red, Light Brown and Blonde were best separated along the horizontal axis by Function 1. However, only 74.4% of the original colour categories were correctly classed.

### 2.3.2.3 Summary of Allocation to Categories (Secondary)

Secondary analyses were conducted to decrease the misclassification rate resulting from the preliminary research, though only the more significant observations were investigated further. As prediction accuracy can increase when variables showing low individual coefficients are removed, the data was separated to reflect either nominally Dark or nominally Light categories with analysis limited to only the strongest predicting variables for each respective dataset. As a result, prediction accuracy increased slightly for the nominally ‘dark’ categories while no improvement was observed for the nominally ‘light’ categories.

Overall, statistically moderate prediction accuracies resulted and alternative methods would need to be considered so that a statistical model with greater discrimination between colours can be developed. The applied method would obviously not increase the value of evidence in court; however, it could still find a useful role for training purposes or during the evidence triage process to assist non-experienced hair examiners or scene of crime officers with base level colour assignment.

### 2.3.3. Main Source of Variance

Prior to attempting to allocate individual hairs to the correct participant, mixed-model ANOVA was used to confirm that the main source of variance in the sample population was ‘between participants’. This range of variation is the foundation on which microscopic hair examinations involving colour comparisons rely. Table 2.3-4 illustrates the variance (%) for each factor under investigation. Rows indicate the colour components; columns indicate the variance (%) each factor contributes to the overall variance. Statistically, the overall variance is the standard deviation squared.

Table 2.3-4 – Source of Variance for Sample Population

SOURCE OF VARIANCE				
COLOUR COMPONENT	Within Hair (%)	Within Participants (%)	Between Participants (%)	Overall Variance* (Std Dev <sup>2</sup> )
	R	3.17	16.26	80.90
G	3.84	18.73	77.84	1832
B	4.79	21.80	74.55	1385
CIE L*	3.68	18.11	80.34	337.5
CIE a*	7.90	27.32	69.62	15.55
CIE b*	6.58	23.97	73.19	46.89

\*Overall variance (std dev<sup>2</sup>) is measured in the same units as the original measurement.

The results for all the dependent variables analysed (R, G, B, CIE L\*, a\* and b\*) confirmed that the main source of variance was indeed ‘between participants’ and the least source of variance was within the individual hair strand. This was in contrast to observations by Birngruber and colleagues (2009) who reported extreme intra-individual variability in the colour of individual hairs. Based on results from this research, the view that numerical colour measurements can be used to distinguish between each participants’ hair colour was supported.

### 2.3.4. Allocation to Participants

Canonical discriminant analysis was used to allocate individual hairs to participants, within a population of similar hair colour. The analyses were performed separately for each of the three colour models and for each of the subpopulations.

It was clear from the results that prediction accuracy was largely affected by the sample population. A number of participant samples were dispersed across more than one nominal colour category. For example, a person who self-reported their natural hair colour as ‘Medium Brown’ often had a few hairs from their ten hair sample set in the ‘Light Brown’ and/ or ‘Dark Brown’ categories. Therefore, within any given subpopulation, a participant (grouping variable) could have anywhere between one and ten hairs. That said, in forensic casework situations would arise whereby varying numbers of hairs belonging to multiple individuals may need to be distinguished. This condition most likely affected the prediction accuracy and, similar to the analyses involving allocation of hairs to categories, unequal prior probability of belonging to a participant was assumed.

#### 2.3.4.1 Predicted Participant Allocation

Table 2.3-5 summarises the prediction accuracy of each colour model for the allocation of a hair to the correct participant. For each subpopulation, the number of hairs in the sample is displayed while the colour model with the highest prediction accuracy for each population is shaded.

**Table 2.3-5 – Summary of Prediction Accuracy**

	<b>RGB</b>	<b>CIE XYZ</b>	<b>CIE L*a*b*</b>
<b>Blonde</b> (n = 106)	58.5	43.4	59.4
<b>Red</b> (n = 71)	80.3	69.0	76.1
<b>Light Brown</b> (n = 162)	45.4	37.4	46.0
<b>Medium Brown</b> (n = 361)	36.0	11.1	34.6
<b>Dark Brown</b> (n = 256)	34.4	15.2	25.4
<b>Black</b> (n = 53)	45.3	54.7	56.6

Similar to the category allocation results, the RGB and CIE L\*a\*b\* colour models performed better overall than the CIE XYZ colour model, with the former models equally returning the highest prediction accuracies for three out of the six subpopulations analysed.

Conversely, CIE XYZ had the lowest prediction accuracy for almost all the subpopulations, with the exception of ‘Black’. For this category, CIE XYZ was able to

correctly class hairs to their participants in 54.7% of cases, which was higher than the RGB result of 45.3% correctly classed. This result was unexpected, given that, in the previous category allocation results, CIE XYZ was unable to discriminate between the darker hairs, with 34.8% of the Dark Brown category misclassified as Medium Brown and all of the Black hairs misclassified as Dark Brown (see 2.3.1.2 CIE XYZ Category Allocation)!

#### 2.3.4.2 Summary of Allocation to Participants

Bednarek (2003) was able to assign 91 of 100 hair samples to the correct participant based on intensity coordinates determined by the RGB colour model system, but was only able to assign 74 of 100 hair samples to the correct participant based on the Ogle and Fox method of measuring hair against colour standards (see Ogle & Fox, 1999). Though correct classification was not as high as Bednarek (2003), Brooks and colleagues (2011) also observed higher results than those observed in the current research, based on ten brown hair samples for each of ten participants. Those researchers reported 64% correct classification based on intensity coordinates determined by the RGB colour model, 68% correct classification using the CIE XYZ colour model and 58% correct classification using the CIE L\*a\*b\* colour model.

Aside from the Red category that returned moderate results between 69.0 and 80.3% prediction accuracy, the results in this research were generally too low for the method to be considered a routine tool in forensic hair examination. These results were analogous to those of Barrett and colleagues (2011) who found that the microspectrophotometry technique was not able to successfully discriminate between 25 natural hair samples, with only 22% of participant hair correctly classed. Birngruber and colleagues (2009) also concluded that it was not possible to provide identification using a compound light microscope and the spectral imaging device *SpectraCube*<sup>®</sup> based solely on the colour of a single hair. Finally, even though the application of the statistical methods in their research were questioned here, Vaughn and colleagues (2009b) also concluded that the digital imaging method (macroscopic) was inaccurate and inconsistent, and thus of limited use in forensic science.

### 2.3.5. Discriminative Analysis Considerations

A number of reasons were considered for why the predictive analyses were of limited value when applied to the discrimination of hair colour. Primary among those was that colour models describe a certain number of specific attributes that combine to produce a ‘colour’ that is, essentially, a visual experience dependant on the human observer for description. The Wilks’ lambda stepwise method was chosen for this research, as there was no reason for assigning one colour component a higher priority than the other two, for any given colour model. However, with any stepwise method, it is solely the statistical criterion that are used to determine the order of entry of predictor variables into the discriminant model (Tabachnick & Fidell, 2001) while the meaning or interpretation of the predictor variables is not relevant. Incorporating subjective observer–reported colours to facilitate the allocation of categories to overcome this drawback subsequently decreased the prediction accuracy rates.

Moreover, discriminant analyses focus on linear relationships. The goal of the analyses in this research was therefore to find the *linear* combination of values of the colour model components that best separate one hair colour from the other hair colours or that best separate the hair of one participant from the hair of other participants. If a *non-linear* relationship between the individual components of a particular colour model existed, it would not have been represented by the discriminant model. For example, when distinguishing a population of medium brown hairs from a population of dark brown hairs, it would be assumed that all hairs in the latter population have equivalently lower scores for all three components measured. It is just as likely that only one or two lower scores affect the overall human perception of darker hair rather than all three components uniformly.

Finally, correct classification can also be affected by departures from homogeneity of the covariance matrix. Box Ms produced by *PASW* were used to test this assumption however, the test is notoriously sensitive and small observed significance levels, especially for large sample sizes, can be ignored (Norusis, 2008; Kinnear & Gray, 2010) as was the case here. Therefore, if the covariance matrix of the predictor variables was not the same for each colour category population, this could additionally explain why the predictive models were of limited value when applied to the discrimination of hair colour

Alternative statistical methods should be considered in order to develop a model that shows greater discrimination between colours. Colour categories need to reflect the human perception of colour yet equally correspond to differences between the numerical coordinates that are measured. The predictive statistical tests applied in this research so far do not have the high discriminating power that is required for a continuous variable such as hair colour. Furthermore, while this research compared three colour models, there is some colour visible to the human eye that is located outside the sRGB colour gamut. This constriction may have limited the potential of this part of the research and a wider RGB gamut, such as Adobe RGB, may have been a better choice.

### 2.3.6. Colour Comparison between Two Samples

The following analyses were designed to investigate whether numerical measurements could assist the experienced forensic hair examiner with colour comparisons. Specifically, confidence intervals were used here to determine whether numerical colour measurements could aid the examiner with comparisons between the individual, questioned hair and a sample from a known source. In the previous discriminant analyses, colour model measurements were considered collectively as multivariate components. For the probability distributions utilised here, the measurements were analysed as individual variables regardless of the overall colour perceived by an observer; that is, the variables were tested on a purely numerical basis. The results below pertain to a hypothetical examination policy declaring that:

- Values within the 95% confidence intervals ( $\alpha = 0.05$ ) for R, G and B measurements are similar in colour

Thus, we would state a similar colour on 95% of occasions when the hair samples were actually from the same source but we would be wrong on 5.0% of those occasions. A greater level of significance (e.g.,  $\alpha = 0.01$ ) could be selected.

The sample standard deviation can be substituted for the unknown population standard deviation as long as the sample size is greater than 30. Given that only ten hairs from each known sample population were obtained (albeit, triplicate measures per hair were included), the analyses were limited to a demonstration for potential future work that could assist the experienced forensic examiner with colour comparisons between a question and known source.

### 2.3.6.1 Individual, Questioned Hair

Figure 2.3-6 displays a montage from the hair selected to represent an individual, questioned hair. The triplicate measures acquired from that individual hair were found to have a mean R value of 86.3, a mean G value of 59.2, and a mean B value of 40.4.



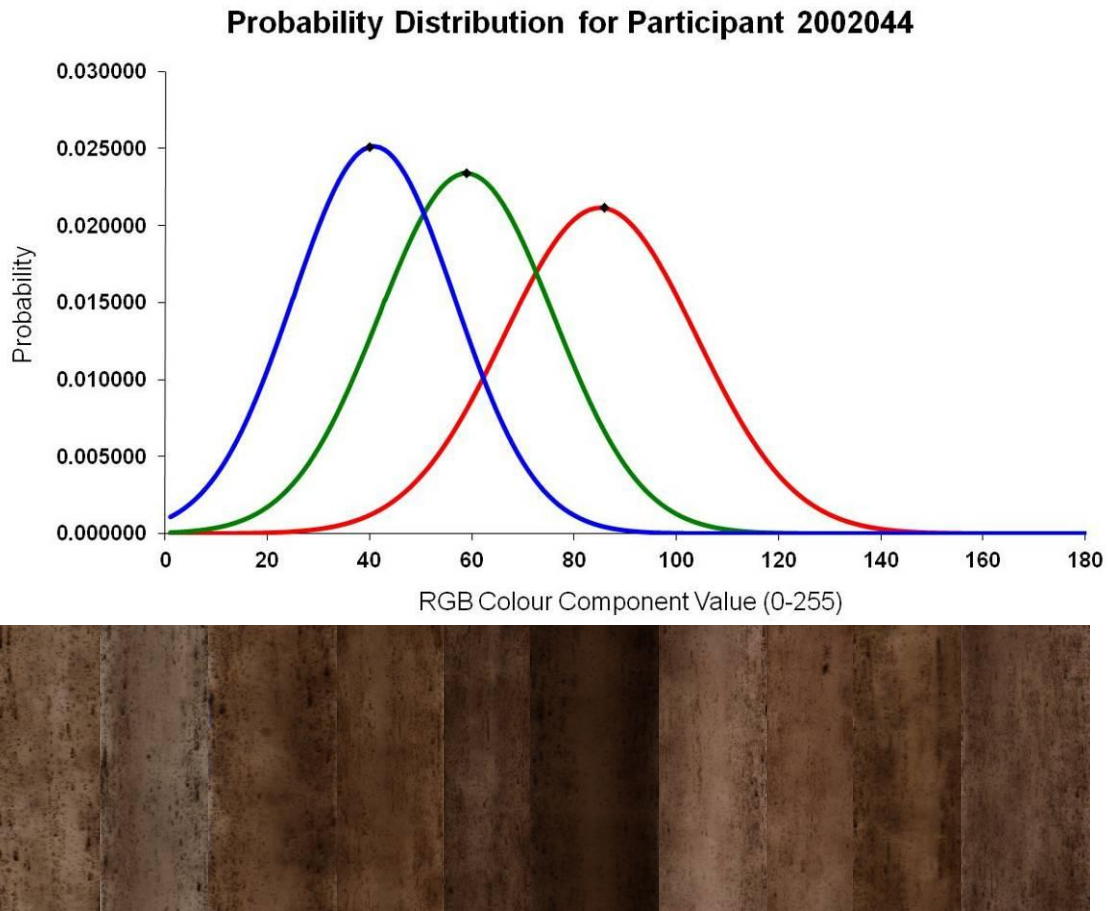
**Figure 2.3-6 –Montage Representing a Individual, Questioned Hair**

One of the three montage images acquired from the hair selected to represent the individual, questioned hair.

### 2.3.6.2 Known Participant 2002044

Triplicate measures acquired from ten hairs belonging to Participant 2002044 were found to have an overall mean R value of 85.1 and standard deviation of 18.8, a mean G value of 58.9 and standard deviation of 17.0 and a mean B value of 40.8 and standard deviation of 15.9. The probability distribution curves derived from those measures of central tendency are displayed in Figure 2.3-7. Generally, each distribution reflects the variation in Participant 2002044's hair colour and the probability of observing those measurements in hair samples from that participant. The distributions include a mark (♦) indicating the point where the individual, questioned hair mean values were located. Figure 2.3-7 also displays a series of ten montage images selected at random from the ten hairs belonging to Participant 2002044 to visually illustrate the hair colour variation represented in the distributions.





**Figure 2.3-7 – Probability Distribution and Colour Variation of Participant 2002044**

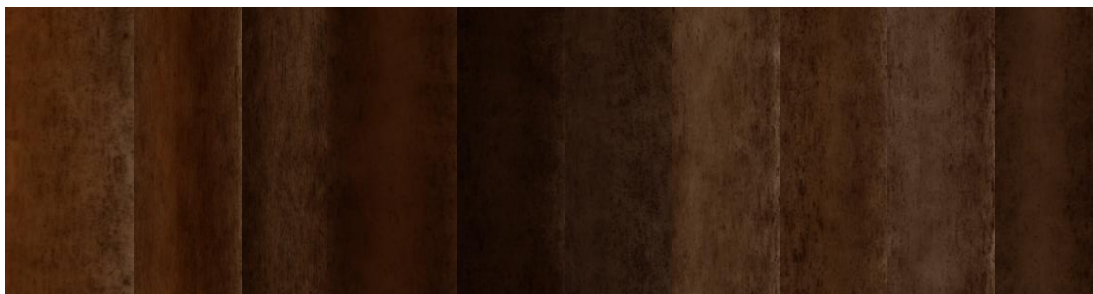
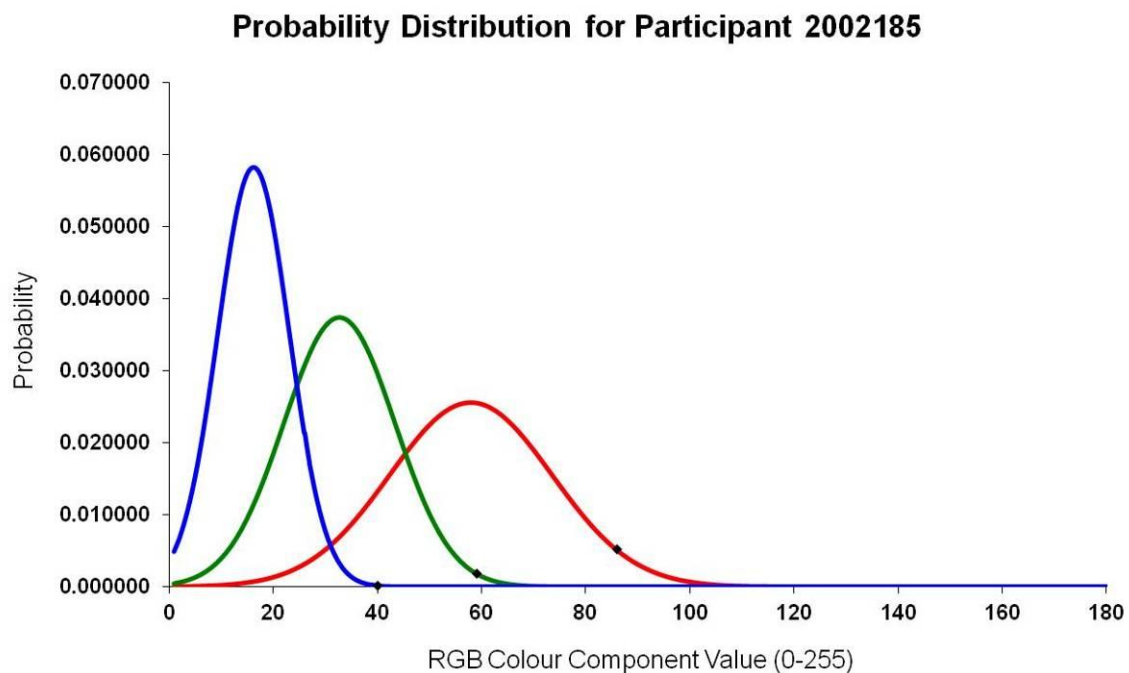
(Top) Probability distribution curves derived from the R, G and B mean and standard deviations for participant 2002044. A mark (♦) along each curve indicates the point where the individual, questioned hair mean values were located. (Bottom) A series of ten montages randomly selected from the ten hairs belonging to known participant 2002044, to illustrate that participant's hair colour variation.

If the individual, questioned hair did indeed come from Participant 2002044, the measured R, G and B variables would be expected to lie near the distribution centres and would have a probability of less than 5% of laying more than 1.96 standard deviations away. For each measured variable, the questioned hair was very close to the sample mean for Participant 2002044 and hence fell within the 95% confidence intervals. Thus, differences between the colour of the questioned hair and that of Participant 2002044 could be explained by chance due to the range of variability in the participant's hair.

### 2.3.6.3 Known Participant 2002185

Participant 2002185 was found to have an overall mean R value of 58.0 and standard deviation of 15.6, a mean G value of 32.8 and standard deviation of 10.7 and a

mean B value of 16.3 and standard deviation of 6.86. The probability distribution curves derived from those measures of central tendencies are displayed in Figure 2.3-8. A mark (♦) along each curve indicates the point where the questioned hair mean values were located. Figure 2.3-8 also displays a series of ten montage images belonging to Participant 2002185 to illustrate their hair colour variation.



**Figure 2.3-8 – Probability Distribution and Colour Variation of Participant 2002185**

(Top) Probability distribution curves derived from the R, G and B mean and standard deviations for participant 2002185. A mark (♦) along each curve indicates the point where the individual, questioned hair mean values were located. (Bottom) A series of ten montages randomly selected from the ten hairs belonging to known participant 2002185, to illustrate that participant’s hair colour variation.

For each measured variable, the questioned hair was lighter than the sample mean for Participant 2002185. For R, the individual, questioned hair fell just within the 95% confidence interval but for G and B the individual, questioned hair fell outside -1.96 and +1.96 standard deviations of the mean. That is, there was a 95% probability of obtaining a

smaller difference in colour (i.e., a more similar colour) if the questioned hair was indeed from Participant 2002185. The differences in colour were so great they were unlikely to have occurred by chance, had the questioned hair actually come from this participant.

### 2.3.6.1 Comparison to another Individual Hair

A forensic hair examiner not only compares an individual, questioned hair to a range of hairs from a known source but also to other individual hairs from the known source. For a comparison between an individual, questioned hair and an individual, known hair it would be unreasonable for an examiner to acquire 30 image acquisitions from either of the single hair strands. Therefore, 95% confidence intervals determined from probability distribution curves should not be applied for such comparisons.

For an examiner to make numerical colour assessments and draw comparisons between two individual hairs, the best method would at least require replicate measurements from both samples. The National Association of Testing Authorities (NATA) (2009) recommend seven replicate measurements for the evaluation of measurement uncertainty and/or bias. However, similar to other research on hair colour (Shriver & Parra, 2000; Naysmith *et al.*, 2004), triplicate measures from each hair were obtained here, so the following is again provided as a demonstration for future work only. Figure 2.3-9 displays two montages from hairs selected to represent the individual, questioned hair (top) and an individual, known hair from Participant 2002044 (bottom).



**Figure 2.3-9 – Montages Representing a Question and Known Comparison Hair**

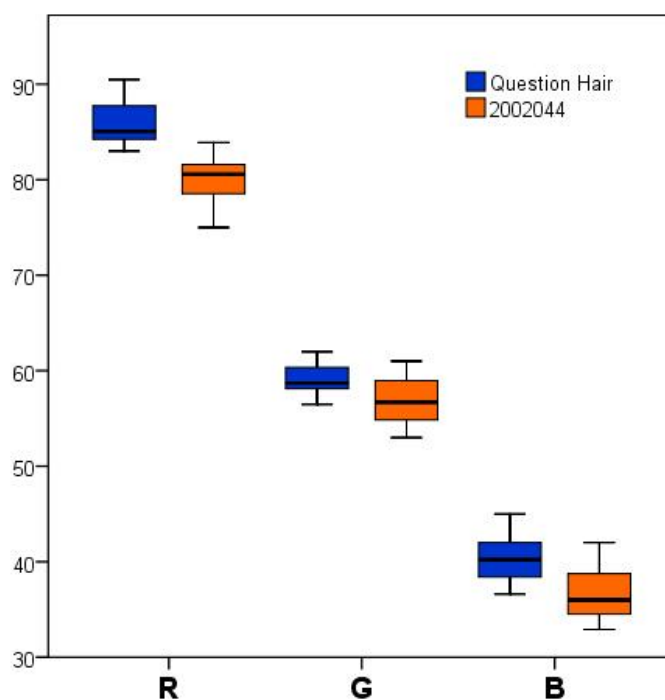
Two montages from hairs selected to represent the individual, questioned hair (top) and an individual, known hair from Participant 2002044 (bottom).

Seven theoretical measurements from each hair were determined to have the mean, upper and lower R, G and B measurements provided in Table 2.3-6. The theoretical

replicate measurements were best represented visually using box-plots, as illustrated in Figure 2.3-10.

**Table 2.3-6 – RGB Values of an Individual, Questioned hair and a Comparison Hair**

	Measurement	Lower Value	Mean	Upper Value
<b>Individual, Questioned hair</b>	R	83.0	86.3	90.5
	G	56.5	59.2	62.1
	B	36.6	40.4	45.5
<b>Participant 2002044</b>	R	75.0	80.0	83.9
	G	53.2	56.9	61.3
	B	32.9	36.8	42.1



**Figure 2.3-10 – Box Plots of Mean, Upper and Lower RGB Measurements**

Box plots providing a visual representation of the mean, upper and lower RGB measurements calculated from seven montage images acquired from an individual, questioned hair and a comparison hair selected from known participant 2002044.

Measurement for the questioned hair were within the same (partial) range as the replicate measures for the comparison hair from Participant 2002044 for the G and B variables only. For the R variable, the lower quartile for the questioned hair was within the same range as the upper quartile for Participant 2002044.

### 2.3.7. Confidence Interval Considerations

These analyses were designed to emulate the forensic hair examination process and investigate whether numerical colour measurements could assist the experienced microscopist, post-triage with colour comparisons between question and known sources. In the first analyses, an individual, questioned hair was compared to two known participant samples. As observed, the mean R, G and B measurements from the three montage images acquired from the questioned hair, fell within the 95% confidence intervals for Participant 2002044. Typically, at this point the examiner would need to consider the odds against obtaining the result by chance if the samples did not come from the same source. This would involve assessing the frequency of hair colours occurring at random from sources other than the comparable participants. These data were outside the scope of the project as a stratified sampling approach was chosen and not a random sampling approach that would be required to obtain frequency information pertaining to the true population.

That said, the role of the forensic hair examiner is to determine whether a questioned hair should be included or excluded as probative evidence and this decision is based on the degree of difference assessed between the question and known samples. The hair examination and comparison process follows defined protocols established by the forensic community and includes an assessment of not only colour, but also length, shaft profile (curly, straight), diameter (fine, coarse), root type, hair tip shape (taper, cut), any treatment or disease condition, pigmentation patterns (distribution, aggregation, density), cortical features, cuticle features and medullar characteristics (Brooks, 2007). Thus, while the follow-up analyses presented may not provide the experienced forensic examiner with information on hair colour frequency and probability in the true population, they could still assist with exclusion of samples at the preliminary stages of the examination and comparison process, given the number of other characteristics that are considered by an examiner.

Following the assessment of multiple hairs from the known source, seven replicate measurements from individual hairs could be obtained in order to determine the mean, upper and lower colour boundaries of a given sample. An examiner, who observes little difference in colour between a questioned hair and a known hair, could use numerical colour assessments to present that observation as inclusionary or exclusionary evidence.

## 2.4. Conclusion

A number of researchers have investigated the application of numerical colour measurements for the forensic examination of human hair. A common statistical approach, including the initial approach taken in this research, involved the application of discriminant analyses – specifically, cluster and canonical discriminant analyses – for the purpose of allocating nominal colour classifications such as ‘Brown’ and ‘Blonde’ to a given hair sample (see Vaughn *et al.*, 2008; Vaughn *et al.*, 2009b; Barrett *et al.*, 2011; Brooks *et al.*, 2011). Based on that approach, correct classification of individual hairs to six nominal categories resulted in a statistically moderate overall prediction accuracy for the RGB and CIE L\*a\*b\* colour models. The rate of misclassification associated with the statistical model, was too high to provide any useful application for court reporting purposes. This statistical approach is therefore only recommended for training new forensic hair examiners or for the evidence triage process to assist inexperienced hair examiners or scene of crime officers with the initial processing of multiple questioned hairs or bulk samples.

Conversely, correct classification of multiple individual hairs to the correct participant in a subpopulation of similarly coloured hairs generally resulted in statistically low overall prediction accuracy. This statistical model would therefore not be recommended for the purpose investigated. A number of reasons were considered for why the discriminant analyses applied, were of limited value when applied to the discrimination of hair colour. Primary among those was that general colour categories that reflect the human perception of colour do not equally correspond to differences between the numerical coordinates tested by the applied statistic. In order for numerical measurements to assist the experienced forensic hair examiner, it is recommended that future research consider the colour components as individual variables, similar to the approach taken by Bednarek (2003) and the follow-up approach applied in this research. Further investigations involving confidence intervals for the comparison of numerical hair colour measurements are therefore recommended. Moreover, while comparisons in this research involved three colour models, a wider RGB gamut such as Adobe RGB may have been a preferable option and would also be recommended for research of this kind undertaken.

## Chapter 3. PIGMENTATION

---

### **3.1. Introduction**

#### **3.1.1. Hair Colour**

Natural hair colour is a consequence of the amount and type of pigmentation located within the keratinocytes of the hair shaft. In human hair, the pigment ‘melanin’ occurs as two types—eumelanin, a black–brown pigment, and phaemelanin, a yellow–red pigment (Jimbow *et al.*, 1983; Robins, 1991; Ito & Wakamatsu, 2003; Rees, 2003). Research by Jimbow and colleagues (1983) involving red hair participants suggests that pure eumelanin or pure phaemelanin seldom exists in mammals. Rather, the majority of melanin present in hair and skin are heteropolymers, comprising varying proportions of both eumelanin and phaemelanin (Ito & Wakamatsu, 2003).

Natural hair colour is also influenced by the number, size and density of the melanin granules. Darker hair colour is correlated with increasing pigmentation and therefore increasing light absorption, while white hair that has no melanin, reflects almost all incident light (Robins, 1991; Rees, 2003). Hair colour will also vary over time and at different somatic areas. As noted by Rees (2003), an individual with a red beard or red pubic hair may simultaneously have black head hair; while children with blonde hair can grow to have brown hair during adolescence then white hair in old age (Tobin & Paus, 2001).

#### **3.1.2. Melanogenesis and Pigment Patterns**

Routine forensic hair examinations typically begin with a detailed microscopic evaluation of each hair, followed by a side–by–side comparison between the unknown and exemplar hair samples. Morphological patterns or trends are often apparent throughout the length of the shaft and may be recognised in hairs from the same or different sources (Verma *et al.*, 2002). Melanin is synthesised by a specific dendrite cell known as the melanocyte, that makes contact with the surrounding keratinocytes into which they discharge the melanin containing melanosomes (Robins, 1991). It is these individual pigment features of the keratinocytes that combine to form trends or patterns along the hair shaft.

In the hair bulb, melanocytes are confronted with seven potential targets for pigmentation – three types of hair cells, three types of inner root sheath cells, and the



undifferentiated cells of the hair matrix (Weiner *et al.*, 2007). Yet, pigment is transferred to only two types of precursor cells, being those of the cortex predominately and, to a lesser extent, the medulla (Tobin *et al.*, 1999; Weiner *et al.*, 2007). One melanocyte donates melanin to between 20 and 40 surrounding keratinocytes (Robins, 1991). Once transferred, the granules arrange into one of two configurations depending on their size—large granules arrange into non-aggregated configurations whereby they remain as single particles, while small granules group within membrane-bound vesicles (Robins, 1991). Recent studies indicate that keratinocytes don't just receive melanin, they influence and regulate melanocyte behaviour as well. Weiner and colleagues (2007) describe a mechanism whereby specific pigment-recipient cells provide the blueprint that instructs the melanocytes on where to place pigment. To summarise their findings, the *Foxn1* gene (Whn, Hfh11) confers special properties on a cell, allowing the cell to emit signals that are recognised by melanocytes. The melanocytes then connect to the target cells via dendrites and transfer the melanin granules.

Studies on mice have indicated that at least 150 genes at over 50 loci control eye, skin and hair colour by regulating such features as melanoblast development and melanin size, shape and transfer processes (Robins, 1991). Thus, a clear relationship exists between genotype and hair melanin content, and between melanin content and the patterns they form.

Typical production of a pigmented human hair shaft lasts as long as the anagen hair cycle—many years duration—demonstrating the phenomenal synthesising capacity of melanocytes (Tobin *et al.*, 1999). During youth, a small number of melanocytes have the potential to produce sufficient melanin pigment for up to 1.5 m of hair, in a single hair growth cycle (Tobin *et al.*, 1999; Tobin & Paus, 2001). The complex process is regulated by a series of enzymes, proteins, transporters, receptors and ligands that act on the development, cellular and hair follicle levels (Slominski *et al.*, 2005). The early anagen cycle coincides with melanocyte proliferation, while in late anagen, melanocytes retract their dendrites, reduce melanogenesis and disappear from the follicular epithelium (Tobin & Paus, 2001).

The cessation of melanogenesis towards the end of the anagen cycle results in the pigment-free proximal ends that are observed in telogen hairs (Tobin *et al.*, 1999; Weiner *et al.*, 2007). In early catagen, Langerhans cells may remove pigment from the regressing

hair matrix to the dermal papilla (Tobin *et al.*, 1999). The non-pigmented area directly above the root of telogen hairs may also contain numerous cortical fusi, being air bubbles trapped in the cortex of the hair (Houck & Bisbing, 2005).

### 3.1.3. Research on Hair Pigmentation

Significant biological differences are reflected by the melanogenesis process, producing a range of inter- and intra-individual variation (Verma *et al.*, 2002). The most variable pigmentation patterns are observed in head hairs, while pubic hairs offer slightly less variation (Smith & Linch, 1999). The density of pigment granules in hair from four races of men, namely Western European, Asiatic Indian, Chinese and Negroid were evaluated by Vernall (1963). The study determined that although cortex pigment granules within an individual hair section appear to be relatively uniform in size, shape and colour, their frequency and distribution varied considerably, decreasing from the peripheral to the innermost area. In addition to variations within hair, pronounced differences were also observed in colour and pigmentation density among hairs from the same individual. However, significantly greater variances were observed between participants within each racial group and were greater still between participants from different racial groups. Later, a separate study on the identification of Polynesian head hair based on hair index and cross-sectional area, found that homogeneity for any racial trait is rare, as there is a wide range of variation within every genetic population (Kerley & Rosen, 1973). The latter study also observed the range of variation within a sample from the same individual and cautioned that several hairs should be sampled from participants in such studies rather than only one or two.

These early papers on racial identification by Vernall (1963) and Kerley & Rosen (1973) demonstrate a reality that can complicate forensic hair examination when only a single or few questioned hairs are recovered from a crime scene. That is, no two hairs will possess indistinguishable features along their entire length—even two hairs belonging to the same individual—making definitive association to a single source impossible. It is the forensic examiner's goal to recognise a pigment pattern in the questioned hair that is representative of the pattern found in the exemplar set (Gaudette, 1999; Smith & Linch, 1999). While one or two hairs may not represent the full range of pigment pattern variation of the individual when several questioned hairs are available, the unique intra-individual variation that occurs over the head can strengthen an examiner's finding of association

(Bisbing & Wolner, 1984). Where possible, a sufficient hair exemplar should not only aim to adequately represent the pigment pattern variation, but also to possess intact roots, represent anagen and telogen phases, and be collected as soon after the event as possible (Smith & Linch, 1999). It is recommended that approximately 40 head hairs and 20 pubic hairs be collected (Smith & Linch, 1999).

#### 3.1.4. Quantification of Pigmentation

A further complication encountered during forensic examinations is that, although differences between pigmentation may be visually observed, such differences can resist quantification. A number of studies involving numerical measures of hair have been reported; however, the methods described rarely involve pigmentation or their derived patterns. Verma and colleagues (2002) describe an automated Hair-MAP system that involves a digitised evaluation of microscopic images for medulla type, cuticle texture and shaft diameter that then undergo multivariate analysis to indicate whether two hairs were from the same source (Verma *et al.*, 2002). Hair-MAP was used to image, segment and extract five common characteristic values found across the hair samples from 25 hairs of nine participants; accurate hair associations were returned 83% of the time (Verma *et al.*, 2002). Sato (2003) investigated hair form using indices derived from hair length, distance and area, obtained by image analysis of the hairs of eight Japanese males. Following statistical analysis (t-test and stepwise linear discriminant analysis), six values were derived that showed larger inter-individual variation than intra-individual variation (Sato, 2003). Based on this preliminary study, the author proposed that numerical data obtained from image analysis is important for constructing an objective screening procedure for evidential hairs (Sato, 2003). Ball and colleagues (2002) used image analysis to determine whether morphological differences could be demonstrated between head hair from 26 Egyptian mummies and 35 living Caucasoid and Oriental individuals. An image analyser was used to scan images that were then measured in respect of hair area, perimeter, length, breadth, width and radius, and analysed using multivariate and discriminate analysis (ANOVA, Tukey HSD multiple comparison tests and discriminant analysis). The authors concluded that there were significant morphometric differences between head hair from different races and from different genders within the same race.

Brooks (2007), however, described a digital analysis method for analysing pigment patterns along the hair shaft. To summarise that research, colour montage images from hair

shafts were converted to monochrome to ensure that only single values were generated per pixel position (x, y) in the range 0–255, rather than three sets of values for red, green and blue. Applying V++ Digital Optics software, a small area representing pigmentation along the shaft was extracted from a single montage. The representative extract was then measured against the patterns of the entire image of an area of the hair shaft. The V++ algorithms were designed to subtract the value (0–255) of each individual pixel within the extract, from the pixel values (0–255) within the comparison image, by successively examining along the x-axis. A value was produced that reflects the mean degree of “mismatch” between pixels—zero represents a perfect match while 75–255 represents a high degree of mismatch. Inter- and intra-individual pigment pattern variations could then be statistically determined. Using samples from ten brown-haired participants, the research resulted in two main outcomes: first, it showed that it was technically possible to develop an objective set of hair colour coordinates (previously described); and second, it showed that confidence intervals and probability inferences could be assessed for pigment characteristics using pattern recognition data (Brooks, 2007).

### **3.1.5. Research Focus**

Forensic hair examinations involve a detailed microscopic evaluation as well as a side-by-side comparison between the unknown and exemplar hairs. A sufficient hair exemplar aims to adequately represent the pigment variation, as morphological patterns or trends are often apparent throughout the length of the shaft and may be recognised in hairs from the same source, given the relationship between genotype and hair melanin content. However, while pigmentation may be visually observed, such differences resist quantification. The research focus of this chapter therefore involved assigning numerical values to hair pigmentation.

As few studies have been conducted in this area, these preliminary analyses were designed to measure hair pigment morphology in terms of density, size and shape, as represented by pixel variations in montage digital images. Two pigmentation pattern analyses were evaluated in the preliminary stages of this research, including the automated V++ script described by Brooks (2007) and a novel analysis. Following this evaluation, Analysis of Variance (ANOVA) was used to determine whether the morphological trends and unique intra-individual variations that are often observed by examiners, could be quantified by the selected analyses and if so, whether the highest measured variance in the

sample population tested was ‘between participants’ (inter-individual). Discriminant analysis was then used to investigate whether pigmentation measurements in respect of density, size and shape, can discriminate between participants with similar shaded hair based on the selected analyses.

## 3.2. Materials and Method

### 3.2.1. Preliminary Evaluation – Sample Preparation

In the preliminary stages of the method design, two pigmentation pattern analyses were evaluated. One analysis was based on the method described by Brooks (2007) (Analysis 1) and the second analysis was based on a novel method (Analysis 2). Three montage images were acquired for each of the ten hairs provided by 154 participants, comprising males and females aged between 18 and 65 years. The images were acquired on the *DM6000*, as 1392 x 1040 pixels (full-frame HQ) and were saved as TIFF files (montage acquisition is described in detail in 2.2.1 Sample Preparation). Not all images were used in this part of the research due to the complexity of data preparation involved. Therefore, three separate hair populations were compared—Fair, Medium and Dark shaded hair—and, within each population, one montage from each of ten hairs from five representative participants was selected.

Pigmentation observed within the montage images were measured using Digital Optics *V++ Precision digital imaging software*, version 5.0 (*Digital Optics Limited*, Auckland, New Zealand). Images for Analysis 1 and Analysis 2 were normalised prior to the pigmentation measurements. Normalisation involved first using the *V++ Geometry* function to align each image so that the hair appeared horizontal across the monitor. As the angle of rotation varied for each montage and the image boundary was not enlarged during the process, the final normalised images differed markedly in size. From this point onwards, images for Analysis 1 and Analysis 2 were prepared differently.

#### 3.2.1.1 Analysis 1




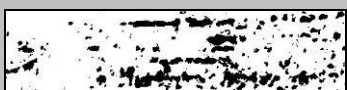





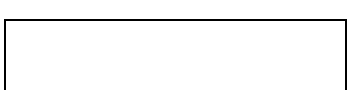


For Analysis 1, each montage was transformed to a greyscale image using the *V++ Colour Intensity* function. Thus, each pixel in the image array was associated with a single intensity value on a scale from black (0) to white (255), instead of the three intensity values that are typically associated with colour digital images. The entire greyscale image was also cropped to 781 pixels in height (y) using the *Region of Interest (ROI) V++* function to map a boundary rectangle. A small area representing pigmentation along the hair shaft was extracted from each greyscale image using the *ROI* function. The height (y) of the two images had to be the same pixel length for the analysis to precede therefore each

extract was also 781 pixels in height. The entire image and the extract were saved as a new TIFF file for analysis.

### 3.2.1.2 Analysis 2

For Analysis 2, a small area representing pigmentation along the hair shaft was extracted from each montage using the *V++* ROI function to map a boundary rectangle of 120 x 500 pixels in size. A threshold operation was then applied to each image depending on the general shade of the hair. Thresholding transforms an image to binary by converting all the pixels above the threshold level to 1 (white) and all the pixels below the threshold level to 0 (black) (Digital Optics Ltd., 2009). Determining the correct threshold level is critical. The array of pixels in an image of dark hair would comprise mostly low values therefore Dark images transformed at a high threshold level would appear almost black. Conversely, the array of pixels in an image of fair hair would comprise mostly high values so lighter images transformed at a low threshold level would appear almost white. The application of various threshold levels to images of three shades of hair is displayed in Table 3.2-1.

**Table 3.2-1 – Threshold levels for Fair, Medium and Dark Shaded Hair**

			
50%			
35%			
25%			

Cells that are shown as grey in Table 3.2-1, correspond to the ideal threshold level for each shade, as determined by experimentation on the three hair populations selected for this part of the research. For images of Fair shaded hair the threshold level was set to 50% of the original image, for Medium shaded hair the threshold level was set to 35% of the original image and for Dark shaded hair the threshold level was set to 25%. Given the intra-individual variability known to exist, occasionally a hair sample was thresholded at an

unsuitable level due to the population shade the participant was selected for. (For example, a participant in the Fair population may have 9 fair shaded hairs and 1 medium shaded hair. The Fair population threshold limit of 50% would be unsuitable for the medium hair and the resulting image would appear almost black.)

### **3.2.2. Preliminary Evaluation – Pigmentation Measurement**

#### **3.2.2.1 Analysis 1**

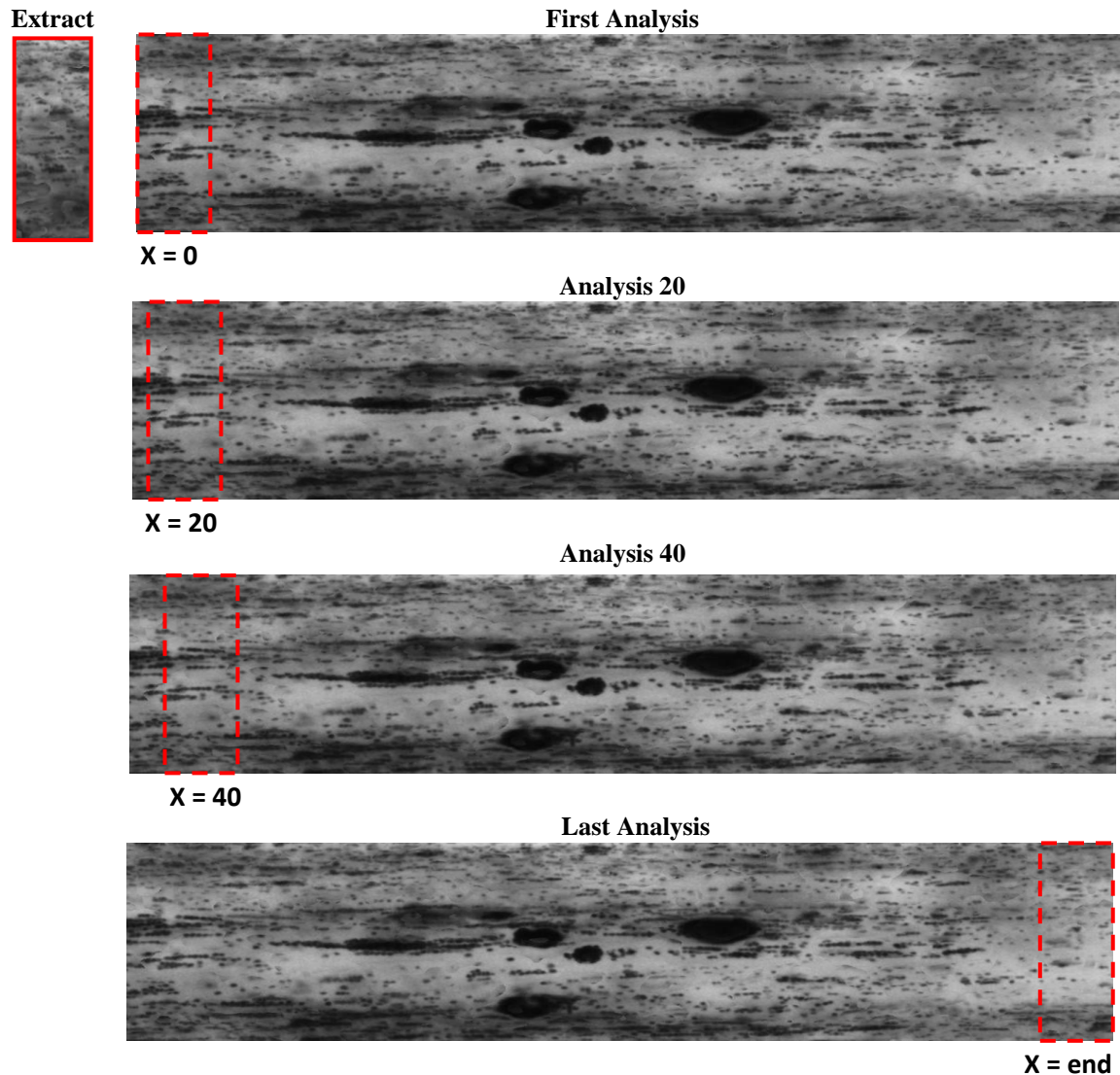
The *VPascal* programming software associated with *V++* was used to automate most of the pigmentation measurements for Analysis 1. The original *VPascal* script for Analysis 1 was provided by Comber (2006b) and small changes not affecting the script's function were performed. The *VPascal* script used to generate pigmentation pattern matching values is provided in Appendix C.

To generate a set of pigmentation pattern matching values, both an extract and an entire image were required. A matching value was produced for each pixel position along the entire image x axis, as illustrated in Figure 3.2-1. The automated process involved:

- Calculating a mean of the pixel values (0 to 255) in the extract array;
- Starting at the location  $x = 0$  and determining the section of the entire array that corresponds in spatial (x, y) dimensions to the size of the extract array;
- Calculating the mean of the pixel values (0 to 255) in this section;
- Subtracting the mean pixel value of the extract from the mean pixel value of the section to produce a “matching” value. Zero indicated a perfect match between mean pixel values, while values above 75 (up to 255) indicated a high degree of mismatch;
- This process was repeated for every pixel location along the x axis of the entire image (i.e.,  $x = 1, x = 2 \dots x = \text{final } x \text{ position}$ ).

Generally, more than 1000 values were produced for each extract-to-entire image analysis. Analyses were performed between hairs belonging to the same participant and between hairs belonging to different participants.





**Figure 3.2-1 – Pigment Pattern Matching Value Generation for Analysis 1**

The mean of the pixel values in the extract array was calculated then subtracted from the mean of pixel values in a section of the entire array, whereby the section corresponds to the same spatial dimensions ( $x$ ,  $y$ ) as the extract. This subtraction was repeated at each pixel position along the  $x$ -axis of the entire array, beginning with the location  $x = 0$  and continuing until the final pixel location along the  $x$ -axis. Analyses were performed between images belonging to the same participant and images belonging to different participants.

### 3.2.2.2 Analysis 2

To measure pigmentation within the image, the *V++* Object Analysis function was employed. As a threshold operation had already been applied to the images, this function could analyse the black on white objects in each array and produce an *Excel* spreadsheet containing measurements of each object. The complete list of parameters available for measurement using Object Analysis is provided in Table 3.2-3 (Digital Optics Ltd., 2009). This function can also be automatically performed with the appropriate *VPascal* script.

**Table 3.2-2 – V++ Object Analysis Measured Parameters**

<b>Parameter</b>	<b>Description</b>
Id	Identifying serial number of the object
Area	Total number of pixels contained in the object
Perimeter	The distance around the traced edge of the object, in pixels
Major	The approximate length of the object's major axis
Minor	The approximate length of the object's minor axis
Angle	The angle between the major axis and the horizontal
Xc	X-coordinate of the centre of mass (centroid) position
Yc	Y-coordinate of the centre of mass (centroid) position
Left	Left boundary of the object
Top	Top boundary of the object
Right	Right boundary of the object
Bottom	Bottom boundary of the object
Frame	The sequence frame in which the object is found
XSeed	X-coordinate of a single boundary pixel
YSeed	Y-coordinate of a single boundary pixel
M10 (SumX)	Sum of x coordinates for all pixels in the object
M01 (SumY)	Sum of y coordinates for all pixels in the object
M20 (SumX <sup>2</sup> )	Sum of squares of x coordinates for all pixels in the object
M02 (SumY <sup>2</sup> )	Sum of squares of y coordinates for all pixels in the object
M11 (SumXY)	Sum of the products of the x and y coordinates for all pixels in the object
Mxx ( $\mu_{20}$ )	Sum of squares of $(X-X_c)$ for all pixels in the object
Myy ( $\mu_{02}$ )	Sum of squares of $(Y-Y_c)$ for all pixels in the object
Mxy ( $\mu_{11}$ )	Sum of $(X-X_c)*(Y-Y_c)$ for all pixels in the object
Border	Contains 1 if the object touches the image boundary, 0 otherwise
Sum	Sum of intensities of all pixels contained in the object
Min	Minimum intensity of any pixel contained in the object
Max	Maximum intensity of any pixel contained in the object
Mean	Mean intensity of all pixels contained in the object

Not all the parameters measured by the Object Analysis function were exploited in this research. The ‘Area’ parameter was used to measure the pigmentation density, that is, the number of black (pigment) pixels divided by the total number of pixels in the 120 x 500 array. The Area parameter was also used to determine the size of the objects. Finally, the ‘Major’ and ‘Minor’ parameters were used to determine the average shape of the pigment; however, only two nominal aggregations were considered, namely streaks or clumps.

### 3.2.3. Preliminary Evaluation – Summary

Evaluation of hair pigmentation patterns using Analysis 1 provided a number of benefits. For instance, locating the actual area of pattern match between the extracted pattern and entire image was possible as the analysis sequentially followed the order of pixels along the x-axis and that the degree of match (or mismatch) could be assessed from the subtraction calculation (Brooks, 2007). Furthermore, in a forensic context, it was possible to determine the probability of whether the pattern from a questioned hair also belonged to a known set of hairs. To attain these benefits, Brooks (2007) compared the mean (log +1) distributions for pigment pattern values of persons matched with themselves (e.g., Participant A extract with Participant A entire image 1 to 5) versus the mean (log +1) distributions for pigment pattern values of persons matched with others (e.g., Participant A extract with Participant B entire image 1 to 5, Participant C entire image 1 to 5, etc.). It was determined that extracts compared to entire images from the same participant returned a high probability, such as 89.9% and extracts compared to entire images from other participants returned a low probability, such as 0.3% (Brooks, 2007).

Despite the potential of Analysis 1 to separate or associate patterns between hairs from the same participant and between other participants, it was determined that this method did not meet the aims of the current investigation. Specifically, regardless of the sequential generation of pattern matching values along the x-axis, it is the mean value from each comparison that is recorded then a further mean of those individual comparisons that is used to create the distributions for analysis. Thus, theoretically, simply subtracting the mean pixel value of the extract from the mean pixel value of the entire image should produce the same result as that generated by the pigmentation pattern matching values of the V++ script (provided in Appendix C). Three montages were used to validate this theory, as displayed in Table 3.2-3.

Table 3.2-3 – Manual versus Automatic Generation of Pigmentation Measurements

Mean Intensity of Entire minus Mean Intensity of Extract	Script Generation of Matching Values
7.1	8.2
95.0	95.2
0.0	1.5

Chapter 2: COLOUR was concerned with the investigation of numerical hair *colour* measurements, while the present chapter was concerned more specifically with the *pigmentation* that produces that overall hair colour. Notwithstanding the obvious relationship between the two entities, for the purpose of this research, it was necessary to avoid repeating measurements investigated in the previous chapter. It was decided not to proceed further with Analysis 1 given the close relationship between the measurements produced by this analysis and those of the previous chapter. That is, focus was retained on measuring the *morphology* of the pigmentation rather than the *intensity values* associated with the pigmentation in a hair image.

Evaluation of hair pigmentation patterns using Analysis 2, while being a novel, untested technique also provided a number of benefits. For instance, the analysis aimed to numerically measure the density, size and shape of pigmentation common to a participant's hair shaft—characteristics that were not targeted by Analysis 1 that instead

only focused on average intensity values within the image. Density, size and shape of pigmentation are typically evaluated during a routine forensic hair examination therefore, Analysis 2 attempts to compliment standard forensic procedures already employed in routine casework. Based on results from the preliminary evaluation, it was decided to proceed with this novel analysis and, therefore retain a focus on measuring the morphology of the pigmentation.

### 3.2.4. Data Preparation

This chapter involved assigning numerical values to hair pigmentation. The analysis was designed to measure hair pigment morphology in terms of density, size and shape by relying on only a few of the parameters listed in Table 3.2-2. Notwithstanding, all of the raw parameters available in *V++ Object Analysis* would be worth investigating to determine their ability to assist in the objective discrimination of hair samples. The numerical parameters employed here, were pasted directly from the *V++* clipboard to an *Excel* spreadsheet for initial observations and further calculations. Raw data from *Excel* was then exported directly to *PASW (Predictive Analytical Software) Statistics for Windows*, version 17.0.2 (SPSS Statistics IBM Corporation, 2008) for analysis.

#### 3.2.4.1 Density

Each black on white object in the thresholded 120 x 500 image was allocated an 'Area' value, being the number of black pixels in each object. The sum of the Area measurements determined the total number of black pixels in the whole image, with each array containing a total of 60,000 pixels (120 x 500). The following calculation was therefore used to determine the density of each image:

- $Density = (\sum Area / 60,000) * 100$

#### 3.2.4.2 Size

An average of the Area parameter represented the average number of pixels contained in each of the black on white objects in the thresholded image. The following *Excel* syntax was employed to allocate one of three sizes to each object; an example calculation of the values employed here, is provided:

- *Size* = IF (logical test [1], value if [1] true, IF (logical test [2], value if [2] true), value if [1] [2] false)
- *Size* = IF (Area > 1000, "large", IF(Area < 100, "small", "medium"))

Following the allocation of the small, medium and large sizes, the percentage occurrence of each size in the image was calculated (i.e., the percentage of black objects that are small, medium and large; %Small, %Med and %Large).

### 3.2.4.3 Shape

The 'Major' and 'Minor' parameters were used to determine the nominal shape of the pigment. Where the length of the major axis of an object was more than two times greater than the minor axis, this was considered a nominal "streak" pigment configuration, while an object with two axes of similar length (+/- 1 pixel) was considered a nominal "clump" pigment configuration. The following example *Excel* syntaxes were employed to define these aggregation types:

- *Streak* = IF (major > 2\*minor, "streak", ".")
- *Clump* = IF (major > minor +1, ".", IF (major < minor -1, ".", "clump"))

Following the determination of the two nominal configurations, the percentage of the shape's occurrence in each image was calculated (i.e., %Streak and %Clump).

### 3.2.5. Analysis of Variance

Analysis of variance (ANOVA) is used to compare two or more sample means, by focusing on the variance within the data being compared. A one-way ANOVA measures the variability in scores between different groups believed to be due to the independent variable, compared with the variability within each of the groups believed to be due to chance (Pallant, 2005). An F ratio is calculated that indicates whether there is more variability between the groups as a result of the independent variable than there is within each group (Pallant, 2005). An F-ratio significant value (sig-F) less than or equal to  $\alpha$ , where  $\alpha = 0.05$ , indicates there is a significant difference somewhere among the mean scores of the dependent variable.

One-way ANOVA was used to confirm whether the main source of variance in the sample populations for each shade was 'between participants' for each of the pigmentation

raw measurements or final calculations. Attempting to distinguish one participant's hair pigmentation from another's based on numerical measurements would be unnecessary if 'within participant' variance was found to be greater for any of the given measurements. The raw measurements, being Area, Major and Minor, and the calculated measurements, being Density, %Small, %Med and %Large, %Streak and %Clump, were the dependent variables while 'within participant' and 'between participants' were the factors under investigation. Where it was determined that sig-F was less than  $\alpha$  for a particular raw or calculated measurement, indicating more variability between groups, the null hypothesis was rejected and the measurement was included in further analyses (i.e., the variance between participants was found to be greater than the intra-individual, for the given measurement).

#### 3.2.5.1 Assumptions

The ANOVA statistic is only reliable when applied to normally distributed data. Normality was determined by observing histograms, QQ- and stem-and-leaf plots produced by *PASW*. Homogeneity of variance is also required and the Levene test for equality is included as part of the *PASW* analysis. The ANOVA test is reasonably robust to violations of the assumption of homogeneity of variance, provided the group sizes are reasonably similar and they were all of equal size in this research.

#### 3.2.6. Discriminant Analysis

The underlying principles of discriminant analysis have been described in detail in section 2.2.8 Discriminant Analysis. Chiefly, discriminant analysis is used to determine whether two or more groups can be distinguished from each other, based on a linear combination of multiple variables. In this chapter, the discriminant function coefficients categorised cases by allocating them to one group when the pigmentation measurements placed them within a certain category or to another group when the coordinates placed within another category. The more widely separated the discriminant function distributions, the more successful the prediction of group membership from those functions (Kinnear & Gray, 2010).

Discriminant analysis [probability of F criteria (0.05, removal 0.10) and Wilks' lambda stepwise method] was used to allocate each of the ten hairs to one of five participants within a sample population of similarly shaded hair, being Fair, Medium or

Dark in shade. The participant numbers were the grouping variables, while the numerical pigmentation measurements that returned a significance value less than 0.05 (One-way ANOVA) were the regressors from which group membership was predicted.

### 3.2.6.1 Canonical Discriminant Analysis

Canonical discriminant analysis was used here to evaluate whether numerical measurements of hair pigmentation could be allocated to one of five participants of similarly shaded hair with a high degree of accuracy. This test measures the degree of association between discriminant scores and the predicted groups and is used when the group membership for a set of cases is known. Where most of the observed variability is explained by differences between the groups, a high canonical correlation will result. Misclassification results from a lack of separation between the groups. The canonical discriminant function plot, incorporating Function 1 versus Function 2, visually represents the discriminant scores of the predictor variables that showed the greatest discriminating power (Norusis, 1985; Brooks, 2007). For canonical discriminant analyses performed in this chapter, prior probabilities were considered equal.

### 3.2.6.2 Assumptions

Discriminant scores are sensitive to outliers because they are based on the calculated mean of the group centroid. Histograms produced by *PASW* were used to check for any outlying cases. Further, the covariance matrix of the predictor variables should be the same for all populations. ‘Box Ms’ also produced by *PASW* were used to test this assumption; however, the test is notoriously sensitive with even minor departures from homogeneity resulting in small observed significance levels, especially when routine  $\alpha$  levels are used (Tabachnick & Fidell, 2001).

Overall, this chapter was designed to investigate whether numerical measurements could assist the forensic hair examiner with pigmentation pattern evaluations. Specifically, discriminant analyses were used to address the question:

- Can images of hair pigmentation measured in respect of density, size and shape, be used to discriminate between participants possessing similarly shaded hair?



### 3.3. Results and Discussion

Approximately 3150 montage images were acquired from the hair samples of 105 participants. From those images, only five representative participants were selected for each of the ‘Fair’, ‘Medium’ and ‘Dark’ sample populations created for this chapter. Respective threshold operations were applied to a 120 x 500 pixel extract of each image then the total pixel area of each black on white object was measured as well as the length of their major and minor axes. These measurements were used to create numerical representations of the morphology captured in each image in terms of pigment density, size and shape. One-way ANOVA was employed to determine whether the main source of variance in the three sample populations were ‘between participants’ for each variable. Finally, discriminant analyses were performed in *PASW* to assess whether such quantitative methods could be used to discriminate between participants with similar shaded hair.

#### 3.3.1. Main Source of Variance

##### 3.3.1.1 Fair Samples

The ten image extracts acquired from each of five participants selected to represent the Fair sample population are displayed in Figure 3.3-1.

Participant 2002107



Participant 2002121



Participant 2002175



Participant 2002187



Participant 2002200



**Figure 3.3-1 – Images Acquired for Fair Sample Population**

Five participants were selected to represent the Fair hair sample population. One montage image from each of the participants ten hairs, were prepared for the analysis. Normalised extracts from those images are provided.

One-way ANOVA was used to confirm whether the greater source of variance in each of the three sample populations was between participants. For the five Fair sample population participants, large F ratio values—indicating that there was significantly greater inter-participant variability—were obtained for the variables Area ( $F = 3.639$ , sig. 0.01), %Small ( $F = 7.25$ , sig. 0.00), %Medium ( $F = 6.75$ , sig. 0.00), %Large ( $F = 3.30$ , sig. 0.02), Density ( $F = 7.53$ , sig. 0.00), %Clumps ( $F = 5.73$ , sig. 0.00), %Streaks ( $F = 19.35$ , sig. 0.00) and the Major axis ( $F = 6.68$ , sig. 0.00). These variables were therefore considered suitable for the discriminant analysis, while the Minor axis ( $F = 2.11$ , sig. 0.09) was determined to be unsuitable and therefore excluded from further analysis of the Fair samples.

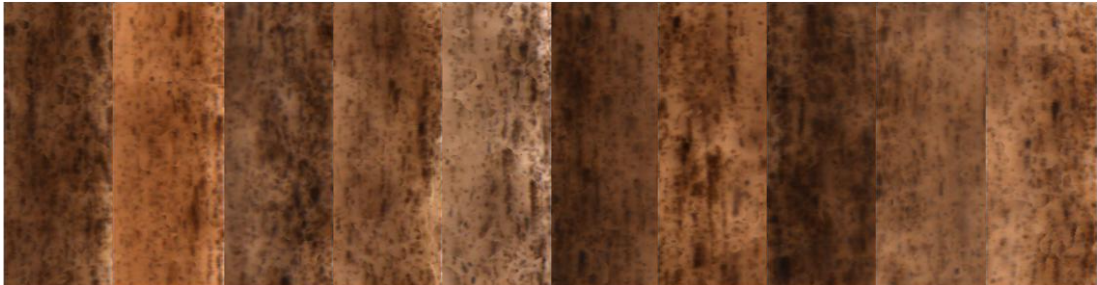
**3.3.1.2 Medium Samples**

The ten image extracts acquired from each of five participants selected to represent the Medium sample population are displayed in Figure 3.3-2.

Participant 2002038



Participant 2002086



Participant 2002093

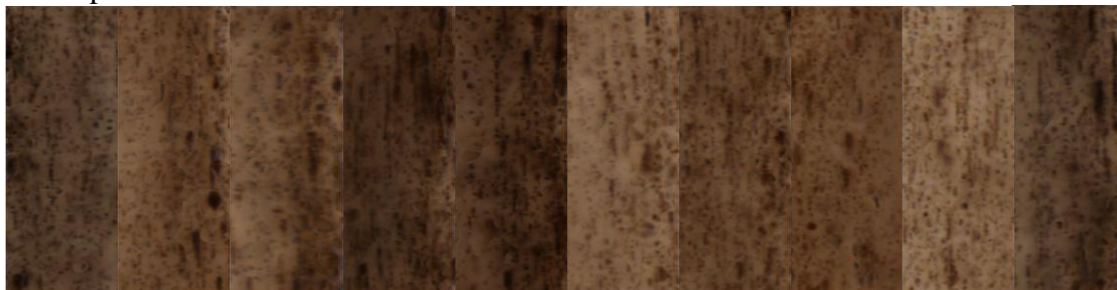


Participant 2002165





Participant 2002167



**Figure 3.3-2 – Images Acquired for Medium Sample Population**

Five participants were selected to represent the Medium hair sample population. One montage image from each of the participants ten hairs, were prepared for the analysis. Normalised extracts from those images are provided.

For the five Medium sample population participants, a large F ratio value was determined for the variables Area ( $F = 2.77$ , sig. 0.04), %Large ( $F = 3.91$ , sig. 0.01), Density ( $F = 5.99$ , sig. 0.00) and the Major ( $F = 4.41$ , sig. 0.01) and Minor ( $F = 4.39$ , sig. 0.01) axes. These variables were therefore considered suitable for the discriminant analysis, while the %Small ( $F = 1.01$ , sig. 0.41), %Medium ( $F = 0.25$ , sig. 0.91), %Clumps ( $F = 1.14$ , sig. 0.35) and %Streaks ( $F = 0.94$ , sig. 0.45) were determined to be unsuitable and therefore excluded from further analysis of the Medium samples.

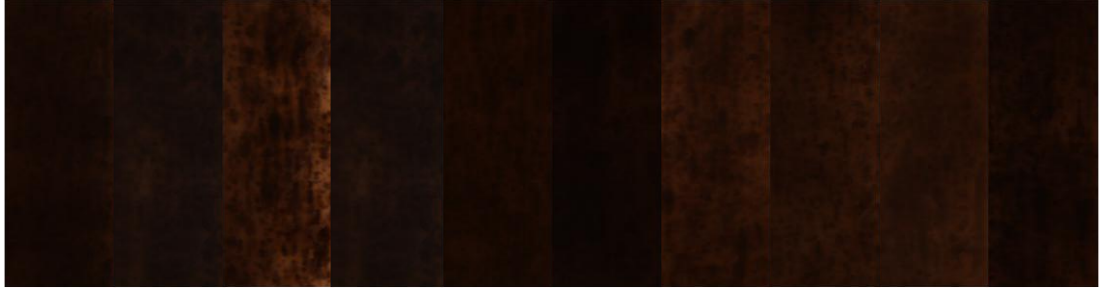
### **3.3.1.3 Dark Samples**

The ten image extracts acquired from each of five participants selected to represent the Dark sample population are displayed in Figure 3.3-3.

Participant 2002064



Participant 2002120



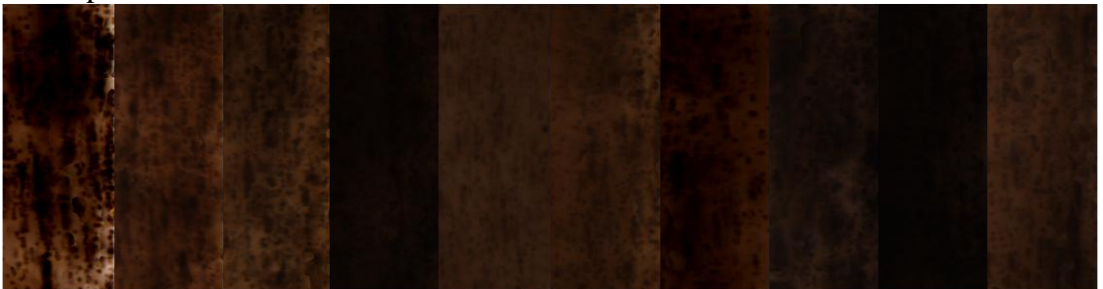
Participant 2002147



Participant 2002185



Participant 2002203



**Figure 3.3-3 – Images Acquired for Dark Sample Population**

Five participants were selected to represent the Dark hair sample population. One montage image from each of the participants ten hairs, were prepared for the analysis. Normalised extracts from those images are provided.

For the five Dark sample population participants, a large F ratio value was determined for the variables %Small (F = 6.36, sig. 0.00), %Medium (F = 5.39, sig. 0.00), %Large (F = 6.67, sig. 0.00), Density (F = 7.39, sig. 0.00), %Clumps (F = 3.03, sig. 0.03) and the Minor axis (F = 11.73, sig. 0.00). These variables were therefore considered

suitable for the discriminant analysis, while the Area ( $F = 1.88$ , sig. 0.13), %Streaks ( $F = 1.39$ , sig. 0.25) and the Major axis ( $F = 2.10$ , sig. 0.10) were determined to be unsuitable and therefore excluded from further analysis of the Dark samples.

### 3.3.1.4 Summary of Main Source of Variance

These analyses were designed to measure hair pigment morphology in terms of density, size and shape by relying on both raw numerical measurements such as the average pixel area and the length of the major and minor axes, as well as calculated measurements such as density, the percentage of small, medium and large objects, and the percentage of two nominal configurations—‘streaks’ and ‘clumps’. Where it was determined that the significance value was less than  $\alpha$  (0.05) for a particular raw or calculated measurement, indicating greater variability between groups, the measurement was included for further analyses. Different outcomes resulted for the variables tested, depending on the sample population under consideration. The overall results are summarised in Table 3.3-1, where ‘Yes’ denotes a statistically significantly large F value result and ‘No’ denotes an insignificant result.

**Table 3.3-1 – Summary of Main Source of Variance**

Measurement	Fair	Med	Dark
Area	Yes	Yes	No
% Small	Yes	No	Yes
% Med	Yes	No	Yes
% Large	Yes	Yes	Yes
Density	Yes	Yes	Yes
% Clumps	Yes	No	Yes
% Streaks	Yes	No	No
Major	Yes	Yes	No
Minor	No	Yes	Yes

As displayed, overall the variables returned the lowest discriminating power for the Medium shade sample population. In this sample set, only five variables showed greater inter-participant variability than intra-participant variability, compared with the Dark population that had six variables showing greater inter-participant variability and the Fair

population that had eight variables. It is important to note that, while a significant F test result indicates that an appreciable difference exists between the participant's scores, the test does not indicate where that difference occurs (Pallant, 2005). Thus, whether one participant or all five participants were appreciably different in any given sample population, a significant F test would result. As the objective for applying the one-way ANOVA in this research was to assist in selecting variables for the following discriminant analyses, identifying the variables with significant discriminating power was important, while actually identifying those participants was not as important.

### 3.3.2. Allocation to Participants

#### 3.3.2.1 Fair Participant Allocation

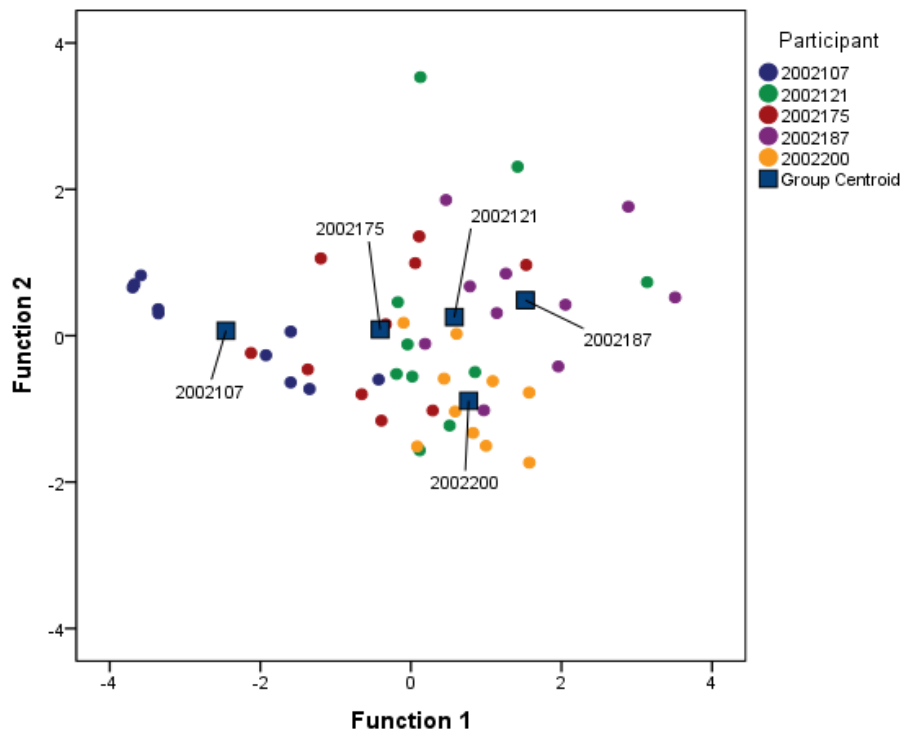
Canonical discriminant analysis was used to allocate hair images to participants, within one of three populations of similar hair shades, being Fair, Medium or Dark. The analyses were performed separately for each of the populations. The Fair sample population analysis involved Area, % Small, % Medium, % Large, Density, % Clumps, % Streaks and Major axis as the predictor variables and resulted in the second highest number of images correctly allocated, with 54% prediction accuracy. Table 3.3-2 illustrates the predicted categories (%) where rows indicate the original participant and columns indicate the participant predicted based on the numerical pigmentation measurements.

**Table 3.3-2 – Fair Participant Predicted Allocation (%)**

		PREDICTED					
		2002107	2002121	2002175	2002187	2002200	Total %
ORIGINAL	2002107	80		20	0		100
	2002121		10	40	20	30	100
	2002175	10	20	40	10	20	100
	2002187		30	0	60	10	100
	2002200		10	10		80	100

As illustrated, three of the participants individually scored above 60% correct allocation, while the remaining two participants scored relatively poorly, one participant as low as only 10% correct classification. Figure 3.3-4 represents discriminant scores for the Fair shade population. Each image is chromatically represented by the correct participant

but located in canonical space with respect to the two highest discriminant functions. It was observed that the group centroids for all five participants, were best separated by Function 1 along the horizontal axis. For this function, the %Streaks and Density variables were the strongest predictors, showing individual coefficients of 0.879 and 0.451, respectively. The canonical correlation indicates that Function 1 explained 82.3% of the data variance.



**Figure 3.3-4 – Fair Participant Canonical Discriminant Functions**

The *PASW* canonical plot illustrates the two highest discriminant functions for the Fair hair sample population. Group centroids for all five participants were best separated along the horizontal axis by Function 1.

### 3.3.2.1 Medium Participant Allocation

The Medium sample population discriminant analysis involved the predictor variables Area, % Large, Density, Major and Minor axes and of the three sample populations tested, resulted in the lowest number of images correctly allocated, with only 32% prediction accuracy. Table 3.3-3 illustrates the predicted categories (%).



**Table 3.3-3 – Medium Participant Predicted Allocation (%)**

		PREDICTED					
		2002038	2002086	2002093	2002165	2002167	Total %
ORIGINAL	2002038	60	10	10	20		100
	2002086	10	20	40	30		100
	2002093	10	20	60	10		100
	2002165	50	10	10	20	10	100
	2002167	60		10	30		100

As illustrated, two of the participants individually scored 60% correct allocation, while the remaining three participants scored relatively poorly. For two of the latter, the majority of samples were incorrectly allocated to participant 2002038 with one of these participants having no correct classifications at all. A combined canonical discriminant plot was unavailable for the Medium shade sample population, as only a single discriminant function resulted from the analysis. That is, Density was found to be the strongest and only predictor variable (1.0 individual coefficient).

### 3.3.2.1 Dark Participant Allocation

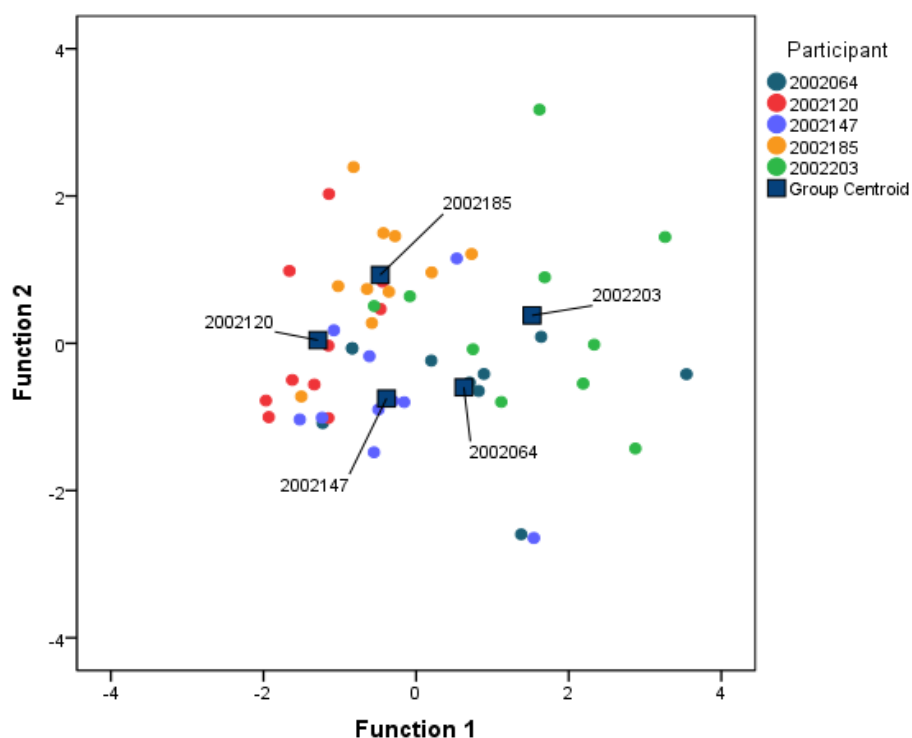
The Dark sample population discriminant analysis involved % Small, % Medium, % Large, Density, % Clumps and Minor axis as the predictor variables and resulted in the highest number of images correctly allocated, with 62% prediction accuracy. Table 3.3-4 illustrates the predicted categories (%).

**Table 3.3-4 – Dark Participant Predicted Allocation (%)**

		PREDICTED					
		2002064	2002120	2002147	2002185	2002203	Total %
ORIGINAL	2002064	50	20	10		20	100
	2002120		60	10	30		100
	2002147	10	20	60	10		100
	2002185		10		80	10	100
	2002203	20			20	60	100

As illustrated, all five of the participants individually scored 50% or above correct allocation. Figure 3.3-5 represents discriminant scores for the Dark shade population. Each image is chromatically represented by the correct participant, but located in canonical

space with respect to the two highest discriminant functions. It was observed that group centroids were well separated by both Function 1 and Function 2. The Minor axis and % Medium variables were the strongest predictors, showing individual coefficients of 1.039 and -0.115, respectively. The canonical correlation indicates that Function 1 explained 71.6% of the data variance and Function 2 explained 54.8%.



**Figure 3.3-5 – Dark Participant Canonical Discriminant Functions**

The *PASW* canonical plot illustrates the two highest discriminant functions for the Dark shade population. Group centroids for all five participants were well separated by both Function 1 and Function 2.

### 3.3.2.2 Summary of Allocation to Participants

The focus of this chapter involved assigning numerical values to hair pigmentation. Unfortunately, this novel methodology did not support discrimination between the selected participants. The nine measured variables returned the lowest discriminating power for the Medium hair sample population, with only five variables showing greater variance between participants than within participants. The Dark hair population comprised six variables showing greater variance between participants while the Fair hair comprised eight variables. The respective variables indicated that an appreciable difference existed between the participants' scores but did not indicate where the difference occurred—either

one participant or all five participants in each population may have been appreciably different from the others.

Furthermore, no obvious relationships were observed between each of the populations in terms of the number of variables selected, the strongest predicting variable or the overall prediction accuracy. The Medium sample population resulted in the lowest number of images correctly allocated, with only 32% prediction accuracy. Three of the five participants in this population scored less than 60% correct allocation, with one receiving zero correct classifications. The Fair hair sample population resulted in the second highest correct allocation, with 54% prediction accuracy and the Dark hair sample population showed the highest correct allocation, with 62% prediction accuracy. All five of the Dark hair participants scored 50% or above correct classification. Density was found to be the strongest and only predictor variable for the Medium hair sample population, %Streaks and Density were the strongest predictors for the Fair hair population, while the Minor axes and %Medium were the strongest predictors for the Dark hair population.

Although the selected methodology did not support discrimination between participants, other research supports the proposal that there is a strong relationship between genotype and pigmentation. As previously discussed, studies on mice indicate that at least 150 genes at over 50 loci control eye, skin and hair colour (Robins 1991) and specific pigment-recipient cells provide the blueprint that instructs melanocytes on where to place pigment (Weiner et al, 2007). The automated Hair-MAP system described by Verma and colleagues (2002) involving measures of medulla type, cuticle texture and shaft diameter resulted in 83% correct allocation; indices derived from measures of hair length, distance and area employed by Sato (2003) demonstrated larger inter-individual variations than intra-individual variations; while raw measurements and calculations derived from hair area, perimeter, length, breadth, width and radius employed by Ball and colleagues (2002) demonstrated significant morphometric differences between head hair from different races and from different genders within the same race. A number of factors were considered in terms of why the numerical approach applied in this research did not support discrimination between participants.

First, while no two hairs from the same individual will have indistinguishable features along the entire length of the shaft, the goal of the forensic examiner is to recognise pigmentation patterns that are similar in both the questioned hair and the

exemplar set. To achieve this outcome, an examiner will evaluate the entire hair shaft of all hairs available. The present study, however, only evaluated a representative extract from a high resolution image of approximately 204 x 152  $\mu\text{m}$  of each sample (see 2.2.2 Image Acquisition) and was therefore limited in the information available for evaluation, in comparison to that available during a routine forensic examination.

Second, during method development of this part of the research, the threshold level was found to be critical. While the best average threshold was determined for the three separate populations (i.e., 50% for Light hair, 35% for Medium hair and 25% for Dark hair), given the intra-individual variability that is known to exist and that can be observed, for example, in the images displayed in section 3.3.1 Main Source of Variance, occasionally a hair sample was unavoidably thresholded at an unsuitable level. An incorrect threshold level results in the misrepresentation of available data, as demonstrated in Table 3.2-1. Addressing such limitations through an evaluation of the entire shaft and a reassessment of threshold levels, may assist future investigations into numerical measures of pigmentation to improve the discrimination of hairs from different individuals.

Alternatively, to extract information from pigmentation patterns, the fractal dimension of the configurations could be determined (McNevin, 2012). Fractal dimensions describe the complexity of detail in a pattern rather than merely its size as described by a spatial dimension. Fractal dimensions rely on the concept that changes in scale, changes the detail in the pattern. For example, the distance of a coast line measured with a scale of 1.0 km will yield one distance, but when measured with a scale of 0.001 km following the geometry of the coast line, will yield a greater distance (see Mandelbrot, 1967); the ratio of the two measured distances provides an indication of the complexity of the line measured. One study involving the determination of fire accelerants, successfully applied fractal dimension as a parameter for soot aggregates (Pinorini *et al.*, 1994). In that study, soot aggregates were characterised by size and form in terms of perimeter, surface area, circularity and principal surface moments ratio; however, those physical measures did not have the discriminatory power required to separate the rich soot aggregates from those coming from the weak smoke products, so measures of fractal dimensions were successfully employed as an alternative (Pinorini *et al.*, 1994). Statistical indices provided by fractal dimensions may similarly be suitable for comparing hair pigmentation within and between participants and further investigation is warranted.

### 3.4. Conclusion

The research focus of this chapter involved investigating whether numerical measurements could be used to quantify and discriminate pigmentation pattern evaluations. Previously reported studies involving the numerical classification of hair characteristics have focused on hair morphology in terms of the form or structure of the shaft or on comparisons between pixel intensity values rather than the pigmentation itself. This preliminary study was designed to measure the density, size and shape of the pigment configurations, as represented by pixel variations within montage images. Specifically, discriminant analyses were used to address the question of whether the selected measurements could discriminate between participants with similar shaded hair. Unfortunately, the selected methodology did not support discrimination between the selected participants and a number of limitations were considered for potential future research.

First, the forensic hair examiner will evaluate the entire length of hairs available in a questioned and exemplar set of hairs. The present study only evaluated an extract taken from an area approximately 204 x 152  $\mu\text{m}$  in size. This methodology was therefore limited in the information available for evaluation, in comparison to that available during a routine forensic examination. Future research should consider a method that involves a greater representation of the available hair sample. Second, during method development, the most appropriate average threshold level was determined experimentally for the three separate populations, i.e., 50% for Light hair, 35% for Medium hair and 25% for Dark hair. Occasionally a hair sample was unavoidably thresholded at an unsuitable level. It is recommended that future research consider multiple threshold levels for each image (i.e., 25%, 35% and 50% for a single light hair image) that could be subjected to object analysis. While the data would be more cumbersome, the misrepresentation of information in any individual samples would be avoided.

Furthermore, to measure pigmentation in each threshold image, the V++ Object Analysis function was employed to analyse black on white objects. Only a limited number of the parameters available in this function were exploited in this research, including the average pixel area and the length of the major and minor axes, as well as values calculated from those parameters, including density, size (percentage small, medium and large) and

two nominal configurations, namely the percentage of ‘streaks’ and ‘clumps’. Future research could consider a wider range of the 28 Object Analysis parameters available in *V++*; a complete list is provided in Table 3.2-3 (Digital Optics Ltd., 2009). Due to the complexity of data preparation involved in the current method design, only a small cohort of images and participants were evaluated here, namely one montage from each of ten hairs from five representative participants in each population. Investigating a greater number of parameters would only increase this complexity; however, once an appropriate method was determined, the Object Analysis function could be automatically performed with the appropriate *VPascal* script. This approach is recommended to enable a greater number of comparisons to be evaluated more easily.

Alternatively, to extract information from pigmentation patterns, fractal dimensions that describe the complexity of detail in a pattern rather than merely its size, could be determined. Fractal dimensions rely on the concept that changes in scale by which a pattern is measured, changes the detail in the pattern and have been successfully applied in other research that required statistical discrimination between measures of structure morphology (see Pinorini *et al.*, 1994). Statistical indices provided by fractal values may also be suitable for comparing hair pigmentation within and between participants and further investigation is warranted.

As noted by Tontarski and Thompson (1998), traditional approaches to pattern recognition rely on the human element to make observations and interpretations, and this depends heavily on the brain’s ability to correlate hundreds of data points and on consistency when repeating these tasks. Emerging technologies in image processing, pattern recognition and computer science could assist future examinations with classifying—or potentially individualising—forensic hair evidence. However, no method has yet been reported for the successful quantification and discrimination of hair pigmentation. Until there is a universally applicable technique that will mimic the microscopic analysis of pigmentation and the patterns they form, current evaluations by an experienced examiner, while subjective, is the best option available.

## Chapter 4. SPECTROSCOPY

---

## **4.1. Introduction**

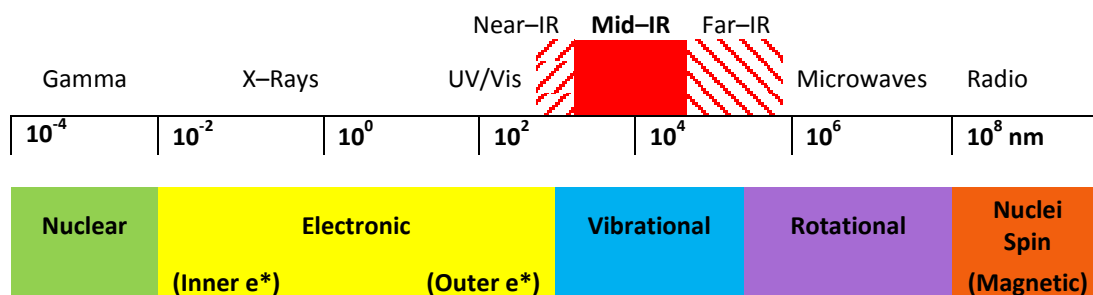
The characterisation of molecules can be performed by spectroscopy, whereby radiant energy is absorbed, reflected or transmitted by a substance. By examining the frequencies where interaction has occurred, as well as the degree of interaction, information on the molecular structure of the substance can be obtained. Chemical analysis of many substances can be performed by conventional spectroscopy or by chemical imaging, which essentially combines molecular spectroscopy with digital imaging. Both qualitative and quantitative information can be rapidly captured with little sample preparation, decreasing the potential for sample contamination.

### **4.1.1. Principles of Molecular Spectroscopy**

#### **4.1.1.1 Electromagnetic Radiation**

Electromagnetic radiation consists of alternating electric and magnetic fields that oscillate in phase with each other and that are propagated through space as waves. Radiation is conveniently divided into regions depending on the frequency of wave oscillation and the joules of energy per photon of light. Regions of the electromagnetic spectrum, including gamma rays, X-rays, ultra violet (UV) radiation, visible light, infrared (IR) radiation, microwaves and radio waves, are associated with one or two types of quantum transitions including nuclear, electronic, rotational and vibrational transitions, as depicted in Figure 4.1-1.





**Figure 4.1-1 – Electromagnetic Spectrum**

The Electromagnetic Spectrum represented by regions of radiant energy, their corresponding wavelengths and the quantum transitions typically associated with their absorption. Long wavelength, low energy radio waves are associated with nuclei spin, microwaves with rotational transitions around chemical bonds, IR radiation with vibrational transitions, UV-visible radiation with transitions of the valence electrons and X-rays with transitions of the core electrons. Short wavelength, high energy gamma waves are highly penetrating, associated with removal of electrons from the atom; such energy is used for identifying radioactive isotopes.

Radio waves are the lowest energy form of electromagnetic radiation. Generally, the absorption of radio waves can cause nuclei spin that subsequently creates a small magnetic field, while microwaves have enough energy to cause chemical groups to rotate around some bonds (Skoog *et al.*, 2007). IR radiation absorption is associated with vibrational transitions, whereby atoms of a molecule stretch symmetrically or asymmetrically, and bend in or out of plane (Rouessac & Rouessac, 2007; Blackman *et al.*, 2008). While IR radiation has insufficient energy to cause electronic transitions, UV-visible radiation has enough to illicit transitions of the valence (bonding) electrons and X-ray radiation can interact with core electrons plus, along with gamma rays, can generate ions by removing electrons (Skoog *et al.*, 2007; Blackman *et al.*, 2008). Gamma rays are the highest energy form of electromagnetic radiation and are useful for identifying unstable, radioactive isotopes. When gamma rays interact with a substance, they lose energy by three mechanisms: the photoelectric effect, the Compton effect or pair production (Skoog *et al.*, 2007). (Discussion of each gamma ray mechanism is outside the scope of this chapter.)

#### 4.1.1.2 Spectroscopy

Atoms have unique, quantised energy levels therefore, in order for absorption to occur, the energy of the radiation must exactly match the quantised energy levels of the atoms under analysis (Blackman *et al.*, 2008). Wavelengths that are not absorbed are either

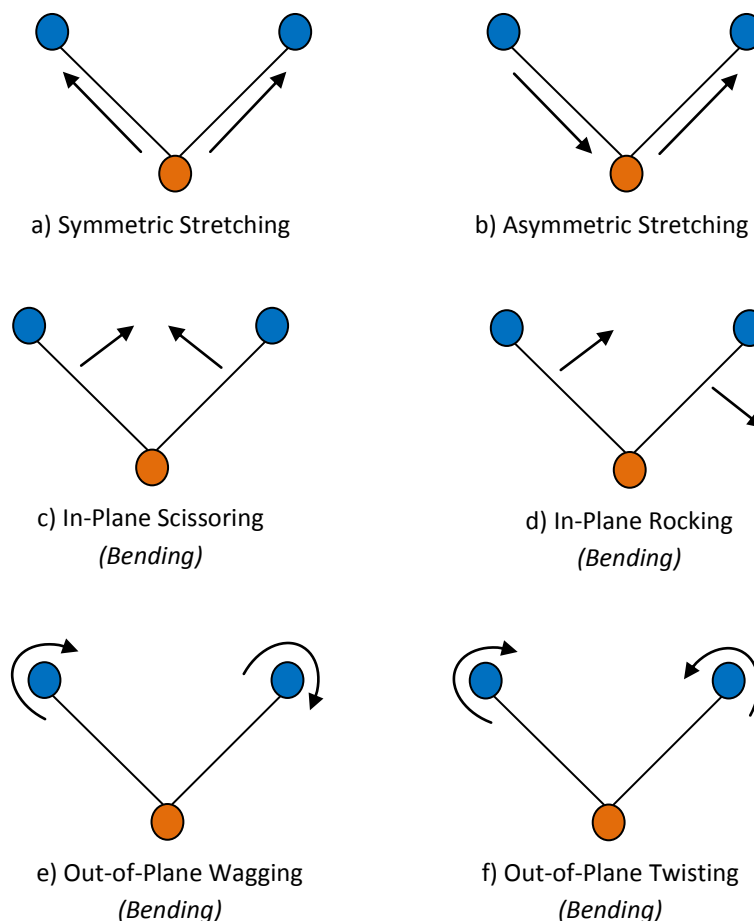
transmitted through the sample or reflected from the surface, unchanged. The spectroscopy technique essentially involves irradiating a sample thereby causing the atoms, molecules or ions to undergo transition to an excited state. Information on molecular structure and concentration can be acquired from a spectrum, being a measurement of the electromagnetic radiation absorbed (reflected or transmitted) as a result of the excitation.

#### 4.1.1.3 Mid-Infrared Spectroscopy

IR radiation incorporates all the wavelengths between approximately 780 and  $10^6$  nm and is located between visible light and microwaves in the electromagnetic spectrum. IR radiation is often subdivided into three approximate regions. The near-IR region corresponds to wavelengths between 780 and 2500 nm, the mid-IR to wavelengths between 2500 and  $5.0 \times 10^4$  nm (typically represented as wavenumbers, being 4000 to 400  $\text{cm}^{-1}$ ) and the far-IR to wavelengths between  $5.0 \times 10^4$  to  $1.0 \times 10^6$  nm (Rouessac & Rouessac, 2007; Skoog *et al.*, 2007). Near-IR spectroscopy is often used for the quantitative determination of low molecular weight and simple compounds, while the primary use of far-IR spectroscopy is for structural determination of some inorganic and metal-organic species (Skoog *et al.*, 2007). In comparison, collecting spectra at mid-IR frequencies provides greater chemical specificity because mid-IR radiation is associated with pure vibrational quantum transitions and the vibrational spectra of most organic compounds consist of an abundance of narrow, well-resolved bands that represent discrete functional groups (Flynn *et al.*, 2005; Tahtouh *et al.*, 2005; Flynn *et al.*, 2006). Compared with the near-IR and far-IR regions, mid-IR spectroscopy provides greater information on molecular structure so it is routinely employed for qualitative and quantitative analyses of functional groups and for identifying organic compounds.

Bonded atoms undergo continuous vibrations relative to each other and, where the atoms are different (i.e., non-symmetrical) they form an electric dipole with specified frequency (Rouessac & Rouessac, 2007). When a non-symmetrical bond is irradiated with mid-IR radiation, those frequencies with energy exactly equal to the vibrational energy levels of the molecule are absorbed, producing a change in the amplitude of the molecular vibration (Skoog *et al.*, 2007). As different functional groups require different quantised energy to bring about a vibrational transition, the groups can be identified by evaluating the frequencies where radiation is absorbed. However, the bond undergoing vibration must be a polar bond and must undergo a net change in dipole moment as it vibrates. The

stronger the bond the higher the vibrational frequency; the greater the polarity of the bond, the more intense the absorption (Blackman *et al.*, 2008). For example, O=O, N≡N and Cl–Cl have non-polar bonds so do not absorb infrared radiation; C≡C absorbs at a higher vibrational frequency ( $\sim 2200\text{ cm}^{-1}$ ) than C=C ( $\sim 1650\text{ cm}^{-1}$ ) or C–C ( $\sim 1000\text{ cm}^{-1}$ ), while C=O is characterised by a strong intensity absorption band and C≡C by a weak intensity absorption band.



**Figure 4.1-2 – Molecular Vibrations**

Stretching and bending are the two main types of molecular vibrations. Stretching vibrations involve an (a) symmetric or (b) asymmetric change in distance along the axis of a bond. Bending vibrations involve a change in the angle between two bonds and are further characterised as in-plane (c) scissoring and (d) rocking, or out-of-plane (e) wagging or (f) twisting.

There are two main categories of molecular vibration, as illustrated in Figure 4.1-2. Stretching vibrations involve a symmetric or asymmetric change in distance along the axis of a bond between two atoms, while bending vibrations involve a change in the angle

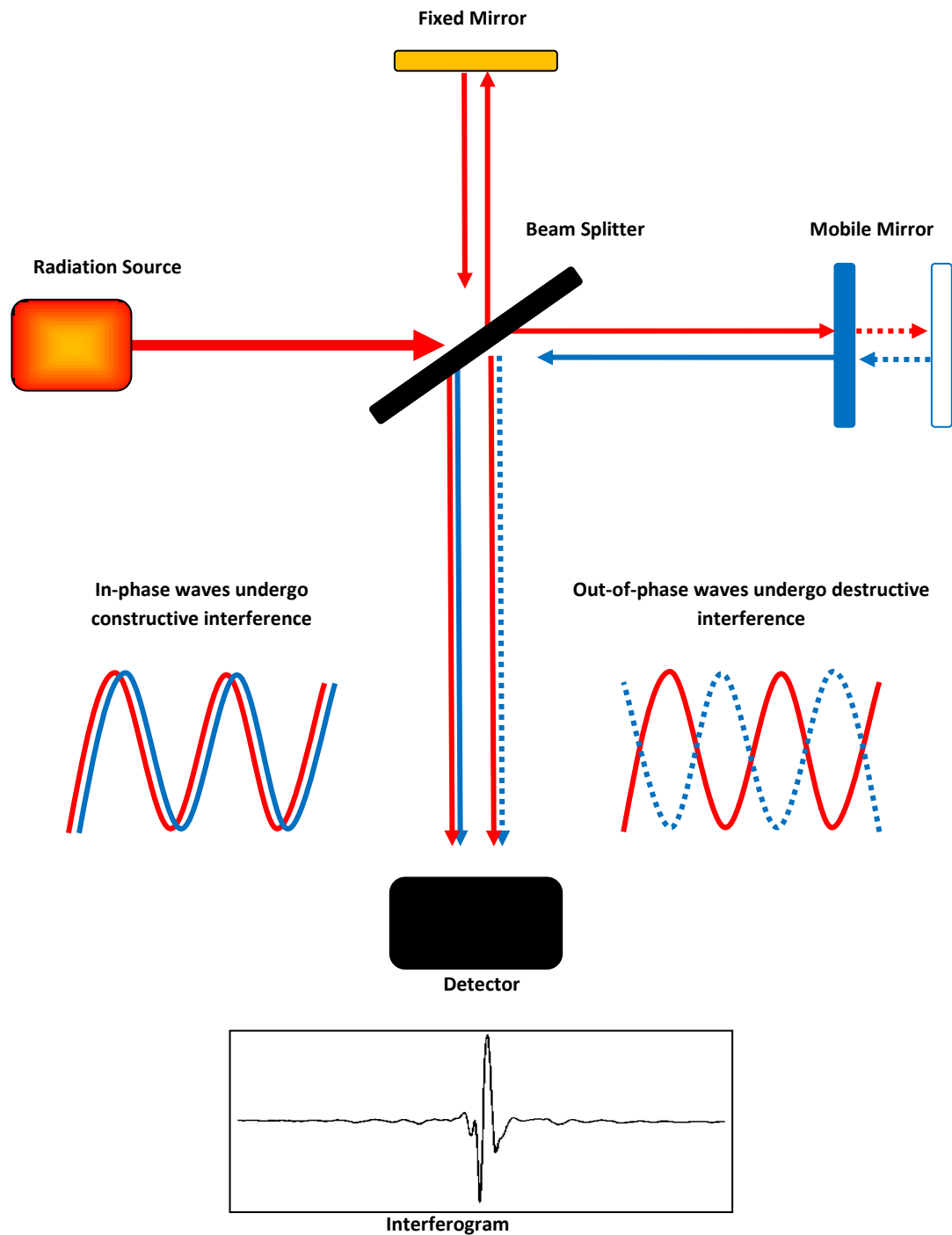
between two bonds, which are further characterised as four types, namely, scissoring, rocking, wagging and twisting.

## 4.1.2. Spectroscopy Instrumentation and Sampling Techniques

### 4.1.2.1 Interferometer

The interferometer is an essential component of the Fourier Transform Infrared (FTIR) spectrometer. It consists of three components, namely a beam splitter, a mobile mirror and a fixed mirror. As depicted in Figure 4.1-3, the beam splitter divides the spectrometer's infrared polychromatic radiation source into parallel beams of equal intensity, with one half transmitted toward the mobile mirror and the other half reflected toward the fixed mirror (Rouessac & Rouessac, 2007; Skoog *et al.*, 2007). The beams are then reflected from each mirror back to the beam splitter, where they recombine and are directed toward the sample. Oscillation of the mobile mirror creates an interference pattern by introducing a phase difference between the parallel beams. At one mirror position, waves of the recombined beam are in phase and undergo constructive interference to create maximum signal power (Rouessac & Rouessac, 2007; Skoog *et al.*, 2007) referred to as the 'centre burst' at zero path difference. When the mobile mirror changes from this position, the two waves are out of phase and undergo destructive interference, reducing the radiant power of the recombined beams to zero (Rouessac & Rouessac, 2007; Skoog *et al.*, 2007).

The interferogram relates the detector signal to the mobile mirror position, thus representing the various phase changes between the two beams. Sample analysis requires two interferograms: the first of the background alone and the second of the sample and background. A microprocessor coupled to the interferometer calculates the final spectra as a function of the wavenumber ( $\text{cm}^{-1}$ ).



**Figure 4.1-3 – Depiction of the FTIR Interferometer**

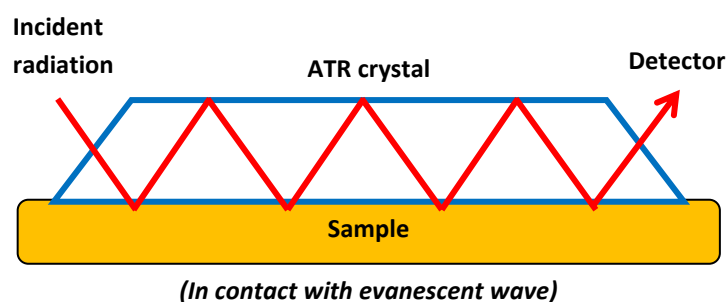
A beam splitter divides the radiation into parallel beams that are directed toward a mobile mirror and a fixed mirror. The beams return to the beam splitter, recombine and are directed toward the sample and/or detector. Oscillation of the mobile mirror creates an interference pattern by introducing in-phase and out-of-phase wave differences for the recombined beams. Phase changes are represented by the interferogram that relates the signal intensity to the position of the mobile mirror.

#### 4.1.2.2 Fourier Transform

As frequency responses are collected simultaneously, it is necessary to decode the intensity for each of the individual signal components. The Fourier transform is a mathematical operation used to transform an interferogram into its component waves. The spectrum produced displays the intensity (energy transmitted, absorbed or reflected) as a function of wave frequency. Fourier transform instruments offer a number of major advantages. Greater signal-to-noise ratios are observed due to an increase in radiant energy reaching the detector, analysis of complex spectra are possible due to the extremely high resolving power and wavelength reproducibility, and an entire spectrum can be collected in 1 second or less because all wavelength components of the source reach the detector simultaneously (Skoog *et al.*, 2007).

#### 4.1.2.3 Attenuated Total Reflectance

When radiation is passed from a material with a high refractive index (RI), such as germanium (RI = 4.0) or diamond (RI = 2.4), to a lower refractive index sample, a fraction of light will be reflected. When the angle of incident radiation is greater than the critical angle (approximately  $45^\circ$ ), the crystal or diamond will experience total internal reflection also known as an evanescent wave (Rouessac & Rouessac, 2007; Skoog *et al.*, 2007). As depicted in Figure 4.1-4, during total internal reflection the evanescent wave extends into the lower index sample.



**Figure 4.1-4 – Total Internal Reflection**

Internal reflection spectroscopy involves passing radiation through a transparent material with a high refractive index, such as a crystal or diamond, causing the radiation to undergo single or multiple internal reflections. A sample with a lower refractive index that is in direct contact with the crystal or diamond partially absorbs the beam of radiation before it is passed to a detector and the corresponding spectrum produced.

The attenuated total reflectance (ATR) FTIR sampling technique is based on the principle of internal reflection, whereby the incident radiation is passed through a transparent, flat or hemispherical crystal or diamond and the radiation undergoes single or multiple internal reflections. The lower refractive index sample that is in direct contact with the crystal or diamond partially absorbs the evanescent radiation that is then passed to the detector.

ATR–FTIR spectral band intensities are proportional to concentration thereby permitting quantitative measures to be made; however, the spectra can differ from conventional absorption spectra due to distortions that occur where the sample refractive index changes rapidly (Skoog *et al.*, 2007). Moreover, because the depth of penetration into the sample depends on the refractive indices of the two materials, the angle of incidence and the wavelength, lower–frequency radiation penetrates the sample deeper than the higher frequencies, causing ATR–FTIR spectral band intensities to skew toward the lower frequencies. The depth of penetration can be calculated as follows (where  $\lambda$  is wavelength,  $n_1$  is the diamond or crystal RI,  $n_2$  is the sample RI and  $\phi$  is the angle of incidence):

$$\bullet \quad D_{\text{penetration}} = \lambda / 2\pi n_1 [(\sin^2 \phi) - (n_2/n_1)]^{1/2}$$

For example, the depth of penetration for a typical hair sample (RI ~1.53) using a germanium crystal (RI = 4.0), incident angle of 45° and at a frequency of 5.0  $\mu\text{m}$  (2000  $\text{cm}^{-1}$ ) would be:

$$\begin{aligned} \bullet \quad D_{\text{penetration}} &= 5.0 \mu\text{m} / 2 * 3.14159265 * 4.0 [(\sin 45)^2 - (1.53 / 4.0)^2]^{1/2} \\ &= 0.335 \mu\text{m} \end{aligned}$$

Conversely, at the lower frequency of 25  $\mu\text{m}$  (400  $\text{cm}^{-1}$ ) the depth of penetration would be:

$$\begin{aligned} \bullet \quad D_{\text{penetration}} &= 25 \mu\text{m} / 2 * 3.14159265 * 4.0 [(\sin 45)^2 - (1.53 / 4.0)^2]^{1/2} \\ &= 1.67 \mu\text{m} \end{aligned}$$

Corrections that involve multiplying the sample spectrum by a frequency–dependent factor must therefore be applied to adjust the relative intensities. (ATR correction algorithms are included in most conventional FTIR software programs.)

The ATR–FTIR sampling technique can be applied to a wide variety of solid and liquid forms, such as textile fabrics, individual fibres, pastes, powders, aqueous solvents, polymers and rubbers. Continual research concerning the potential application of ATR–FTIR in forensic science has extended its application to a variety of samples, including paint chips, vehicle bumpers, photocopy toners, carbon copies, writing inks on paper, lipsticks on tissue and black electrical tapes (Bartick *et al.*, 1994), sunscreens on the skin surface (Rintoul *et al.*, 1998), shampoo and liquid soap surfactants (Carolei & Gutz, 2005), skin surface proteins and pharmaceutical tablets (Chan & Kazarian, 2006b; 2006a; Kazarian & Chan, 2006), latent fingerprints, and residues from fingerprints and drugs on tape lift surfaces (Ricci *et al.*, 2006; Ricci *et al.*, 2007a).

#### 4.1.2.4 Sample Thickness and Shape

For transmission analyses, electromagnetic radiation is partially absorbed by the sample with the remainder transmitted to the detector at a reduced intensity. According to Beer’s law, as the path length through the sample increases, absorbance levels increase proportionally. For IR analyses, a sample thickness of approximately 10–20  $\mu\text{m}$  is ideal for good spectral representation and for Beer’s law to be obeyed (Schiering, 1988; Kirkbride & Tungol, 1999). Beyond this path length, diffusion of the radiation increases as the sample thickness increases, and zero radiation may be transmitted to the detector if the sample possesses high absorptivity (Tungol *et al.*, 1990; Kirkbride & Tungol, 1999).

Different methods can be used to reduce sample thickness prior to analysis. Commonly, these methods include sectioning the sample with a microtome, using a small metallic roller to flatten the sample, or sampling through a diamond compression cell. The micro compression diamond cell (or “micro diamond anvil cell”) accessory consists of an upper and lower diamond window, between which the sample is placed, and a screw cap that flattens the sample when it is tightened. For some analyses, it can be better to acquire spectra using only the lower diamond window (Kirkbride & Tungol, 1999). Flattening has the benefit of increasing the sample’s surface area thereby enhancing the signal–to–noise ratio, diminishing stray light effects and increasing the energy throughput, although minor changes in frequency and intensities have been known to result from changes in the crystalline composition of some flattened fibres (Tungol *et al.*, 1990). Flattening can also improve the shape of the sample. Circular fibres can divert the radiation enough so it is not



detected, while those with irregular cross sections can refract the radiation, also distorting the spectral representation (Kirkbride & Tungol, 1999).

Finally, smoothness of the sample surface can also be an issue. Fibres with a flat, smooth surface can generate interference fringing whereby some of the radiation transmitted to the detector has undergone internal reflection, having traversed the sample multiple times (Kirkbride & Tungol, 1999). An interference fringe results when two signals reach the detector, yielding a second burst in the interferogram. One arises from the radiation beam that passes the sample once and the other arises from the beam that traverses the sample multiple times (Kirkbride & Tungol, 1999). Interference fringes can cause problems when interpreting spectra and can even obscure weak absorption bands (Harrick, 1977). One study found that flattening samples with a metallic roller or a diamond compression cell did not prevent interference fringes resulting in the spectra (Tungol *et al.*, 1990). An advantage of the attenuated total reflection technique over transmission analyses is that interference fringes do not occur (Harrick, 1977).

#### 4.1.3. Chemical Imaging

Chemical imaging combines digital imaging with conventional spectroscopy techniques, including UV–visible absorption, photoluminescence emission, Raman scattering, mid–IR or near–IR spectroscopy (Payne *et al.*, 2005a) to generate information on the identity, distribution and concentration of substances present in a sampled area. The transmitted, absorbed or reflected intensity is not only recorded as a function of wavelength ( $\lambda$ ) – as with conventional spectroscopy – but a variable liquid crystal tuneable filter (LCTF) also records a fully resolved spectrum for each pixel location ( $x, y$ ) (Payne *et al.*, 2007). Three–dimensional images ( $x, y, \lambda$ ) of the sample – where wavelength ( $\lambda$ ) is the third dimension – are presented as false colour maps, with an arbitrary colour attributed to each pixel according to the spectral intensity at a selected wavenumber (Tahtouh *et al.*, 2005). Typically, red represents high spectral intensity and blue represents low spectral intensity.

One of the main advantages of chemical imaging over traditional techniques is the utilisation of a focal plane array (FPA) detector that permits collection of spectral data from the entire field of view simultaneously. Analysis time is greatly reduced compared with techniques that require the measurement of multiple discrete spectra to obtain an

average profile of the sample (Payne *et al.*, 2005b). Also, by selecting the wavenumber corresponding to the spectral band of a specific molecule, its spatial distribution can be selectively mapped across the sampled area, revealing any inhomogeneity present (Flynn *et al.*, 2005; Flynn *et al.*, 2006; Ricci *et al.*, 2007b). This capability has been investigated for untreated latent fingerprints and those developed by DFO (1, 8-diazafluoren-9-one), ninhydrin, cyanoacrylate fuming and/or luminescent staining, as a way to maximise ridge-to-background contrast on surfaces with high colour content and complex patterns, including the Australian polymer banknote (Exline *et al.*, 2003; Payne *et al.*, 2005a; Tahtouh *et al.*, 2005). In addition to fingerprints, chemical imaging has also been successfully investigated for multi-component automotive paint samples (Flynn *et al.*, 2005; Payne *et al.*, 2005b), bicomponent textile fibres (those with two polymers of different properties) (Flynn *et al.*, 2006), tapes and other adhesives, the sequence of intersecting ball-point pen and toner lines, and firearm discharge residues (Payne *et al.*, 2005b) and for the age estimation of bruises (Payne *et al.*, 2007).

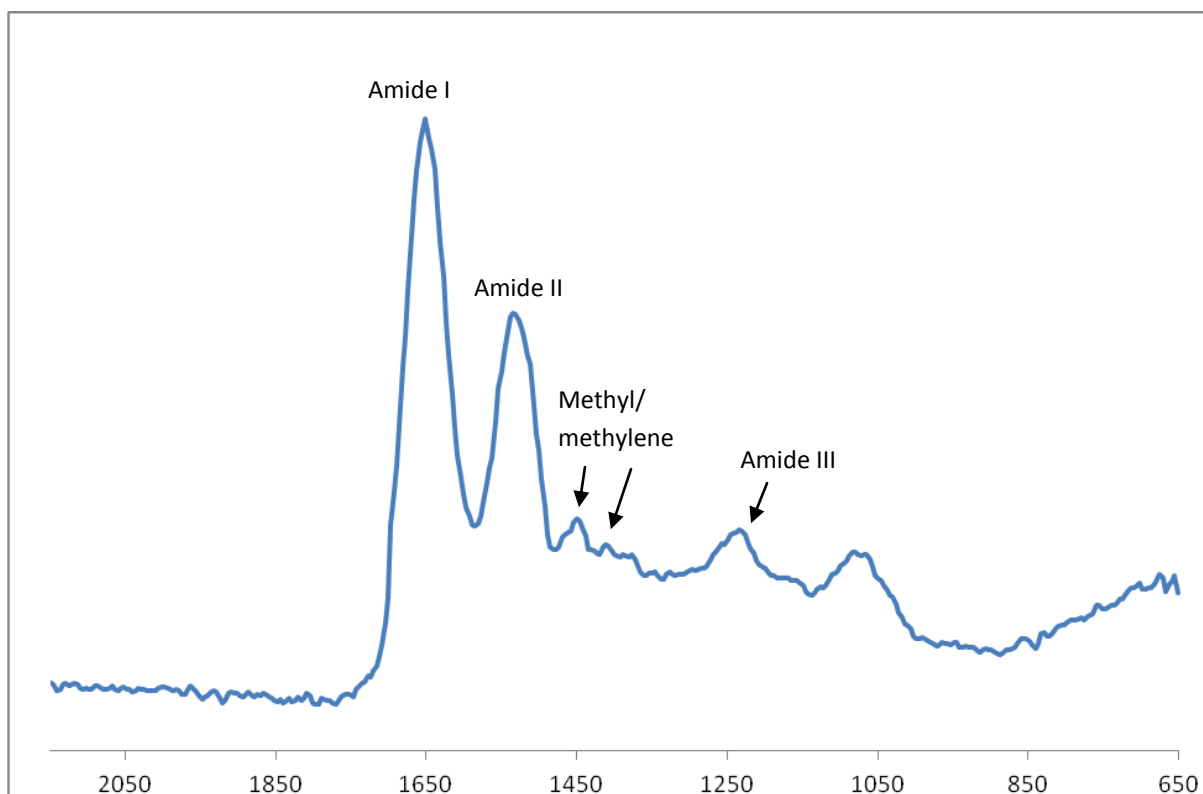
Furthermore, to investigate the aging of fingerprints, ATR-coupled chemical imaging has been used to spatially locate proteins and lipids in fingerprint residues over time (Ricci *et al.*, 2007b). However, it has been observed that a much higher number of ATR image scans (1024 scans, approximately 25 minutes) is required to obtain an acceptable signal-to-noise ratio compared with transmission imaging (256 scans, approximately 6 minutes). In addition, the high refractive index of the ATR crystal employed results in a smaller field of view (90 x 90  $\mu\text{m}$ ) (Flynn *et al.*, 2006). With respect to human hair, preliminary chemical imaging studies by Chan and colleagues (2005; 2008) suggested that ATR-coupled imaging could potentially provide a further level of discrimination by identifying chemical components typically associated with hair.

#### 4.1.4. Research on Hair

A key structural component of the hair keratin protein is cystine, a dimeric amino acid that is formed by the oxidation of two cysteine residues covalently linked by a disulfide bond. The hair bleaching process involves oxidative cleavage of the disulfide bond producing a sulfonic acid (Brenner *et al.*, 1985). This reaction is also naturally promoted following the exposure of hair to UV radiation from sunlight (Signori & Lewis, 1997). Most permanent waving treatments also involve a re-oxidation process following

initial reduction of the disulfide cross links and this produces a sulfonic acid (Brenner *et al.*, 1985).

The major FTIR absorbance bands for human hair keratin correspond to the functional groups Amide I (C=O, NH), Amide II (CN, CH) and Amide III (NH, CN, O=CN), carbonyl (C=O), hydrocarbon (CH), methylene (CH<sub>2</sub>) and methyl (CH<sub>3</sub>) (Panayiotou & Kokot, 1999), as shown in Figure 4.1-5.



**Figure 4.1-5 – Typical Hair Keratin Spectra**

The major FTIR absorbance bands for human hair keratin correspond to the functional groups Amide I (C=O, NH) at approximately 1650–1630 cm<sup>-1</sup>, Amide II (CN, CH) and Amide III (NH, CN, O=CN) at approximately 1550–1510 and 1320–1230 cm<sup>-1</sup>, respectively, carbonyl (C=O) at approximately 1735–1710 cm<sup>-1</sup> often masked by the Amide I band, hydrocarbon (CH) at approximately 1470–1460 cm<sup>-1</sup> also often masked by the Amide II band, and methylene (CH<sub>2</sub>) and methyl (CH<sub>3</sub>) at approximately 1453–1390 cm<sup>-1</sup>. These peak frequencies are approximate as slight variations will occur between instruments.

The FTIR spectra of chemically treated or sun damaged hair have been found to include an additional absorbance band, corresponding to the oxidation of the cysteine thiol (SH) bond or the cystine disulfide (S–S) bond. Table 4.1-1 displays the name, structure and major FTIR absorbance bands (cm<sup>-1</sup>) for human hair keratin and their oxidative products (Joy & Lewis, 1991; Signori & Lewis, 1997; Panayiotou & Kokot, 1999; Barton, 2011). These

peak frequencies are approximate as slight variations are known to occur between instruments.

**Table 4.1-1 – Hair Keratin Components and Oxidation Products**

Name	Functional Group	Structure	Abs (cm <sup>-1</sup> )
<b>Cysteine &amp; Cystine</b>		<b>HOOC—CH(NH<sub>2</sub>)—CH<sub>2</sub>—SH</b>	
		<b>HOOC—CH(NH<sub>2</sub>)—CH<sub>2</sub>—S—S—CH<sub>2</sub>—CH(NH<sub>2</sub>)—HOOC</b>	
	Carbonyl	C=O stretch	1735–1710
	Amide I	C=O stretch and NH bend	1650–1630
	Amide II	CN stretch and NH bend	1550–1510
	Hydrocarbon	CH deformation	1470–1460
	Methylene/ Methyl	CH <sub>2</sub> /CH <sub>3</sub> bend	1453–1390
	Amide III	NH bend, CN stretch and O=C–N bending	1320–1230
<b>Cystine monoxide</b>		<b>HOOC—CH(NH<sub>2</sub>)—CH<sub>2</sub>—SO—S—CH<sub>2</sub>—CH(NH<sub>2</sub>)—HOOC</b>	
	Sulfinyl	SO	1072–1070
<b>Cystine dioxide</b>		<b>HOOC—CH(NH<sub>2</sub>)—CH<sub>2</sub>—SO<sub>2</sub>—S—CH<sub>2</sub>—CH(NH<sub>2</sub>)—HOOC</b>	
	Sulfonyl	SO <sub>2</sub>	1121–1114
<b>Cysteine S-sulfonate</b>		<b>HOOC—CH(NH<sub>2</sub>)—CH<sub>2</sub>—S—SO<sub>3</sub>H</b>	
	Sulfur–Sulfo	S—S=O	1022–1020
<b>Cysteic acid</b>		<b>HOOC—CH(NH<sub>2</sub>)—CH<sub>2</sub>—SO<sub>3</sub>H</b>	
	Sulfo	S=O	1040–1035

To date, hair research involving FTIR spectroscopy has primarily focused on the effects of chemical hair treatments and/or sunlight exposure on keratin protein. Brenner and colleagues (1985) investigated the degree of discrimination between treated and untreated hair samples collected from 135 male and female participants, aged 6 months to 83 years. The researchers prepared 0.5 to 0.7 mm hair fragments that were analysed using a diamond cell micro sampler. Spectra (1000 scans at 8 cm<sup>-1</sup> resolution) were collected using a *Digilab FTS-10 C/D* FTIR Spectrometer with cesium iodide optics, a triglycine sulfide (TGS) detector and a diamond cell with x4 beam condenser. They observed that untreated hair did not present a sulfonic acid (sulfo group) absorption peak or shoulder at 1044 cm<sup>-1</sup> in the FTIR spectrum. The researchers also report that natural hair colour or the

absence of melanin (white hair), moisture and the age of the hair samples had little to no effect on the sulfonic acid absorption peak (Brenner *et al.*, 1985).

Joy and Lewis (1991), and later Signori and Lewis (1997), investigated the effects of chemical treatments and natural weathering on the oxidation products of cystine. Spectra were collected on a *Perkin Elmer 1740* FTIR Spectrophotometer with TGS and mercury cadmium telluride (MCT) detectors and coupled to a Spectra-Tech IR Plan optical microscope. In total, the researchers compared five sampling techniques. One technique was conducted in transmission mode involving a Spectra-Tech ‘Sample Plan’ BaF<sub>2</sub> compression cell (single hairs) and the second was conducted in reflectance mode involving a diffuse reflectance attachment with KBr pellets (multiple hairs). The third, fourth and fifth techniques involved various ATR attachments including a multi-reflection KRS-5-ATR accessory (multiple hairs), a *Spectra-Tech* ZnSe-ATR accessory (single hair) and a *Bio-Rad* elliptical shape diamond-ATR accessory (multiple hairs) (Joy & Lewis, 1991; Signori & Lewis, 1997).

Joy and Lewis (1991) observed that the diffuse reflectance and KRS-5-ATR methods both produced mediocre results, including spectra with narrow transmission ranges and unacceptable noise levels. Similarly, Signori and Lewis (1997) observed that the ZnSe-ATR produced high noise and low reproducibility, while the diamond-ATR results only showed high sensitivity when seven to nine hairs were analysed simultaneously. Conversely, both papers report that reproducible, noise-free spectra were obtained with the ‘Sample Plan’ BaF<sub>2</sub> compression cell technique. Cysteic acid and cystine-S-sulfonate levels were found to be higher for naturally weathered hair than for chemically bleached hair, while cystine monoxide showed no significant variation between the two types of hair (Joy & Lewis, 1991). Cysteic acid content was also found to increase from the mid-point of the hair shaft to the distal end, though a standard variation of up to 11% occurred for the intensity absorption of cysteic acid in hairs from the same sample tress, particularly for naturally weathered hair (Signori & Lewis, 1997).

FTIR spectroscopy has also been used to investigate the Amide I and II residues alone, to determine whether genetic variations between the quantity and type of amino acids present in human hair were distinctive enough to individualise hair samples. Using the same sample set as Brenner and colleagues (1985) described above, a later study by Hopkins and colleagues (1991) examined differences between amide absorption band

ratios. Analyses in the later study again employed the diamond cell micro sampler, but spectra (128 scans,  $4\text{ cm}^{-1}$  resolution) were collected with a *Mattson Polaris* FTIR spectrometer and a deuterated triglycine sulfate (DTGS) detector. Reportedly, the spectra showed little to no difference in the amide band ratio that could be correlated to gender, age, hair colour or chemical treatment. The authors concluded that, if such differences did exist, they would have “little influence on the ability to analyse for other chemicals such as hair spray, conditioner” (Hopkins *et al.*, 1991, pp65).

Rintoul and colleagues (1998) reported the effects of race on the major amide and CH deformation spectral bands while, the following year, Panayiotou and Kokot (1999) reported the effects of race as well as gender, age and hair oxidation. In both studies, hair samples were flattened with a metallic roller and taped to a gold mirror for spectra collection (256 scans,  $8\text{ cm}^{-1}$  resolution) using a *Perkin Elmer* FTIR 2000 System spectrometer coupled to a *Perkin Elmer i-series* IR microscope and MCT detector (Rintoul *et al.*, 1998). Reportedly, Rintoul and colleagues (1998) could distinguish between spectra collected from nominally black Caucasian hair and nominally black Asian hair, while Panayiotou and Kokot (1999) could discriminate between two similarly aged female Caucasians with the same hair colour, length and treatment, as well as between hair collected from the left and right side of the participant’s heads. Similar to previous studies, discrimination between treated and untreated hair was also reported and, for the first time, spectra of single hairs were also successfully discriminated on the basis of gender (Panayiotou & Kokot, 1999). However, as noted in both reports, these results were only possible once chemometric methods for data interpretation, including principal component and fuzzy cluster analysis, were applied as opposed to conventional statistical methods.

Bartick and colleagues (1994) reported on the FTIR–ATR analysis of single hairs with hair spray contamination to determine whether hair spray or other contaminants on a hair may increase the evidential value of the sample. The IR spectra (250 scans,  $4\text{ cm}^{-1}$  resolution) of clean hair, hair coated with hairspray and hairspray reference samples, were collected on a *Nicolet 20SXC* FTIR spectrometer coupled to a Spectra–Tech IR Plan microscope and a single–reflection hemispherical ATR (ZnSe) microscope objective (Bartick *et al.*, 1994). The researchers subtracted a clean hair spectrum from a hairspray coated spectrum and observed that the difference spectrum closely resembled that of the hairspray reference. However, two residual amide bands near  $1650$  and  $1530\text{ cm}^{-1}$  could

not be subtracted and the researchers recommended that the compositional variation of hairsprays be further investigated to establish the capability to discriminate between these products.

While investigating the FTIR spectra of hair from different genders and racial origins, Barton (2011) followed the approach used by Bartick (1994), whereby the spectra of clean hair was subtracted from the spectra of the contaminated hair to identify the components responsible for the atypical spectral results. Atypical spectra from two participants were observed by Barton (2011), one who used an intense hair moisturiser as part of the hair straightening process and the other who used hair gel. In the difference spectrum of the participant using the intense moisturiser, broad absorptions in the 3430 to 3090  $\text{cm}^{-1}$  region were observed, indicative of carboxylic acid (COOH) and alcohol (OH) functional groups, three absorption bands in the 2950 to 2820  $\text{cm}^{-1}$  region were observed, indicative of the hydrocarbons (CH) of saturated and unsaturated long chain fatty acids, alcohols and esters, as well as two sharp bands at 1106 and 991  $\text{cm}^{-1}$ , characteristic of carbonyl (CO) from the ester functional group. Absorbance bands in the difference spectrum from the sample of the participant using the hair gel were determined to be consistent with a long-chain siloxane resin commonly observed in cosmetic hair formulations and fixatives such as gel, hairspray and mousse (Barton, 2011). Specifically, two absorption bands at 1260 and 800  $\text{cm}^{-1}$  were observed and attributed to the Si-CH<sub>3</sub> bond and two absorption bands at 1095 and 1020  $\text{cm}^{-1}$  attributed to the Si-O bond.

#### 4.1.5. Research Focus

Unlike the biological structure of hair, it is proposed that the chemical components associated with hair are quite dissimilar. When considering intrinsic factors, human hair plays a role in the excretion of waste from the body such as heavy metals, chemicals and toxins, by binding these substances to the melanin in cortical keratinocytes (Tobin & Paus, 2001). The extent of binding and retention differs between hairs depending on, for example, the level of pigmentation (Rothe *et al.*, 1997; Kidwell *et al.*, 2000), cosmetic treatments and hygiene (Kidwell *et al.*, 2000). Conversely, considering environmental contaminants, the outer surface of the hair shaft also binds molecules in order to prevent foreign material from accessing the living tissue of the scalp. Environmental stressors that can effect hair include climate, pollutants, exposure to toxins (Tobin & Paus, 2001), as well as personal grooming habits (Gurden *et al.*, 2004).

Through microscopic examination and comparison, the forensic examiner assesses and scores such hair characteristics as colour, pigmentation, chemical treatments, spatial configuration, length and coarseness (Petraco, 1999; Biological Criminalistics, 2004). However, identifying hair surface contamination resulting from the popular use of cosmetic products such as hairsprays, gels and mousse, is not currently part of the examination process. Hair research involving ATR–FTIR spectroscopy, to date, has focused on the effects of chemical–based hair treatments and/or sunlight exposure, and very few studies have been reported on hair surface contamination. The research focus of this chapter involved assessing the potential for identifying traces of cosmetic product on the hair surface. Such a process could increase the evidential value of human hair by producing an additional level of discrimination.

Evaluation of the potential of ATR–FTIR spectroscopy to detect hair surface contamination commenced from a broad perspective. First, visual spectral assessments and spectral interpretation software were used to establish whether popular hair product constituents absorbed in the infrared region and, therefore, could be detected by the selected method. Discriminant analysis (canonical correlation) was then used to determine whether multiple spectra of the products could be broadly distinguished or classed based on product type including hairspray, gel, mousse, moisturiser, finishing gloss, styling wax or smoothing balm. The final analyses were designed to address hair evidence in the context of forensic casework. Discriminant analysis (hierarchical cluster) was used to determine whether the spectra of a particular product type could be distinguished from other products types, following application to a single hair.



## 4.2. Materials and Methods

### 4.2.1. Sample Preparation

Hair samples were received from 154 participants, comprising males and females aged between 18 and 65 years, as described in section 2.2.1 Sample Preparation. For this part of the project, additional hair samples were received from one female Caucasian (participant number 2002038). The participant's hair was washed, blow-dried and collected by cutting tresses approximately 8 cm from the distal ends then placing the tresses together in a plastic snap-seal bag. The participant's hair had not been chemically treated in any way nor did the hair contain any cosmetic product immediately prior to sample collection.

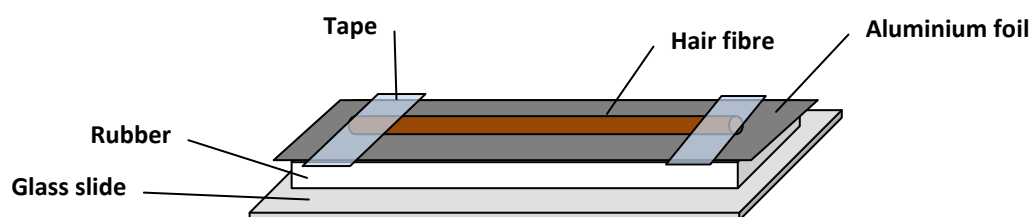
Hair products are manufactured using a diverse range of organic compounds to various degrees, depending on the product type. Common organic functional groups found in cosmetic products include aliphatic hydrocarbons (CH), aromatic derivatives (C<sub>6</sub>H<sub>5</sub>), carboxylic acids (COOH), esters (COOR), alcohols (OH), amides (CONR<sub>2</sub>) and silicone oils (SiO). Seven types of hair products were targeted, namely, hairspray, gel, mousse, moisturiser, finishing gloss, styling wax and smoothing balm. A description of the seven products is provided in Appendix F, including the product type, brand and a complete list of contents as described by the respective manufacturers.

Four sample sets were prepared overall. With the exception of the reference spectra, the other three sample sets each comprised five single hairs:

- Product alone (reference spectra);
- Hair without product (control);
- Hair with product densely applied; and
- Hair with product sparsely applied.

The reference spectra were comprised of five samples with hair product alone (no hair). Each of the products was directly applied to five 10 cm<sup>2</sup> sheets of aluminium foil that were left to dry naturally at room temperature, for between two and seven days. Two spectra from different locations on each dried product sample were collected, yielding ten spectral

references for each product. The five single hairs that comprised the control samples (no product) were removed from the snap-seal bag with tweezers, individually fixed to a pre-cleaned laboratory bench with double sided tape at either end and hand rolled with a small (approximately 5 mm) metallic roller to flatten the hair surface area. The metallic roller and the bench top were cleaned with ethanol in between samples to avoid cross-contamination. Each flattened hair was individually fixed with tape, at either end, to a Livingstone Premium Microscope Glass Slide (76.2 x 25.4 mm, thickness 1.0 – 1.2 mm). A thin slice of rubber, approximately 3 mm in depth, was placed between the sample and the glass slide to provide a resilient surface for the ATR crystal. In addition, as rubber is known to absorb IR radiation, it was first covered in heavy-duty aluminium foil to ensure that it did not contribute to the recorded spectra. A depiction of the sampling substrate is provided in Figure 4.2-1. Two spectra from each hair were collected, yielding ten spectra for the ‘without product’ sample set.



**Figure 4.2-1 – Depiction of FTIR Sampling Substrate**

For spectral data collection, a 3 mm slice of rubber was placed on a glass microscope slide and covered in heavy duty aluminium foil. The flattened hair fibre was fixed over the top with tape at either end.

The other two sample sets were similarly prepared; however, instead of removing the single hairs from the bag, 14 small tresses of hair were removed with tweezers then taped to aluminium foil. Seven of the small tresses were heavily coated with one each of the products and this formed the ‘product densely applied’ sample set. The other seven small tresses were sparingly coated with one each of the products to simulate “normal” product use and this formed the ‘product sparingly applied’ sample set. Both sample sets were left to dry naturally for between two days and one month, then five single hair samples were removed from each of the tresses, taped to the laboratory bench, flattened and prepared in a manner similar to the ‘without product’ hair samples. Two spectra from different locations on each hair were collected, yielding ten spectra for each product in the

‘product sparingly applied’ sample set and ten spectra for each product in the ‘product densely applied’ sample set.

#### 4.2.2. Instrumentation

All data collection was performed with a *Thermo–Nicolet* Micro–FTIR Nexus bench coupled to a Continuum FTIR Microscope as well as its associated spectral analysis software, *OMNIC* version 7.3 (*Thermo–Electron*, Madison, Wisconsin, USA). The microscope was fitted with a 15x Infinity Refflachromat objective, a germanium slide–on ATR accessory and a contact alert sensor pad (supplied by *Thermo–Fisher Scientific*, Scorseby, Victoria). Operating parameters for the FTIR are provided in Table 4.2-1:

**Table 4.2-1 – *Thermo–Nicolet* FTIR Operating Parameters**

Parameter	Setting
Detector	Mercury Cadmium Telluride (MCT)
Beam Splitter	Potassium Bromide (KBr)
Spectral Range	4000 to 650 $\text{cm}^{-1}$
Gain	Autogain
Moving Mirror Velocity	1.8988 $\text{cm/s}$
Aperture	100 $\mu\text{m}$
Apodization	Happ–Genzel
Fourier Transform Phase Correction	Mertz algorithm

In addition to the operating parameters of the instrument, standard data collection conditions were likewise maintained throughout the research. These conditions included obtaining a background spectrum in air before every sample, accumulating 128 scans for every spectrum (57 second collection time) at  $8 \text{ cm}^{-1}$  resolution. Product contamination on the hairs was visually located with the Refflachromat objective and the slide–on ATR in view mode (i.e., microscope only). The Continuum microscope stage was raised toward the ATR germanium crystal (analysis mode) no further than when the contact alert pad indicated that contact had been made with the sample. However, contact with the sample was usually indicated by a change in the *OMNIC* Live Spectrum Collection Preview prior to any indication of contact by the alert pad. For the ‘product densely applied’ sample set, Live Preview spectra resembling hair keratin on its own or product contamination on its own was often observed depending on the degree of contact pressure applied between the crystal and sample. A spectrum of product on its own was observed when little pressure

was applied, while a spectrum of keratin on its own was observed when slightly more pressure was applied. The difference in pressure between these two observations was minuscule. For this research, only spectra resembling a combination of both keratin and product together were collected for the relevant samples.

Raw data spectral intensity was collected in the percent reflectance mode that was mathematically transformed to absorbance using the *OMNIC* Advanced ATR Correction function that corrects for both the effects of variation in the depth of penetration and the shifting of IR absorption bands. The crystal was wiped with a cotton tip and occasionally with ethanol to avoid product residue cross-contamination between samples.

### 4.2.3. Data Preparation

A qualitative visual evaluation was performed on each spectrum. The *OMNIC* IR Spectral Interpretation function was used to help evaluate the functional groups represented in each spectrum and, more specifically, to identify which bonds corresponded to each major absorbance band. This function examined the location and intensity of peaks in the spectrum (or a specified region), then provided a list of functional groups that may be present in the sample.

All spectra were saved as Comma Separated Value (CSV) data files. The individual CSV spectral intensity measurements (absorbance) were copied and transposed to *Excel for Windows* where a single spreadsheet was prepared and exported directly to *PASW (Predictive Analytical Software) Statistics for Windows*, version 18.0.0 (SPSS Statistics IBM Corporation, 2009) for analysis. As the data collection conditions produced a data spacing of  $3.857\text{ cm}^{-1}$ , this resulted in an absorbance measurement for every 3 to 4 wavenumbers (e.g., an absorbance measurement at 710, 714, 717, 721 ...  $\text{cm}^{-1}$ ). For each of the sample sets statistically analysed, the *PASW* input datasheet contained ten absorbance measurements for 254 wavenumbers between  $1632$  and  $652\text{ cm}^{-1}$ .

### 4.2.4. Chemical Imaging

For the collection of spectra from the ‘product densely applied’ and ‘product sparingly applied’ sample sets, contamination on the hair surface was located visually through the 15x Infinity Replachromat objective with the slide-on ATR in view mode (microscope only). In addition to the methods described above, chemical imaging was also used to determine whether spatial data could assist the forensic examiner locate product

contamination on the hair surface. This part of the study was designed to provide a “proof-of-concept” for potential future work. Hair samples were sprayed with hairspray as per the ‘product densely applied’ sample preparation previously described (see 4.2.1, Sample Preparation). The spatial and spectral data were collected simultaneously on a *Digilab* FTS 7000 series FTIR spectrometer, coupled to a *Digilab* UMA 600 microscope. The microscope was fitted with a Stingray Large Sampling Accessory (LSA) that incorporates a germanium ATR crystal and a Lancer 64 x 64  $\mu\text{m}$  focal plane array (FPA) detector. The data were collected (64 scans at  $8\text{ cm}^{-1}$  resolution) over a spectral range of 4000 to  $900\text{ cm}^{-1}$  and with the instrument’s associated software, the *Digilab* Win-IR Pro software. False colour maps corresponding to the spectra for hair keratin and product contamination were saved in Bitmap Image File (bmp) format, while the spectral measurements were saved as CSV files.

#### 4.2.5. Discriminant Analysis

The underlying principles of discriminant analysis have been described in detail in the previous chapter (section 2.2.8 Discriminant Analysis). Chiefly, discriminant analysis is used to determine whether two or more known groups can be distinguished from each other, based on a linear combination of multiple variables. The discriminant function coefficients would categorise cases by allocating them to one group when the absorbance measurements were placed within a certain criterion or to another group when the coordinates were placed within another criterion. The more widely separated the discriminant function distributions, the more successful the prediction of group membership from those functions (Kinnear & Gray, 2010).

Discriminant analysis [probability of F criteria (0.05, removal 0.10) and Wilks’ lambda stepwise method] was used in this research, first to allocate 60 reference spectra to one of six product categories (NB – attempts to collect spectra for the product ‘moisturiser’ were unsuccessful, so this product was discontinued from further analyses; See 4.3.1.4, Leave-In Moisturiser Reference Spectra). The six types of hair product, namely, hairspray, gel, mousse, finishing gloss, styling wax and smoothing balm, were the grouping variables, while the absorbance measurements for 254 wavenumbers between  $1632$  and  $652\text{ cm}^{-1}$  were the regressors from which group membership was predicted. Once it was observed that discriminant analysis could distinguish between the spectral references with high prediction accuracy, the analysis was used to allocate 60 ‘product

densely applied' spectra to one of six product categories. Two types of discriminant analysis were used in this research, canonical and hierarchical cluster. Principal component and fuzzy cluster analysis were used by Panayiotou and Kokot (1999) to discriminate between hair fibres based on chemical treatment and gender, and used by Barton (2011) to discriminate between hair fibres based on chemical treatment, gender and racial origin. Such statistical techniques were not applied here because principal component analysis assumes that any prior sub-structuring in the data is unknown prior to analysis (Brooks, 2007), which was not the case with the product reference samples, while fuzzy cluster analysis assumes that each case belongs to every cluster so only maintains a likelihood of belonging to any given cluster, which was not the objective of the present investigation.

#### **4.2.5.1 Canonical Discriminant Analysis**

Canonical discriminant analysis was used here to evaluate whether the individual reference spectra could be allocated to one of six product types. Where such discrimination could be made with a high degree of accuracy, it follows that the potential to discriminate between products after application to hair warranted investigation. Canonical discriminant analysis measures the degree of association between discriminant scores and the predicted groups, and is used when the group membership for a set of cases is known. Where most of the observed variability is explained by differences between the groups, a high canonical correlation (up to 100%) will result, whereas misclassification will result from a lack of separation between the groups.

Individual function coefficients produced by *PASW* represent the discriminating power of each of the variables, with Function 1 explaining the greatest variance in the data and Function 2 explaining the second greatest variance in the data, etc. (Norusis, 2008). Thus, the associated canonical discriminant function plot (i.e., Function 1 versus Function 2) visually represents discriminant scores of the predictor variables that showed the greatest discriminating power (Norusis, 1985; Brooks, 2007).

#### **4.2.5.2 Hierarchical Cluster Analysis**

Hierarchical cluster analysis is used when the group membership for a set of cases is not known. For each of the spectral references, information about the product type was known whereas any products used by the owner of a hair recovered as evidence in forensic casework would not be known. Therefore, hierarchical cluster analysis (Squared Euclidean

distance and Ward's Method) was used to facilitate the allocation of spectra from hairs with 'product densely applied' to one of six product types.

#### 4.2.5.3 Assumptions

Firstly, discriminant scores are sensitive to outliers because they are based on the calculated mean of the group centroid. Simple histograms produced by *PASW* can be used to check for any outlying cases. Second, the covariance matrix of the predictor variables, being the absorbance measurements for each wavenumber, should be the same for all populations and violations of this assumption can affect both hypothesis testing and classification (Norusis, 2008). 'Box Ms' produced by *PASW* can be used to test whether the population covariance matrices are equal; however, this test could not be performed for the present data because there were fewer than two non-singular group covariance matrices (SPSS Statistics IBM Corporation, 2008). That is, due to the size of each group (spectra per product) being less than the number of variables (wavenumbers between 1632 and 652 with  $3.857\text{ cm}^{-1}$  data spacing), the covariance matrix for each group was essentially singular. Proceeding with the discriminant analysis without testing equality of the covariance matrices could risk incorrectly fitting the data.

Overall, the analyses in this chapter investigated whether traces of product on the hair surface could be used to increase the evidential value of human hair in a forensic context, by introducing an additional level of discrimination. Specifically, visual evaluations and discriminant analyses were used to address the questions:

- Can the FTIR spectra of a particular product type (sans hair) be distinguished from that of other product types;
- Can the FTIR spectra of a particular product type be distinguished from that of other product types following dense application to a single hair;
- Can the FTIR spectra of a particular product type be distinguished from that of other product types following sparse application to a single hair; and
- Can chemical imaging assist the forensic examiner locate contamination on the hair surface.

### 4.3. Results and Discussion

Hair samples were received from a female Caucasian (participant number 2002038). The hair was washed and dried, then collected by cutting tresses approximately 8 cm from the distal hair end and placing them directly in a plastic snap-seal bag. Seven types of hair products were targeted, namely, hairspray, gel, mousse, moisturiser, finishing gloss, styling wax and smoothing balm. One set of five samples for each of the seven products alone was prepared as reference spectra. Three sample sets each comprising five single hairs were also prepared, including hair without product (control), hair with the seven products densely applied and hair with the seven products sparingly applied. Two spectra from each of the samples—either single hair or product alone—were collected, yielding ten spectra per product within a sample set as well as ten controls (spectra of hair alone). Visual evaluations and *OMNIC* Spectral Interpretation were used to establish whether hair product constituents could be detected by ATR-FTIR spectroscopy. Discriminant analysis was used to determine whether multiple spectra of the absorbing constituents could be broadly distinguished and classed based on product type. Discriminant analysis was then used to determine whether the spectra of a particular product type could be distinguished from other product types after application to a single hair.

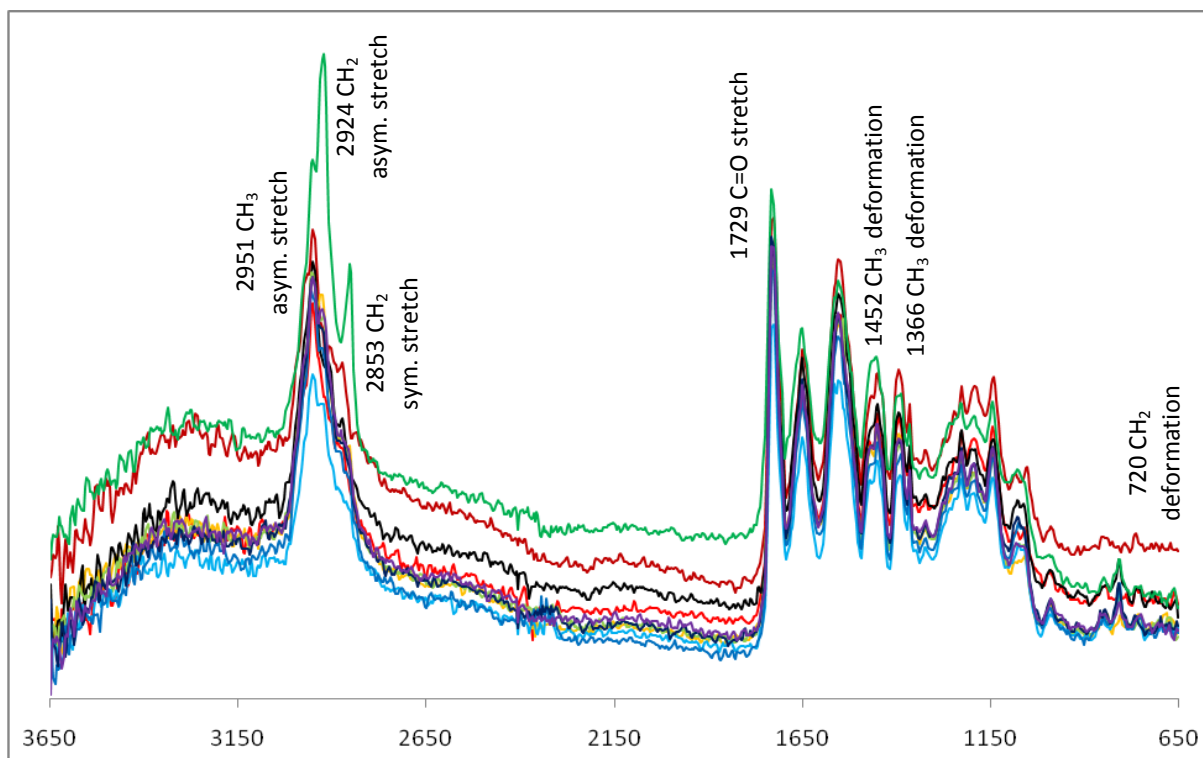
#### 4.3.1. Hair Product References

##### 4.3.1.1 Hairspray Reference Spectra

Visual evaluation of the ten hairspray spectra established that some constituents of the product absorbed in the infrared region and therefore could be identified by the ATR-FTIR spectroscopy method. This was confirmed by spectral interpretation software that assessed the location and intensity of absorbance bands and determined that functional groups consistent with aliphatic hydrocarbons (CH) were present in the samples analysed. Figure 4.3-1 illustrates the main vibrational bands present, including the asymmetric stretching vibration of CH<sub>3</sub> occurring at 2951 cm<sup>-1</sup> and CH<sub>2</sub> at 2924 cm<sup>-1</sup>, the symmetric stretching vibration of CH<sub>2</sub> at 2853 cm<sup>-1</sup>, the CH<sub>3</sub> deformations at 1452 cm<sup>-1</sup> (asymmetric bending) and at 1366 cm<sup>-1</sup> (symmetric bending) and the CH<sub>2</sub> deformation at 720 cm<sup>-1</sup> (rocking) (Pavia *et al.*, 1979; Thermo Electron Corporation, 2006). A carbonyl (C=O)



stretching frequency consistent with carboxylic acid (COOH) was also observed at  $1729\text{ cm}^{-1}$  (Pavia *et al.*, 1979).



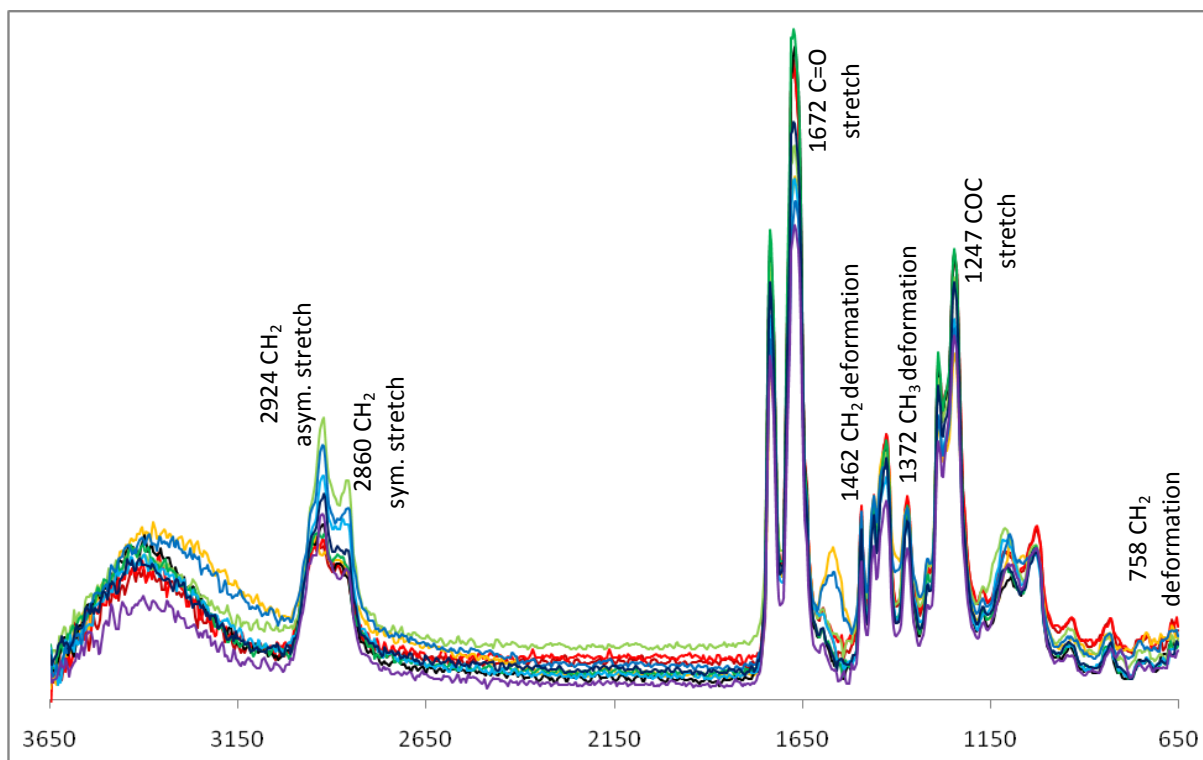
**Figure 4.3-1 – Hairspray Reference Spectra**

Spectral interpretation software used to assess the hairspray reference spectra confirmed the presence of aliphatic hydrocarbons. The main vibrational bands included the asymmetric stretching vibration of  $\text{CH}_3$  at  $2951\text{ cm}^{-1}$  and  $\text{CH}_2$  at  $2924\text{ cm}^{-1}$ , the symmetric stretching vibration of  $\text{CH}_2$  at  $2853\text{ cm}^{-1}$ , the  $\text{CH}_3$  deformations at  $1452\text{ cm}^{-1}$  (asymmetric bending) and at  $1366\text{ cm}^{-1}$  (symmetrical bending) and the  $\text{CH}_2$  deformation at  $720\text{ cm}^{-1}$  (rocking). A carbonyl stretch at  $1729\text{ cm}^{-1}$  consistent with carboxylic acid was also observed.

The spectral interpretation results were partially consistent with the product content, particularly the carbonyl stretch of the acrylate and methacrylates polymers (see *Coles Smart Buy Hairspray*, Appendix F). Visually, the hairspray spectra collected were inconsistent with the hairspray reference reported by Bartick and colleagues (1994). However, spectral frequencies for the main absorbance bands were not reported by Bartick and colleagues (1994), so an accurate comparison could not be performed; also, different hairspray brands most likely contain different compounds and ratios.

#### 4.3.1.2 Gel Reference Spectra

Visual evaluation of the ten gel spectra also established that some product constituents could be identified by the ATR–FTIR spectroscopy method. This was confirmed by spectral interpretation software that determined that functional groups consistent with aliphatic tertiary amides ( $\text{CONR}_2$ ), aliphatic hydrocarbons (CH) and aromatic ethers ( $\text{C}_6\text{H}_5\text{—OCO}$ ) were present. Figure 4.3-2 illustrates the main vibrational bands present in the samples analysed. Those absorbances attributed to the CH functional groups include the asymmetric stretching vibration of  $\text{CH}_2$  at  $2924\text{ cm}^{-1}$ , the symmetric stretching vibration of  $\text{CH}_2$  at  $2860\text{ cm}^{-1}$ , the  $\text{CH}_2$  deformations at  $1462\text{ cm}^{-1}$  (scissoring) and  $758\text{ cm}^{-1}$  (rocking) and the  $\text{CH}_3$  deformation (symmetrical bending) at  $1372\text{ cm}^{-1}$  (Pavia *et al.*, 1979; Thermo Electron Corporation, 2006). The carbonyl group ( $\text{C=O}$ ) stretching vibration at  $1672\text{ cm}^{-1}$  and the absence of a NH absorbance band at approximately  $3500\text{ cm}^{-1}$  was attributed to the tertiary amide, while the asymmetric stretching vibration of COC at  $1247\text{ cm}^{-1}$  was attributed to the aromatic ether (Pavia *et al.*, 1979; Thermo Electron Corporation, 2006).



**Figure 4.3-2 – Gel Reference Spectra**

Spectral interpretation software used to assess the gel reference spectra confirmed the presence of aliphatic hydrocarbons, aliphatic tertiary amides and aromatic ethers. The main vibrational bands included the asymmetric stretching vibration of  $\text{CH}_2$  at  $2924\text{ cm}^{-1}$ , the symmetric stretching vibration of  $\text{CH}_2$  at  $2860\text{ cm}^{-1}$ , the  $\text{CH}_2$  deformations at  $1462\text{ cm}^{-1}$  (scissoring) and  $758\text{ cm}^{-1}$  (rocking), the  $\text{CH}_3$  deformation (symmetrical bending) at  $1372\text{ cm}^{-1}$ ; the stretching vibrations of  $\text{C}=\text{O}$  at  $1672\text{ cm}^{-1}$ ; and the asymmetric stretching vibration of  $\text{COC}$  at  $1247\text{ cm}^{-1}$ .

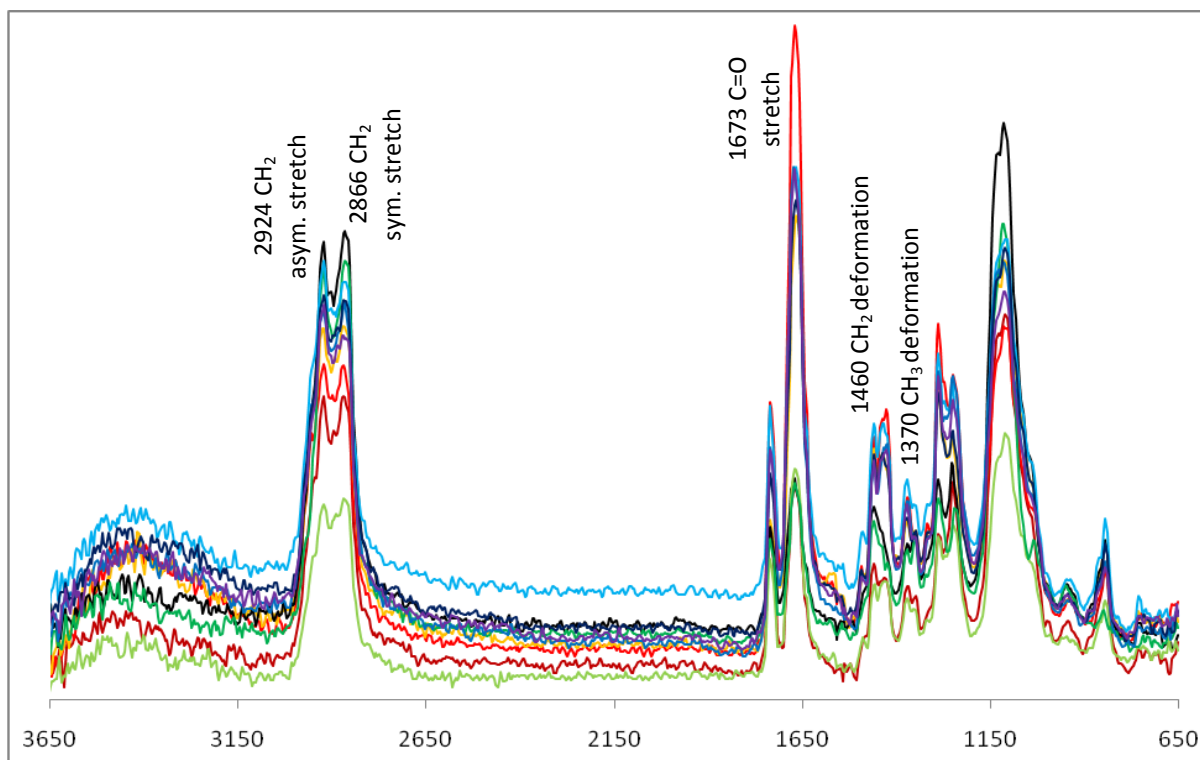
The spectral interpretation results were partially consistent with the product content, particularly the hydrocarbon backbone of the glycols and glycerides, and the polyethylene glycol (PEG) poly ethers (see *Garnier Fructis Style Styling Gel*, Appendix F). The carbonyl group ( $\text{C}=\text{O}$ ) stretching vibration occurring at a frequency below  $1700\text{ cm}^{-1}$  was attributed to the presence of a tertiary amide, although there were no amides listed in the manufacturer's product content. This could have derived from a reaction involving triethanolamine which, being a tertiary amine, does not contain a  $\text{C}=\text{O}$  bond, but this is unlikely.

Surprisingly, dimethicone (polydimethylsiloxane), a type of silicone oil that vitrifies rather than evaporates, did not appear to contribute to any of the ten gel spectra even though it was the second compound listed by the manufacturers after water, implying a greater concentration in the product content than the other compounds listed. Conversely,

the gel spectra obtained by Barton (2011) only had four distinguishable vibrational bands at 1260, 1095, 1020 and 800  $\text{cm}^{-1}$  that were each attributable to the Si-CH<sub>3</sub> and Si-O stretches of a siloxane resin. However, as with the hairspray reference comparison, it is again worth noting that different hair gel brands are likely to contain different compounds and relative concentrations.

#### 4.3.1.3 Mousse Reference Spectra

Visual evaluation of the ten mousse spectra established that some product constituents could be identified by the ATR-FTIR spectroscopy method. The spectral interpretation software determined that functional groups consistent with aliphatic hydrocarbons (CH) and aliphatic tertiary amides (CONR<sub>2</sub>) were present. Figure 4.3-3 illustrates the main vibrational bands present in the samples analysed. Those absorbances attributed to CH functional groups include the asymmetric stretching vibration of CH<sub>2</sub> at 2924  $\text{cm}^{-1}$ , the symmetric stretching vibration of CH<sub>2</sub> at 2866  $\text{cm}^{-1}$ , the CH<sub>2</sub> deformation at 1460  $\text{cm}^{-1}$  (scissoring) and the CH<sub>3</sub> deformation (symmetrical bending) at 1370  $\text{cm}^{-1}$  (Pavia *et al.*, 1979; Thermo Electron Corporation, 2006). Similar to the gel reference spectra, the carbonyl group (C=O) stretching vibration at 1673  $\text{cm}^{-1}$  was attributed to tertiary amides, as absorbance occurred at a frequency below 1700  $\text{cm}^{-1}$  and no NH absorbance bands were present at approximately 3500  $\text{cm}^{-1}$  (Pavia *et al.*, 1979; Thermo Electron Corporation, 2006).



**Figure 4.3-3 – Mousse Reference Spectra**

Spectral interpretation software used to assess the gel reference spectra confirmed the presence of aliphatic hydrocarbons and aliphatic tertiary amides. The main vibrational bands included the asymmetric stretching vibration of  $\text{CH}_2$  at  $2924\text{ cm}^{-1}$ , the symmetric stretching vibration of  $\text{CH}_2$  at  $2866\text{ cm}^{-1}$ , the  $\text{CH}_2$  deformations at  $1460\text{ cm}^{-1}$  (scissoring) and the  $\text{CH}_3$  deformation (symmetrical bending) at  $1370\text{ cm}^{-1}$ ; and the carbonyl group ( $\text{C}=\text{O}$ ) stretching vibration at  $1673\text{ cm}^{-1}$ .

The mousse spectral interpretation was in consistent with the product's content (see *Toni & Guy Boost-It Mousse*, Appendix F). Similar to the gel spectral references, the carbonyl group ( $\text{C}=\text{O}$ ) stretching vibration was attributed to the presence of a tertiary amide. Again, no amides were listed in the product content list, but could have formed from a reaction involving the tertiary amine triethanolamine, but this is unlikely. Furthermore, another silicone derivative, phenyl trimethicone, surprisingly could not be resolved from all of the ten mousse spectra.

#### 4.3.1.4 Leave-In Moisturiser Reference Spectra

Multiple attempts to collect spectra of the leave-in moisturiser samples were unsuccessful. Three likely possibilities were considered, including:

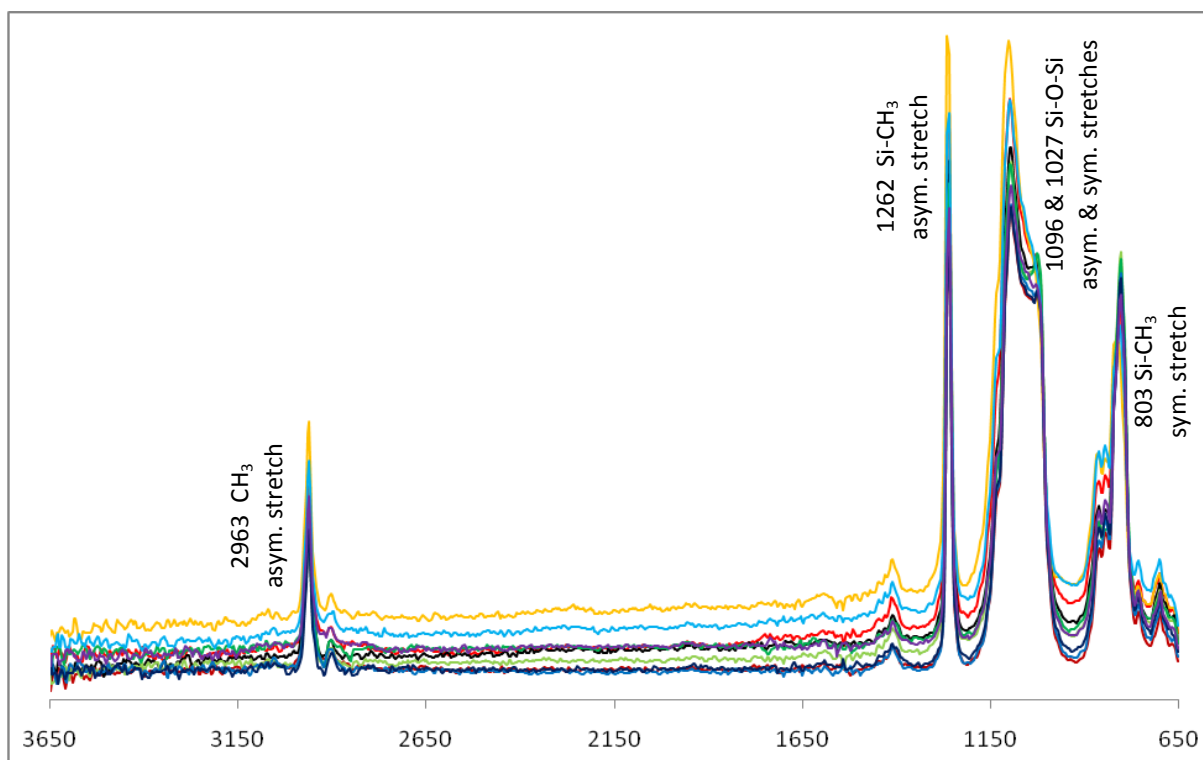
- The primary constituents evaporated during the drying process;

- The primary constituents did not absorb in the infrared region of the spectrum (i.e., they were compounds with non-polar bonds that could not undergo a dipole moment net change); and/or,
- The constituents that did not evaporate and could absorb in the infrared region were in quantities below the detectable limit of the instrument.

The reference spectra (product alone) sample set were the broadest experiments incorporated in this research for evaluating whether the ATR-FTIR spectroscopy method could identify traces of product contamination on the hair surface. As detection of the leave-in moisturiser was not achievable at this broad, product only level, further analysis of the product after heavy or sparse application to single hairs was considered unwarranted. Therefore, the leave-in moisturiser was discounted from any further analyses.

#### **4.3.1.5 Finishing Gloss Reference Spectra**

Visual evaluation of the ten finishing gloss spectra established that some of the product constituents could be identified by the ATR-FTIR spectroscopy method. This was confirmed by spectral interpretation software that determined that functional groups consistent with silicone oils (siloxanes) (SiO) were present. Figure 4.3-4 illustrates the main vibrational bands present in the samples analysed, including the asymmetric stretching vibration of CH<sub>3</sub> occurring at 2963 cm<sup>-1</sup>, the Si-CH<sub>3</sub> asymmetric and symmetric stretches at 1262 and 803 cm<sup>-1</sup> respectively, and the Si-O-Si asymmetric and symmetric stretches at 1096 and 1027 cm<sup>-1</sup> respectively (Thermo Electron Corporation, 2006).



**Figure 4.3-4 – Finishing Gloss Reference Spectra**

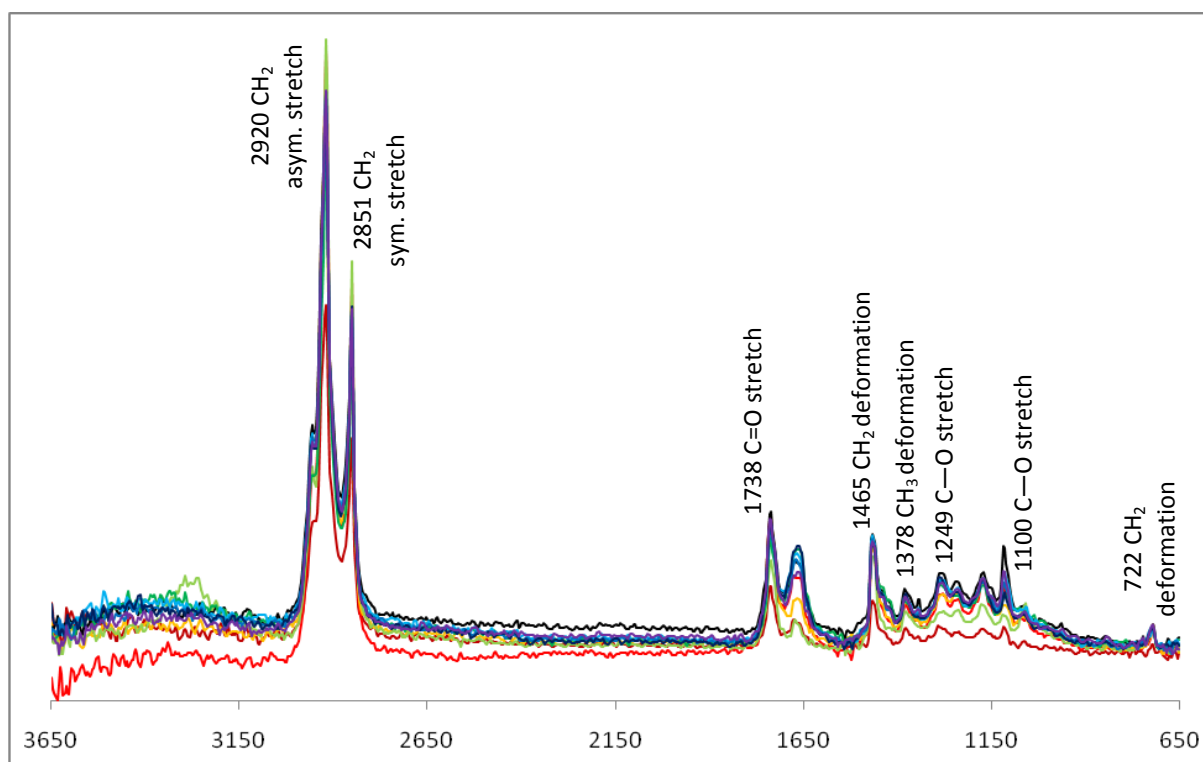
Spectral interpretation software used to assess the gloss reference spectra confirmed the presence of silicone oils (siloxanes). The main vibrational bands included the asymmetric stretching vibration of  $\text{CH}_3$  at  $2963\text{ cm}^{-1}$ , the  $\text{Si-CH}_3$  asymmetric and symmetric stretches occurring at  $1262$  and  $803\text{ cm}^{-1}$  respectively, and the  $\text{Si-O-Si}$  asymmetric and symmetric stretches at  $1096$  and  $1027\text{ cm}^{-1}$  respectively.

An *OMNIC* Library Search with each of the ten finishing gloss spectra, returned an average match of 91% with the compound dimethicone (polydimethylsiloxane). This was expected as dimethicone was the first compound listed in the product formulation (see *Paul Mitchell Smoothing Gloss Drops*, Appendix F) and, because silicone oils vitrify rather than evaporate, this increases the likelihood of being detected post-drying. The finishing gloss spectral references were virtually identical to the gel spectra obtained by Barton (2011) that had four distinguishable vibrational bands at  $1260$ ,  $1095$ ,  $1020$  and  $800\text{ cm}^{-1}$  attributable to the  $\text{Si-CH}_3$  and  $\text{Si-O}$  stretches of a siloxane resin.

#### 4.3.1.6 Styling Wax Reference Spectra

Visual evaluation of the ten styling wax spectra established that some product constituents could be identified by the ATR-FTIR spectroscopy method. Spectral interpretation software determined that functional groups consistent with aliphatic hydrocarbons (CH) and aliphatic acetate esters (COOR) were present. As illustrated by Figure 4.3-5, the CH functional group absorbances include the asymmetric stretching

vibration of  $\text{CH}_2$  at  $2920\text{ cm}^{-1}$ , the symmetric stretching vibration of  $\text{CH}_2$  at  $2851\text{ cm}^{-1}$ , the  $\text{CH}_2$  deformations at  $1465\text{ cm}^{-1}$  (scissoring) and  $722\text{ cm}^{-1}$  (rocking) and the  $\text{CH}_3$  deformation (symmetrical bending) at  $1378\text{ cm}^{-1}$  (Pavia *et al.*, 1979; Thermo Electron Corporation, 2006). The carbonyl group ( $\text{C}=\text{O}$ ) stretching vibration at  $1738\text{ cm}^{-1}$  and the  $\text{CO}$  absorbance bands at  $1249$  and  $1100\text{ cm}^{-1}$  were attributed to the aliphatic acetate esters (Pavia *et al.*, 1979; Thermo Electron Corporation, 2006).



**Figure 4.3-5 – Styling Wax Reference Spectra**

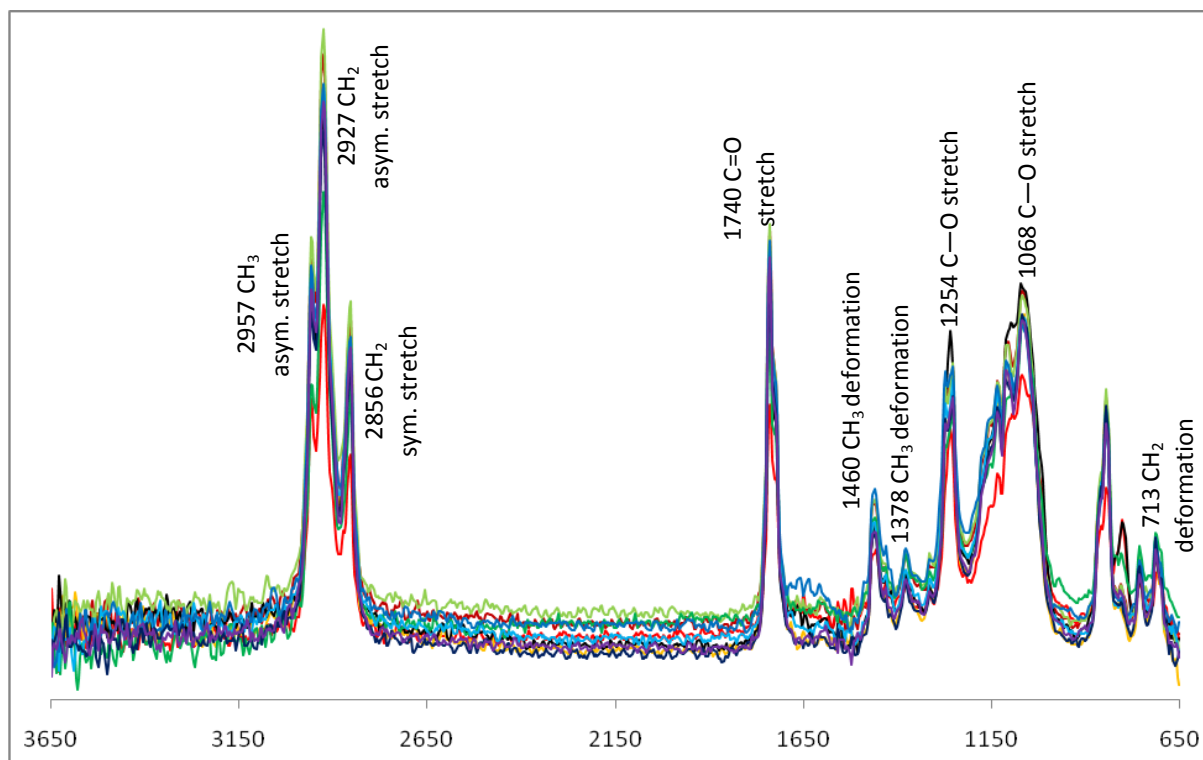
Spectral interpretation used to assess the styling wax reference spectra confirmed the presence of aliphatic hydrocarbons and aliphatic acetate esters. The main vibrational bands included the asymmetric stretching vibration of  $\text{CH}_2$  at  $2920\text{ cm}^{-1}$ , the symmetric stretching vibration of  $\text{CH}_2$  at  $2851\text{ cm}^{-1}$ , the  $\text{CH}_2$  deformations at  $1465\text{ cm}^{-1}$  (scissoring) and  $722\text{ cm}^{-1}$  (rocking) and the  $\text{CH}_3$  deformation (symmetrical bending) at  $1378\text{ cm}^{-1}$ ; and, the carbonyl group ( $\text{C}=\text{O}$ ) stretching vibration at  $1738\text{ cm}^{-1}$  and the  $\text{CO}$  absorbance bands at  $1249$  and  $1100\text{ cm}^{-1}$ .

The spectral interpretation was consistent with the product content, particularly lanolin wax that comprises approximately 97% long chain esters (Imperial Oel Import, 2011). Other aliphatic acetate esters listed in the content include, tridecyl stearate, dipentaerythryl hexacaprylate/ hexacaprinate, tridecyl trimellitate and alkyl acrylate crosspolymer (see *American Crew Fiber Pliable Molding Cream*, Appendix F).



#### 4.3.1.7 Smoothing Balm Reference Spectra

Finally, visual evaluation of the ten smoothing balm spectra established that some product constituents could be identified by the ATR–FTIR spectroscopy method. Similar to the wax reference spectra, spectral interpretation software determined that functional groups consistent with aliphatic hydrocarbons (CH) and aliphatic acetate esters (COOR) were present. As illustrated by Figure 4.3-6, the hydrocarbon absorbances include the asymmetric stretching vibrations of CH<sub>3</sub> at 2957 cm<sup>-1</sup> and CH<sub>2</sub> at 2927 cm<sup>-1</sup>, the symmetric stretching vibration of CH<sub>2</sub> at 2856 cm<sup>-1</sup>, the CH<sub>2</sub> deformations at 1460 cm<sup>-1</sup> (scissoring) and 713 cm<sup>-1</sup> (rocking) and the CH<sub>3</sub> deformation (symmetrical bending) at 1378 cm<sup>-1</sup> (Pavia *et al.*, 1979; Thermo Electron Corporation, 2006). The carbonyl group (C=O) stretching vibration at 1740 cm<sup>-1</sup> and the CO absorbance bands at 1254 and 1068 cm<sup>-1</sup> were attributed to the aliphatic acetate esters (Pavia *et al.*, 1979; Thermo Electron Corporation, 2006).



**Figure 4.3-6 – Smoothing Balm Reference Spectra**

Spectral interpretation software used to assess the smoothing balm reference spectra confirmed the presence of aliphatic hydrocarbons and aliphatic acetate esters. The main vibrational bands included the asymmetric stretching vibrations of  $\text{CH}_3$  at  $2957$  and  $\text{CH}_2$  at  $2927$   $\text{cm}^{-1}$ , the symmetric stretching vibration of  $\text{CH}_2$  at  $2856$   $\text{cm}^{-1}$ , the  $\text{CH}_2$  deformations at  $1460$   $\text{cm}^{-1}$  (scissoring) and  $713$   $\text{cm}^{-1}$  (rocking) and the  $\text{CH}_3$  deformation (symmetrical bending) at  $1378$   $\text{cm}^{-1}$ ; and, the carbonyl group ( $\text{C}=\text{O}$ ) stretching vibration at  $1740$   $\text{cm}^{-1}$  and the  $\text{CO}$  absorbance bands at  $1254$  and  $1068$   $\text{cm}^{-1}$ .

The spectral interpretation was consistent with the aliphatic acetate esters listed in the product content, such as the diester propylene glycol dicarprylate/ dicaprinate, decyl oleate and alkyl benzoate (see *Joico K-Pak Smoothing Balm*, Appendix F). Similar to the mousse and gel reference spectra, peaks attributed to silicone derivatives were not observed in any of the ten smoothing balm spectra, albeit that peaks from this type of compound were the most predominant in the finishing gloss spectra.

#### 4.3.1.8 Summary of Product Reference Spectra

Visual evaluations and *OMNIC* Spectral Interpretation analyses established that many hair product constituents could be detected by ATR-FTIR spectroscopy. Of the seven products targeted, the leave-in moisturiser was the only product where no significant molecular absorption was observed in the mid-IR region of interest. Three explanations were considered, including: (i) the primary constituents evaporated during

sample preparation; (ii) the primary constituents did not absorb in the mid-IR; and/or (iii) the quantities were below the detectable limit of the instrument. As detection of the leave-in moisturiser was not achievable at this broad level of evaluation, it was discontinued from further analyses.

For the remaining six products evaluated, CH<sub>2</sub> and CH<sub>3</sub> vibrations were the most common spectral intensities between 3000 and 2800 cm<sup>-1</sup> that were identified. For product classification purposes, therefore, detailed analyses of hydrocarbon absorptions bands in this region are not recommended (Pavia *et al.*, 1979). With the exception of the finishing gloss reference spectra, methylene (CH<sub>2</sub>) and methyl (CH<sub>3</sub>) groups were commonly observed at lower frequencies, particularly the CH<sub>3</sub> symmetrical bend at approximately 1370 cm<sup>-1</sup> and the CH<sub>2</sub> scissoring and rocking vibrations at approximately 1460 and 720 cm<sup>-1</sup>, respectively.

The reference spectra were partially consistent with the product content as listed by the respective manufacturer, with a few exceptions. Tertiary amides (CONR<sub>2</sub>) were identified in both the gel and mousse spectra because the carbonyl group (C=O) stretching vibrations occurred at a frequency below 1700 cm<sup>-1</sup> and NH absorbance bands in the 3500 cm<sup>-1</sup> region were absent. Neither the gel nor the mousse formulations listed amides in their content, yet both listed triethanolamine, a tertiary amine that does not contain a C=O or an NH bond. Amines can react to form amides; typically this occurs when carboxylic acids are present but generally does not extend to the formation of tertiary amines so was considered unlikely to have occurred here. Furthermore, dimethicone (polydimethylsiloxane) and phenyl trimethicone were listed in the product content of the gel, the mousse and the smoothing balm. Both compounds were classed as silicone oils that do not evaporate, so their corresponding vibrational bands were expected in the resulting spectra. Four distinguishable bands attributable to Si-CH<sub>3</sub> and Si-O were reportedly the only absorbance bands observed in the gel reference spectra obtained by Barton (2011) and, in addition to a sole hydrocarbon vibrational stretch, were the only absorbances observed in the finishing gloss reference spectra obtained in this research. The latter spectra returned an average software match (from ten spectra) of 91% with dimethicone (Thermo Electron Corporation, 2006).

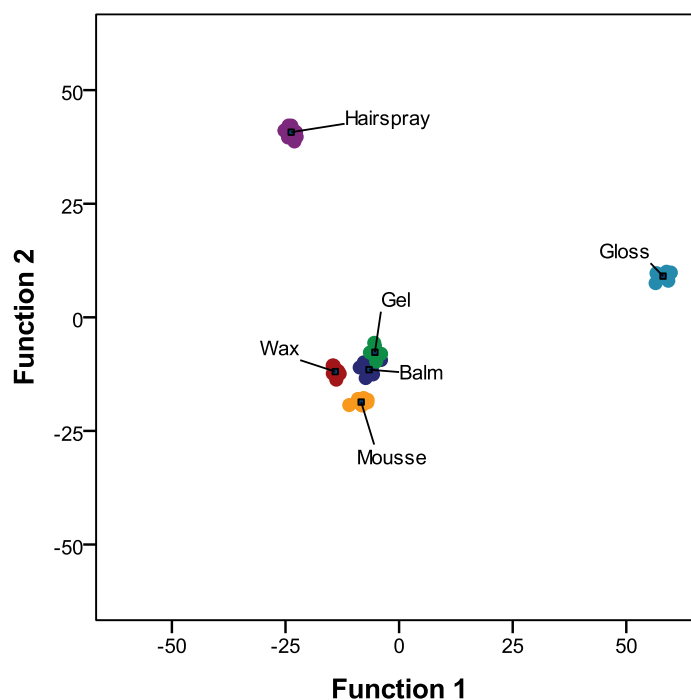
Finally, while visually the wax and smoothing balm were considered to be very different hair products, the resulting spectra were similar at the lower mid-IR frequencies.

The wax and smoothing balm spectra included a carbonyl group (C=O) absorption band at 1738 and 1740  $\text{cm}^{-1}$ , respectively, and two CO stretches at 1249 and 1100  $\text{cm}^{-1}$  and 1254 and 1068  $\text{cm}^{-1}$ , respectively.

#### 4.3.2. Allocation to Product Class

Hydrocarbon absorption bands occurring in the region 3000 and 2800  $\text{cm}^{-1}$  were excluded from the statistical analyses as they were common to the spectra of each product, thereby providing little discriminatory power. The statistical analyses were confined to include only the 254 wavenumbers between 1632 and 652.

The discriminant analysis (canonical correlation) comprising wavenumbers between 1632 and 652 (with a data point spacing of 3.857  $\text{cm}^{-1}$ ) as the predictor variables resulted in 100% prediction accuracy. That is, all 60 spectra were correctly classified as belonging to one of six product categories. Only one brand of product per product type was included in this analysis. Figure 4.3-7 represents the discriminant scores for the product reference model. Each spectrum is represented by a colour in accordance with the true product type (e.g., all ten hairspray spectra are coloured purple) but is located in canonical space with respect to the two highest discriminant functions. It was observed that group centroids for the hairspray and finishing gloss reference spectra were well separated by both Function 1 and Function 2; however, the styling wax, gel, smoothing balm and mousse reference spectra were not well separated by either function.



**Figure 4.3-7 – Product Reference Spectra Canonical Discriminant Functions**

Output from *PASW* illustrates the discriminant scores for each spectrum (independent variables). Group centroids for the hairspray and finishing gloss reference spectra were well separated by Function 1 and Function 2 while, conversely, the styling wax, gel, smoothing balm and mousse reference spectra were not well separated by either function. Overall, 100% of the product spectra were correctly classed.

Analysing the individual coefficients for each wavenumber (predictor variables) with respect to discrimination between the products would be complicated. First, the shoulders of a number of absorption bands accumulate over a range of wavenumbers, second, some shoulders are proximal enough to form duplicate peaks and third, given data was collected every  $3.857\text{ cm}^{-1}$ , precise vibrational absorption for each consecutive frequency was not available. Notwithstanding, for Function 1 the strongest predictor variables were generally between  $1300$  and  $1000\text{ cm}^{-1}$  corresponding to the CO absorbance bands for ethers and esters, with the first and third highest individual coefficients occurring at  $1227$  and  $1242\text{ cm}^{-1}$  ( $-12.137$  and  $10.364$ , respectively). The second highest individual coefficient occurred at  $1450\text{ cm}^{-1}$  ( $-11.271$ ) corresponding to the  $\text{CH}_3$  asymmetrical bend vibration. Similarly for Function 2, the strongest predicting variable was  $1450\text{ cm}^{-1}$  showing the highest individual coefficient ( $8.867$ ) and the third strongest was  $1227\text{ cm}^{-1}$  ( $6.083$ ). The canonical correlation indicated that Function 1 explained 78% of the data variance while Function 2, being uncorrelated to Function 1, explained 11.8% of the data variance. Overall, the discriminant analyses confirmed that multiple spectra of various hair

products, including hairspray, gel, mousse, finishing gloss, styling wax and smoothing balm, could be distinguished from one another at a broad level of enquiry (i.e., product only analyses).

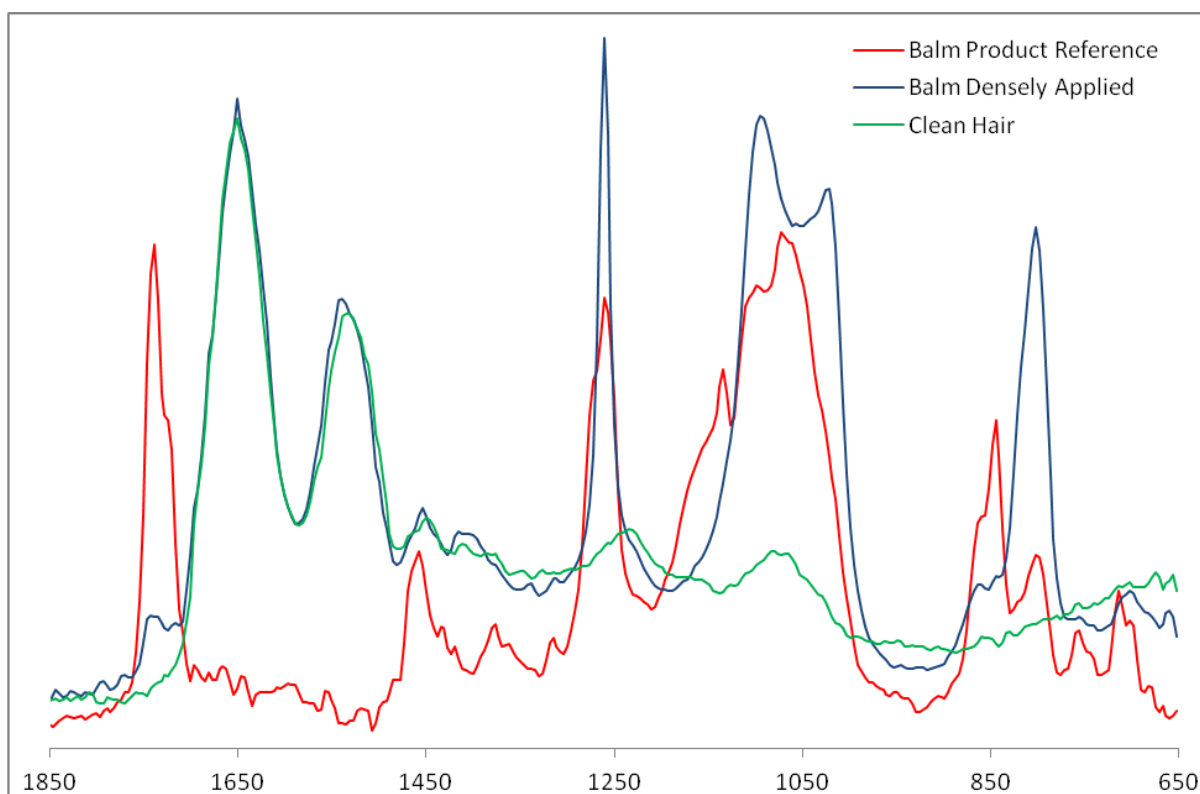
### 4.3.3. Product Densely Applied

These analyses were designed to investigate whether the spectra of a particular product type could still be distinguished following dense application to a single hair. Cosmetic product contamination on the hair was visually located using the 15x Infinity Reflachromat objective with the slide-on ATR in view mode (i.e., microscope only). It was established that contact had been made between the ATR crystal and the sample (analysis mode) by observing a change in the spectrum on the *OMNIC* Live Spectrum Collection Preview. As described in 4.2.2 Instrumentation, a spectrum of product contamination alone was observed on the Live Preview when little pressure was applied, while a spectrum of keratin alone was observed when slightly more pressure was applied. Hair keratin was not the focus of this investigation while, in the previous section (4.3.2 Allocation to Product Class) it was established that spectra of the contamination could be distinguished from other contamination on the basis of product type. Therefore, only spectra resembling a *combination* of both hair keratin and contamination were collected.

Presumably, the different hair products tested were designed to undergo different molecular reactions with the hair, for example, hydrogen bonding, depending on the product's purpose. This was evident when the product densely applied spectra (hair with product) were visually compared with their respective reference spectra (product alone) counterparts. For example, some of the uncharacterised absorbance bands that were evident in the ten smoothing balm reference spectra were absent from the ten smoothing balm densely applied spectra.

Specifically, for the smoothing balm densely applied spectra, a medium intensity band occurring on the shoulder of the characteristic CO stretch at approximately  $1140\text{ cm}^{-1}$  and a low intensity band occurring at approximately  $850\text{ cm}^{-1}$  were absent. Moreover, the characteristic  $\text{CH}_3$  deformation at  $1460\text{ cm}^{-1}$  was also no longer evident given that absorbance by the hair keratin occurred at similar frequencies, as displayed in Figure 4.3-8. As a result of these variations, in the frequency region under analysis the smoothing balm densely applied spectra were visually similar to the finishing gloss densely applied

spectra (displayed in Figure 4.3-9). That is, following application to hair, the smoothing balm spectra resembled silicone oils (siloxanes).

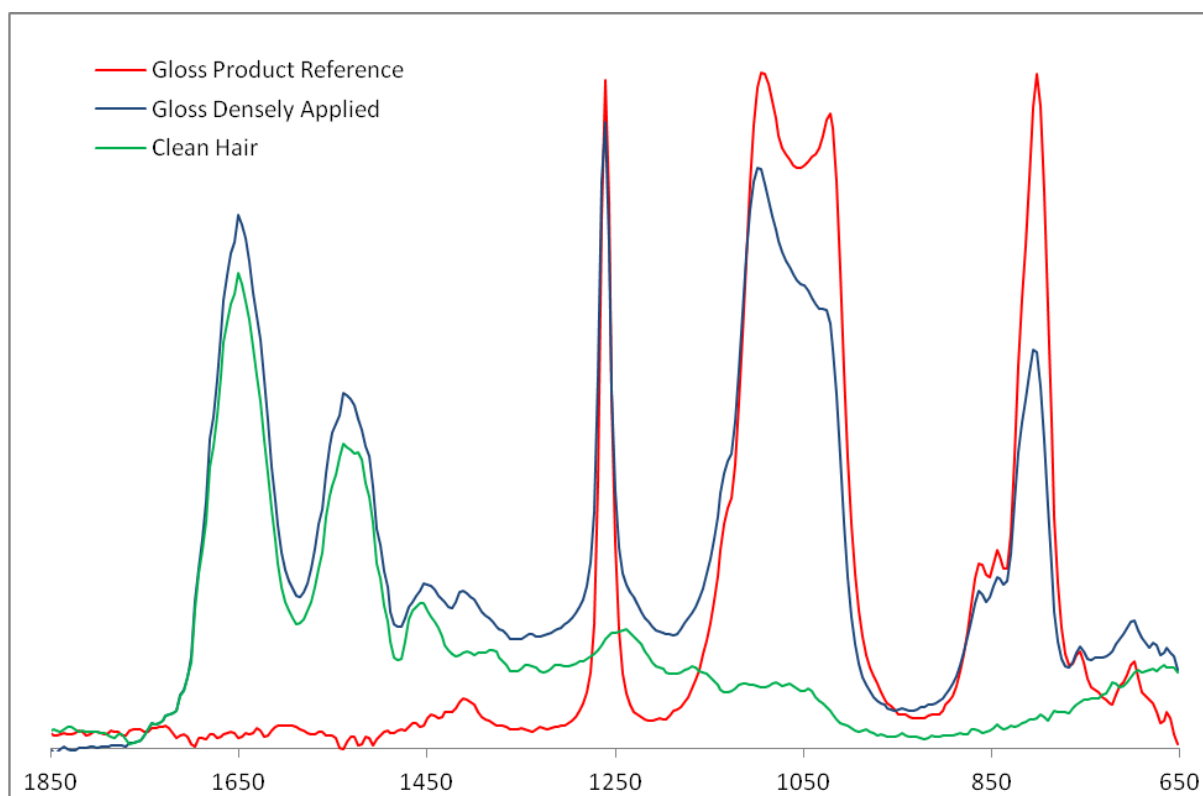


**Figure 4.3-8 – Smoothing Balm Reference and Densely Applied Spectra**

Variations were observed between the spectra of hair with smoothing balm densely applied and the smoothing balm spectral references in the mid-IR frequency region under analysis. With the absence of some of the uncharacterised absorbance bands that appear in the product reference spectra, specifically, the peaks occurring at approximately 1140 and 850  $\text{cm}^{-1}$ , the smoothing balm densely applied spectra were visually similar to the finishing gloss densely applied spectra illustrated in the next Figure.

As discussed throughout section 4.3.1 Hair Product References, the spectra of gel on hair obtained by Barton (2011) resembled a siloxane spectrum. However, of the gel, mousse, finishing gloss and smoothing balm reference spectra obtained in this research, the spectral evaluation only determined the presence of silicone oils in the finishing gloss spectra despite dimethicone (polydimethyl siloxane) and/or phenyl trimethicone being listed in the formulations for each of these products. Given that the smoothing balm spectra resembled silicone oils (siloxanes) following application to hair, this could support the presumption that different product types were designed to undergo various molecular reactions with the hair, depending on the respective product's purpose. The spectral changes could also be a result of extended drying times (leading to increased product oxidation).

As displayed in Figure 4.3-9, variations between the finishing gloss densely applied spectra and the finishing gloss reference spectra were not observed in the frequency region under analysis, with the obvious exception of the additional hair keratin absorbance bands. A slight reduction in the intensity of the Si–O–Si asymmetrical and symmetrical stretches occurring at 1096 and 1027  $\text{cm}^{-1}$ , respectively, and of the Si–CH<sub>3</sub> symmetrical stretch occurring at 803  $\text{cm}^{-1}$ , were observed.

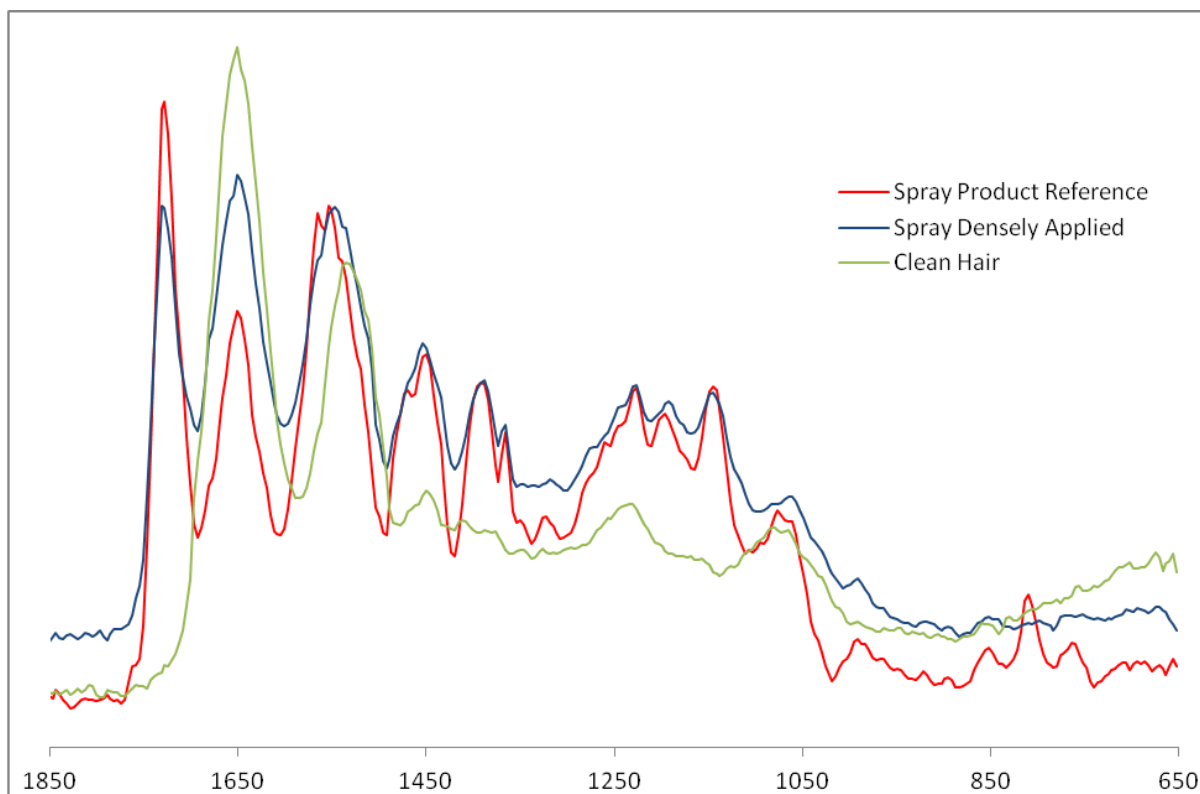


**Figure 4.3-9 – Finishing Gloss Reference and Densely Applied Spectra**

With the obvious exception of the additional hair keratin absorbance bands, the finishing gloss densely applied spectra were visually similar to the finishing gloss reference spectra and no major variations were observed. Albeit, a slight reduction in the intensity of the silicone oil absorbance bands occurring at 1096, 1027 and 803  $\text{cm}^{-1}$  was observed.

For the hairspray densely applied spectra, both the two major Amide I and Amide II absorbance bands occurred at similar frequencies as those of the product, while no significant peaks were absent. As a result, overall, the product reference spectra appeared almost identical to the densely applied spectra, as displayed in Figure 4.3-10.

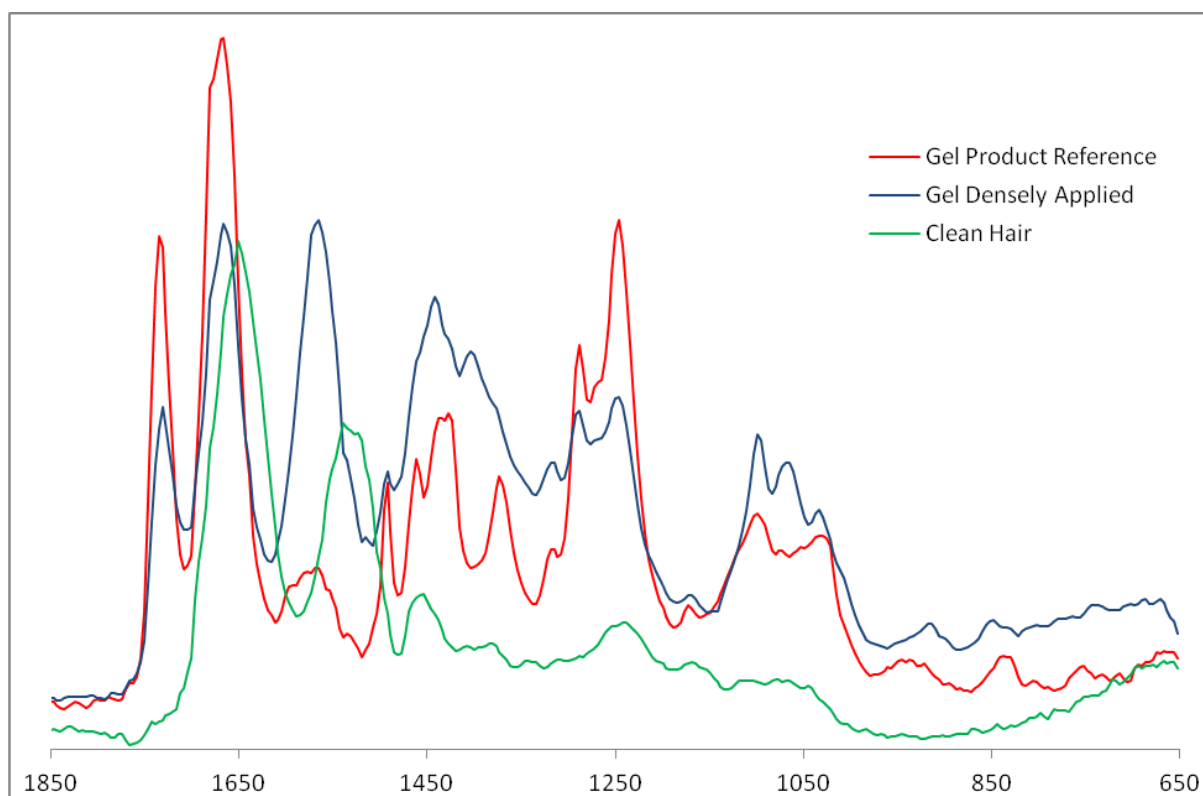




**Figure 4.3-10 – Hairspray Reference and Densely Applied Spectra**

The major absorbance bands for hair keratin, being peaks for Amide I and Amide II, occurred at the same frequencies as the absorbance bands for the hairspray product. As there were also no spectral intensities absent from the hairspray densely applied spectra, both sample sets appeared almost identical.

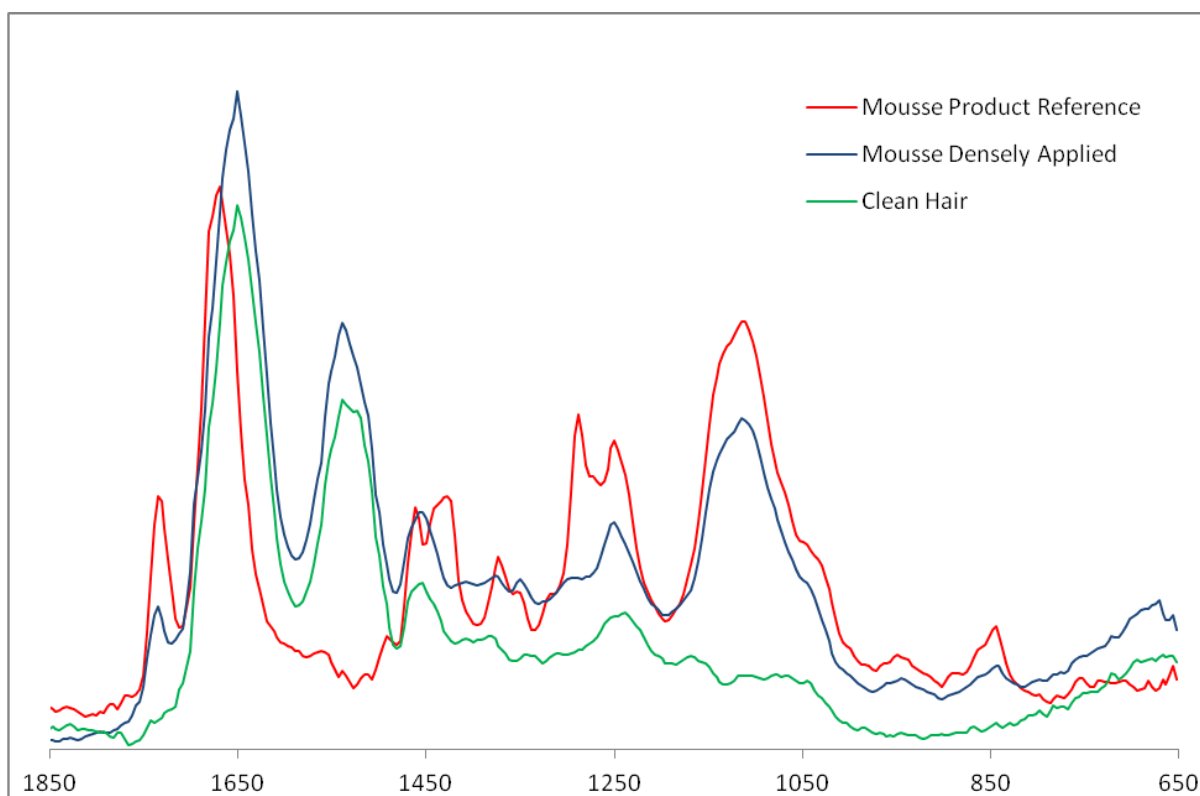
Similarly, for the gel product densely applied spectra, one of the major amide absorbance bands for hair keratin occurred at the same frequency as an absorbance band for the gel reference spectra. Therefore, variations between the spectra were observed due to the additional amide absorbance band for hair keratin occurring in the product densely applied spectra and because there was a slight increase in the intensity of the uncharacterised bands occurring between approximately 1450 and 1400  $\text{cm}^{-1}$ , and between approximately 1150 and 1000  $\text{cm}^{-1}$ , as displayed in Figure 4.3-11.



**Figure 4.3-11 – Gel Reference and Densely Applied Spectra**

Variations between the gel densely applied spectra and gel reference spectra were observed due to the additional hair keratin amide absorbance band and the slight increase in the intensity of the uncharacterised bands occurring between approximately 1450 and 1400  $\text{cm}^{-1}$  and between approximately 1150 and 1000  $\text{cm}^{-1}$ . A slight reduction in the spectral intensity of the double peak occurring at approximately 1250  $\text{cm}^{-1}$  was also observed.

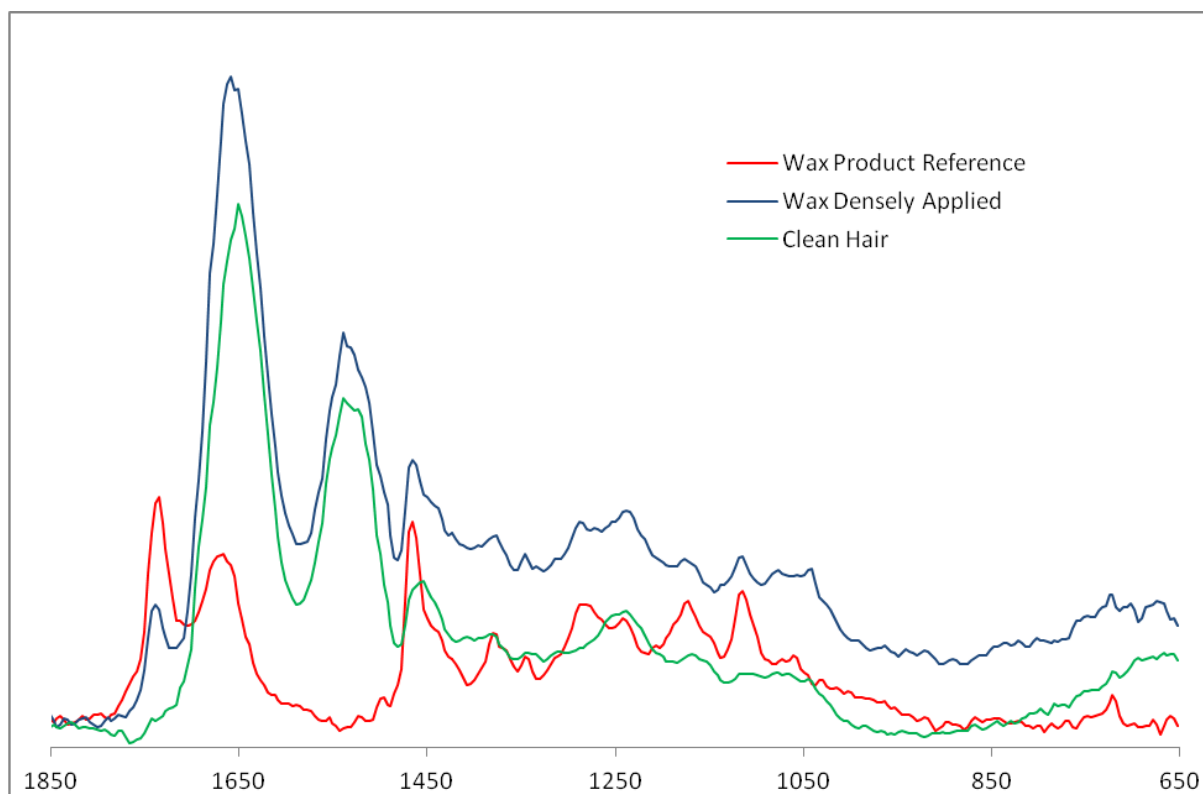
Variations between the mousse densely applied spectra and the mousse product reference spectra were observed due to the additional amide absorbance bands for hair keratin and because there was a slight increase in the intensity of the uncharacterised bands occurring between approximately 1200 and 1000  $\text{cm}^{-1}$ , as displayed in Figure 4.3-12. For both the mousse and gel product densely applied spectra, a slight reduction was observed in the spectral intensity of the uncharacterised double peak occurring at approximately 1250  $\text{cm}^{-1}$ .



**Figure 4.3-12 – Mousse Reference and Densely Applied Spectra**

Variations between the mousse densely applied spectra and mousse product reference spectra were observed due to the additional amide absorbance bands for hair keratin. An increase in the uncharacterised spectral intensities occurring between approximately 1200 and 1000  $\text{cm}^{-1}$  were observed as well as a reduction in intensity of the uncharacteristic double peak occurring at approximately 1250  $\text{cm}^{-1}$ .

Finally, as displayed in Figure 4.3-13, no medium or strong absorbance bands were observed in the frequency region under analysis between 1632 and 652  $\text{cm}^{-1}$  for the styling wax spectra. Therefore, while variations between the styling wax densely applied and the styling wax reference spectra were observed, few absorbance bands distinguishing the product contamination as styling wax could be observed on the styling wax densely applied hair spectra in that region (i.e., they resembled the hair without product (control) spectra).



**Figure 4.3-13 – Styling Wax Reference and Densely Applied Spectra**

No medium or strong absorbance bands were observed in the frequency region under analysis between 1632 and 652  $\text{cm}^{-1}$ . Few absorbance bands distinguishing the product contamination as styling wax could be observed on the wax densely applied hair spectra.

#### 4.3.3.1 Summary of Product Densely Applied

Only spectra resembling a combination of both hair keratin and contamination on the *OMNIC* Live Spectrum Collection Preview were collected for analysis. The two major Amide I and Amide II absorbance bands were apparent on all the data collected. In addition, visual evaluations of the product densely applied spectra in comparison with the spectral references established that other variations to the absorbing constituents occurred. This was most likely due to molecular reactions that the respective products were designed to perform on application to hair.

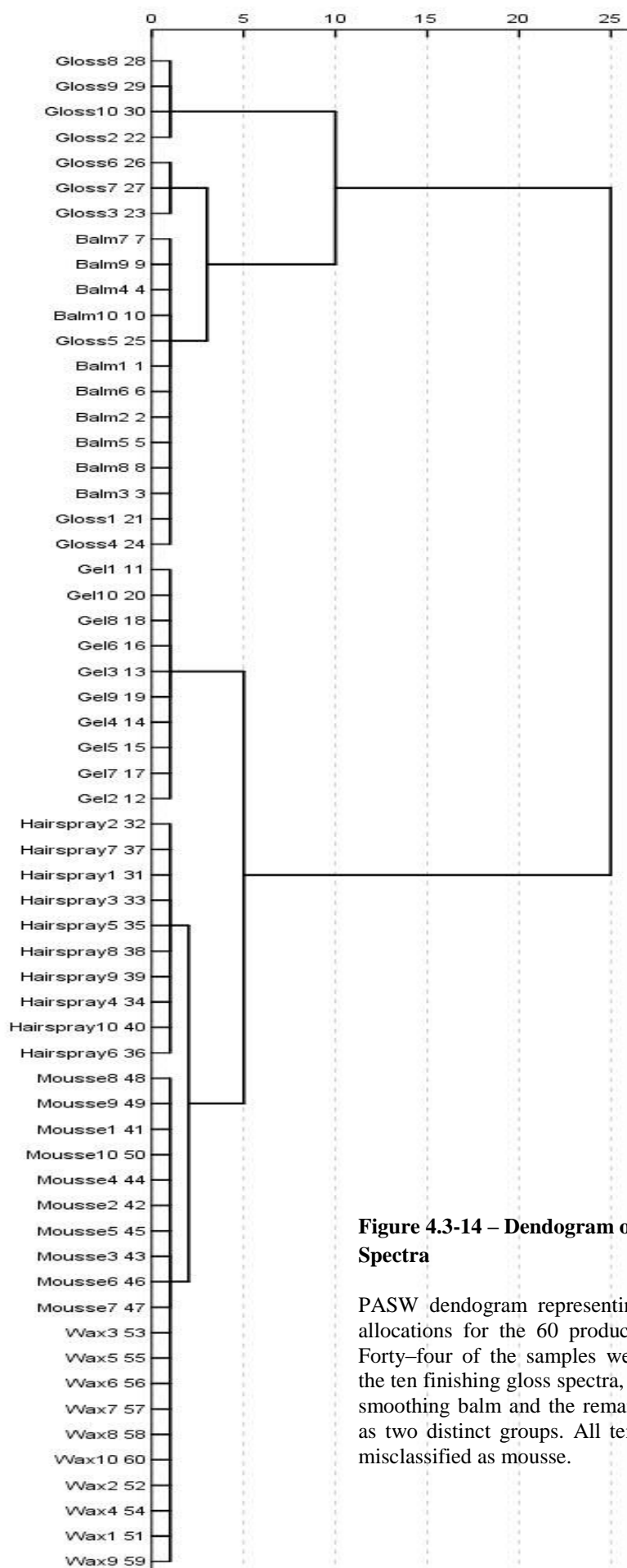
A number of uncharacterised absorbance bands were absent (or reduced in intensity) in the smoothing balm densely applied spectra. This resulted in the smoothing balm spectra being visually similar to the finishing gloss densely applied spectra. Only slight reductions in the spectral intensity of the finishing gloss absorbance bands were observed. The hairspray densely applied spectra were considered almost identical to the

hairspray reference spectra, due to the absorbance bands of the hairspray constituents occurring at similar frequencies as the hair keratin absorbance bands. Only the Amide II absorbance band occurred at the same frequency as the gel absorbance bands, although there was a slight increase in the spectral intensity of a number of uncharacterised peaks. This was also the case with the mousse densely applied spectra; however, only the Amide I absorbance band occurred at the same frequency as for product constituents. Finally, the wax densely applied spectra practically resembled hair without product (control), as there were no medium or strong absorbance bands and few low intensity absorbance bands occurring in the frequency region under analysis, that could distinguish the presence of any product contamination.

#### 4.3.4. Allocation to Product Class

Aliphatic C–H absorption bands occurring in the region 3000 and 2800  $\text{cm}^{-1}$  were excluded from the statistical analyses as they were common to the spectra of each product, thereby providing little discrimination. The statistical analysis was confined to include only the 254 wavenumbers between 1632 and 652 (at a spacing of 3.857  $\text{cm}^{-1}$ ).

The discriminant analysis (hierarchical cluster) comprising 254 wavenumbers as the predictor variables resulted in 73% prediction accuracy. That is, 44 spectra were correctly classified as belonging to one of six product categories and 16 were misclassified. The dendrogram produced by *PASW* and provided in Figure 4.3-14 represents the hierarchical cluster allocations for the 60 product densely applied spectra, whereby each spectrum is named in accordance with the true product type, sample number (1 to 10) and case number (1 to 60) but is located on the dendrogram with respect to the cluster allocation or statistical similarity to the other spectra. It was observed that three of the finishing gloss densely applied spectra were misclassified as smoothing balm and the remaining seven finishing gloss spectra were clustered as two distinct groups, while all ten of the styling wax densely applied spectra were misclassified as mousse product type.



**Figure 4.3-14 – Dendrogram of Densely Applied Spectra**

PASW dendrogram representing the hierarchical cluster allocations for the 60 product densely applied spectra. Forty-four of the samples were correctly classified. Of the ten finishing gloss spectra, three were misclassified as smoothing balm and the remaining seven were clustered as two distinct groups. All ten of the wax spectra were misclassified as mousse.

The visual evaluation determined that spectra of the smoothing balm appeared similar to the spectra of the finish gloss, following application to the hair. Therefore, it is not surprising that a number of those spectra were indistinguishable. However, as spectra of the styling wax densely applied samples appeared, visually, very different from that of the mousse spectra, the close location of those two sets of samples on the dendrogram was not expected.

Further statistical analyses that excluded all ten of the finishing gloss spectra from the test resulted in the correct allocation of the remaining 50 spectra to five product classifications.<sup>2</sup> Although the densely applied spectra were not statistically distinguishable, the visual evaluations suggest that employing FTIR spectroscopy to identify hair surface contamination could potentially increase the evidential value of human hair. It was determined that further exploration of whether a particular product type could be distinguished from other product types following sparse application to a single hair was warranted.

#### 4.3.5. Product Sparsely Applied

These analyses were designed to investigate whether the spectra of a particular product type could still be distinguished following sparse application to a single hair, simulating normal product usage. Cosmetic product contamination on the hair was visually located using the 15x Infinity Replachromat objective with the slide-on ATR in view mode (i.e., microscope only). It was established that contact had been made between the ATR crystal and the sample (analysis mode) by observing a change in the spectrum on the *OMNIC* Live Spectrum Collection Preview. During data collection of the densely applied samples, a spectrum of product contamination alone was observed on the Live Preview when little pressure was applied, while a spectrum of keratin alone was observed when slightly more pressure was applied. This was not the case with the sparsely applied samples, most likely due to the significantly smaller quantity of contamination on the hair surface.

---

<sup>2</sup> NB: A *PASW* K-Cluster (or “Quick Cluster”) test was also briefly explored, as the test uses a typology similar to a fuzzy clustering algorithm that has been applied in other research involving hair spectroscopy (e.g., Panayiotou & Kokot, 1999). Greater misclassification resulted from the K-Cluster statistic, with the ten styling wax, ten mousse and ten hairspray spectra all incorporated in a single cluster, and the smoothing balm and finishing gloss divided across four clusters. All ten gel spectra were correctly allocated to the final cluster.

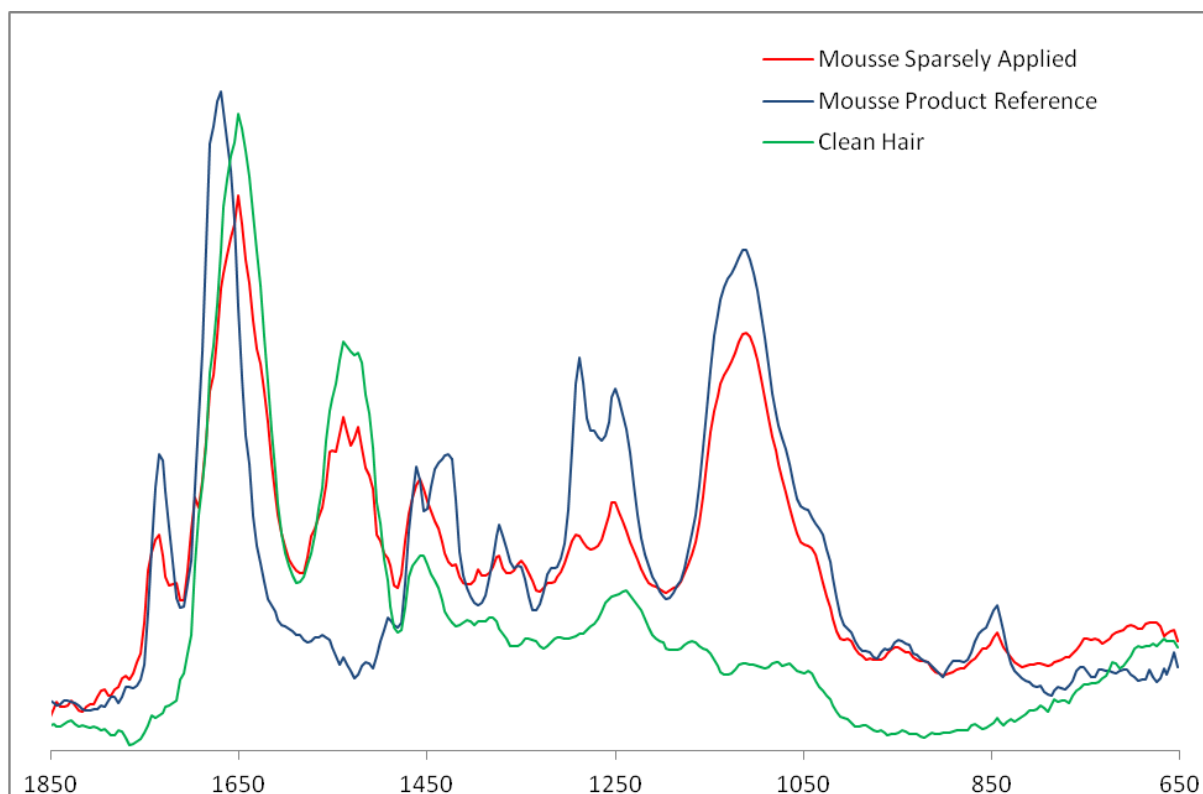
With the ATR in view mode, contamination was not observed on the majority of sparsely applied samples. Furthermore, on the few samples where contamination was observed, spectra of neither the contamination alone nor contamination in combination with the hair keratin could be resolved despite numerous attempts. Table 4.3-1 summarises those samples where contamination was observed with the ATR view mode and/or on the Live Preview spectrum.



Table 4.3-1 – Product Sparsely Applied Summary of Spectra Resolved

Product	Hair	Sample	Contamination Observed?	Spectra of Contamination Resolved?
Hairspray	1	1	No	—
		2	No	—
Hairspray	2	3	Yes	No
		4	No	—
Hairspray	3	5	Yes	No
		6	No	—
Hairspray	4	7	No	—
		8	No	—
Hairspray	5	9	No	—
		10	No	—
Gel	1	1	Yes	No
		2	Yes	No
Gel	2	3	No	—
		4	Yes	No
Gel	3	5	Yes	No
		6	Yes	No
Gel	4	7	No	—
		8	Yes	No
Gel	5	9	Yes	No
		10	Yes	No
Gloss	1	1	No	—
		2	No	—
Gloss	2	3	No	—
		4	No	—
Gloss	3	5	No	—
		6	No	—
Gloss	4	7	No	—
		8	No	—
Gloss	5	9	No	—
		10	No	—
Wax	1	1	Yes	Yes
		2	Yes	Yes
Wax	2	3	Yes	No
		4	Yes	Yes
Wax	3	5	Yes	Yes
		6	Yes	Yes
Wax	4	7	No	—
		8	No	—
Wax	5	9	Yes	Yes
		10	Yes	No
Balm	1	1	No	—
		2	No	—
Balm	2	3	No	—
		4	No	—
Balm	3	5	No	—
		6	No	—
Balm	4	7	No	—
		8	No	—
Balm	5	9	No	—
		10	No	—
Mousse	1	1	No	—
		2	No	—
Mousse	2	3	No	—
		4	Yes	Yes
Mousse	3	5	Yes	No
		6	No	—
Mousse	4	7	Yes	No
		8	Yes	Yes
Mousse	5	9	Yes	No
		10	No	—

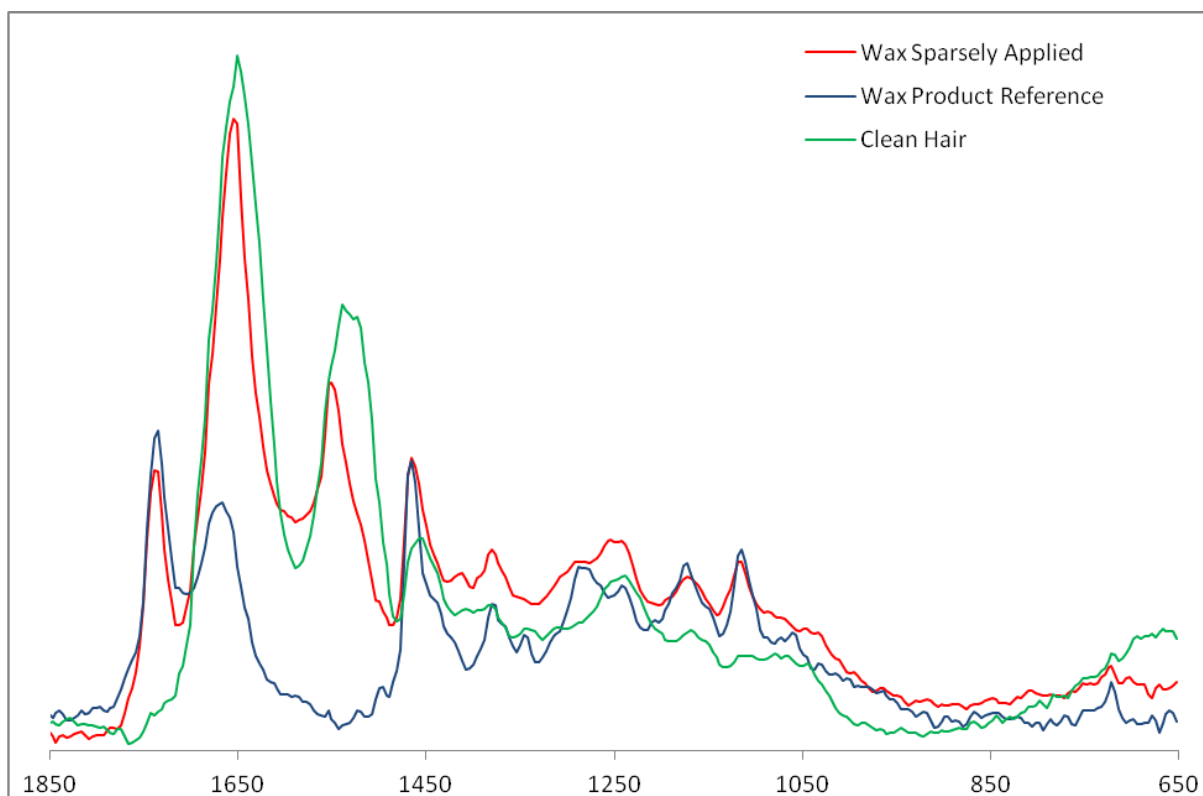
No contamination was observed on any of the smoothing balm or finishing gloss hair samples. Potential hairspray contamination was observed at single locations on two individual hair samples; however, all spectrum collection attempts resembled keratin only and the source of the contamination could not be resolved. Potential gel contamination was also observed at single locations on two individual hair samples and at two or more locations on three individual hair samples yet, similar to the hairspray samples, all spectra resembled keratin alone and the source of the contamination could not be resolved. Potential mousse contamination was observed at single locations on three individual hair samples and at multiple locations on a single hair sample; however, two spectra resembling a combination of both mousse and keratin were successfully resolved. A spectrum from the mousse sparsely applied samples is provided in Figure 4.3-15, along with the mousse product reference for comparison.



**Figure 4.3-15 – Mousse Reference and Sparsely Applied Spectra**

An increase in spectral intensities occurring between approximately 1200 and 1000  $\text{cm}^{-1}$  along with an additional band at approximately 1700  $\text{cm}^{-1}$  on the shoulder of Amide I, indicated the presence of mousse contamination on the sparsely applied samples. Of the four samples comprising potential contamination, only two spectra resembling mousse could be resolved, with all others resembling hair keratin alone.

Unlike the other five products analysed, potential styling wax contamination was observed on the majority of sparsely applied wax samples, specifically, contamination was observed at multiple locations on four out of five hair samples. Furthermore, where contamination was observed the resulting spectrum resembled a combination of both the styling wax contamination and hair keratin on all but two locations, albeit, only a few additional low intensity absorbance bands indicating the presence of wax occurred in the frequency region under analysis, as illustrated in Figure 4.3-16.



**Figure 4.3-16 – Styling Wax Reference and Sparsely Applied Spectra**

A number of low intensities bands occurred in the frequency region under analysis, including one at approximately  $1750\text{ cm}^{-1}$  and two between approximately  $1200$  and  $1100\text{ cm}^{-1}$ , indicated the presence of styling wax contamination on the sparsely applied sampled. Of the four hair samples that comprised potential contamination, all produced spectrum resembling wax from at least one location along the hair.

The distinctive styling wax results were most likely due to the viscous texture of the product that in turn produced a firm bond with the hair fibre. The styling wax was not designed to partially evaporate on application and drying, such as the hairspray and smoothing balm products that, most likely, resulted in minimal product residues that were below the detection limit of the instrument.

#### 4.3.5.1 Summary of Product Sparsely Applied

The sparse application analyses were designed to address hair evidence in the context of forensic casework. Contamination was not observed on the majority of samples, including the samples prepared with smoothing balm, finishing gloss, hairspray and styling gel. Furthermore, on the few samples where contamination of these products was observed, spectra of the contamination could not be resolved. Conversely, for almost all the samples prepared with styling wax, and to a lesser extent those prepared with mousse, spectra resembling the respective product contamination were observed.

With all samples, attempts to locate product contamination on the hair surface were undertaken using the 15X Infinity Reflachromat objective with the Slide-on ATR in view mode. During data collection of the sparsely applied samples, dried product contamination without interference from the hair keratin was generally not observed on the *OMNIC* Live Preview screen due to, most likely, the low concentration of the contamination. As previously discussed (4.1.2.3 Attenuated Total Reflectance), radiation at the lower frequencies penetrates deeper than at higher frequencies, causing ATR-FTIR spectral bands to skew. Given the low concentration of the contaminants, the keratin amide bands present at the low frequencies may have overwhelmed the contaminants for these analyses. The detection limit of the instrument was therefore considered a major drawback of the method presented for this type of analysis. Chemical imaging was identified as a potential alternative for locating and analysing contamination on the hair surface, and this technique is discussed further below (4.3.6 Chemical Imaging).

Moreover, Raman spectroscopy was identified as a potential alternative for this type of analysis (Maynard, 2012). Raman is considered a complimentary technique to IR spectroscopy that can similarly be used for sample identification and quantification and additionally, the depth of focus (z plane) can be adjusted to enable characterisation of different sample layers. Fourier Transform Raman spectroscopy has already been evaluated elsewhere to assess the state of degraded archaeological hair samples collected from various burial sites, including different coffin materials, caves, exposed conditions and museum storage facilities (Wilson *et al.*, 1999). That study identified the impact of environmental contaminants, for example, a  $\text{CO}_3^{2-}$  vibration at  $1047\text{ cm}^{-1}$  was consistently observed on spectra of hair collected from lead lined coffins, while a  $\text{CaCO}_3$  vibration at  $1086\text{ cm}^{-1}$  was observed on spectrum of hair collected from cave sites (Wilson *et al.*,

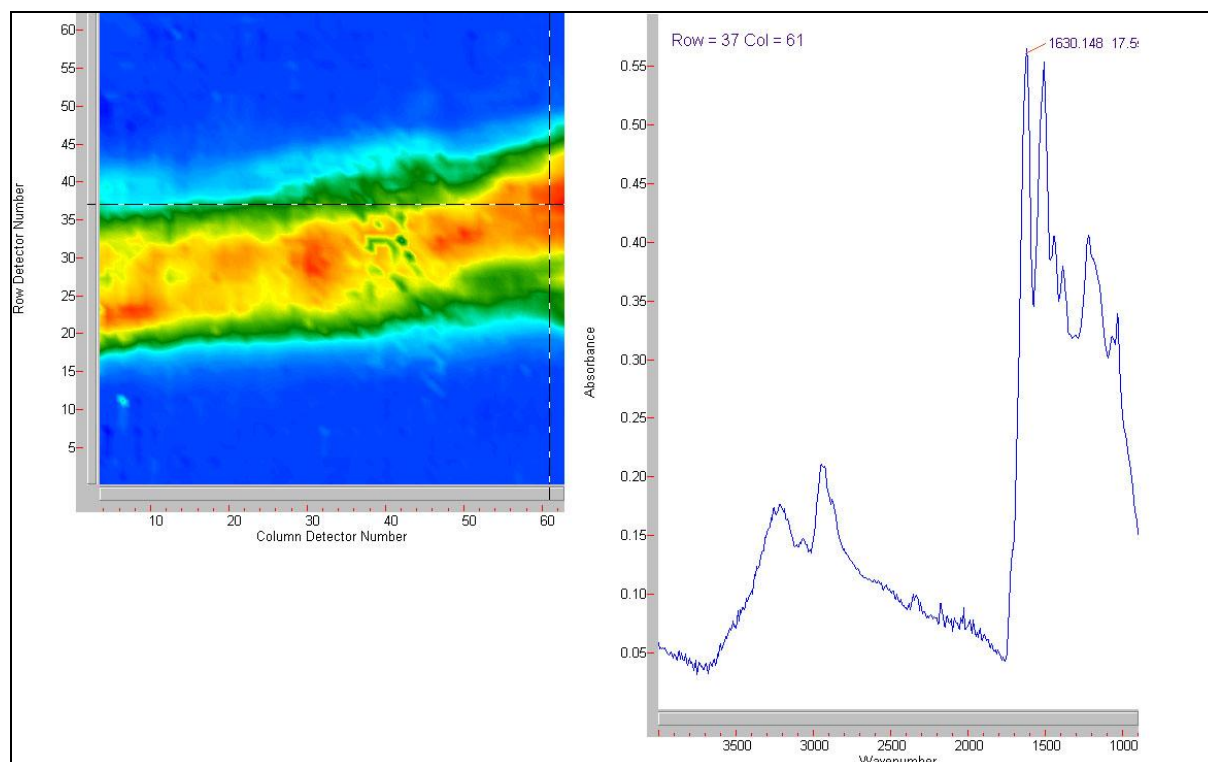
1999). Thus, Raman is recommended for further investigation to evaluate its suitability for the detection of hair surface contaminants within a forensic context.

### 4.3.6. Chemical Imaging

Mid-IR chemical imaging was used to determine whether spatial data (false colour map) could assist the forensic examiner with locating product contamination on the hair surface. This part of the research was designed to provide a “proof of concept” for future research. Individual hair samples were densely coated with hairspray and analysed using the *Digilab* Stingray Imaging System. By selecting a wavenumber that corresponds to the spectral band of a specific compound, the spatial distribution of that compound across the sampled area can be selectively mapped, revealing the samples’ inhomogeneity.

#### 4.3.6.1 Hair Keratin

Figure 4.3-17 illustrates the spatial data corresponding to the spectrum for hair keratin, being the Amide I absorption band at  $1630\text{ cm}^{-1}$ . As illustrated, an arbitrary colour was attributed to each pixel according to the spectral intensity at  $1630\text{ cm}^{-1}$  with red representing high spectral intensity and blue representing low spectral intensity. Thus, while the hair surface was coated in product, the hair keratin Amide I compounds were still identifiable by the ATR-FTIR technique. This could be as a result of the inhomogeneous application of hairspray, or as a result of the hemispherical shape of the germanium crystal down the longitudinal centre of the hair shaft, forcing the contamination to the outer edges. In her work on chemical imaging of hair cross-sections, Lee (2008) recommended the use of a flat diamond ATR for hair surface contamination to allow greater contact between the hair surface the crystal.



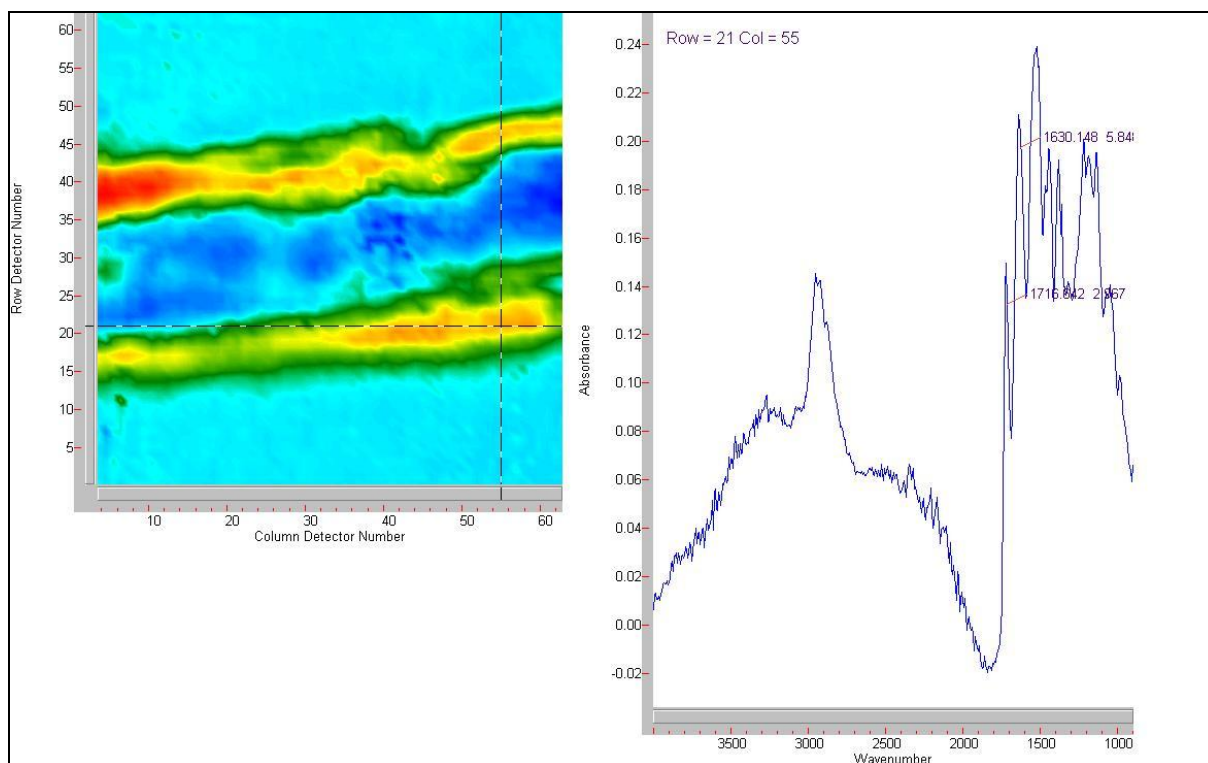
**Figure 4.3-17 – Chemical Image of Keratin**

Spatial representation of the hair keratin Amide I absorption band at  $1630\text{ cm}^{-1}$  from chemical imaging data generated from a hair with hairspray densely applied. The inhomogeneity of the sample is evident, with red representing areas of high spectral intensity of the selected wavenumber ( $1630\text{ cm}^{-1}$ ) and blue representing low spectral intensity.

#### 4.3.6.2 Hairspray Contamination

The spatial data corresponding to the spectrum for the hairspray, being the aliphatic tertiary amide carboxyl group ( $\text{C}=\text{O}$ ) absorption band at  $1716\text{ cm}^{-1}$ , is presented in Figure 4.3-18. As illustrated, an arbitrary colour is attributed to each pixel according to the spectral intensity at  $1716\text{ cm}^{-1}$  with red representing high spectral intensity and blue representing low spectral intensity. While the hair sample had a dense application of hairspray, product contamination is only identifiable along the outer longitudinal lines of the hair shaft by this technique. Similar to the hair keratin spatial data, this could be as a result of the inhomogeneous application of hairspray or, dried hairspray from the longitudinal centre of the hair shaft may have been removed during sample preparation when the hair was flattened with a metallic roller. Moreover, with the previous ATR-FTIR analysis, spectra resembling hair keratin on its own or product contamination on its own was often observed depending on the degree of contact pressure applied between the crystal and sample. Similarly here, as a result of a greater depth of penetration by the

hemispherical crystal at the centre, the keratin absorbance bands may have been more intense toward the centre of the shaft.



**Figure 4.3-18 – Chemical Image of Hairspray**

Spatial representation of the aliphatic tertiary amide C=O absorption band at  $1716\text{ cm}^{-1}$  from chemical imaging data generated from a hair with hairspray densely applied. The inhomogeneity of the sample is evident, with red representing areas of high spectral intensity of the selected wavenumber ( $1716\text{ cm}^{-1}$ ) and blue representing low spectral intensity.

#### 4.3.6.3 Summary of Chemical Imaging

This part of the spectroscopic analyses was designed to provide an example of potential future work by demonstrating that the spatial data obtained by chemical imaging could be employed to assist the forensic examiner with locating product contamination on the hair surface. That is, by selecting a wavenumber that corresponds to the spectral band of a known molecule, specifically aliphatic hydrocarbons (CH), carboxylic acids (COOH), esters (COOR), amides (CONR<sub>2</sub>) and silicone oils (SiO), the spatial distribution of that molecule could be selectively mapped to reveal the samples inhomogeneity. This could assist the examiner with locating then identifying traces of cosmetic hair products on the hair surface. Such a process is not currently part of the examination sequence, but has the potential to increase the evidential value of human hair by providing an additional level of

discrimination and by associating a crime-related sample with an individual's environment.



#### 4.4. Conclusion

Identifying hair surface contamination that occurs from the popular use of cosmetic products such as hairsprays, gels and mousse, is not currently part of the routine forensic examination process. Such analyses could increase the evidential value of human hair by producing an additional level of discrimination. Hair research involving ATR–FTIR spectroscopy, to date, has focused on the effects of chemical based hair treatments and/or sunlight exposure, and very few studies have been reported on hair surface contamination. The research focus of this chapter involved assessing the potential for identifying traces of cosmetic product on the hair surface with ATR–FTIR spectroscopy.

Visual evaluations and *OMNIC* Spectral Interpretation analyses established that many hair product constituents from seven targeted product types could be detected by ATR–FTIR spectroscopy. Of the seven products targeted, the leave–in moisturiser was the only product where significant mid–IR absorption bands were not observed, so this product was excluded from further evaluation. The discriminant analysis (canonical correlation) comprising 254 wavenumbers between 1632 and 652 (at a spacing of 3.857  $\text{cm}^{-1}$ ) as the predictor variables resulted in 100% accuracy. That is, all 60 reference spectra were correctly classified as belonging to one of six product categories.

Spectra collected of the six product types following dense application to a single hair showed some variations when compared to the respective reference spectra (in addition to the presence of the hair keratin Amide I and Amide II absorbance bands that were apparent in each spectrum). The spectral intensity of some absorbance bands increased, others reduced, and a few bands were absent altogether. The discriminant analysis (hierarchical cluster) resulted in only 73% prediction accuracy, with 16 of the 60 spectra misclassified. While some misclassifications were not surprising given the visual similarities, the styling wax spectra and the mousse spectra were, visually, very different so the close location of those two sample sets on the dendrogram was surprising. All ten finishing gloss spectra had to be removed in order for the statistical analyses to succeed. As some discrimination between the densely contaminated hair samples could be determined, it was decided that investigation of whether a particular product type could be distinguished following sparse application to a single hair was warranted.

The sparse application analyses were designed to address hair evidence in the context of forensic casework by simulating normal product usage. However, with the exception of styling wax, and to a lesser extent mousse, contamination was not observed on the majority of samples and, on the few samples where it was observed, spectra of the contamination could not be resolved. The distinctive styling wax results were most likely due to the viscous texture of the product that in turn produced a firm bond with the hair fibre. Conversely, the poor results involving the other products, particularly those products designed to partially evaporate on application and drying, such as the hairspray and smoothing balm, would produce contamination of low concentration along the hair fibre. This may have been due to the significant keratin bands overwhelming the contamination, given the greater depth of penetration at the lower frequencies on ATR analyses. The detection limit of the instrument was therefore considered a major drawback for the purpose of this research. Identifying alternative methods for locating and analysing contamination on the hair surface was thus considered for potential future work, including Raman spectroscopy. Alternatively, visually locating hair contamination with a high power objective and/or analysing spatial data provided by mid-IR chemical imaging, were also recommended as techniques to assist the examiner with locating hair surface contamination, although more research is required in this area.

Finally, it is recommended that future work also involves investigating the ability to discriminate between different brands within the same product type. It is reasonable to expect that where within-product differences were found to exist, the 100% correct classification of reference spectrum to product class would reduce concurrently. Common hair surface contaminants resulting from occupational or environmental means, for example, specks of paint or machine oil resulting from employment in the automotive industry, might also be considered.

## Chapter 5. CONCLUSION

---

## 5.1. Conclusion

The role of the forensic hair examiner is to determine whether a questioned hair recovered from a crime scene could or could not be from the same source as a known sample and therefore whether it should be included or excluded as probative evidence. Arguably, traditional hair microscopy is a largely subjective process that relies heavily on the training and experience of the examiner. The aim of this project was to investigate three objective analytical methods to produce a hair examination protocol that balances qualitative microscopic observations with quantitative measures. Hair samples were received from 154 participants, with 20 participants from each of six nominal hair colour categories actively sought. Combed head hair was requested to increase the number of telogen hairs in each sample set, though only samples comprising at least ten hairs with the root end attached and natural, untreated colouring were retained for use in this study. Approximately 3150 montage images were acquired at three equidistant points along the proximal end of the hair shaft for all ten hairs belonging to each participant. The montage images were utilised in both the colour and pigmentation components of this research (Chapter 2 and Chapter 3, respectively). For the spectroscopy component of this research (Chapter 4), additional hair samples were received from one female Caucasian. The participant's hair was washed, blow-dried and collected by cutting tresses approximately 8 cm from the distal ends. Four sample sets were prepared, including a 'reference spectra', 'hair with product sparsely applied', 'hair with product densely applied' and a control set. Two spectra from each sample were collected, yielding ten spectra per product within each sample set.

### 5.1.1. Colour

#### 5.1.1.1 Allocation to Categories

Numerical colour measurements derived from three colour models were assessed to determine which produced the best statistical model for allocating hair to one of six nominal colour categories. Between 69.3 and 76.2% correct classification to the categories was achieved, with RGB and CIE L\*a\*b\* returning the highest prediction accuracy and CIE XYZ returning generally poor results, particularly among the darker categories. In an effort to refine and improve these results, analyses were repeated that incorporated only a

limited set of categories and predictor variables. Correct allocation increased slightly for the darker samples while no improvement was observed for the lighter samples.

A number of reasons were considered for why the predictive analyses were of limited value when applied to the discrimination of hair colour. First, numerical models describe *colour* that is, essentially, a visual experience dependant on the human observer for description. Colour categories need to reflect the human perception of colour, yet equally correspond to differences between the numerical coordinates that were measured. Subjective observer–reported colours were incorporated in the hierarchical cluster analyses used to facilitate the allocation of categories, but the predictive model relied solely on numerical criterion. Moreover, discriminant analyses focus on linear relationships, so where a non–linear relationship between the individual components of a particular colour model existed, it also would not have been reflected by the resulting model. Finally, Box Ms were used to test the assumption of homogeneity of the covariance matrix. The test is notoriously sensitive and small observed significance levels for large sample sizes can be ignored; albeit, this could additionally explain why the predictive models were of limited value.

The predictive statistical tests applied in this research did not have the high discriminating power that would otherwise be expected for a continuous variable such as hair colour. The rate of misclassification associated with the statistical model was too high to provide support for routine application in operational casework. Furthermore, while this research compared three colour models, sRGB may have been an unsuitable choice given that some colours visible to the human eye are located outside the sRGB gamut. The potential of this part of the research may have been limited as a result and a wider gamut, such as Adobe RGB, should be considered for future research of this kind.

#### **5.1.1.2 Allocation to Participants**

This part of the colour component was designed to emulate the forensic hair examination process and investigate whether numerical colour measurements could assist the experienced microscopist, post–trriage with colour comparisons between samples from questioned and known sources. Importantly, this research found the range of variation for the present sample population was greater between people than within one person, confirming the view that numerical colour measurements can be used to distinguish

between participant hair colour. Likewise, this range of variation is the foundation on which microscopic hair examinations involving colour comparisons rely.

Discriminant analyses were used to distinguish between individual hairs within a subpopulation of similarly coloured hair. The RGB and CIE L\*a\*b\* colour models again performed better overall than the CIE XYZ colour model; however, aside from the Red hair category (up to 80.3% prediction accuracy), the overall prediction accuracy was low (between 11.1 and 59.4%) and did not provide support for application of the method as a routine tool in forensic hair examination.

Confidence intervals that test colour components as individual variables were considered as an alternative to discriminant analyses, which rely on multivariate evaluations. In order for numerical measurements to assist the experienced forensic hair examiner, it was recommended that future research consider the colour components as individual variables, similar to the approach taken by Bednarek (2003) as well as the follow-up approach demonstrated in Chapter 2 of this research.

### **5.1.2. Pigmentation**

A novel image analysis technique was investigated for quantifying and discriminating pigmentation pattern evaluations. The study was designed to measure the density, size and shape of the pigment configurations, as represented by pixel variations within montage images. Specifically, statistical analyses were used to address the question of whether the selected measurements could discriminate between participants with similar shaded hair. Unfortunately, the selected methodology did not support discrimination between the selected participants and a number of limitations were considered.

First, the forensic hair examiner will evaluate the entire length of hairs available in a questioned and an exemplar set, while the present study only evaluated an extract taken from an area approximately 204 x 152  $\mu\text{m}$  in size. Future research should consider a method that involves a greater representation of the entire shaft. Second, during method development, the most appropriate threshold level was determined experimentally for the three separate populations, i.e., 50% for Light, 35% for Medium and 25% for Dark. Occasionally, a hair sample was unavoidably thresholded at an unsuitable level. Third, to measure pigmentation in each threshold image, only a limited number of the 28 parameters available from the V++ Object Analysis function were employed to analyse the black on

white objects. Future research could consider all of the parameters available in *V++*; a complete list is provided in Table 3.2-3 (Digital Optics Ltd., 2009). Due to the complexity of data preparation involved in the current method design, only a small cohort of images and participants were evaluated in this part of the research and this would be more cumbersome with a greater number of parameters considered. Once appropriate discriminating measures had been determined, the Object Analysis function could be automatically performed with the appropriate *VPascal* script and this approach would be recommended to enable a greater number of comparisons to be evaluated more easily. Finally, fractal dimensions that describe the complexity of detail in a pattern rather than its spatial dimensions could provide an alternative tool for extracting information from pigmentation patterns.

### 5.1.3. Spectroscopy

The potential for identifying trace contaminants on the hair surface using ATR–FTIR spectroscopy was assessed. Visual evaluations and *OMNIC* Spectral Interpretation analyses established that many constituents from seven targeted product types could be detected by ATR–FTIR spectroscopy. Of those contaminants, the leave–in moisturiser was the only product where mid–IR absorption was not observed, so this product was excluded from further evaluations. Discriminant analysis comprising 254 wavenumbers between 1632 and 652 (at a spacing of  $3.857\text{ cm}^{-1}$ ) as the predictor variables, resulted in 100% classification accuracy. Albeit, this analysis only included one brand of product per product type and it is reasonable to assume that had numerous brands per product been tested, the prediction accuracy may have been reduced. For the analysis conducted, the strongest predictor variables were generally between 1300 and  $1000\text{ cm}^{-1}$  corresponding to the CO absorbance bands for ethers and esters, and at  $1450\text{ cm}^{-1}$  ( $-11.271$ ) corresponding to the  $\text{CH}_3$  asymmetrical bend vibration.

Spectra collected following dense application to single hairs showed some variations when compared to the reference spectra. The spectral intensity of some absorbance bands increased, others reduced, and a few bands were absent altogether. The discriminant analysis resulted in 44 out of 60 correct classifications (73%). The ‘sparse application’ analyses were designed to address hair evidence in the context of forensic casework by simulating normal product usage. However, with the exception of styling wax, and to a lesser extent mousse, contamination was not observed on the majority of

samples and, on the few samples where it was observed, spectra of the contamination could not be clearly resolved. Those products designed to partially evaporate on application and drying, would most likely produce low concentration traces along the hair fibre that likely contributed to the poor results. Similarly, greater depth of penetration at the lower frequencies often experienced by the ATR technique may have resulted in the keratin bands overwhelming any contaminants present. The limited sensitivity and specificity of the technique (i.e., its ability to detect low-level surface contamination against the strong signal from the air shaft itself) was therefore considered a major drawback for this application.



## 5.2. Conclusion – Recommendations for Future Research

Following from the research results detailed in this thesis, recommendations for future research resulting from this study include the following:

- Discriminant analysis is only recommended for distinguishing between nominal hair colour categories in the case of training new forensic hair examiners or for the evidence triage process to assist inexperienced hair examiners or scene of crime officers with the initial processing of multiple questioned hairs or bulk samples;
- Alternative statistical methods should be investigated in order to achieve greater discrimination between colours. However, the nominal categories need to reflect the human perception of colour, yet equally correspond to differences between the numerical coordinates that were measured;
- Future research relying on RGB colour measurements should consider a wider gamut such as Adobe RGB. This option may depend on the capture device employed;
- Discriminant analysis is not recommended for distinguishing between individual hairs of similar colour. Future research should consider the colour components as individual variables, such as confidence intervals determined from probability distribution curves;
- Future research could consider multiple threshold level images of pigmentation, prior to object analysis that could involve a greater number of parameters not investigated here;
- Performing numerical analysis of pigmentation using appropriate automated script is recommended to enable a greater number of comparisons to be evaluated more easily;
- The statistical indices provided by fractal dimensions may be suitable for comparing pigmentation within and between participants and further investigation is warranted;

- Research involving ATR–FTIR spectroscopy to investigate hair surface trace contaminants resulting from occupational or environmental means, for example, specks of paint or machine oil resulting from employment in the automotive industry, should be considered. Research involving different brands within the same product type should also be considered;
- Raman spectroscopy is recommended for future investigations, to evaluate its suitability for the detection of hair surface contaminants in a forensic context; and
- Locating hair surface contaminants with a high power objective and/or analysing spatial data provided by mid–IR chemical imaging, should be investigated further.

Finally, difficulties associated with improving the discriminating power of hair examinations were identified two decades ago, specifically that considerable variation exists in hairs from a single individual and that microscopic features of hair are difficult to assess objectively (Robertson, 1982). Emerging technologies in image processing, pattern recognition and computer science could assist future examinations with classifying—or potentially individualising—forensic hair evidence. However, despite attempts made in this research, successful quantification and discrimination of hair characteristics has not been achieved. Until there is a universally applicable technique that will mimic microscopic analysis, current evaluations made by an experienced examiner are the best option available.

# References

---

*United States v Frye* (1923) 293 F 2d (DC Cir)

*Daubert v Merrell Dow Pharmaceuticals Inc.* (1993) 509 US, 579, 113 S Ct 2786, 125 L Ed 2d 469

*Williamson v Reynolds* (1995) 904 F Supp 1529, 1558 (ED, Oklahoma)

*State v McGrew* (1997) 682 NE 2d 1289 (Ind)

Aitken C & Robertson J (1986) 'The value of microscopic features in the examination of human head hairs: statistical analysis of questionnaire returns' *Journal of Forensic Sciences*, vol.31(2), pp.546-562

Akyildiz E, Uzun I, Inanici M & Baloglu H (2009) 'Computerized image analysis in differentiation of skin lesions caused by electrocution, flame burns, and abrasions' *Journal of Forensic Sciences*, vol.54(6), pp.1419-1422

Australia National Association of Testing Authorities, 'Technical note 17: guidelines for the validation and verification of chemical test methods' Retrieved 29 April 2011, from <http://www.nata.com.au/publications/category/9-nata-technical-notes>

Ball T, Griggs W, Kuchar M, R P & Hess W (2002) 'Image analysis of Egyptian mummy hair' *Microscopy and Microanalysis*, vol.8(S02), pp.922-923

Barrett J, Siegal J & Goodpaster J (2010) 'Forensic discrimination of dyed hair color: I. UV-visible microspectrophotometry' *Journal of Forensic Sciences*, vol.55(2), pp.323-333

Barrett J, Siegal J & Goodpaster J (2011) 'Forensic discrimination of dyed hair color: II. multivariate statistical analysis' *Journal of Forensic Sciences*, vol.56(1), pp.95-101

Bartick E, Tungol M & Reffner J (1994) 'A new approach to forensic analysis with infrared microscopy - internal reflection spectroscopy' *Analytica Chimica Acta*, vol.288(1-2), pp.35-42

Barton P (2011) 'A forensic investigation of single human hair fibres using FTIR-ATR spectroscopy and chemometrics'. *School of Physical and Chemical Sciences, Discipline of Chemistry*, Queensland University of Technology, Brisbane

## REFERENCES

- Beach J (2009) 'Scientific evidence: a need for caution in decision making'. *Judicial Reasoning: Art or Science?*, National Judicial College of Australia, ANU College of Law, Australian Academy of Forensic Sciences
- Bednarek J (2003) 'An attempt to establish objective criteria for morphological examinations of hairs using the image analysis system' *Problems of Forensic Sciences*, vol.56, pp.65-77
- Biological Criminalistics (2004) 'Hair examination procedure manual'. *Laboratory Services*, Australian Federal Police (AFP), Weston ACT
- Birngruber C, Ramsthaler F & Verhoff M (2009) 'The color(s) of human hair - forensic hair analysis with SpectraCube®' *Forensic Science International*, vol.185(1), pp.e19-23
- Bisbing R & Wolner M (1984) 'Microscopical discrimination of twins' head hair' *Journal of Forensic Sciences*, vol.29(3), pp.780-786
- Blackman A, Bottle S, Schmid S, Mocerino M & Wille U (2008) *Chemistry*, John Wiley & Sons Australia Ltd., Milton QLD
- Blackwell R & Crisci W (1975) 'Digital image processing technology and its application in forensic sciences' *Journal of Forensic Sciences*, vol.20(2), pp.288-304
- Boonen T, Vits K, Hoste B & Hubrecht F (2008) 'The visualisation and quantification of cell nuclei in telogen hair roots by fluorescence microscopy, as a pre-DNA analysis assessment' *Forensic Science International: Genetics Supplement Series 1*, pp.16-18
- Brenner L, Squires P, Garry M & Tumosa C (1985) 'A measurement of human hair oxidation by Fourier transform infrared spectroscopy' *Journal of Forensic Sciences*, vol.30(2), pp.420-426
- Brinkman R (2008) *The Art and Science of Digital Composition*, Morgan Kaufmann Publishers, Burlington USA
- Brooks E (2007) 'An appraisal of the use of numerical features in the forensic examination of hair'. *School of Health Sciences, Division of Health, Design and Science*, University of Canberra, Canberra
- Brooks E (2009), Biological Criminalistics, Forensic and Data Centre, Australian Federal Police
- Brooks E, Comber B, McNaught I & Robertson J (2011) 'Digital imaging and image analysis applied to numerical applications in forensic hair examination' *Science and Justice*, vol.51(1), pp.28-37

- Brown M (2004) *The Choice Guide to Digital Photography*, CHOICE Books, Marrackville NSW
- Carolei L & Gutz I (2005) 'Simultaneous determination of three surfactants and water in shampoo and liquid soap by ATR-FTIR' *Talanta*, vol.66(1), pp.118-124
- Chan K & Kazarian S (2006a) 'ATR-FTIR spectroscopic imaging with expanded field of view to study formulations and dissolution' *Lab on a Chip*, vol.6(7), pp.864-870
- Chan K & Kazarian S (2006b) 'High-throughput study of poly(ethylene glycol)/Ibuprofen formulations under controlled environment using FTIR Imaging' *Journal of Combinatorial Chemistry*, vol.8(1), pp.26-31
- Chan K, Kazarian S, Mavraki A & Williams D (2005) 'Fourier transform infrared imaging of human hair with a high spatial resolution without the use of a synchrotron' *Applied Spectroscopy*, vol.59(2), pp.149-155
- Chan K, Tay F, Taylor C & Kazarian S (2008) 'A novel approach for study of in situ diffusion in human hair using Fourier transform infrared spectroscopic imaging' *Applied Spectroscopy*, vol.62(9), pp.1041-1044
- Chase H (1954) 'Growth of the hair' *Physiological Reviews*, vol.34(1), pp.113-126
- Christie R, Mather R & Wardman R (2000) *The Chemistry of Colour Application*, Blackwell Science Ltd, Carlton VIC
- Clement JL, Hagege R, Le Pareux A, Connet J & Gastaldi G (1981) 'New concepts about hair identification revealed by electron microscope studies' *Journal of Forensic Sciences*, vol.26(3), pp.514-517
- Clement JL, Le Pareux A & Ceccaldi P (1982) 'The specificity of the ultrastructure of human hair medulla' *Journal of the Forensic Science Society*, vol.22(4), pp.396-398
- Comber B (2006a) 'Version 4.0 *VPascal* program for conversion of RGB images to L\*a\*b\* images', Australian Federal Police, Canberra ACT
- Comber B (2006b) 'Version 4.0 *VPascal* program for generating pigment pattern matching values', Australian Federal Police, Canberra ACT
- Devore J & Peck R (2005) *Statistics: the Exploration and Analysis of Data*, Thomson Learning, Belmont USA
- Digital Optics Ltd. (2009) 'V++ Precision Digital Imaging, version 5.0', Auckland NZ

## REFERENCES

- Djozan D, Baheri T, Karimian G & Shahidi M (2008) 'Forensic discrimination of blue ballpoint pen inks based on thin layer chromatography and image analysis' *Forensic Science International*, vol.179(2-3), pp.199-205
- Exline D, Wallace C, Roux C, Lennard C, Nelson M & Treado P (2003) 'Forensic applications of chemical imaging: latent fingerprint detection using visible absorption and luminescence' *Journal of Forensic Sciences*, vol.48(5), pp.1047-1053
- Facey O, Hannah I & Rosen D (1992) 'Shoe wear patterns and pressure distribution under feet and shoes, determined by image analysis' *Journal of the Forensic Science Society*, vol.32(1), pp.15-25
- Flynn K, O'Leary R, Lennard C, Roux C & Reedy B (2005) 'Forensic applications of infrared chemical imaging: multi-layered paint chips' *Journal of Forensic Sciences*, vol.50(4), pp.832-841
- Flynn K, O'Leary R, Roux C & Reedy B (2006) 'Forensic analysis of bicomponent fibers using infrared chemical imaging' *Journal of Forensic Sciences*, vol.51(3), pp.586-596
- Forensic Standards Working Group (2012) 'Forensic Analysis Part 3: Interpretation', Draft Standard V11
- Formanek F, De Wilde Y, Luengo G & Querleux B (2006) 'Investigation of dyed human hair fibres using apertureless near-field scanning optical microscopy' *Journal of Microscopy*, vol.224(2), pp.197-202
- Gaudette B (1999) 'Evidential value of hair examination' in *Forensic Examination of Hair*, Robertson, J (Eds.), Taylor & Francis, CRC Press, London UK, pp.243-260
- Gaudette B (2000) 'Hair - overview' in *Encyclopedia of Forensic Sciences*, Siegel, J, Saukko, P & Knupfer, G (Eds.), Academic Press, London UK, vol.3, pp.999-1002
- Grey T (2006) *Color Confidence (2nd ed.)*, Wiley Publishing Inc., Indiana USA
- Gurden S, Monteiro V, Longo E & Ferreira M (2004) 'Quantitative analysis and classification of AFM images of human hair' *Journal of Microscopy*, vol.215(1), pp.13-23
- Hadjur C, Daty G, Madry G & Corcuff P (2002) 'Cosmetic assessment of the human hair by confocal microscopy' *Scanning*, vol.24(2), pp.59-64
- Hancock D, 'CIE 1931 Chromaticity Diagram' Retrieved 17 December 2010, from <http://hancocktechnologies.com/Color%20Basics.html>

- Harrick N (1977) 'Transmission spectra without interference fringes' *Applied Spectroscopy*, vol.31(6), pp.548-549
- Hopkins J, Brenner L & Tumosa CS (1991) 'Variation of the Amide I and Amide II peak absorbance ratio in human hair as measured by Fourier transform infrared spectroscopy' *Forensic Science International*, vol.50(1), pp.61-65
- Houck M, 'Hair bibliography for the forensic scientist' Retrieved 12 October 2012, from <http://www.fbi.gov/about-us/lab/forensic-science-communications/fsc/jan2002/houck.htm>
- Houck M & Bisbing R (2005) 'Forensic human hair examination and comparison in the 21st Century' *Forensic Science Review*, vol.17, pp.51-66
- Houck M, Bisbing R, Watkins T & Harmon R, 'Locard exchange: the science of forensic hair comparison and the admissibility of hair comparison evidence: Frye and Daubert considered' Retrieved 27 February 2010, from <http://www.modernmicroscopy.com/main.asp?article=36&searchkeys=>,
- Huang Y & Xu B (2002) 'Image analysis for cotton fibers, Part I: Longitudinal measurement' *Textile Research Journal*, vol.72(8), pp.713-720
- Hunt R (1987) *The Reproduction of Colour (4th ed.)*, Fountain Press, England UK
- Imperial Oel Import, 'Lanolin' Retrieved 25 October 2011, from <http://www.lanolin.com/lanolin-basics/lanolin-refinement.html>
- Ito S & Wakamatsu K (2003) 'Quantitative analysis of eumelanin and pheomelanin in humans, mice, and other animals: a comparative review' *Pigment Cell Research*, vol.16(5), pp.523-531
- Jimbow K, Ishida O, Ito S, Hori Y, Witkop C & King R (1983) 'Combined chemical and electron microscopic studies of pheomelanosomes in human red hair' *Journal of Investigative Dermatology*, vol.81(6), pp.506-511
- Joy M & Lewis D (1991) 'The use of Fourier transform infra-red spectroscopy in the study of the surface chemistry of hair fibres' *International Journal of Cosmetic Science*, vol.13(5), pp.249-261
- Kaszynski E (1985) 'Hair growth: mechanism and regulation'. *Proceedings of the International Symposium on Forensic Hair Comparisons*, FBI Academy, Quantico, Virginia USA, pp.25-27
- Kay S, 'RGB gamut' Retrieved 17 December 2010, from <http://www.flickr.com/photos/stevefaembra/2075918823/>

## REFERENCES

- Kazarian S & Chan K (2006) 'Applications of ATR-FTIR spectroscopic imaging to biomedical samples' *Biochimica et Biophysica Acta*, vol.1758(7), pp.858-867
- Kelch A, Wessel S, Will T, Hintze U, Wepf R & Wiesendanger R (2000) 'Penetration pathways of fluorescent dyes in human hair fibres investigated by scanning near-field optical microscopy' *Journal of Microscopy*, vol.200(3), pp.179-186
- Kerley E & Rosen S (1973) 'The identification of Polynesian head hair' *Journal of Forensic Sciences*, vol.18(4), pp.351-355
- Kidwell D, Lee E & DeLauder S (2000) 'Evidence for bias in hair testing and procedures to correct bias' *Forensic Science International*, vol.107(1-3), pp.39-61
- Kinneer P & Gray C (2010) *PASW 17 Statistics Made Simple (replaces SPSS Statistics 17)*, Psychology Press, East Sussex UK
- Kirkbride K & Tungol M (1999) 'Infrared microspectroscopy of fibres' in *Forensic Examination of Fibres*, Robertson, J & Grieve, M (Eds.), Taylor & Francis, CRC Press, London UK, pp.179-222
- Kolowski J, Petraco N, Wallace M, De Forest P & Prinz M (2004) 'A comparison study of hair examination methodologies' *Journal of Forensic Sciences*, vol.49(6), pp.1253-1255
- Lamb P & Tucker L (1994) 'A study of the probative value of Afro-Caribbean hair comparisons' *Journal of the Forensic Science Society*, vol.34(3), pp.177-179
- Lee L, Ludwig K & Baden H (1978) 'Matrix proteins of human hair as a tool for identification of individuals' *Forensic Science*, vol.11(2), pp.115-121
- Lee V (2008) 'Discrimination of human hair using infrared hyperspectral image data'. *School of Chemistry and Forensic Science, Faculty of Science, University of Technology, Sydney*
- Leech N, Barrett K & Morgan G (2008) *SPSS for Intermediate Statistics: Use and Interpretation*, Taylor & Francis Group, New York USA
- Linch C (2009) 'Degeneration of nuclei and mitochondria in human hairs' *Journal of Forensic Sciences*, vol.54(2), pp.346-349
- Linch C & Prahlow J (2001) 'Postmortem microscopic changes observed at the human head hair proximal end' *Journal of Forensic Sciences*, vol.46(1), pp.15-20
- Linch C, Smith S & Prahlow J (1998) 'Evaluation of the human hair root for DNA typing subsequent to microscopic comparison' *Journal of Forensic Sciences*, vol.43(2), pp.305-314



- Logicol Color Technology, 'Easy RGB - The Inimitable RGB and Colour Search Engine'  
Retrieved various dates, 2010, from <http://www.easyrgb.com/index.php?X=CALC>
- Mandelbrot B (1967) 'How long is the coast of Britain? Self-similarity and fractional dimension' *Science*, vol.156(3775), pp.636-638
- Maynard P (2012), School of Chemistry and Forensic Science, University of Technology, Sydney
- McClellan J P (2009) 'Admissibility of expert evidence under the Uniform Evidence Act'.  
*Emerging Issues in Expert Evidence Workshop*, Judicial College of Victoria, Melbourne
- McNevin D (2012), Forensic Studies, Faculty of Applied Science, University of Canberra
- Meyer W, Schnapper A, Hulmann G & Seger H (2000) 'Domestication-related variations of the hair cuticula pattern in mammals' *Journal of Animal Breeding and Genetics*, vol.117(4), pp.281-283
- Meyer W, Seger H, Hülmann G & Neurand K (1997) 'A computer-assisted method for the determination of hair cuticula patterns in mammals' *Berliner und Münchener Tierärztliche Wochenschrift*, vol.110(3), pp.81-85
- Miyata H, Shinozaki M, Nakayama T & Enomae T (2002) 'A discrimination method for paper by Fourier transform and cross correlation' *Journal of Forensic Sciences*, vol.47(5), pp.1125-1132
- National Research Council of the National Academies (2009) 'Strengthening forensic science in the United States: a path forward', Washington DC USA: The National Academies Press,
- Natural Nigerian, 'Hair 101 - hair growth starts here ... the hair bulb' Retrieved 23 March 2012, from <http://naturalnigerian.com/2012/01/hair-101-hair-growth-starts-here-the-hair-bulb/>
- Naysmith L, Waterson K, Ha T, Flanagan N, Bisset Y, Ray A, Wakamatsu K, Ito S & Rees J (2004) 'Quantitative measures of the effect of the melanocortin 1 receptor on human pigmentary status' *Journal of Investigative Dermatology*, vol.122(2), pp.423-428
- Norusis M (1985) *SPSS-X Advanced Statistics Guide*, McGraw-Hill, New York USA
- Norusis M (2008) *SPSS Statistics 17.0 Statistical Procedures Companion*, Pearson Prentice Hall, New Jersey USA

## REFERENCES

- Ogle R & Fox M (1999) *Atlas of Human Hair Microscopic Characteristics*, CRC Press, Boca Raton USA
- Overheim R & Wagner D (1982) *Light and Colour*, John Wiley & Sons Inc, New York USA
- Pallant J (2005) *SPSS Survival Manual*, Allen & Unwin, Crows Nest NSW
- Panayiotou H & Kokot S (1999) 'Matching and discrimination of single human-scalp hairs by FT-IR micro-spectroscopy and chemometrics' *Analytica Chimica Acta*, vol.392(2-3), pp.223-235
- Parakkal P & Matoltsy A (1964) 'A study of differentiation products of the hair follicle cells with the electron microscope' *Journal of Investigative Dermatology*, vol.43(1), pp.28-34
- Pavia D, Lampman G & Kriz G (1979) *Introduction to Spectroscopy: A Guide for Students of Organic Chemistry*, WB Saunders Company, Philadelphia USA
- Payne G, Langlois N, Lennard C & Roux C (2007) 'Applying visible hyperspectral (chemical) imaging to estimate the age of bruising' *Medicine, Science and the Law*, vol.47(3), pp.225-232
- Payne G, Reedy B, Lennard C, Comber B, Exline D & Roux C (2005a) 'A further study to investigate the detection and enhancement of latent fingerprints using visible absorption and luminescence chemical imaging' *Forensic Science International*, vol.150(1), pp.33-51
- Payne G, Wallace C, Reedy B, Lennard C, Schuler R, Exline D & Roux C (2005b) 'Visible and near-infrared chemical imaging methods for the analysis of selected forensic samples' *Talanta*, vol.67(2), pp.334-344
- Petraco N (1999) 'Forensic human hair identification and comparison guidelines'. *Scientific Working Group for Material Analysis (SWGMAT)* Federal Bureau of Investigation, Washington DC USA
- Petraco N, Fraas C, Callery F & de Forest P (1988) 'The morphology and evidential significance of human hair roots' *Journal of Forensic Sciences*, vol.33(1), pp.68-76
- Pinorini M, Lennard C, Margot P, Dustin I & P F (1994) 'Soot as an indicator in fire investigations: physical and chemical analyses' *Journal of Forensic Sciences*, vol.39(4), pp.933-973
- Rees J (2003) 'Genetics of hair and skin color' *Annual Review of Genetics*, vol.37, pp.67-90

- Ricci C, Bleay S & Kazarian S (2007a) 'Spectroscopic imaging of latent fingermarks collected with the aid of a gelatin tape' *Analytical Chemistry*, vol.79(15), pp.5771-5776
- Ricci C, Chan K & Kazarian S (2006) 'Combining tape-lift method and fourier transform infrared spectroscopic imaging for forensic applications' *Applied Spectroscopy*, vol.60(9), pp.1013-1021
- Ricci C, Phiriavityopas P, Curum N, Chan K, Jickells S & Kazarian S (2007b) 'Chemical imaging of latent fingerprint residues' *Applied Spectroscopy*, vol.61(5), pp.514-522
- Rieke G (1994) *Detection of Light: From the Ultraviolet to the Submillimeter*, Cambridge University Press, Cambridge UK
- Rintoul L, Panayiotou H, Kokot S, George G, Cash G, Frost R, Bui T & Fredericks P (1998) 'Fourier transform infrared spectrometry: a versatile technique for real world samples' *Analyst*, vol.123(4), pp.571-577
- Rivard P (2006) *Digital Color Correction*, Thomson Delmar Learning, New York USA
- Robertson J (1982) 'An appraisal of the use of microscopic data in the examination of human head hair' *Journal of the Forensic Science Society*, vol.22(4), pp.390-395
- Robertson J (1999) 'Forensic and microscopic examination of human hair' in *Forensic Examination of Hair*, Robertson, J (Eds.), Taylor & Francis, CRC Press, London UK, pp.79-154
- Robertson J & Aitken C (1986) 'The value of microscopic features in the examination of human head hairs: analysis of comments contained in questionnaire returns' *Journal of Forensic Sciences*, vol.31(2), pp.563-573
- Robertson J & Roux C (2010) 'Trace evidence: here today, gone tomorrow?' *Science and Justice*, vol.50(1), pp.18-22
- Robins A (1991) *Biological Perspectives on Human Pigmentation*, Cambridge University Press, Cambridge UK
- Robson D (1993) 'Fibre surface imaging' *Journal of the Forensic Science Society*, vol.34(3), pp.187-191
- Rofin (2006) *Getting Started With V++ Precision Digital Imaging System*, Digital Optics Limited, Auckland NZ
- Roth S & Helwig E (1964) 'The cytology of the cuticle of the cortex, the cortex, and the medulla of the mouse hair' *Journal of Ultrastructure Research*, vol.11(1-2), pp.52-66

## REFERENCES

- Rothe M, Pragst F, Thor S & Hunger J (1997) 'Effect of pigmentation on the drug deposition in hair of grey-haired subjects' *Forensic Science International*, vol.84(3), pp.53-60
- Rouessac F & Rouessac A (2007) *Chemical Analysis: Modern Instrumentation Methods and Techniques*, John Wiley & Sons Ltd., West Sussex England
- Sato H (2003) 'Preliminary study of hair form of Japanese head hairs using image analysis' *Forensic Science International*, vol.131(2), pp.202-208
- Schiering D (1988) 'Infrared microspectroscopic solutions to manufacturing and quality control problems' in *Infrared Microspectroscopy: Theory and Applications*, Messerschmidt, R & Harthcock, M (Eds.), Marcel Dekker Inc., New York USA, pp.229-243
- Shaikhzadeh Najar S, Amani M & Hasani H (2003) 'Analysis of blend irregularities and fibre migration index of wool/acrylic blended worsted yarns by using an image-analysis technique' *Journal of the Textiles Institute*, vol.94(3), pp.177-185
- Shriver M & Parra E (2000) 'Comparison of narrow-band reflectance spectroscopy and tristimulus colorimetry for measurements of skin and hair color in persons of different biological ancestry' *American Journal of Physical Anthropology*, vol.112(1), pp.17-27
- Signori V & Lewis DM (1997) 'FTIR investigation of the damage produced on human hair by weathering and bleaching processes: implementation of different sampling techniques and data processing' *International Journal of Cosmetic Science*, vol.19(1), pp.1-13
- Skoog D, Holler E & Crouch S (2007) *Principles of Instrumental Analysis*, Thomson Higher Education, Belmont USA
- Slominski A, Wortsman J, Plonka P, Schallreuter K, Paus R & Tobin D (2005) 'Hair Follicle Pigmentation' *Journal of Investigative Dermatology*, vol.124(1), pp.13-21
- Smith J (1998) 'A quantitative method for analysing AFM images of the outer surfaces of human hair' *Journal of Microscopy*, vol.191(3), pp.223-228
- Smith S & Linch C (1999) 'A review of major factors contributing to errors in human hair association by microscopy' *The American Journal of Forensic Medicine and Pathology*, vol.20(3), pp.269-273
- SPSS Statistics IBM Corporation (2008) 'PASW for Windows, version 17.0.2', New York USA

- Stenn K & Paus R (2001) 'Controls of hair follicle cycling ' *Physiological Reviews*, vol.81(1), pp.449-494
- Swift J & Smith J (2000) 'Atomic force microscopy of human hair' *Scanning*, vol.22(5), pp.310-318
- Tabachnick B & Fidell L (2001) *Using Multivariate Statistics*, Allyn and Bacon, Massachusetts USA
- Tafaro J (2000) 'The use of microscopic postmortem changes in anagen hair roots to associate questioned hairs with known hairs and reconstruct events in two murder cases' *Journal of Forensic Sciences*, vol.45(2), pp.495-499
- Tahtouh M, Kalman J, Roux C, Lennard C & Reedy B (2005) 'The detection and enhancement of latent fingerprints using infrared chemical imaging' *Journal of Forensic Sciences*, vol.50(1), pp.64-72
- Taupin (1996) 'Hair and fiber transfer in an abduction case - evidence from different levels of trace evidence transfer' *Journal of Forensic Sciences*, vol.41(4), pp.697-699
- Thermo Electron Corporation (2006) 'OMNIC version 7.3', Thermo Electron Corporation, Madison, Wisconsin USA
- Theuwissen A, 'It is time to switch on the light' Retrieved 19 January 2011, from <http://harvestimaging.com/index.php>
- Thyon Design, 'CIE LAB Colour Space' Retrieved 17 December 2010, from <http://www.thyon.com/lab.html>
- Tobin D & Paus R (2001) 'Graying: gerontobiology of the hair follicle pigmentary unit' *Experimental Gerontology*, vol.36(1), pp.29-54
- Tobin D, Slominski A, Botchkarev V & Paus R (1999) 'The fate of hair follicle melanocytes during the hair growth cycle' *Journal of Investigative Dermatology Symposium Proceedings*, vol.44(3), pp.323-332
- Tontarski R & Thompson R (1998) 'Automated firearms evidence comparison; a forensic tool for firearms identification - an update' *Journal of Forensic Sciences*, vol.43(3), pp.641-647
- Trotter M (1939) 'Classifications of hair colour' *American Journal of Physical Anthropology*, vol.25(2), pp.237-260
- Tungol M, Bartick E & Montaser A (1990) 'The development of a spectral data base for the identification of fibers by infrared microscopy' *Applied Spectroscopy*, vol.44(4), pp.543-549

## REFERENCES

- Vaughn M, Brooks E, van Oorschot R & Baindur-Hudson S (2009a) 'A comparison of macroscopic and microscopic hair color measurements and a quantification of the relationship between hair color and thickness' *Microscopy & Microanalysis*, vol.15(3), pp.189-193
- Vaughn M, van Oorschot R & Baindur-Hudson S (2008) 'Hair Color Measurement and Variation' *American Journal of Physical Anthropology*, vol.137(1), pp.91-96
- Vaughn M, van Oorschot R & Baindur-Hudson S (2009b) 'A comparison of hair colour measurement by digital image analysis with reflective spectrophotometry' *Forensic Science International*, vol.183(1), pp.97-101
- Verma M, Pratt L, Ganesh C & Medina C (2002) 'Hair-MAP: a prototype automated system for forensic hair comparison and analysis' *Forensic Science International*, vol.129(3), pp.168-186
- Vernall D (1963) 'A study of the density of pigment granules in hair from four races of men' *American Journal of Physical Anthropology*, vol.21(4), pp.489-496
- Wagner J (1998) 'Product characterisation and problem solving using an image analyser' *TAPPI Journal*, vol.81(6), pp.155-162
- Weiner L, Han R, Scicchitano B, Li J, Hasegawa K, Grossi M, Lee D & Brisette J (2007) 'Dedicated epithelial recipient cells determine pigmentation patterns' *Cell*, vol.130(5), pp.932-942
- Wilson A, Edwards H, Farwell D & Janaway R (1999) 'Fourier Transform Raman spectroscopy: evaluation as a non-destructive technique for studying the degradation of human hair from archaeological and forensic environments' *Journal of Raman Spectroscopy*, vol.30(5), pp.367-373
- Wilson A & Gilbert A (2006) 'Hair and nail' in *Forensic Human Identification: An Introduction*, Thompson, T & Black, S (Eds.), Taylor & Francis, London UK, pp.147-174

# Appendices

---

## Appendix A

### *Example Sample Collection Documents*

#### Participant Information Form

#### *New analytical approaches to advance & enhance the forensic value of human hair*

##### Sample Identification Number

This number cannot be linked to the identity of the participant hair donor. It should be retained by the participant and quoted to the researchers if at any stage the participant wishes to withdraw from the study.

2002 XXX

##### Researchers

Dr Dennis McNevin, PhD  
Forensic Studies  
Faculty of Applied Science  
University of Canberra  
[dennis.mcnevin@canberra.edu.au](mailto:dennis.mcnevin@canberra.edu.au)  
(02) 6201 2634

Professor Alan Cooper, PhD  
Australian Centre for Ancient DNA  
School of Earth & Environmental Sciences  
The University of Adelaide  
[alan.cooper@adelaide.edu.au](mailto:alan.cooper@adelaide.edu.au)  
(08) 8303 5950

Ms Carolyn McLaren  
Forensic Studies  
Faculty of Applied Science  
University of Canberra  
[carolyn.mclaren@canberra.edu.au](mailto:carolyn.mclaren@canberra.edu.au)  
(02) 6201 5879

Ms Janette Edson  
Australian Centre for Ancient DNA  
School of Earth & Environmental Sciences  
The University of Adelaide  
[janette.edson@uqconnect.edu.au](mailto:janette.edson@uqconnect.edu.au)  
(08) 8303 3952

##### Project Aims

The aims of the project are to:

1. develop a protocol for recovery and characterisation of nuclear DNA (nuDNA) from naturally shed human hair.
2. refine new methods for image analysis of hairs;
3. compare the identification success rates of microscopic hair examination, nuDNA genotyping and image analysis; and
4. design a screening sequence and protocol for forensic hair examination based on these methods that minimises resource usage and maximises statistical (and hence evidential) power.



## Benefits of the Project

Human hairs have several features that make them attractive as trace evidence in forensic examinations. The most important feature is that hairs are a ubiquitous material in our environment and are the most common form of evidence found at crime scenes. Pubic hairs are a very common evidence type associated with sexual assault. Humans shed 50 – 150 telogen (resting phase) hairs per person per day and so an offender will typically leave multiple hairs at a crime scene. Hairs have the potential to contribute to the classic ‘roles’ for trace evidence; namely, they can:

- associate an individual with a crime;
- dissociate an individual from a crime; and
- help reconstruct the events that may have taken place.

For this reason, there is a great interest in the potential use of human hair for forensic analysis, with both disaster victim identification and criminal applications.

Traditionally, hair evidence has been provided to the courts in the form of expert testimony from hair examiners, with no statistical probability of association or dissociation. The value of this evidence depends heavily on the experience of the hair examiner, who must be well trained in their sole tool: microscopic hair comparison. By combining this technique with genetic profiling and image analysis, we will provide the forensic community, both nationally and internationally, with new forensic protocols for hair analysis that can be validated and calibrated numerically. It will allow cataloguing of hair characteristics from the general population in a form that will be amenable to database storage, thereby placing hair examination on a similar numerical footing to nuDNA evidence from other sources.

A major outcome of this project will be new methods for the forensic examination of hair that will compliment standard microscopic comparison:

- Advanced genotyping. We will apply and evaluate newly developed DNA characterisation techniques developed for ancient and highly damaged specimens to the forensic analysis of hair.
- Microscopic ‘optical sectioning’ through the full depth of a hair sample. By montaging different sections into one ‘in-focus’ image, this method can provide colour and pigmentation pattern analysis, and the base data from which numerical values can be derived for these distinguishing features.
- Chemical imaging of hair using FTIR spectroscopy. This technique is already applied to fibre analysis and will be used to provide insight into the chemical structure of hair providing a further basis for discrimination.

## General Outline of the Project

Hairs will be collected from participants and then sorted according to:

- racial origin
- gender (male, female)
- age
- hair growth cycle stage (anagen, telogen)

Hairs will then be stored under various conditions according to:

- hydration (dry, humid, wet)
- temperature

## APPENDICES

Hairs will be further treated by cleaning with:

- detergent
- alcohol
- bleach

The hairs will then be analysed in parallel to allow comparison of the efficiency of three proposed methodologies for discriminating between hairs:

1. Hairs will be initially screened by microscopic examination to establish base level data for samples.
2. A range of DNA analysis methods will be used to characterise trace amounts of degraded DNA in the hairs.
3. Image analysis techniques will be applied to the hairs. These techniques are:
  - microscopic optical sectioning;
  - colour imaging;
  - pigmentation pattern analysis; and
  - chemical imaging

We will then compare the identification success rates of microscopic hair examination, nuDNA genotyping and image analysis and design a screening sequence and protocol for forensic hair examination that minimises resource usage and maximises statistical (and hence evidential) power.

The results of the study can be made available to participants by contacting one of the researchers.

### **Participant Involvement**

The project is a voluntary activity and participants may decline to take part or withdraw at any time without providing an explanation. Participants must be aged 18 years or over.

Participants will provide hair samples (scalp) which will be collected using Collection Kits. Each Collection Kit contains the following items:

- Participant Information form
- Informed Consent form
- Participant Questionnaire
- sterile cheek swab (x2)
- sterile disposable gloves (x2 pair)
- sterile plastic comb
- A3 paper (folded) (x2)
- snap-seal bag
- numbered Collection Envelope

### Sample Collection Procedure

The procedure for collecting hairs and DNA is as follows:

1. Read the Participant Information Form.
2. Sign the Informed Consent Form and keep a copy.
3. Fill out the Participant Questionnaire.
4. Self administer a cheek swab by removing the swab from its sheath and wiping it on the inside of one cheek. Return the swab to its sheath. Use the second cheek swab for the other cheek.
5. Cut a small section from the corner of the sheath (see diagram) to allow the saliva to dry and prevent bacterial growth. Return both cheek swabs to the Collection Envelope (please do not place in the snap-seal bag).



6. Perform all hair collection immediately before washing hair.
7. Perform all hair collection while wearing the sterile disposable gloves provided.
8. Holding your head over the unfolded A3 paper (single sheet), gently and slowly run the sterile comb through your scalp hair. Pick out individual hairs from the teeth of the comb and place them on the paper as well. Collect **at least** 20 hairs.
9. Refold the A3 paper, ensuring your hair sample is in the centre. Place this in the snap-seal bag.
10. If your sample appears low (less than 20 hairs) an additional pair of sterile disposable gloves and A3 paper is provided for collection at a second time (immediately before washing hair). Paper containing the second hair sample should be refolded and placed in the same snap-seal bag.
11. Place the Participant Questionnaire and the snap-sealed hair sample(s) in the Collection Envelope. The comb and gloves may be discarded.
12. Please contact one of the nominated researchers to organise return of your Informed Consent Form and the Collection Envelope. Keep the Participant Information Form with the Sample Identification Number recorded on it.

### **Confidentiality**

Only the nominated researchers will have access to the Participant Questionnaires, Informed Consent forms, cheek swabs and hair samples provided by participants. They will not be able to link these to the identities of the participants.

### **Anonymity**

The anonymity of each participant will be preserved. The Participant Questionnaire answers, cheek swabs and hair samples will be identified by a Sample Identification Number that will not be recorded with the personal identity of any participant. The Informed Consent form will be the only document that records participants' names and signatures and these will not have any Sample Identification Number recorded and they will not be stored with the questionnaire answers, cheek swabs or hair samples. Thus, after collection of samples, there will be no means to associate the personal identity of any participant with their Participant Questionnaire, cheek swab or hair samples.

Each participant will retain a Participant Information form with their Sample Identification Number recorded on it. This may be quoted to any of the nominated researchers if any participant wishes to withdraw from the study at any time. If a participant notifies a nominated researcher of their intention to withdraw, their Participant Questionnaire, cheek swab and hair samples will be destroyed.

### **Data Storage**

Participant Questionnaires will be stored in a locked room (7D10) on Level D of Building 7 at the University of Canberra. Cheek swabs and hair samples will be stored in a locked -80 °C freezer on Level D of Building 7 at the University of Canberra. Sub-samples from cheek swabs and hairs will be stored in a restricted access laboratory (7D25) on Level D of Building 7 at the University of Canberra. Sub-samples will be destroyed upon completion of the project. Participant Questionnaires, cheek swabs and hair samples will be stored for five years and then destroyed.

### **Ethics Committee Clearance**

This project has been approved by the Committee for Ethics in Human Research of the University of Canberra.

### **Queries and Concerns**

Any queries or concerns about this project can be addressed to one of the nominated researchers. Any participant may withdraw from the project at any time.

## Informed Consent Form

### *New analytical approaches to advance & enhance the forensic value of human hair*

#### Consent

I have read and understood the information about the research contained in the Participant Information form. I am not aware of any condition that would prevent my participation, and I agree to participate in this project. I have had the opportunity to ask questions about my participation in the research. All questions I have asked have been answered to my satisfaction.

Name .....

Signature .....

Date .....

A summary of the research report can be forwarded to you when published. If you would like to receive a copy of the report, please include your mailing address below.

Address .....

.....

.....

**Carolyn McLaren**  
Forensic Studies  
Faculty of Applied Science  
T (02) 6201 5879  
F (02) 6201 2461  
E [carolyn.mclaren@canberra.edu.au](mailto:carolyn.mclaren@canberra.edu.au)

## Participant Questionnaire

### *New analytical approaches to advance & enhance the forensic value of human hair*

#### Sample identification number

This number cannot be linked to the identity of the participant hair donor.

2002 XXX

#### Questions

Please tick (✓) or cross (✗) the most appropriate answers. If there are any questions you do not wish to answer or where you do not have the information, please leave them blank.

1. Your ethnic origin is best described as:
  - Sub-Saharan African
  - North African
  - Northern European (Celtic, Scandinavian)
  - Western European
  - Southern European (Italian, Greek)
  - Eastern European (Slavic)
  - Middle Eastern
  - West Asian (Indian, Pakistani)
  - East Asian (Chinese, Japanese)
  - South East Asian
  - Polynesian
  - Melanesian
  - Australasian (Australian Aboriginal)
  - Native North American
  - Native South American
  - Other (please specify)
  
2. Your gender is:
  - male
  - female
  
3. Your age is:  
\_\_\_ years
  
4. Your natural hair is best described as:

- dry
  - normal
  - oily
5. Your natural hair type is best described as:
- straight
  - wavy
  - curly
  - other
6. Your natural hair colour is best described as:
- black
  - brown
  - blonde
  - red
  - grey
  - white
7. Your natural hair shade is best described as:
- dark
  - medium
  - light
8. Has your hair been treated in the last year?
- yes (go to question 9)
  - no (go to question 15)
9. How long ago was your hair treated?
- \_\_\_ days, or  
\_\_\_ weeks, or  
\_\_\_ months
10. How has your hair been treated?
- permanent dye
  - semi-permanent dye
  - wash-out dye
  - bleach
  - streaks or foils
  - permanent wave
  - straightened
11. Your treated hair is best described as:
- dry
  - normal
  - oily
12. Your treated hair type is best described as:
- straight

## APPENDICES

- wavy
- curly
- other

13. Your treated hair colour is best described as:

- black
- brown
- blonde
- red
- grey
- white

14. Your treated hair shade is best described as:

- dark
- medium
- light

15. The last hair product used in your hair was:

- none
- hair spray
- mousse
- gel
- moisturiser

16. How long ago did you last apply hair product?

- \_\_\_ days, or
- \_\_\_ weeks, or
- \_\_\_ months, or
- \_\_\_ years, or
- never

*Thank you for your time and co-operation!*

**Carolyn McLaren**

Forensic Studies

Faculty of Applied Science

T (02) 6201 5879

F (02) 6201 2461

E [carolyn.mclaren@canberra.edu.au](mailto:carolyn.mclaren@canberra.edu.au)



## Appendix B

### *VPascal Script for Transformation between Colour Coordinates*

```

button btn_text,'caz3';
var
qq, img,im,iml,m;
temp_small,temp_big;
r,g,b,lr,lg,lb,xn,yn,zn,x,y,z,xx,yy,zz;
l,a;
imgl,imga,imgb,imgxyz;
rgb_mean, rgb_StdDev;
l_mean, a_mean, b_mean;
l_StdDev, a_StdDev, b_StdDev;
x_mean, y_mean, z_mean;
x_StdDev, y_StdDev, z_StdDev;
csv_output;
aa;
lmg8 ;
nImages ;
Msg ;
// r, g and b are standard RGB values; lr, lg and lb are linear RGB values

function powerof(s,t);
var
value,result;
begin
value:=Ln(s);
result:=Exp(value*t);
powerof:=result;
end;

begin
getactiveimage(img);
rgb_mean := MeanOf(img) ;
rgb_StdDev := StdOf(img) ;
r:=single(red(img))/255;
g:=single(green(img))/255;
b:=single(blue(img))/255;

// Standard R,G,B values are transformed to linear R,G,B values

temp_small:=r*(r<=0.04045)/12.92;
temp_big:=powerof(((r+0.055)/1.055),2.4)*(r>0.04045);
lr:=temp_small+temp_big;
// r is the linear red value in the interval 0 to 1

temp_small:=g*(g<=0.04045)/12.92;
temp_big:=powerof(((g+0.055)/1.055),2.4)*(g>0.04045);
lg:=temp_small+temp_big;

```

APPENDICES

```

// g is the linear green value in the interval 0 to 1

temp_small:=b*(b<=0.04045)/12.92;
temp_big:=powerof(((b+0.055)/1.055),2.4)*(b>0.04045);
lb:=temp_small+temp_big;
// b is the linear blue value in the interval 0 to 1

// Linear R,G,B values are transformed to CIE X,Y,Z values

xn := 0.412453 + 0.357580 + 0.180423;
yn := 0.212671 + 0.715160 + 0.072169;
zn := 0.019334 + 0.119193 + 0.950227;
// xn, yn and zn are the CIE XYZ tristimulus values of the reference white

x := 0.412453 * lr + 0.357580 * lg + 0.180423 * lb;
y := 0.212671 * lr + 0.715160 * lg + 0.072169 * lb;
z := 0.019334 * lr + 0.119193 * lg + 0.950227 * lb;
// x, y, and z are the CIE XYZ tristimulus values

x_mean := MeanOf( x ) * 100;
y_mean := MeanOf( y ) * 100;
z_mean := MeanOf( z ) * 100;
x_StdDev := StdOf( x ) * 100;
y_StdDev := StdOf( y ) * 100;
z_StdDev := StdOf( z ) * 100;

// CIE XYZ values are transformed to CIE L*a*b* values

xx := x/xn;
yy := y/yn;
zz := z/zn;

temp_big := (116* powerof(yy,1/3) -16 )*(yy>0.008856);
temp_small := yy*(yy<=0.008856)*903;
l := temp_big+temp_small;
// l is the CIE L* value between 0 to 100

temp_big := powerof(xx,1/3)*(xx>0.008856);
temp_small := (7.787*xx+0.1379310345)*(xx<=0.008858);
xx := temp_big + temp_small;

temp_big := powerof(yy,0.3333) *(yy>0.008856);
temp_small := (7.787*yy + 0.1379310345)*(yy<=0.008856);
yy := temp_big + temp_small;

temp_big := powerof(zz,0.3333)*(zz>0.008856);
temp_small := (7.787*zz + 0.1379310345)*(zz<=0.008856);
zz := temp_big + temp_small;

a := 500*(xx-yy);
b := 200*(yy-zz);
// a is the CIE a* value between -100 to 100

```

```
// b is the CIE b* value between -100 to 100
```

```
// The CIE L*a*b* values are transformed to values between 0 and 255
```

```
SetDisplayRange(img,0,255 ); SetDisplayMode( img,dm_fixed );
show(l,getname(img)+' l');SetDisplayRange(l,-100,100 ); SetDisplayMode( l,dm_fixed );
show(a,getname(img)+' a'); SetDisplayRange(a,-100,100 ); SetDisplayMode( a,dm_fixed );
show(b,getname(img)+' b'); SetDisplayRange(b,-100,100 ); SetDisplayMode( b,dm_fixed );
```

```
l_mean := MeanOf( l );
a_mean := MeanOf( a );
b_mean := MeanOf( b );
l_StdDev := StdOf( l );
a_StdDev := StdOf( a );
b_StdDev := StdOf( b );
```

```
// Format results into a comma separated output (RGB mean, LAB Mean, XYZ Mean, RGB
StdDev, LAB StdDev, XYZ StdDev)
```

```
csv_output := str
(rgb_mean,chr(44),l_mean,chr(44),a_mean,chr(44),b_mean,chr(44),x_mean,chr(44),y_mean,chr(
44),z_mean,chr(44),rgb_StdDev,chr(44),l_StdDev,chr(44),a_StdDev,chr(44),b_StdDev,chr(44),x_
StdDev,chr(44),y_StdDev,chr(44),z_StdDev);
```

```
writeln(csv_output);
writeln;
```

```
getactiveimage(qq);
Delete (qq);
getactiveimage(qq);
Delete (qq);
getactiveimage(qq);
Delete (qq);
getactiveimage(qq);
Delete (qq);
```

```
free(img);
free(l);
free(a);
free(b);
free(x);
free(y);
free(z);
```

```
end
```

## Appendix C

### *VPascal Script for Pigmentation Analyses*

```
button btn_text,'Caz2 PPR';
```

```
var
```

```
img1, img2, pos;
```

```
//pixel_comparison procedure; at each x position, mean extract image values are subtracted from  
the mean entire images values
```

```
procedure pixel_comparison;
```

```
var
```

```
a;
```

```
begin
```

```
a:=img1[pos..pos+getxsize(img2)-1,..];
```

```
writeln(pos,chr(9),abs(meanof(single(a)-single(img2))));
```

```
end;
```

```
begin
```

```
if selectimage('entire image',img1)=id_cancel then halt;
```

```
if selectimage('section image',img2)=id_cancel then halt;
```

```
//Loop command; the above procedure 'pixel_comparison' is executed once at each x position in  
the range x=0 to x=(width of entire image minus width of section image)
```

```
for pos:= 0 to getxsize(img1)-getxsize(img2)-1 do
```

```
begin
```

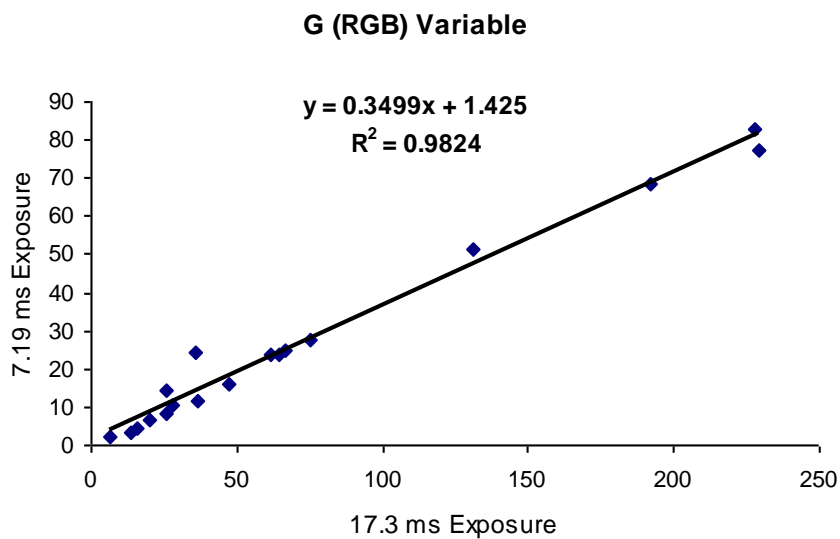
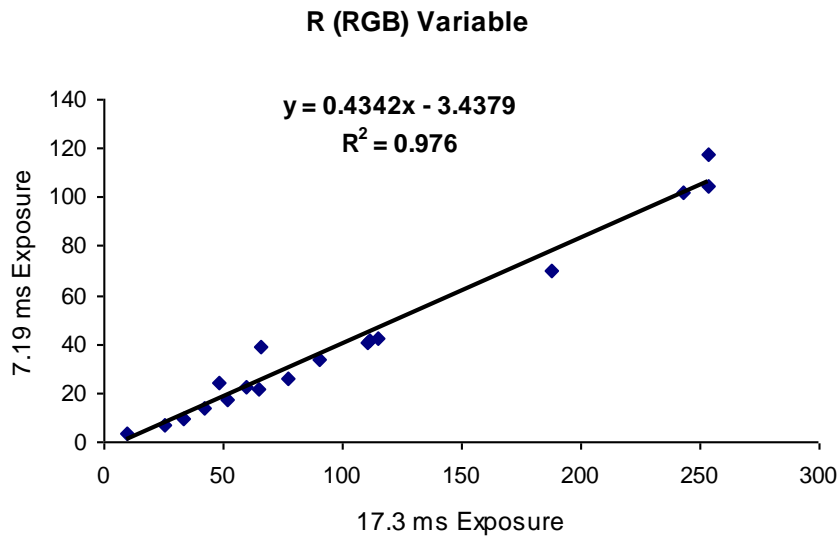
```
overlay_section;
```

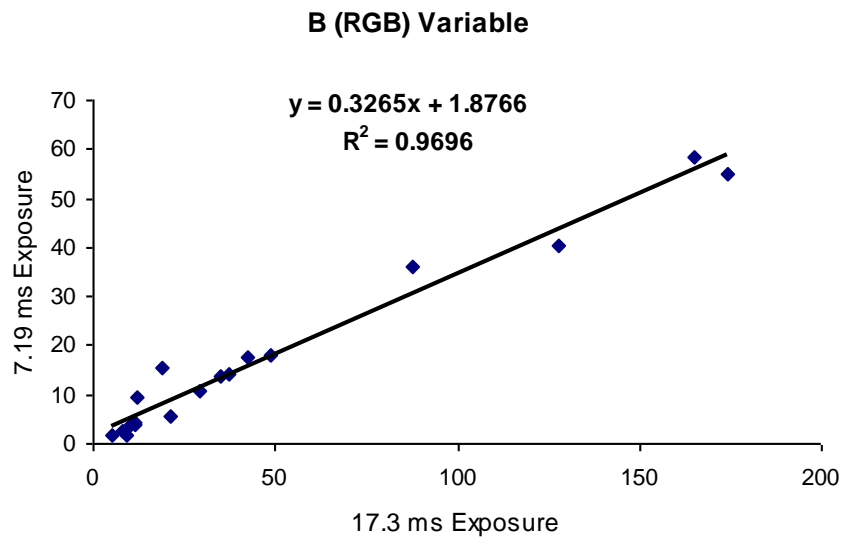
```
end;
```

```
end
```

## Appendix D

### Linear Regression for Correcting Exposure









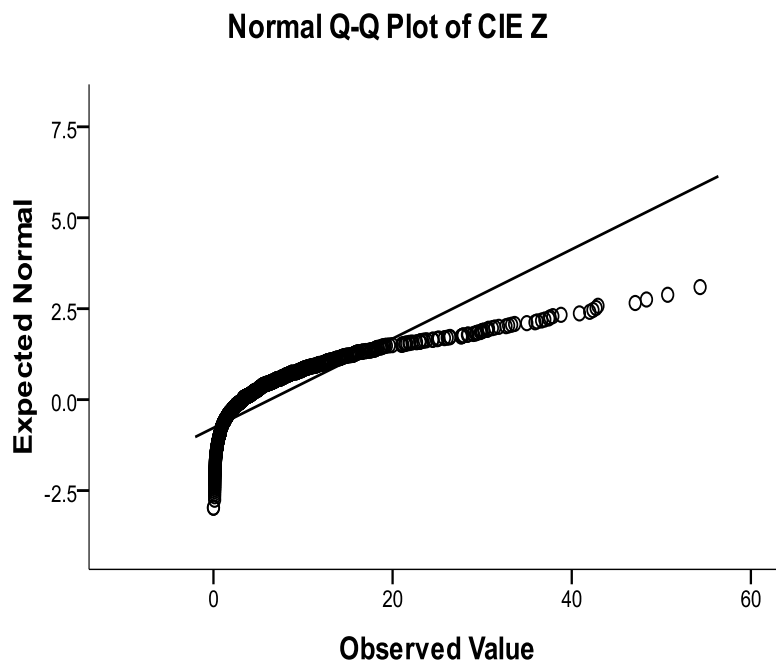


**CIE Z Variable**  
Stem and Leaf Plot

```

245  0 . 01111111111222222222222333333333344444444444555555556666667777777777888
      88889999999
141  1 . 000001111112222333333344445555566666677778889999
92   2 . 00001111222333344444556677788899
78   3 . 00011112222233344456677899
65   4 . 00112222344455567788999
56   5 . 000111223344456788&
39   6 . 013344567889&
34   7 . 01255666899&
31   8 . 0012345677
28   9 . 234456889&
21  10 . 0113568&
18  11 . 0145678&
21  12 . 1345669&
14  13 . 3457&
15  14 . 12458&
14  15 . 679&&
8   16 . 06&
7   17 . 5&&
13  18 . 01378&
72  Extremes (>=19.0)
    
```

(& denotes fractional leaves.)



## Appendix F

### Brand, Type and Content of Analysed Hair Products

Brand & Product Type	Product Content (Manufacturer)
<p><b>Coles Smart Buy Hairspray</b></p>	<p>Alcohol, Butane, Isobutane, Propane, Water, Octylacrylamide/ Acrylates/ Butylaminoethyl Methacrylate Copolymer, Aminomethyl Propanol, Fragrance</p>
<p><b>Garnier Fructis Style Styling Gel</b></p>	<p>Water, Dimethicone, Propylene Glycol, VP/VA Copolymer, Triethanolamine, Carbomer, Phenoxyethanol, PEG 40 Hydrogenated Castor Oil, PEG 192 Apricot Kernel Glycerides, PEG 70 Mango Glycerides, Chlorphenesin, Polyethylene Glycol, Limonene, Pentasodium Penetrate, Linalool, Citrus Limonum/ Lemon Fruit Extract, Cinnamal Fragrance (FIL C256281)</p>
<p><b>Toni &amp; Guy Boost-It Mousse</b></p>	<p>Water, Dimethyl Ether, Alcohol, Butane, PVP/VA Copolymer, PPG 5 Ceteth 20, Polysorbate 20, PVP, Isobutane, Phenyl Trimethicone, Triethanolamine, Fragrance, Carbomer, Propane, Disodium EDTA, Benzophenone 4, Butylphenyl Methylpropanol, Hydroxyisohexyl 3 cyclohexene Carboxaldehyde, Polyquaternium 7, Hydroxycitronellal, Linalool, Methylparaben, Propylparaben</p>
<p><b>Joico Moisture Recovery Leave-In Moisturiser</b></p>	<p>Water, Hydrolysed Keratin, Cocodimonium Hydroxypropyl Hydrolysed Keratin, Hydrolyzed Algin, Oenothera Biennis (Evening Primrose) Oil, Simmonosia Chinensis (Jojoba) Seed Oil, Panthenol, Chlorella Vulgaris Extract, Seawater, Amodimethicone, Cocamidopropyl PG-Dimonium Chloride, PEG 7 Glyceryl Cocoate, Dimethicone, Propoxytetramethyl, Piperidinyl, Dimethicone, Benzophenone 4, Lysine HCL, Quaternium 80, Trideceth 12, Trideceth 6, Triethanolamine, Cetareth 20, Cetrimonium Bromide, Cetrimonium Chloride, C11-15 Pareth 7, Citric Acid, Disodium EDTA, Diazolidinyl Urea, DMDM Hydantoin, Iodopropynyl Butylcarbamate, Limonene, Fragrance</p>
<p><b>Paul Mitchell Smoothing Gloss Drops</b></p>	<p>Dimethicone, Cyclomethicone, Phenyltrimethicone, SD Alcohol 40 B, Bisamino PEG/PPG 41/3 Aminoethyl PG Propyl Dimethicone, Hedychium Coronarium (White Ginger), PEG 12 Dimethicone, Algae (Seaweed) Extract, Aloe Vera (Aloe Barbadensis) Extract, Anthemis Nobilis (Roman Chamomile) Flower Extract, Lawsonia Inermis (Henna) Extract, Simmondsia Chinensis (Jojoba) Seed Extract, Rosmarinus Officinalis (Rosemary) Extract, Isopropyl Alcohol, Fragrance, Benzoate, Benzyl Salicylate, Butylphenyl Methylpropional, Citronellol, Geraniol, Hexylcinnamal, Hydroxycitronellal, Limonene</p>

Brand &Product Type	Product Content (Manufacturer)
<p data-bbox="252 573 523 696"><b>American Crew Fiber Pliable Molding Cream (Wax)</b></p> <p data-bbox="288 1055 486 1128"><b>Joico K-Pak Smoothing Balm</b></p>	<p data-bbox="576 535 1401 745">Water, Lanolin Wax, Cetearyl Alcohol (Coconut), PVP, Tribehenin, Propylene Glycol, Tridecyl Stearate, Dipentaerythryl Hexacaprylate/Hexacaprate, Cetareth 25 (Coconut), PEG 8 Beeswax, Tridecyl Trimelitate, PEG 40 Castor Oil, Acrylates/C10 30 Alkyl Acrylate Crosspolymer, Triethanolamine, Tetrasodium EDTA, Fragrance, Methylparaben, Propylparaben, Butylparaben, Isobutylparaben, Phenoxyethanol, Caramel, Yellow 5 Lake (CI 19140)</p> <p data-bbox="576 808 1401 1384">Water, Polyquaternium 37, Phenyl Trimethicone, Propylene Glycol Dicaprylate/Dicaprate, Cyclopentasiloxane, Decyl Oleate, Propoxytetramethyl Piperidinyl Dimethicone, Cetrimonium Chloride, C12–15 Alkyl Benzoate, Polyquaternium 11, Hydrolyzed Keratin (Quadramine Complex), Cocodimonium Hydroxypropyl Hydrolyzed Keratin, Hydrolyzed Keratin PG–Propyl Methylsilanediol, Thioctic Acid, Butyl Methoxydibenzoylmethane, Psidium Guajava Fruit Extract, Sodium Ascorbyl Phosphate, Dimethicone, Tocopheryl Acetate, Oenothera Biennis (Evening Primrose) Oil, Aleurites Moluccana Seed Oil, Glycolipids, Hyaluronic Acid, Allantoin, Aloe barbadensis Leaf Juice, Benzophenone–4, Glycerin, Hydrolyzed Wheat Protein, Polyquaternium–59, Butylene Glycol, Bisamino PEG/PPG–41/3 Aminoethyl PG–Propyl Dimethicone, Polyquaternium–46, Hydroxyethylcellulose, PPG–1 Trideceth–6, Quaternium–80, Trideceth–3, Trideceth–6, Tetrasodium EDTA, Methylparaben, Propylparaben, Aminomethyl Propanol, Diazolidinyl Urea, Benzyl Benzoate, Benzyl Salicylate, Citronellol, Geraniol, Hexyl Cinnamal, Hydroxyisohexyl–3–Cyclohexene Carboxaldehyde, Hydroxycitronellal, Limonene, Butylphenyl Methylpropional, Fragrance, Mica (CI 77019), Titanium Dioxide (CI 77891), Iron Oxides (CI 77491)</p>